# Subglacial water storage in an Alpine glacier

*Including hydrometeorological and glaciological influences on flooding in Alpine glacierised basins.*

**A thesis submitted to the Division of Life and Environmental Sciences,**

**University of Oxford for the degree of Doctor of Philosophy.**

**By**

**Nicholas J. Rutter**

**B.A.(Hons), Geography, University of Oxford, 1997.**

**School of Geography and the Environment,**

**University of Oxford.**

**2002**

## ABSTRACT

Glaciated catchments increasingly accommodate rising populations. As glaciers are capable of modifying peak flows and releasing floodwaters, understanding and developing models of subglacial water storage and release has significance to the safety of resident populations and land use decision-making.

Glaciological and hydrometeorological processes play a critical role in determining water storage within the subglacial drainage system of Alpine glaciers. However, our understanding of spatial variations of these processes throughout the ablation season remains incomplete. Field results and modelling studies of the glacial hydrological system at Findelengletscher, Canton Valais, Switzerland are presented with a view to improving understanding of physical mechanisms controlling water flow within glacierised catchments.

A physically-based model of surface runoff incorporating meltwater and precipitation has been developed. This model has limited data requirements using only air temperature, solar radiation, precipitation and elevation of the transient snow line in a simple, spatially distributed energy balance model. It has been used to predict surface runoff at an hourly resolution for the 1999 ablation season.

Methodological advances have been made by creating conceptual models of water flow through the subglacial drainage system. Models are used for semi-quantitative interpretation of water level variations in boreholes, as surrogate measures of subglacial water pressures. The boreholes either directly intersect subglacial channels or hydraulically connect to subglacial channels through a subglacial sediment layer. Variations in borehole water levels are considered at both diurnal and seasonal timescales.

Water storage has been calculated within the subglacial drainage network and interpretations are made of temporal variations in subglacial water storage. Borehole water levels indicate that the glacier subsole can be spatially separated into those areas that are hydraulically connected or unconnected to the subglacial drainage system. Hydraulically connected areas may further be subdivided into areas of efficient and inefficient subglacial drainage. These may intermittently connect and influence water balance within a glacier. Increasing and decreasing trends in water balance cycles are initiated by glaciohydrological mechanisms. These control the activity of intermittent hydraulic connections between efficient and inefficient areas of subglacial drainage. Connections form in response to two hydrometeorological factors: high elevation rainfall and short duration decreases in elevation of either the snowline or the 0°C isotherm. Increasing trends in water balance over successive days are associated with preferential routing of inputs into, and retention within, hydraulically inefficient areas of the subglacial drainage system.

Occasionally the release of water from temporary subglacial storage is not synchronous with either hydrometeorological causal factor. Measurements of fall-line velocity and vertical displacement suggest that basal sliding may alter preferential subglacial flow pathways. However, uncertainty exists as to whether such changes may be the result of lagged effects of either high water pressures from rainfall or low water pressures from low daily surface runoff. These uncertainties are due to system response times affecting the time taken to transfer longitudinal strain within glacier ice.

In the late ablation season the potential for rapid surface runoff over the annual maximum snow-free area within the catchment is high. In the event of a large rainfall event the capacity of a tunnel-conduit system to discharge may have decreased sufficiently to cause temporary retention

of a large proportion of surface runoff, predominantly within distributed drainage. Temporary storage followed by re-integration of hydraulic connections formed earlier in the ablation season, increases the potential for proportionally large discharge events (relative to the volumes of inputs) in the late ablation season. Flooding in glacierised basins becomes more likely as a result.

**Table of Contents**

**Abstract……..…...i**

**List of Figures……..….vii**

**List of Tables……...….xiv**

**Acknowledgements……...xv**

**SECTION I - INTRODUCTION .....1**

**1 INTRODUCTION.....2**
**1.1 Problem and context.....2**
**1.2 Document overview.....3**
**2 INPUTS, STORAGE AND OUTPUT OF WATER IN GLACIERISED SYSTEMS: A REVIEW.....7**
**2.1 Introduction.....7**
**2.2 A systems approach to water movement in glacial environments.....9**
**2.3 Energy balance and glacier surface ablation.....11**
2.3.1 Radiation as a cause of ablation.....11
2.3.2 Conduction as a cause of ablation.....17
2.3.2.1 Sensible heat.....18
2.3.2.2 Latent heat.....22
2.3.3 Terrestrial influences on glacier energy balance and direct measurement of ablation.....26
2.3.4 Temporal variation of ablation in the Swiss Alps.....29
**2.4 Theory of drainage in temperate Alpine glaciers.....35**
2.4.1 Inter-granular water flow.....40
2.4.1.1 Inter-granular water flow through ice.....40
2.4.1.2 Inter-granular water flow through consolidated sediment.....41
2.4.1.3 Inter-granular water flow through deformable sediment.....43
2.4.2 Englacial drainage.....47
2.4.3 Subglacial water flow.....52
2.4.3.1 Concentrated subglacial drainage.....53
2.4.3.2 Distributed subglacial drainage.....65
**2.5 Influence of subglacial water pressure on glacier sliding and uplift.....72**
**2.6 Permanency of sub-glacial drainage structures in temperate Alpine glaciers.....74**
2.6.1 Seasonal evolution and deterioration.....78
2.6.2 Coexistence of multiple drainage systems.....84
2.6.3 Influence of outburst flooding.....86
**2.7 Field instrumentation and methodology.....88**
2.7.1 Boreholes.....88
2.7.2 Proglacial solute and suspended sediment fluxes.....95
2.7.2.1 Solute fluxes.....96
2.7.2.2 Suspended sediment fluxes.....98

2.7.3 Tracer studies ..... 101
**2.8 Summary ..... 104**
**3 AIMS AND OBJECTIVES ..... 106**
**SECTION II - FIELD METHODS, SURFACE RUNOFF MODELS AND THEORETICAL DEVELOPMENT OF SUBGLACIAL WATER STORAGE ..... 108**
**4 RESEARCH DESIGN AND FIELD METHODS ..... 109**
**4.1 Introduction ..... 109**
**4.2 Location of study site ..... 110**
**4.3 Selection of study site ..... 112**
**4.4 Field Methods ..... 112**
4.4.1 Hydrometeorological ..... 113
4.4.2 Borehole drilling ..... 115
4.4.3 Borehole water level monitoring ..... 117
4.4.4 Dye tracing ..... 119
4.4.5 Solute load ..... 120
4.4.6 Surface velocity and vertical displacement ..... 120
**4.5 Data Management ..... 123**
4.5.1 Identification of faulty data ..... 124
4.5.2 Reconstruction of missing data ..... 126
**5 SURFACE RUNOFF MODEL DEVELOPMENT ..... 132**
**5.1 Introduction ..... 132**
**5.2 Model development ..... 133**
5.2.1 Temporal variation in surface runoff at a single point on the glacier surface ..... 136
5.2.2 Runoff across the glacier surface ..... 143
**5.3 Model application and parameter optimisation ..... 148**
**5.4 Summary ..... 158**
**6 THEORETICAL DEVELOPMENT OF SUBGLACIAL WATER STORAGE USING BOREHOLES ..... 159**
**6.1 Introduction ..... 159**
**6.2 Conceptualisation of the glacial hydrological network ..... 160**
**6.3 Diurnal variations of water levels in boreholes directly intersecting a subglacial channel ..... 163**
6.3.1 Connection with an unobstructed channel ..... 164
6.3.2 Connection with an obstructed channel ..... 167
6.3.2.1 Down-glacier obstruction ..... 167
6.3.2.2 Up-glacier obstruction ..... 170
**6.4 Affect of subglacial channel size on borehole water levels ..... 173**
6.4.1 Diurnal variations ..... 174
6.4.2 Seasonal variations ..... 176
**6.5 Diurnal variations of water levels in boreholes hydraulically connected to a subglacial channel through subglacial sediment ..... 180**
6.5.1 Confined, saturated sediment of constant hydraulic conductivity ..... 180
6.5.2 Unconfined sediment ..... 182
6.5.3 Unsaturated sediment ..... 184
6.5.4 Variable hydraulic conductivity of sediment ..... 186
**6.6 Summary ..... 188**

**SECTION III - RESULTS AND SYNTHESIS ..... 190**

**7 WATER STORAGE ..... 192**
**7.1 Introduction ..... 192**
**7.2 Comparison of modelled surface runoff and proglacial discharge ..... 193**
**7.3 Variations in the water balance ..... 199**
**7.4 Detailed observations of water storage ..... 203**
**7.5 Affect of seasonal variation in subglacial drainage on water storage ..... 210**
7.5.1 Subglacial drainage in the early ablation season ..... 211
7.5.2 Subglacial drainage in the mid ablation season ..... 215
7.5.3 Subglacial drainage in the late ablation season ..... 223
**7.6 Summary ..... 225**
**8 HYDRO-GLACIOLOGICAL INFLUENCES ON SUBGLACIAL WATER STORAGE ..... 228**
**8.1 Introduction ..... 228**
**8.2 Topographic influences on subglacial drainage ..... 229**
**8.3 Spatial and temporal variations of water storage within the subglacial drainage network ..... 232**
8.3.1 Detailed observations of borehole water levels ..... 236
8.3.2 Interpretation of water balance using borehole water levels ..... 250
8.3.2.1 Water balance period one (WB1) ..... 250
8.3.2.2 Water balance period two (WB2) ..... 258
8.3.2.3 Water balance period three (WB3) ..... 262
8.3.2.4 Water balance period four (WB4) ..... 267
8.3.2.5 Water balance period five (WB5) ..... 271
8.3.2.6 Water balance period six (WB6) ..... 275
8.3.2.7 Water balance period seven (WB7) ..... 278
**8.4 Water balance and ice motion ..... 281**
8.4.1 Detailed observations of ice motion ..... 282
8.4.2 Affect of ice motion on water balance ..... 284
8.4.2.1 Mean fall line velocities and water balance ..... 284
8.4.2.2 Vertical displacement and water balance ..... 289
**9 WATER BALANCE AND SUBGLACIAL DRAINAGE STRUCTURE ..... 294**
**9.1 Introduction ..... 294**
**9.2 Hydraulic connection of boreholes ..... 295**
**9.3 Configuration of subglacial drainage ..... 300**
**9.4 Causes of storage and release of subglacially routed water ..... 304**
9.4.1 Precipitation ..... 308
9.4.2 Low daily surface runoff ..... 310
9.4.3 Glaciological changes ..... 311
9.4.4 Implications for high magnitude runoff in the late ablation season ..... 313
**9.5 Conclusions ..... 317**

**SECTION IV - CONCLUSIONS ..... 320**

**10 CONCLUSIONS ..... 321**
**11 REFERENCES ..... 326**
**12 APPENDICES ..... 350**
**12.1 Data processing ..... 350**
**12.2 Calibration of pressure transducers ..... 354**
**12.3 Pressure sensor construction, operation and overburden ..... 360**
**12.4 Worked example of curve fitting ..... 363**
**12.5 Borehole Summary - spot height measurements ..... 367**

**12.6 Drilling Record.....373**
**12.7 Surface runoff model computer code (FORTRAN 90).....375**
**12.8 Time lags between stationary points in BWL time series.....383**

## List of Figures

*Figure 1.1 - Thesis structure (chapter headings in bold).....6*
*Figure 2.1 - Feedback effects of climate on glacier movement (Modified from Meier 1965 in Benn and Evans 1998).....9*
*Figure 2.2 – Phase changes between ice, water and vapour (Benn and Evans, 1998).....24*
*Figure 2.3 – Daily mean values of air temperature (upper panel, smoothed curve also shown) and global radiation (lower panel) (Oerlemans and Knap, 1998). .....32*
*Figure 2.4 – Calculated net radiation on north- and south-facing slopes of 30° in the Caucasus at 3600m (modified from Barry 1992). .....33*
*Figure 2.5- Typical variations of radiation input and loss at ground level (Linacre and Geerts, 1997). .....34*
*Figure 2.6 – Hourly values of energy budget components, 12 July 1997, Hohe Mut (2560m), Austrian Tirol (Rott 1979 in Barry 1992). S = net radiation; B = soil heat flux; F = sensible heat flux; L = latent heat flux; MEZ = Central European Time.....35*
*Figure 2.7 – Schematic diagram of englacial equipotential surfaces that control direction of water movement (Lawson 1993 after Hooke 1989 and Shreve 1972). .....38*
*Figure 2.8 – Schematic long-section of hydrological pathways through a temperate glacier (Lawson 1993 modified from Collins 1988). .....39*
*Figure 2.9 – Model of possible active interfaces within an active net-melting subglacial environment (Menzies, 1995).....40*
*Figure 2.10 – Schematic diagram showing variation of mean shear stress ($\tau$) as a function of time (or displacement) in a granular medium that is sheared at a constant rate (Hooke, 1998).....46*
*Figure 2.11 – Hypothesised formation of grain bridges. Large arrows show shear stress applied to material, short arrows indicate component of this stress along grain bridges (Hooke and Iverson, 1995). (a) standard grain bridge; (b) grain fracture; (c) slip between grains; (d) reduction of stress at grain contact points due to additional material.....47*
*Figure 2.12 – Velocity profile for an ice sheet (surface slope of 2.2°, flow law exponent (n) = 3, viscosity parameter = 0.2 MPa $a^{1/n}$). A comparative profile (dashed line) for a linearly viscous material is shown for comparison and the thickness of the till is greatly exaggerated. Surface velocity = $u_s$, basal velocity due to sliding = $u_{sl}$, basal velocity due to deformation of till = $u_d$. (Hooke, 1998). .....49*
*Figure 2.13 – (Upper) Longitudinal velocity distribution ($ma^{-1}$) on Athabasca Glacier (dots indicate points of measurement, dashed contours are extrapolated). (Lower) theoretical distribution of longitudinal velocity in a parabolic channel, scaled to cover approximately the observed range of velocities (Raymond, 1971).....50*
*Figure 2.14 – Hypothetical relationship between the position of potholes and the stress field in the glacier (Röthlisberger and Lang, 1987). .....50*
*Figure 2.15 – Orientation of the principal stress deviator ($\sigma$') as a function of depth (y) in the glacier (Röthlisberger and Lang, 1987). .....51*
*Figure 2.16 – Approximate slope of a moulin conduit, White Glacier, Axel Heiberg Island, Canadian Arctic (Müller and Iken, 1973). .....51*
*Figure 2.17 – Different types of subglacial drainage system. (1) bulk water movement with deforming till; (2) Darcian porewater flow; (3) pipe flow; (4) dendritic channel network; (5) linked cavity system; (6) braided canal network; (7) thin film at ice-rock interface (Benn and Evans, 1998).....54*
*Figure 2.18 – Idealised sketch of effects of ice deformation pressure and channel water pressure within a cylindrical ice walled conduit (in relation to Equation 2.21 and*

*Equation 2.22, u and $P_i$ are defined as positive inward and $\dot{m}$ and $P_w$ are defined as positive outward (Hooke, 1998).....56*
*Figure 2.19 – Differential elements for computation of water pressure in cylindrical ice walled conduits (Röthlisberger and Lang, 1987). .....56*
*Figure 2.20 – Hydraulic grade lines for a circular horizontal channel under ice of 250m thickness (B = ice flow / deformation parameter (B is the same as A in Table 2.3), n' = Manning roughness coefficient, x = distance from glacier snout) (from Hooke 1998 after Röthlisberger and Lang 1987). .....59*
*Figure 2.21 – Geometry of an idealised broad, low subglacial conduit (Hooke et al., 1990). .....62*
*Figure 2.22 – Relationship between angle (θ) controlling the length of arc and the factor (δ) by which the ice-viscosity parameter must be reduced to obtain the same piezometric pressures (Hooke et al., 1990). .....62*
*Figure 2.23 – Schematic diagram of linked-cavity network. Plan view (left) has areas of ice contact with bed shaded and areas of ice-bed separation are blank. Vertical cross-sections (right) along axis AA' and BB' indicate water filled cavities and linking channels (Kamb, 1987). .....66*
*Figure 2.24 – Idealised configurations for cavities in the linked-cavity model; (a) modelled step(Kamb, 1987); (b) wave cavities; (c) bedrock surface; (d) rounded bedrock step; (e) N channel of (Weertman, 1972). .....67*
*Figure 2.25 – Plan views of actual (left) and modelled (right) subglacial morphologies of linked-cavities, showing modelled parameters (Kamb, 1987). .....68*
*Figure 2.26 – (a) Steady-state configurations of step orifice roof profile values for varying values of melt stability parameter (Ξ) where gap height (g(x)) is shown in terms of g/h as a function of dimensionless longitudinal coordinate x/l, where l is the gap length (Kamb, 1987). (b) Steady state configurations of wave orifice roof profile values for varying values of melt stability parameter (Ξ') where the gap height (g(x)) is shown in terms of the ratio $g/g_o$, where $g_o$ is the height midway along the length of the gap (x = ½) in the absence of roof melting (Ξ' = 0). The longitudinal coordinate x is scaled by the gap length l (Kamb, 1987). .....69*
*Figure 2.27 – Comparison of effective confining pressure vs. discharge relationship for linked-cavity and channel-tunnel models (using an ice thickness of 400m) (Kamb, 1987). .....70*
*Figure 2.28 - Schematic diagram to show relative changes in volume of surface runoff (dashed) and capacity to discharge runoff (solid) throughout an annual cycle in a temperate Alpine glacier. .....75*
*Figure 2.29 - Schematic development of a cave system. Future moulins (short dash), course of crevasses due to water pressure (long dash) and potential course of crevasses (dotted) (Röthlisberger, 1996). .....77*
*Figure 4.1 - Location map of the study area, Findelengletscher, Switzerland (Barrett and Collins, 1997). .....110*
*Figure 4.2 - Map of meteorological stations and borehole locations at Findelengletscher, including type of borehole connectivity with the subglacial hydrological system, during 1999. .....114*
*Figure 4.3 - Calculation of borehole water levels .....118*
*Figure 4.4 - Positions of stakes used to determine ice surface movement relative to the positions of boreholes. .....121*
*Figure 4.5 - Faulty borehole water level data from borehole 99.10 .....124*
*Figure 4.6 – Peaks in diurnal cycles before overburden pressures affect the pressure transducer in borehole 99.10 (n.b. water levels drop below that of the transducer at night). .....126*

*Figure 4.7 – Low resolution measurements of borehole water level data ..... 127*
*Figure 4.8 - Regression analysis used to reconstruct data. ..... 131*
*Figure 5.1 - Interaction of vertical movements of the transient snow line with catchment basin hypsometry of Findelengletscher, Switzerland (Collins 1998). ..... 147*
*Figure 5.2 - Typical variations of radiation input and loss at ground level (Linacre and Geerts 1997). ..... 150*
*Figure 5.3 – Extension and compression effects on modelled total surface runoff of variations in the melt factor (MF) parameter (MF = 1.0 pecked line, MF = 3.0 dashed line, MF = 6.0 solid line). ..... 153*
*Figure 5.4 – Optimised values of $R^2$ coefficients derived from comparison of hourly values of modelled total surface runoff and proglacial river discharge using the Nash and Sutcliffe (1970) measure of efficiency. ..... 154*
*Figure 5.5 - Optimised values of $R^2$ coefficients derived from comparison of daily range values of modelled total surface runoff and proglacial river discharge using the Nash and Sutcliffe (1970) measure of efficiency. ..... 154*
*Figure 5.6 – Histograms of hourly values of proglacial river discharge (solid line) and modelled total surface runoff model output (pecked line) using a melt factor value of 3.35, between 31 July and 16 September 1999. ..... 157*
*Figure 5.7 – Cumulative frequency plot of hourly values of proglacial river discharge (solid back line) and modelled total surface runoff using various values for the melt factor parameter (dashed grey line = 1.35, dashed black line = 2.35, pecked line = 3.35 and solid grey line = 4.35), between 31 July and 16 September 1999. ..... 157*
*Figure 6.1 – Conceptual model of the glacial hydrological system as a single store (or reservoir). ..... 160*
*Figure 6.2 – Water levels at night in boreholes directly intersecting an unobstructed subglacial channel where, h, represents the depth of water columns in each borehole. ..... 166*
*Figure 6.3 - Water levels during the day in boreholes directly intersecting an unobstructed subglacial channel. ..... 166*
*Figure 6.4 – Diurnal time series of water levels in boreholes at different elevations directly intersecting an unobstructed subglacial channel. ..... 166*
*Figure 6.5 - Water levels at night in boreholes directly intersecting a subglacial channel that has a temporary obstruction in a down-glacier section where, a, represents the difference between the height of the water level in borehole 1 relative to other boreholes. ..... 169*
*Figure 6.6 - Water levels during the day in boreholes directly intersecting a subglacial channel that has a temporary obstruction in a down-glacier section where, b, represents the difference between the height of the water level in borehole 1 relative to other boreholes. ..... 169*
*Figure 6.7 - Diurnal time series of water levels in boreholes at different elevations directly intersecting a subglacial channel that has a temporary obstruction in a down-glacier section. ..... 169*
*Figure 6.8 - Water levels at night in boreholes directly intersecting a subglacial channel that has a temporary obstruction in an up-glacier section where, a, represents the difference between the height of the water level in borehole 3 relative to other boreholes. ..... 172*
*Figure 6.9 - Water levels during the day in boreholes directly intersecting a subglacial channel that has a temporary obstruction in an up-glacier section where, b, represents the difference between the height of the water level in borehole 3 relative to other boreholes. ..... 172*

*Figure 6.10 - Diurnal time series of water levels in boreholes at different elevations directly intersecting a subglacial channel that has a temporary obstruction in an up-glacier section.* ..... *172*
*Figure 6.11 – Idealised diagram of influences in computation of net effective pressure in an ice walled, cylindrical conduit ($P_w$ = water pressure, $P_i$ = ice overburden pressure) after (Röthlisberger and Lang 1987).* ..... *173*
*Figure 6.12 –Affects of a small sub-glacial channel orifice on diurnal changes in borehole water levels.* ..... *175*
*Figure 6.13 - Affects of a large sub-glacial channel orifice on diurnal changes in borehole water levels.* ..... *175*
*Figure 6.14 - Diurnal time series of water levels in boreholes drilled into sub-glacial channels with small (Figure 6.12) and large (Figure 6.13) sized orifices that receive similar volumes of surface runoff.* ..... *175*
*Figure 6.15 – Diurnal variations in borehole water levels in the early ablation season (May / June) when runoff is low. Boreholes directly intersect sub-glacial channels with a low capacity to discharge (small orifice size).* ..... *176*
*Figure 6.16 - Diurnal variations in borehole water levels in the mid-ablation season (July / August) when runoff is high. Boreholes directly intersect sub-glacial channels with a high capacity to discharge (large orifice size).* ..... *177*
*Figure 6.17 - Schematic diagrams of decrease in the capacity of subglacial channels to discharge (decreasing orifice size) in the late ablation season (September / October) when runoff is decreasing. Boreholes directly intersect subglacial channels.* ..... *178*
*Figure 6.18 – Diurnal variations in water levels of boreholes hydraulically connected to subglacial channels through a sediment layer.* ..... *181*
*Figure 6.19 – Diurnal variations in water levels of boreholes hydraulically connected to subglacial channels through a sediment layer. Where, $I_1$, represents the difference in magnitude of daily maximum water levels between boreholes.* ..... *183*
*Figure 6.20 - Diurnal variations in water levels of boreholes hydraulically connected to subglacial channels through a sediment layer. Where, $I_2$, represents the lag time between daily minimum borehole water levels.* ..... *185*
*Figure 6.21 - Diurnal variations in water levels of boreholes hydraulically connected to subglacial channels through a sediment layer. Where, $I_3$, represents the lag time between daily maximum borehole water levels.* ..... *187*
*Figure 7.1 - Hourly total precipitation (bars), diurnal variation of air temperature (grey solid), incoming solar radiation (black solid), modelled total surface runoff (pecked) and daily estimates of snow line elevation (dashed) at Findelengletscher, 29 July-17 September, 1999.* ..... *194*
*Figure 7.2 - Hourly discharge (solid line) and modelled total surface runoff (pecked line).* ..... *195*
*Figure 7.3 - Cumulative total hourly runoff predicted over 30 consecutive days in 1999 using measurements from discharge in the pro-glacial river (solid line) and modelled estimates of total surface runoff (pecked line).* ..... *196*
*Figure 7.4 - Hourly pro-glacial river discharge in the Findelenbach, 20 May - 27 October 1999. Vertical bars separate hydrological episodes (I - XIV) into distinct hydrological periods.* ..... *197*
*Figure 7.5 – Cumulative total daily runoff from Findelengletscher 1–31 August 1999, using measurements from ablation stakes (dashed), discharge in the Findelenbach (solid) and modelled estimates of total surface runoff (pecked).* ..... *198*
*Figure 7.6 - (a) 24-hour running average of total surface runoff (pecked) and proglacial discharge in the Findelenbach (solid) demarcated into hydrological periods, (b) hourly water balance (pecked) and 24 hour running average (solid) demarcated into periods of rising and falling water balance at Findelengletscher, 31 July - 16 September 1999.* ..... *200*

*Figure 7.7 - (a) Hourly total surface runoff (pecked) and proglacial discharge (solid), (b) hourly water balance (thin solid) and 24 hour running average (thick solid), Findelengletscher and Findelenbach 1–12 August 1999.....204*
*Figure 7.8 - (a) Hourly total surface runoff (pecked) and proglacial discharge (solid), (b) hourly water balance (thin solid) and 24 hour running average (thick solid), Findelengletscher and Findelenbach 10–22 August 1999.....206*
*Figure 7.9 - (a) Hourly total surface runoff (pecked) and proglacial discharge (solid), (b) hourly water balance (thin solid) and 24 hour running average (thick solid), Findelengletscher and Findelenbach 20 August - 17 September 1999. .....208*
*Figure 7.10 - Hourly electrical conductivity (solid) and discharge (pecked) in the Findelenbach, 22 June -10 August 1999. .....211*
*Figure 7.11 - Annual discharge in the Findelenbach, 1991 - 1998 (Collins, Unpublished data).....212*
*Figure 7.12 - Scheme of presumed changes of subglacial drainage at Findelengletscher prior to and during an advance represented by moulins (circles), subglacial R-channels (lines) and zones of interconnected cavities (shaded). (a) and (b) are prior to the advance and (c) and (d) are during; (a) and (c) are early in the ablation season and (b) and (d) are late (Iken and Truffer, 1997).....215*
*Figure 7.13 - Hourly air temperature (grey solid) and pro-glacial discharge (black solid) in the Findelenbach, 7 September - 7 October 1999. .....224*
*Figure 8.1 - Three-dimensional estimate of a section of the subsole of Findelengletscher made from ice depth measurements in boreholes (exaggerated in the vertical axis). .....229*
*Figure 8.2 - Map of ablation area of Findelengletscher, showing contours of ice surface and subsole (Modified from Iken and Bindschadler 1986; from radio-echo soundings by H. P. Wächter Unpublished).....230*
*Figure 8.3 - Englacial channel intersecting borehole 99.55.....233*
*Figure 8.4 – Map of borehole locations, their degree of connectivity with the subglacial hydrological system and measurement resolution at Findelengletscher, 1999. .....234*
*Figure 8.5 - 10-minutely variation in elevation of water levels in borehole 99.30 (solid and pecked - see text for explanation) and elevation of glacier surface at time of drilling (dashed), 20 July - 3 September 1999.....237*
*Figure 8.6 - (a) Hourly water balance (solid) and 24-hour running average (pecked) demarcated into periods of rising and falling water balance at Findelengletscher, (b) 10-minutely variation in elevation of water levels in borehole 99.30 (solid), elevation of glacier surface at time of drilling (dashed), (c) hourly modelled total surface runoff (pecked) and pro-glacial river discharge (solid) in the Findelenbach, 20 July – 1 September 1999. .....238*
*Figure 8.7 - (a) Hourly water balance (solid) and 24-hour running average (pecked) demarcated into periods of rising and falling water balance at Findelengletscher, (b) 10-minutely variation in elevation of water levels in borehole 99.33 (solid), elevation of glacier surface at time of drilling (dashed), estimates of water levels during periods with missing data (pecked) and estimates of diurnal maximum and minimum borehole water level (including error bars at 95% confidence limits), (c) hourly modelled total surface runoff (pecked) and pro-glacial river discharge (solid) in the Findelenbach, 29 July – 2 September 1999.....240*
*Figure 8.8 - (a) Hourly water balance (solid) and 24-hour running average (pecked) demarcated into periods of rising and falling water balance at Findelengletscher, (b) 10-minutely variation in elevation of water levels in borehole 99.52 (solid), elevation of glacier surface at time of drilling (dashed), (c) hourly modelled total surface runoff (pecked) and pro-glacial river discharge (solid) in the Findelenbach, 30 July – 10 August 1999. .....242*

*Figure 8.9 - (a) Hourly water balance (solid) and 24-hour running average (pecked) demarcated into periods of rising and falling water balance at Findelengletscher, (b) 10-minutely variation in elevation of water levels in borehole 99.54 (solid), elevation of glacier surface at time of drilling (dashed), estimates of water levels during periods with missing data (pecked) and estimates of diurnal maximum and minimum borehole water level (including error bars at 95% confidence limits), (c) hourly modelled total surface runoff (pecked) and pro-glacial river discharge (solid) in the Findelenbach, 12 – 24 August 1999. ....244*

*Figure 8.10 – (a) Hourly water balance (solid) and 24-hour running average (pecked) demarcated into periods of rising and falling water balance at Findelengletscher, (b) 10-minutely variation in elevation of water levels in borehole 99.10 (solid), elevation of glacier surface at time of drilling (dashed), estimates of water levels during periods with missing data (pecked) and estimates of diurnal maximum and minimum borehole water level (including error bars at 95% confidence limits), (c) hourly modelled total surface runoff (pecked) and pro-glacial river discharge (solid) in the Findelenbach, 15 August – 16 September 1999. ....246*

*Figure 8.11 - (a) hourly precipitation; (b) hourly water balance at Findelengletscher; (c) 10-minutely variation in elevation of water levels in borehole 99.30 (dashed), borehole 99.33 (grey), borehole 99.52 (pecked), estimates of water levels in borehole during periods with missing data (short dash) and estimates of diurnal maximum borehole water level (including error bars at 95% confidence limits); (d) hourly total surface runoff (pecked) and pro-glacial river discharge (solid) in the Findelenbach, 31 July - 7 August 1999. ....251*

*Figure 8.12 - (a) hourly precipitation; (b) hourly water balance at Findelengletscher; (c) 10-minutely variation in elevation of water levels in borehole 99.30 (dashed), borehole 99.33 (grey), borehole 99.52 (pecked), estimates of water levels in borehole during periods with missing data (short dash) and estimates of diurnal maximum borehole water level (including error bars at 95% confidence limits); (d) hourly total surface runoff (pecked) and pro-glacial river discharge (solid) in the Findelenbach, 7 - 11 August 1999. ....260*

*Figure 8.13 - (a) hourly precipitation; (b) hourly water balance at Findelengletscher; (c) 10-minutely variation in elevation of water levels in borehole 99.30 (dashed), borehole 99.33 (grey), borehole 99.54 (pecked), estimates of water levels in borehole during periods with missing data in boreholes 99.54 (light pecked) 99.33 (short dash) and estimates of diurnal maximum borehole water level (including error bars at 95% confidence limits); (d) hourly total surface runoff (pecked) and pro-glacial river discharge (solid) in the Findelenbach, 10 - 17 August 1999. ....263*

*Figure 8.14 - Hourly boundary layer air temperature measured off-glacier (solid) and on-glacier (pecked), 11 - 14 August 1999. ....265*

*Figure 8.15 - (a) hourly precipitation; (b) hourly water balance at Findelengletscher; (c) 10-minutely variation in elevation of water levels in borehole 99.10 (solid), borehole 99.30 (dashed), borehole 99.33 (grey), borehole 99.54 (pecked), estimates of water levels in borehole during periods with missing data in boreholes 99.10 and 99.54 (light pecked) and estimates of diurnal maximum borehole water level (including error bars at 95% confidence limits); (d) hourly total surface runoff (pecked) and pro-glacial river discharge (solid) in the Findelenbach, 16 - 21 August 1999. ....268*

*Figure 8.16 - (a) hourly precipitation; (b) hourly water balance at Findelengletscher; (c) 10-minutely variation in elevation of water levels in borehole 99.10 (solid), borehole 99.30 (dashed), borehole 99.33 (grey), borehole 99.54 (pecked), estimates of water levels in borehole during periods with missing data in boreholes 99.33 (short dash) 99.10 and 99.54 (light pecked) and estimates of diurnal maximum borehole water level*

*(including error bars at 95% confidence limits); (d) hourly total surface runoff (pecked) and pro-glacial river discharge (solid) in the Findelenbach, 20 - 28 August 1999. ....272*
*Figure 8.17 - (a) hourly precipitation; (b) hourly water balance at Findelengletscher; (c) 10-minutely variation in elevation of water levels in borehole 99.10 (solid), borehole 99.30 (dashed), borehole 99.33 (grey), estimates of water levels in borehole during periods with missing data in borehole 99.10 (light pecked) 99.33 (short dash) and estimates of diurnal maximum borehole water level (including error bars at 95% confidence limits); (d) hourly total surface runoff (pecked) and pro-glacial river discharge (solid) in the Findelenbach, 27 August - 3 September 1999. ....277*
*Figure 8.18 - (a) hourly precipitation; (b) hourly water balance at Findelengletscher; (c) 10-minutely variation in elevation of water levels in borehole 99.10 (solid), estimates of water levels in borehole during periods with missing data (light pecked) and estimates of diurnal maximum borehole water level (including error bars at 95% confidence limits); (d) hourly total surface runoff (pecked) and pro-glacial river discharge (solid) in the Findelenbach, 3 - 17 September 1999. ....280*
*Figure 8.19 - Positions of stakes used to determine ice surface movement relative to the positions of boreholes. ....282*
*Figure 8.20 - (a) Hourly water balance demarcated into periods of rising and falling water balance at Findelengletscher, (b) mean daily horizontal glacier surface velocity along fall line, (c) hourly total surface runoff (pecked) and pro-glacial discharge (solid), (d) hourly precipitation. All other graphs indicate 10-minutely variation in elevation of water levels in boreholes (solid), estimates of water levels during periods with missing data (pecked) and estimates of diurnal maximum and minimum borehole water level (including error bars at 95% confidence limits), 20 July - 1 September 1999. ....288*
*Figure 8.21 - (a) Hourly water balance demarcated into periods of rising and falling water balance at Findelengletscher, (b) hourly total surface runoff (pecked) and pro-glacial discharge (solid), (c) hourly precipitation, (d) mean daily horizontal glacier surface velocity along fall line. All other graphs show vertical displacement of the glacier surface at positions along the fall line, 20 July - 1 September 1999. ....293*
*Figure 9.1 - Sediment in suspension within borehole 99.54 ....296*
*Figure 9.2 - Schematic diagram of subglacial drainage configuration beneath Findelengletscher in the mid to late ablation season (not to scale). ....303*
*Figure 12.1 - Field calibration of Druck and Gems TransInstument pressure transducers. ....357*
*Figure 12.2 – Exploded diagram of a pressure sensor (Honeywell) and a typical housing (Gems sensors) ....361*
*Figure 12.3 – Hysteresis error (combined temperature and mechanical hysteresis). ....362*
*Figure 12.4 – Full Wheatstone bridge arrangement of resistor connections ....362*
*Figure 12.5 - Original scaled data points and new data points raised and lowered to find maximum values from the curve within the 99% confidence limits. ....365*
*Figure 12.6 - Regression curves through original scaled data points and data points lowered and raised to produce a curve of maximum possible values within a 99% confidence range. ....365*
*Figure 12.7 - Observed data and re-scaled regression curves during periods of missing data. .366*

## List of Tables

*Table 2.1 - Albedos (per cent) of snow and ice surfaces (Paterson 1994, pg59).....15*
*Table 2.2 – Summer heat budget of Aletschgletscher, Switzerland (W $m^{-2}$) (Röthlisberger and Lang, 1987).....31*
*Table 2.3 – Physical constants of ice and water at 0°C and related properties (Röthlisberger and Lang, 1987).....58*
*Table 5.1 - Notation used in equations.....137*
*Table 5.2 – Model parameters (MF is in mm $d^{-1}$ $°C^{-1}$ and radiation factors are in $m^2$ $W^{-1}$ mm $h^{-1}$ $°C^{-1}$) at Storglaciären, Sweden (Hock, 1999). .....141*
*Table 5.3 – Comparison of $R^2$ values with increasing delay in the timing of the modelled total surface runoff. .....153*
*Table 5.4 – t-statistics for Student's t-tests between hourly proglacial discharge and modelled total surface runoff, calculated using variations in the melt factor parameter....156*
*Table 6.1 – Theoretical inter-relations between subglacial channel size, water pressure and channel discharge.....164*
*Table 6.2 - Summary table for borehole water levels where an obstruction in the subglacial channel exists between boreholes 1 and 2 (see Figure 6.5 and Figure 6.6). Where, h, represents the height of the water columns in each borehole and, I, represents the volume of surface runoff over an ice surface.....170*
*Table 6.3 - Summary table for borehole water levels where an obstruction in the subglacial channel exists between boreholes 2 and 3 (see Figure 6.8 and Figure 6.9). Where, h, represents the height of the water columns in each borehole and, I, represents the volume of surface runoff over an ice surface.....171*
*Table 7.1 – Summary table of six dye traces of parcels of water from runoff at 2650m of the glacier surface to the gauging station at 2500m on the Findelenbach, 1998.....198*
*Table 8.1 - Data describing boreholes subject to continuous measurement.....233*
*Table 8.2 – Spot height measurements of depth below the ice surface of water levels in boreholes that connected, temporarily or permanently, with the glacial hydrological system. Measurements in all boreholes were taken within a period of one hour between 12:00 and 19:00 each day. (D = borehole drilled, S = water level at surface, U = water level unknown, C = borehole closed through ice deformation). .....235*
*Table 12.1 - Values used in reconstruction of missing data.....364*

## Acknowledgements

The author would like to thank the following people without whom this work would simply not have been completed.

- Prof. David Collins of the University of Salford who provided the stimulus for this research problem and the opportunity to carry out fieldwork in Switzerland as part of the Alpine Glacier Project. Dr Peter Bull of the University of Oxford, Dr Steve Boult of the University of Manchester and Dr Andy Hodson of the University of Sheffield for their comments and advice that helped improve earlier versions of the thesis.

- Grande Dixence S.A. for logistical support in Switzerland.

- Dr Alex Lee formerly of the University of Manchester for processing GPS data, advice, encouragement and sense of humour whilst in Switzerland that helped me conquer the 'worlds of pain' that inevitably came our way. His appreciation of the bigger picture and the restorative properties of a drinking session, no matter how distant, proved essential.

- All the members of the Alpine Glacier Project from the Universities of Oxford, Manchester and Salford who assisted with fieldwork in Switzerland during 1998 and 1999. Their manpower, enthusiasm and friendship made it all an enjoyable experience. Although too numerous to all name individually special thanks must go to Nick Brier, Charlie Nixon, Mark Roberts and David Mallard for carrying equipment equivalent to their own body weight, happily drilling boreholes in horizontal hail and persuading

loggers to log. Never has one willing volunteer been more valuable than a thousand forced workers.

- Dr Mike Bithell, formerly of the University of Oxford, for his help in coding the melt model and for always being available for just one more last question.

- Support staff and graduate students in the SoG. IT, laboratory, photography, cartography and library support from Dave, Mark, Martin, Ailsa, Chris, Linda and Sue; a constant supply of tea and biscuits at eleven and four from Big Steve and Eric; and the company of Presto, Mike, Elaine, Matt, Helen and the good Dr Tracey whilst consuming them.

- Many others during this research have provided me with the enthusiasm and encouragement to complete the thesis when things have looked bleak. Charlie, Toph, Ian and the Big G for the shared graduate experience over lunch or a beer; the Keble lads (Rich, Max, Fleets, O'D, d'Lace and Steveo amongst others) for dragging me away from the computer and Hertford friends past and present for their friendship and support as I continued to dodge tax for longer than is feasibly possible. Both Louise and Shonagh for their care and attention during the good times as well as the bad.

- Finally and most importantly I would like to thank my mum and dad for their unquestioning support throughout the entire research process, especially during times of great personal difficulties. Their patience and bottomless encouragement were essential as deadline after deadline were breached in the seemingly never-ending processes of getting things done. In the end, it really was all about rates.

# SECTION I - INTRODUCTION

# 1 INTRODUCTION

## 1.1 Problem and context

Glaciated catchments increasingly accommodate rising populations. River discharge from glaciated catchments influences development of habitation in high mountain environments, which utilise water supplies for irrigation, drinking and hydro-electric power production. Flooding has a high impact on habitation and agricultural land in these environments as land-use tends to be concentrated in the narrow valley floors in and around the river flood plains. As temperate Alpine glaciers are capable of modifying peak flows and releasing floodwaters, understanding and developing models of subglacial water storage and release has significance for the safety of resident populations and land use decision-making.

Water storage within a temperate Alpine glacier is a function of inputs as melt and outputs via a dynamic drainage system. However, the hydrometeorological and glaciological process that control both inputs and outputs are complex. Chapter 2 shows that although there has been much research has been done into the complexity of these processes our understanding of meltwater production and subglacial drainage remains incomplete. Although much research has focussed on the timing and evolution of subglacial drainage systems early in the ablation season (Hubbard and Nienow, 1997; Iken and Bindschadler, 1986; Iken *et al.*, 1983; Nienow *et al.*, 1996a) there is a relative paucity of information describing its deterioration. Consequently, investigation of rates and glacier wide patterns of subglacial drainage system closure at the end of the summer melt season is a niche that has been highlighted as a current research priority (Hubbard and Nienow, 1997). Also, "the role of sediment beds in water transmission, storage and temporary retention or lags in discharge over days, seasons and longer periods is basically unknown", (Lawson 1993, pg 41). As a result, research into drainage system closure by direct methods in a subglacial

environment that consists at least partially of a sedimentary substrate, will be of value. Consequently, the aim of this thesis is to investigate the impact of subglacial, including within sediment, water storage and release mechanisms on the capacity of a glacial hydrological system to transfer surface runoff during the late ablation season.

Wider implications of this research relate to the response of glaciers to longer-term changes in climate (Collins, 1989a; Dansgaard *et al.*, 1993; Oerlemans, 1989; Rebetez *et al.*, 1997; Zongtai, 1989). Mid-latitude glaciers are especially susceptible to both changes in winter precipitation, which drive mass balance as well as increasing intensities of sensible heat, and solar radiation in summer that may cause the transient snow-line to rise to higher elevations and thus prolong the summer ablation season. Research in high mountain environments suggests glaciers may provide a valuable surrogate for global warming over a number of decades (Pangallo, 1995; Zeller and Röthlisberger, 1988; Zimmermann, 1990). Annual discharges have risen from glaciated catchments in Switzerland over the last thirty years as a response to warm summers (Collins, 1998a). Therefore, if more extreme hydrometeorological events associated with climate change are superimposed on this trend, understanding mechanisms of water storage within glaciated catchments may have large implications for future water resources management and flood prediction.

## 1.2 Document overview

To ease the flow of discussion and argument this thesis is split into four sections (Figure 1.1). **SECTION I** introduces the research problem.

**Chapter 1** states the research problem within a brief glacio-hydrological context and the general aim of the study.

**Chapter 2** provides a comprehensive review of factors that influence subglacial water storage. A thorough discussion describing processes and monitoring techniques of inputs to, throughputs within and outputs from the glacial hydrological system each provide a basis for chapters in Section III.

**Chapter 3** defines the specific aims and objectives of the project.

**SECTION II** describes the monitoring programme, development of a physically based runoff model and a methodological protocol for interpretation of subglacial water pressures.

**Chapter 4** describes the physical characteristics of the study area, monitoring techniques employed in the investigation and methods of data management and data reconstruction.

**Chapter 5** describes the development of a spatially distributed energy balance model that is used to calculate surface runoff. The model calculates inputs to the glacial hydrological system at an hourly resolution throughout the monitoring period, which in combination with discharge measurements allows calculation of temporal variations in the glacial water balance in chapter 7.

**Chapter 6** develops a methodological protocol for interpretation of subglacial water pressures using water levels in boreholes that hydraulically connect to the subglacial drainage system. This provides a new conceptual framework with which to interpret spatial variations in subglacial water storage in chapter 8.

**SECTION III** presents observed subglacial water pressures to identify periods of water storage for comparison with modelled results. Furthermore, observed data are used to develop understanding of subglacial drainage dynamics within the context of the aims defined in chapter 3.

**Chapter 7** presents results of modelled inputs to and measured outputs from the glacial hydrological system. It allows estimates of changes in the glacial water balance to be calculated in addition to preliminary interpretations of the causes.

**Chapter 8** focuses on interpretation of the causes of spatial variations in storage and release of subglacially routed water. Concurrent observations of borehole water levels, fall line velocity and vertical displacement of the ice surface, in combination with data presented in chapter six, allows interpretation of the affect of hydrometeorological and glaciological mechanisms on the water balance.

**Chapter 9** discusses the nature of hydraulic connections between borehole and the subglacial drainage system, configurations of subglacial drainage, causes of water storage and release and their implications for flooding.

**SECTION IV** presents the conclusions and implications of the study.

**Chapter 10** presents conclusions to the principal research aims, producing a better conceptual understanding of physical mechanisms controlling water storage and their influence on subglacial water storage in the late ablation season.

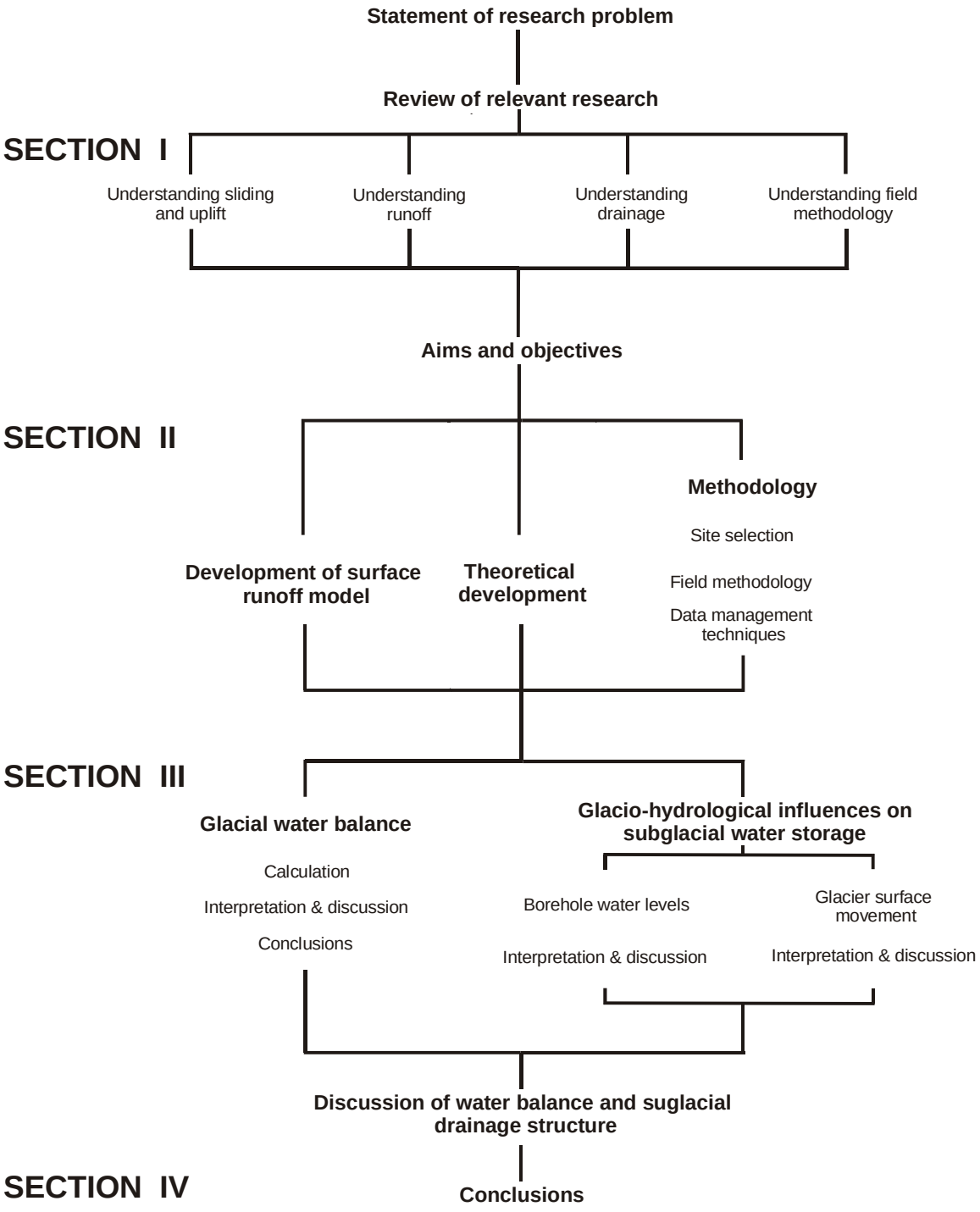



***Figure 1.1 - Thesis structure (chapter headings in bold).***

# 2 INPUTS, STORAGE AND OUTPUT OF WATER IN GLACIERISED SYSTEMS: A REVIEW

## 2.1 Introduction

The purpose of this chapter is to provide a comprehensive review of previous work that concerns hydrological inputs to, throughputs within and outputs from the glacial hydrological system. Each subsection is designed to provide the reader with the required background to understand discussion and analysis in sections II to IV.

Section 2.2 describes how this investigation is part of a systems approach to understanding fluxes of water and ice at a number of temporal and spatial scales. It shows how this research fits into the wider spectrum of current glaciological research that was briefly introduced in chapter 1.

Section 2.3 describes processes that affect rates of surface runoff, which are used in the creation of a surface runoff model in chapter 5 that allows calculation of subglacial water storage in chapter 7. Radiation, sensible heat fluxes, latent heat fluxes and terrestrial affects on meltwater production are described and examples of their combined affect in the Swiss Alps are presented over seasonal and diurnal timescales. Section 2.4 describes processes that affect rates of water flow through the glacier. Principles of micro-scale water flow within ice are initially described. Theories about the size, shape, hydraulic efficiency and connectivity of drainage systems over larger spatial scales are then explained and compared.

Section 2.5 describes processes that cause glacier motion through basal sliding and internal deformation of ice. This focuses on the affect of variations in subglacial water pressure on ice motion, which is directly considered in chapter 8. Section 2.6 combines theory of hydrological

inputs and throughputs to discuss seasonal evolution and deterioration in hydraulic efficiency of the drainage network within temperate glaciers. This provides a robust conceptual basis for methodological development in chapter 6 and all analysis in section III.

Section 2.7 indicates a thorough knowledge of monitoring practices that are relevant to glacial hydrological studies. Four different measurement techniques are examined allowing both the strengths and limitations of different methodologies to be considered. Finally, in section 2.8 a summary is presented of how the processes highlighted in this chapter combine to cause variations in the subglacial drainage network throughout the ablation season. This is presented in relation to the aim of this thesis, which is to investigate the impact of subglacial water storage and release mechanisms on the capacity of a glacial hydrological system to transfer surface runoff during the late ablation season.

## 2.2 A systems approach to water movement in glacial environments

Water flow in glacierised environments are considered in a systems approach as the cryospheric subsection of the whole hydrological cycle. Rates of water input into the cryospheric subsection are overwhelmingly controlled by atmospheric inputs. Alternatively, surface runoff may be derived from geothermal heating of the glacier sole, contributing large amounts of meltwater in spatially distinct tectonically active geological areas; and by surface or groundwater flow from non-glaciated areas at higher elevation within a catchment.

Fluctuations in total volumes of ice and consequently the impact of the cryospheric subsection on the overall hydrological cycle occurs over periodicities of thousands of years as a response to Milankovitch cycles in the earth's orbit affecting incoming solar radiation. The effect of Milankovitch cycles on global climate causes a response in rates of advance and retreat of glacier ice and consequent feedback effects of terrestrial ice coverage on local climate and net mass balance (Figure 2.1) determining the limits of glacial and interglacial periods.

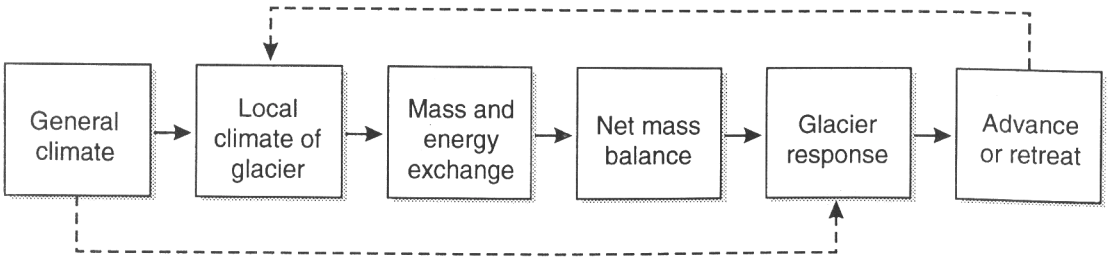



***Figure 2.1 - Feedback effects of climate on glacier movement (Modified from Meier, 1965 in Benn and Evans, 1998).***

During interglacial periods, although the spatial influence of the cryospheric subsection on rates of water movement through the entire hydrological cycle diminishes, the cryospheric system provides a valuable analogue to global and local environmental change. Periods of global

warming during interglacials caused by changes in atmospheric gaseous composition, whether or not enhanced by anthropogenic emissions (e.g. increases in $CO_2$ and other greenhouse gases), will increase the elevation of the 0°C isotherm causing both a decrease in solid precipitation in the accumulation zone and an increase in ice melt in the ablation zone. Although local topographic and atmospheric factors are highly influential on mass balance of valley glaciers, an inter-yearly decrease in net mass balance causes an increase in the equilibrium line altitude and consequently glacial retreat and a reduction in potential glacier ice velocities. Alpine valley glaciers at high elevation in low latitudes are especially sensitive to such changes in mass balance due to large yearly variations in the atmospheric energy budget in comparison to polar glaciers at high latitudes.

As only approximately 3% of the total area of glacier ice on the earth's surface, or approximately 0.6% of global ice by volume (Drewry, 1983; Sugden and John, 1976; both in Benn and Evans, 1998, pg 39), are distributed in ice caps and glaciers in high elevation mountainous areas rather than in large polar ice sheets, global water fluxes as a result of decreasing mass balance do not significantly contribute to rising sea levels through glacioeustacy or glacioisostacy. However, rates of erosion in warm-based alpine glaciers and subsequent evacuation of eroded material by subglacially routed water create a weathering environment that is not supply limited. Limitations to rates of in-stream dissolution of eroded material are instead provided by the rate at which reactants, principally carbonic acid, can be acquired. Consequently, high rates of draw down of $CO_2$ from the atmosphere has been postulated in such glaciated areas, causing high rates of solutional erosion (Sharp *et al.*, 1995a). This has the capacity to represent a potentially important contribution to the global carbon cycle (Raymo and Ruddiman, 1992).

At the catchment scale within the hydrological cycle, release of water from glacierised areas in high mountain environments has important localised effects in terrain that has characteristically steep, impermeable valley sides and constricted, flat valley floors. Water resource uses in such environments, i.e. settlement, agriculture and hydro-electric power, are generally spatially constricted to valley floors due to topographic controls. Consequently water resource requirements rely on seasonal and diurnal variations in the quantity and quality of water draining from heavily glaciated uplands of catchments. Quantity and quality of water available as a resource is a product of variation in atmospheric factors. These factors control the intensity of surface runoff from ice and snowmelt, the intensity and physical state of precipitation and ultimately yearly changes in mass balance interacting with the capacity of the sub- and englacial drainage system to discharge runoff. A systems approach is required to understand physical mechanisms controlling inputs of water to and throughputs within a glacierised catchment over hourly and seasonal timescales. Physical mechanisms that affect the causes and reflect the consequences of water movement over such temporal scales are further discussed in the following sections of this chapter.

## 2.3 Energy balance and glacier surface ablation

### 2.3.1 Radiation as a cause of ablation

The total net energy flux of radiation between the atmosphere and a glacierised catchment is calculated by subdividing the total flux into incoming and outgoing fluxes of short wave and long wave energy (Equation 2.1). The potential maximum seasonal and diurnal variations of total energy flux at a particular latitude are controlled by the earth's orbit and spin. Such potential flux variations may be limited or extenuated by atmospheric, topographic and terrestrial influences as well as their feedback effects at decreasing scales.

$$R_n = (1-\alpha)R_s + R_{ld} - R_{lu}$$

$R_n$ = net radiation flux ($Wm^{-2}$)
$\alpha$ = surface albedo
$R_s$ = global shortwave radiation ($Wm^{-2}$)
$R_{ld}$ = incoming longwave radiation at the surface ($Wm^{-2}$)
$R_{lu}$ = emission of longwave radiation by the surface ($Wm^{-2}$)

***Equation 2.1***

The level of radiance received by a surface at the outermost point of the atmosphere, perpendicular to the sun's rays, is 1368 ± 3 $Wm^{-2}$ (Fröhlich, 1993). Unless the orientation of the ground is parallel to this surface, excluding the effects of atmospheric attenuation, radiation received will reduce as the zenith angle increases. This is because the same amount of incoming solar energy is being dispersed at an increasingly oblique angle over a greater surface area of ground. At high latitudes the curvature of the earth's surface creates an increasingly oblique angle at which solar energy strikes the ground causing the radiance per unit area to be lower than in low latitudes. The degree of seasonal change in energy dispersion relative to a specific latitude is also extenuated by increased scattering of the direct solar beam at low solar elevations, which are controlled by cyclical variations in the sun's declination (Linacre, 1992). As a result, allowing for the effect of clear sky atmospheric transmissivity, the maximum potential incoming solar radiation at any point on the earth's surface can be calculated using Equation 2.2.

$$I = I_0\left(\frac{Rm}{R}\right)^2 \psi^{((P/P_0)/\cos Z)} \cos\phi$$

$I$ = direct short - wave incoming radiation (clear sky) ($Wm^{-2}$)
$I_0$ = solar constant ($Wm^{-2}$)
$Rm$ = mean sun - earth distance (km)
$R$ = instantaneous sun - earth distance (km)
$\psi$ = atmospheric clear sky transmissivity (0.6 - 0.9)
$P$ = atmospheric pressue (Pa)
$P_0$ = mean atmospheric pressure at sea level (Pa)
$Z$ = local zenith angle
$\phi$ = angle of incidence between the normal to the surface and the solar beam

***Equation 2.2***

This has important implications for temporal changes in meltwater production as although seasonal variations in incoming short wave energy are more pronounced at high latitudes than low latitudes, diurnal variations are less extreme. Absolute values of snow and ice melt are not only dependent on the latitudinal position at which extra-terrestrial short wave radiation from the sun strikes the edge of the earth's atmosphere, but also the subsequent diffusion, absorption and reflection of energy within the atmosphere. Global shortwave radiation interacts with clouds, aerosols, gases and particulate matter in the atmosphere that can absorb or scatter extra-terrestrial radiation. Globally, approximately 26% is reflected back out to space, 23% is scattered down to the earth's surface as diffuse radiation with the remaining fraction making up the direct radiation component (Linacre and Geerts, 1997). However, on a local scale the proportions of direct and diffuse radiation can vary greatly due to cloud cover, topographic shading and aspect (altering the angle between the sun's rays and the ground surface). Aspect is especially important in valley glaciers such as Morteratschgletscher, Switzerland, where a combination of shading and atmospheric attenuation means that only 49% of extra-terrestrial irradiance reaches the glacier surface over twelve continuous months of measurements (Oerlemans and Knap, 1998). Although

calculation of the reduction in seasonal and diurnal energy balance changes due to shading, can be achieved by computer simulation using Monte Carlo methods (Hock, 1999; Oerlemans and Knap, 1998) the topographic influences are highly site specific reducing the applicability of this approach to transferable modelling of energy budgets.

Once shortwave radiation strikes a surface ($R_s$), whether it is either direct or diffuse, the degree to which the energy is absorbed or reflected is dependent on the albedo ($\alpha$) of the material. Table 2.1 shows that darker coloured materials have a low albedo thus absorbing more energy than light materials, causing melt rates of dirty ice to be three to four times greater than that of fresh snow (Paterson, 1994). Seasonal melt of Alpine snow packs cause a rise in the elevation of the transient snow line and associated decrease in glacier surface albedo. Consequently, greater energy absorption causes an increase in daily maximums of net radiation, which previously remained very low e.g. below 100 $Wm^{-2}$ (Cline, 1995), and an increase in influence of radiation on the total energy balance e.g. providing 75% of the total energy available for snowmelt (Cline, 1995). Oerlemans and Knap (1998) estimate the efficiency of radiation absorption at the tongue of Morteratschgletscher, Switzerland, to be less than 25% of the total extra-terrestrial radiation (rising to 32% during the ablation season due to less effective shading by surrounding mountains) over an annual cycle using a combination of atmospheric diffusivity, topographic shading and surface albedo.

Energy that is reflected will either escape to space or will be re-absorbed by cloud and atmospheric gases such as ozone, methane and carbon dioxide. Cycles of absorption and re-emittance of long-wave radiation between the ground and various strata of atmospheric gases and particulates will continue until the energy is dissipated within the environment. On a global scale this process causes enhanced warming of the troposphere, maintaining higher air temperatures (i.e. the greenhouse effect) and increasing available thermal energy over inter-annual timescales.

Longwave radiation is preferentially absorbed and emitted (see Equation 2.3) by humid air and solid materials with a low albedo. If either are positioned adjacent to ice or snow, for example rock walls constraining a valley glacier, they can cause highly localised increases in ablation. Intensities of emitted long wave radiated energy fluxes are dependent on the emissivity and temperature of the surface being heated (see Equation 2.3). Müller (1985) estimated emissivity values as 0.98 for wet snow, 0.99 for dry snow and 0.97 for ice. For practical purposes longwave outgoing radiation from a melting surface at 0°C with an emissivity of unity is taken to be 315.6 $Wm^{-2}$ (Hock and Noetzli, 1997).

| | Range |
|---|---|
| Dry snow | 80-97 |
| Melting snow | 66-88 |
| Firn | 43-69 |
| Clean ice | 34-51 |
| Slightly dirty ice | 26-33 |
| Dirty ice | 15-25 |
| Debris-covered ice | 10-15 |

***Table 2.1 - Albedos (per cent) of snow and ice surfaces (Paterson, 1994, pg59).***

$$R_{lu} = \varepsilon\sigma T^4 + (1-\varepsilon)L$$

$R_{lu}$ = outgoing terrestrial (long wave) radiation ($Wm^{-2}$)
$\varepsilon$ = emissivity of surface
$L$ = incoming terrestrial radiation ($Wm^{-2}$)
$\sigma$ = Stefan - Boltzmann constant ($5.67\times10^{-8}\ Wm^{-2}K^{-4}$)
$T$ = surface temperature (°K)

***Equation 2.3***

The proportion of extra-terrestrial radiation that reaches the earth's surface directly varies seasonally as a function of sky transmissivity. Müller (1985) showed that values of sky transmissivity are larger in winter than summer and that the range of annual transmissivity

increases at lower elevations. Diffuse radiation on 'clear sky' days also varies seasonally, controlled predominantly by multiple reflection between the ground and atmosphere, which are sensitive to changes in albedo of both clouds and the ground (Ångström and Tryselius, 1934). The impact of cloud cover on diffuse radiation depends on the albedo of the cloud base. As albedo of a cloud base is generally unknown, albedo from the top of clouds is used as a substitute. Albedo of clouds depends on type, altitude and colour, which in the Alps has as an albedo of around 0.60 (Robinson, 1958 in Müller, 1985). However, variations in diffuse radiation are predominantly controlled by variation in ground albedo (i.e. difference in albedo values of snow and ice between ~0.9 and 0.1) reflecting short-wave energy between the sky and the ground, rather than variations in transmissivity and albedo of cloud cover (Berner, 1963 in Müller, 1985). It is common for heat flux expressions to be parameterised to incorporate measured or estimated values of atmospheric and terrestrial emissivities (Ersi *et al.*, 1995), although the main formats of Equation 2.3 and Equation 2.4 remain. There is some evidence of diurnal variations in albedo of glacier ice and snow, for example a range of 0.3 or more in snow (Hock, 1998; Sauberer and Dirmhirn, 1952). However, even over a sub-diurnal timescale from sunrise to sunset, data reported by these authors are out of phase with each other suggesting interpretation at this timescale may be limited by measurement accuracy, repeatability and spatial difference in ice and snow surfaces between monitoring sites. Oerlemans and Knap (1998) also report some variation in albedo during diurnal cycles but this is attributed to physical factors affecting the measurement sensor (e.g. tilt, riming etc), which could not be corroborated, as measurement stations were unmanned.

Temperature and humidity determines the amount of long wave radiation received at the earth's surface (counter-radiation) when there is no cloud in the sky, which is approximated by Equation 2.4. On cloudy days, levels of counter radiation increase with elevation and type of cloud cover

(from high stratus to low cumulus), also increasing up to 45% in winter compared with summer values.

$$R_{ld} = \varepsilon_f \sigma T^4$$

$R_{ld}$ = incoming terrestrial radiation ($\mathrm{Wm^{-2}}$)
$\varepsilon_f$ = empirical factor dependant on water vapour pressure
$T$ = temperature (°K)
$\sigma$ = Stefan - Boltzmann constant ($5.67 \times 10^{-8}\ \mathrm{Wm^{-2}K^{-4}}$)

***Equation 2.4***

Müller (1985) summarised the relative affects of solar and terrestrial radiation balances. Under clear sky and low surface albedo conditions the Alpine solar radiation balance is large relative to the smaller terrestrial radiation balance and vice versa where skies are overcast and albedo is high. Low surface albedo also causes the solar radiation balance to dominate the terrestrial radiation balance and vice versa. Under either clear or cloudy sky conditions the point at which variation in albedo compensates to the extent that proportions of solar and terrestrial radiation balance the net radiation budget is equal to approximately 0.7.

### 2.3.2 Conduction as a cause of ablation

A proportion of the net radiation flux that is absorbed and not re-emitted by terrestrial or atmospheric compounds can be transferred as a thermal energy flux via intermolecular contact (i.e. conduction). Transfer of thermal energy from one mass to another in this manner is referred to as transfer of sensible heat. Circulation and turbulence characterise movement and transfer of thermal energy via sensible heat fluxes. This affects glacier melt rates both at the global scale, through oceanic and atmospheric currents, and at the catchment scale, through micro-scale eddies caused by surface roughness.

#### 2.3.2.1 Sensible heat

Oceanic circulation, which directly affects ablation of polar glaciers and some temperate valley glaciers that calve directly into maritime waters, controls global thermal energy transfer (Seidov *et al.*, 2001). Cyclonic and anticyclonic frontal systems control synoptic scale energy transfer that heavily influence glacier ablation in the mid-latitudes, such as the European Alps and Himalayas. Catchment scale energy transfer, affecting glaciers at all latitudes and elevations, may be caused by temporal inequalities in heating and cooling of terrestrial and oceanic masses, by atmospheric moisture concentrations and by topographic constraints. More localised sub-catchment scale energy transfers also exist, such as Föhn winds, on and offshore breezes and temperature inversions that can occur more rapidly over diurnal or sub-diurnal timescales. Quantification of melt rates at any point in time relies on accurate interpretation of these factors, both individually and in conjunction with each other (Liestøl, 1967).

Advection of heat through a combination of wind and buoyancy, within a moving fluid such as air, is a consequence of changes in vertical and horizontal pressure gradients with altitude (Benn and Evans, 1998; Tabony, 1985). Rates of air temperature in the free atmosphere decrease with height. They vary between an upper limit of the dry adiabatic lapse rate (9.8°C $km^{-1}$) and the lower saturated adiabatic lapse rate that varies with moisture content but is typically about 6°C $km^{-1}$ (Barry, 1992; Tabony, 1985). However, air temperatures in high mountain glacial environments are very different to those in the free atmosphere due to boundary layer interactions (Barry, 1992; Oke, 1995). Heat transfer becomes increasingly efficient and rapid when winds are strong and turbulent in the boundary layer, caused when air flows across rough surfaces and where there is a big difference between a generally isothermal melting glacier surface and that of the surrounding atmosphere (Benn and Evans, 1998). It is, therefore, important to consider micro-scale variations in energy transfer due to turbulent mixing (through convection and

advection) between an ice or snow surface and the surrounding atmosphere, which are caused by strong winds that vertically redistribute energy producing a localised adiabatic lapse rate (Tabony, 1985). Direct measurements of ablation, and its separation into causal components of radiative and sensible heat fluxes over wide areas are very problematic (see section 2.3.3). Ablation due to sensible heat is more commonly estimated by indirect methods using measurements of air temperature, vapour pressure and variations in wind speed at different heights.

Fluxes of heat and water vapour at the glacier surface, estimated using the bulk aerodynamic method (Ambach, 1986), are best used in an atmosphere that is neutral (i.e. temperature gradients that are equal to the dry adiabatic lapse rate). This uses the assumption that the eddy viscosity of air, the eddy diffusivity of heat and the eddy diffusivity of water vapour remain equal at increasing heights (Paterson, 1994). For this assumption to be correct water vapour, heat and wind speed must vary as a logarithm of height described as a Prandtl-type boundary layer, which is likely to limit estimates to the first 2m above the ice surface in an atmosphere that is very stable (Paterson, 1994). Although atmospheres are unlikely to be this stable, logarithmic profiles have been applied without modification over a range of stability conditions (Braithwaite, 1995). Calculation of energy fluxes using this assumption requires a dimensionless bulk-transfer coefficient, approximately 0.002-0.004 for melting snow and ice surfaces (Paterson, 1994), as well as meteorological data of wind speed, air pressure and both surface and air temperatures (see Equation 2.5). The bulk transfer coefficient is dependent on surface roughness lengths for wind speed and temperature (Braithwaite, 1995). Evidence from field studies shows that surface wind speed over ice varies widely due to effects of micro- and meso-scale topography (Munro, 1989) providing no general consensus on surface roughness coefficients for wind speed over either ice or snow under a variety of meteorological conditions (Braithwaite, 1995).

Although less is known about surface roughness coefficients for temperature it is estimated to be about two orders of magnitude smaller than that for wind (Ambach, 1986; Braithwaite, 1995). Although the two roughness coefficients may be expressed as a ratio (such as the Reynold's number) in practice it is convenient to assume that they, and the effective surface roughness for sensible heat flux, are equal allowing bulk transfer-coefficients to be calculated using Equation 2.6 (Braithwaite, 1995).

$$H_N = \rho c_p APu(T - T_s)$$

$H_N$ = heat available for ablation (in a neutral atmosphere) (W $m^{-2}$)
$\rho$ = density of air (kg $m^{-3}$)
$c_p$ = specific heat of air (1005J $kg^{-1} \circ C^{-1}$)
$A$ = transfer coefficient
$P$ = atmospheric pressure (Pa)
$u$ = wind speed ($ms^{-1}$)
$T$ = air temperature (°C)
$T_s$ = ice surface temperature (°C)

***Equation 2.5***

$$A = \frac{k^2}{(\ln(z/z_0))^2}$$

$A$ = transfer coefficient
$k$ = von Karman's constant (0.41)
$z$ = instrument height (~ 2m)
$z_0$ = surface roughness for sensible heat flux ($1.7 \times 10^{-4}$ m)

***Equation 2.6***

At different wind speeds, an increase in air temperature above a melting glacier surface causes a linear increase in the sensible heat flux. Reliance on the maintenance of a logarithmic wind profile is unrealistic due to relative effects of buoyancy and mechanical forcing of air. This is

reflected through the use of the bulk Richardson Number (Hay and Fitzharris, 1988) that creates or destroys stability in the boundary layer, which is generally considered to be the first 2m above a melting surface (Oke, 1995).

To attempt to mirror reality more closely, incorporation of factors such as different vertical wind profiles, e.g. log-linear profiles based on Monin-Obukhov similarity theory (Grainger and Lister, 1966; Munro, 1989; Munro, 1990), stability corrections (Braithwaite and Olesen, 1990), parameters incorporating wind variations (Hay and Fitzharris, 1988; Kuhn, 1987) and air pressure at different altitudes and surface roughness (Braithwaite, 1995) amongst others have been included in equations of energy balance. Semi-empirical relationships of bulk aerodynamic methods using a combination of meteorological variables and parameters of eddy diffusivity (Escher-Vetter, 1985) make it possible to calculate the whole energy budget at any point on the glacier surface (Baker *et al.*, 1982). Although incorporation of such corrections or parameters may endeavour to increase the accuracy of an energy budget equation it may also add a new subset of assumptions (Hay and Fitzharris, 1988) that violate physical conditions. The Monin-Obukov similarity theory highlights this problem. It can be used under stable and unstable atmospheric conditions, i.e. it can work needing only an approximate constancy of sensible and latent heat fluxes with height (Hock and Holmgren, 1996). However, errors have arisen from investigations as the theory was developed for conditions with quasi-stationarity of average wind speed over horizontal surfaces (Hock and Holmgren, 1996; Paterson, 1994). Such assumptions are particularly violated by valley glaciers with steep inclines and little horizontal homogeneity of the boundary layer (Paterson, 1994).

General inter-relationships indicate that sensible heat fluxes are reduced by aerodynamic stability, which is less likely at high wind speeds (producing a lower flux) than at low wind speeds

(Braithwaite, 1995). The surface roughness coefficient creates uncertainty in estimations of bulk aerodynamic fluxes which, in the case of the Greenland ice sheet, means an underestimation of surface roughness probably offsets neglecting stability itself in flux calculations (Braithwaite, 1995). Despite such counter-uncertainty (Braithwaite, 1995 and Braithwaite *et al.*, 1998) suggests the use of the log-linear wind profile as a more realistic approximation and should be used where wind speed data are available.

The rate of energy exchange between the atmosphere and snow or ice depends on humidity as well as temperature and turbulence of air near the glacier surface. If air has a low humidity, which is a common consequence of the rain shadow effect on the lee side of mountain ranges (e.g. Föhn winds), there is little moisture to conduct any thermal energy that is available. Seasonal variations of energy transferred by sensible heat fluxes in high mountain environments in the mid-latitudes can be large and differ dramatically from that expected in the free atmosphere (Barry, 1992). Localised Föhn winds can rapidly raise air temperatures (as well as influencing snow redistribution) e.g. by 15°C in 3 hours (Aizen *et al.*, 1995) creating a substantial increase in the proportion of the sensible heat flux contribution to the overall energy balance. As a consequence, air temperature gradients over glacial landscapes differ from 0.6°C $100m^{-1}$ in the free atmosphere to 0.4°C $100m^{-1}$ at Storglaciären, Sweden (Hock and Noetzli, 1997) and between 0.4 to 0.8°C $100m^{-1}$ in Kirgizskiy Alato, Tien Shan, China (Aizen *et al.*, 1995). Therefore, the concept of a single continuous temperature gradient over a glacierised catchment remains limited to a theoretical construct in the calculation of spatial difference in melt rates.

#### 2.3.2.2 Latent heat

As surface glacier ice is at or near 0°C, relatively small fluxes of energy into or out from the ice or snowpack may cause a change in phase of water between the gaseous, liquid and solid states.

Surface layer temperature of snow or ice, and its thermal stratigraphy at increasing depth, are affected by consumption and release of latent heat. Resulting ablation (or freezing) alters the thermal profile, making a glacier either more (or less) predisposed to melt without necessarily causing melt itself. Figure 2.2 shows that between seven and eight times as much energy is needed to change the state of water from a solid to a vapour than it does from a solid to a liquid, therefore, evaporation and condensation are a much greater influence on rates of ablation than sublimation. Evaporation occurs if the water vapour pressure in air adjacent to an ice surface at 0°C drops below 611 Pa creating a negative vapour pressure gradient. Conversely, if meteorological conditions create a positive vapour pressure gradient, vapour will condense at the ice surface thus increasing the heat energy and temperature of the ice pack (Paterson, 1994). Consequently, air temperatures below 0°C during a summer ablation season promote evaporation whereas temperatures above 0°C promote condensation. Direct measurements of latent heat fluxes under field conditions are practically impossible although estimates can again be made using bulk aerodynamic methods (Hock and Noetzli, 1997) that employ transfer coefficients in a manner similar to that of sensible heat fluxes (see Equation 2.7).

$$L_v E = 22.2 A u (e - e_s)$$

$L_v$ = specific latent heat of vapourisation ($2.8 \times 10^6$ J kg$^{-1}$)
$E$ = rate of evaporation from surface (negative if condensation)
$e$ = vapour pressure at measurement height
$e_s$ = vapour pressure at ice surface (611 Pa if melting)
$A$ = transfer coefficient
$u$ = wind speed

***Equation 2.7***

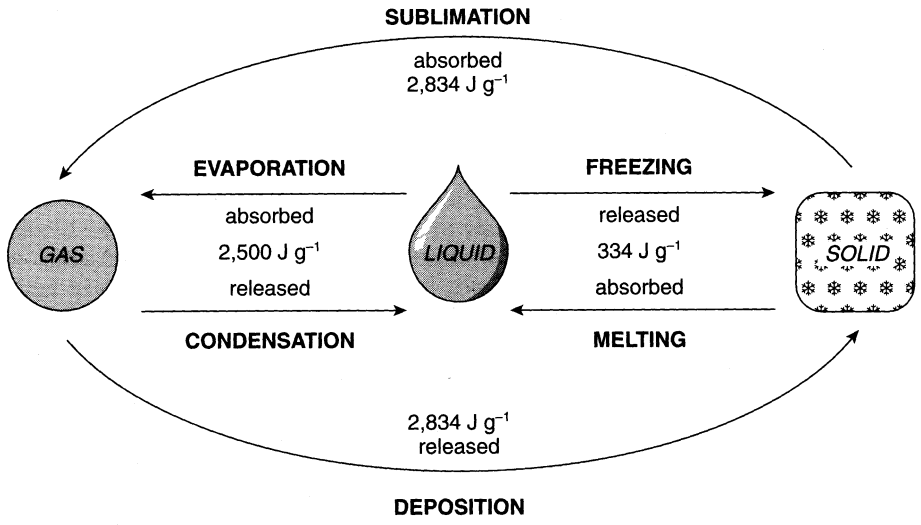



***Figure 2.2 – Phase changes between ice, water and vapour (Benn and Evans, 1998).***

Depending on its physical state, precipitation can either increase or decrease the energy balance of an ice or snow pack. In reality the physical state of precipitation is not partitioned into solids or liquids at exactly 0°C. Partitioning is achieved more accurately using the ambient air temperature relative to thresholds *TL* and *TS* (temperature thresholds delimiting liquid and solid precipitation respectively). If daily minimum air temperature $Tmin \geq TL$, precipitation is liquid; if daily maximum air temperature $Tmax \leq TS$, it is solid. However, if the daily temperature range varies between *TS* and *TL* the ratio of daily solid precipitation $P_s$ to daily liquid precipitation $P_l$ can be calculated using Equation 2.8 (Ersi *et al.*, 1995). Threshold temperature values are highly site specific although for example the value of *TS* and *TL* are 2.8°C and 5.5°C respectively (Ersi *et al.*, 1995) or 1.5°C as a single temperature threshold, i.e. *TS* (Rohrer, 1989).

$$\frac{P_s}{P_l} = \frac{1}{TL - TS}\left(TL - \frac{Td}{2} - \frac{T\max}{4} - \frac{T\min}{4}\right)$$

$Td$ = daily mean air temperature (°C)

***Equation 2.8***

If precipitation falls as a liquid it will raise the energy content through direct conduction of energy as it runs over an ice surface or percolates through a snow pack. Transit times of water percolation through a snow pack, which may decrease in temperature substantially below 0°C with increasing depth, are longer than rapid runoff over an impermeable ice surface (which is likely to be at or near 0°C) creating a greater likelihood of refreezing. Consequently, liquid precipitation falling on snow has a greater effect on the energy balance of a glacier by increasing its propensity to melt if not actually causing melt itself. As rainfall falling at elevations below the snow line coincides with periods of high cloud cover, direct surface runoff will compensate for decreasing melt rates that results from low radiation (Lang, 1973).

Rates of precipitation vary with elevation and thereby affect the spatial distribution of energy input across a catchment. Increase in precipitation with elevation occurs mainly in summer whereas in other seasons there is no obvious relationship (Ersi *et al.*, 1995). Precipitation gradient estimates with increasing elevation were of the order of a 10% linear increase at Storglaciären (Hieltala, 1989). In addition to this linear increase 25% is added for gauge undercatch error (Östling and Hooke, 1986). This addition ranged between about –2 to about 12 mm $100m^{-1}$ in the cold and warm seasons respectively in the Tien Shan region of central Asia, approximately 43°N and predominately glaciated between 3250m – 4500m (Aizen *et al.*, 1995). Ersi *et al.* (1995) report similar values for summer precipitation gradients in the Tien Shan region of China but also warn that strong convection currents, occurring when air temperatures are at their highest in July, may destroy such gradients. Such localised currents and topographic effects cause spatial deviations from standard approximations, creating differences of approximately 2000mm in annual precipitation at equivalent elevations between windward and leeward slopes (Aizen *et al.*, 1995).

If precipitation falls as snow on glacier ice, direct energy conduction has a minimal effect on overall ablation relative to the effect of increasing albedo, which is typically less than 0.3 for ice and over 0.8 for snow (Oerlemans and Knap, 1998). Due to differences in albedo between fresh snow and dirty glacier ice (see Table 2.1) rates of ablation from a glacierised catchment will therefore drop significantly if snow cover reduces the proportion of exposed glacier ice, leading to an increasingly lagged negative correlation between discharge and precipitation (Lang, 1973).

### 2.3.3 Terrestrial influences on glacier energy balance and direct measurement of ablation

The impact of atmospheric energy transfer on snow and ice melt depends on the specific heat capacity, per unit volume, of near surface glacier ice. Heat capacity, per unit volume, of snow and ice is not homogeneous at increasing depth due to variations in density (see Equation 2.9).

$$\Delta G = \int_0^z \rho c(\delta T / \delta t) dz$$

$\Delta G$ = rate heat gain in a vertical column ($^{\circ}C\ m^{-1}$)
$\rho$ = density (kg $m^{-3}$)
$c$ = specific heat capacity (J $kg^{-1} {}^{\circ}C^{-1}$)
$T$ = temperatur e (°C)
$t$ = time (s)
$z$ = depth (m)

***Equation 2.9***

Differences in density alter both the depth to which incoming short wave radiation can penetrate snow and ice, and the degree to which meltwater produced at the surface can percolate through veins and inter-granular voids (Paterson, 1994). Ice and snowpack densities are controlled by

overburden pressure as a function of time. Densities are affected by redistribution of loose snow through strong winds, which force accumulation on lee slopes (Tarboton *et al.*, 1995), and inter-granular compression or expansion, caused by deposition or removal of overlying material. Heat energy that is transmitted to subsurface layers of the ice or snow pack through radiation and conduction may cause no immediate melt at the surface but are very important influences on the susceptibility of surface ice and snow to 'ripen' (i.e. increase in thermal energy towards a threshold of melt).

Direct measurements of glacier melt due to atmospheric energy transfer can be made by monitoring surface lowering and subsurface temperatures. At short hourly monitoring intervals, ablatometers (mechanical devices that directly measure surface lowering) and thermistors that are located at a variety of subsurface depths, may give an indication of the amount of energy absorbed by a glacier (Paterson, 1994). Average diurnal patterns of measured ablation indicate the morning increase is much steeper due to delay in the onset of melt than the afternoon decrease, especially on cloudless days with high radiation, suggesting surface lowering lags input of energy to the surface (Munro, 1990). Accuracy of such direct measurements can be determined by expressing ablatometer measurements as equivalents of the melt energy flux density and comparing them with computed melt energy flux densities. Comparison of average diurnal patterns show that for both calculated and measured values to agree the surface would have to behave as a single plane of energy absorption when in reality it acts more like a three dimensional zone of energy receipt and storage (Munro, 1990). Greater differences between measured and calculated ablation rates of snow rather than ice surfaces are due to differences in processes of energy conduction, storage and consequent meltwater runoff between structures with rigid and 'loose' crystal lattices.

Direct measurements of albedo are made by comparison of incoming and reflected radiation from upward and downward facing radiometers. This technique of surface measurement is complicated due to melt water causing continuous changes in surface relief. Albedo measurement cannot be completely automated over long periods of time. Year round accessibility to measurement sites is necessary to check tilt, condition and accuracy of instruments (e.g. riming of radiometers) due to the sensitivity of the instrument set-up to distortion, resulting from the influence of 'normal' meteorological conditions (Oerlemans and Knap, 1998).

Conductive heat fluxes into subsurface ice can be estimated from temperature depth profiles measured by a series of thermistors drilled at increasing depth into the ice (Hock and Holmgren, 1996; Konzelmann and Braithwaite, 1995). In a polar ice sheet (Kronprins Christian Land, eastern north Greenland) englacial temperature measurements showed the 0°C isotherm to be only 0.2 - 0.3m below the surface and allowed calculations of heat fluxes indicating that they were asymptotic to zero below depths of 4 metres (Konzelmann and Braithwaite, 1995). However, techniques of direct measurement are vulnerable to errors in precision due to unavoidable impact and disruption of the environment they are measuring. Error can be reduced by allowing longer intervals (e.g. daily or weekly) between surface lowering measurements relative to a fixed height using ultrasound techniques that negate surface disturbance by ablatometers or stakes drilled into the ice. Increased accuracy of melt estimates from longer monitoring intervals are a consequence of allowing time for complex physical interactions of energy transfer, resulting in melt and runoff to be averaged.

### 2.3.4 Temporal variation of ablation in the Swiss Alps

Total ablation in glacierised catchments is controlled by the sum of the energy fluxes (see Equation 2.10) upon antecedent energy conditions of terrestrial snow and ice.

$$Q_m = G(1-\alpha) + L_{Net} + Q_H + Q_L + Q_R$$

$Q_m$ = energy available for melt
$G$ = global shortwave radiation
$L_{Net}$ = net longwave radiation
$Q_H$ = sensible heat flux
$Q_L$ = latent heat flux
$Q_R$ = energy supplied by rain

***Equation 2.10***

The relative importance of net radiation, sensible heat fluxes and latent heat fluxes on the overall heat budget of a glacier can be determined using a combination of latitudinal position, relative frequency of weather conditions and the result of complex interactions and feedback effects between the different sources of energy. Arid zones, where there is little moisture or cloud favour an increase in the role of radiation, whereas in moist low latitudes glacier melt is determined more by a combination of air temperature and radiation (Drosdov and Mosolova, 1975). In high polar latitudes radiation is predominantly diffuse, which favours reflection of incoming solar radiation causing melt to be controlled by sensible heat close to the surface layer (Drosdov and Mosolova, 1975). Although relative magnitudes of energy sources vary with location, net radiation is generally the largest energy source (Braithwaite and Olesen, 1990; Paterson, 1994, pg58-61) typically providing 75% of the melt energy, although on lower parts of maritime glaciers this may drop to 50% (Oerlemans and Knap, 1998).

Table 2.2 shows that in Alpine environments, net radiation is generally the dominant component of the overall heat budget and the main influence on ice and snow-melt (Baker *et al.*, 1982; Cline, 1995; Lundquist, 1982). Sensible heat and latent heat also have a small positive or negative impact on the energy balance, e.g. latent heat flux is negative as it consumes energy during evaporation (Röthlisberger and Lang, 1987). Inter-relations of meteorological variables that influence the hierarchy of energy flux parameters in the total glacial heat budget mean that although radiation provides most of the energy for ablation, the existence of a causal relationship between radiation and air temperature is such that temperature may be interpreted as a proxy variable for radiation. However, in glaciers at higher latitudes, there is a very poor correlation between ablation rate and incoming short-wave radiation compared to its correlation with temperature (Braithwaite and Olesen, 1989), suggesting it does not act as a proxy. Willis *et al.* (1991/1992) illustrated this point by using the meteorological variables, daily maximum temperature, daily temperature range and the product of wind speed and air temperature. These meteorological variables were used as surrogates for turbulent heat transfer, incoming radiation and cloud cover (i.e. longwave radiation reflected back towards the earth's surface from clouds) respectively, to explain 73% of variance in daily melt rates over the lower sections of Midtdalsbreen, Norway. Preference for using air temperature in calculations over other variables is illustrated during periods of strong temporal variations in atmospheric energy inputs. It is the most important single variable that correlates with variations in melt. Despite feedback effects between component parts of the budget and time lags between absorption and melt (Lang, 1973).

Figure 2.3 shows seasonal cycles of solar radiation that force similar trends, albeit lagged, in air temperature. Variations in air temperature and solar radiation account for variations in the ablation of snow and ice. They provide an improved correlation with melt over synoptic and shorter time-scales due to highly significant correlations with albedo of snow and ice that dominate surface conditions (Ersi *et al.*, 1995). An increase in sensible heat, causing a decrease

in albedo, will also increase the amount of net radiation that is absorbed, completing a positive feedback effect that increases the overall energy balance. Figure 2.4, shows net radiation at high elevation (3600m) in the Caucasus Mountains, a typically seasonal pattern that approximates to a bell-shaped curve. A rapid increase of net radiation in April / May and decrease in late August / September is associated with a rapid decrease, then increase, in albedo of the land surface (from snow to ice or bare rock and back again) causing increased summer absorption of shortwave radiation. As a consequence of the albedo effect of snow covered slopes that surround a valley glacier in the winter, day-to-day variability of radiation relative to the ablation period is not as accentuated (see Figure 2.3 – lower panel) due to multiple reflections that decrease the contrast between sunny and cloudy days (Oerlemans and Knap, 1998). The spring increase in net radiation is especially rapid due to the feedback effect of melting snow exposing surfaces with a lower albedo that emit greater amounts of longwave radiation energy in close proximity to the retreating snow line.

| | | R | H | $-L_vE$ | Net |
|---|---|---|---|---|---|
| Accumulation area (3366m) | mean | 44 | 4 | -3 | 45 |
| | max | 66 | 1 | 2 | |
| | min | 18 | 0 | -37 | |
| Ablation area (2220m) | mean | 129 | 38 | 14 | 181 |
| | max | 197 | 76 | 86 | |
| | min | 22 | 5 | -89 | |

***Table 2.2 – Summer heat budget of Aletschgletscher, Switzerland (W $m^{-2}$) (Röthlisberger and Lang, 1987).***

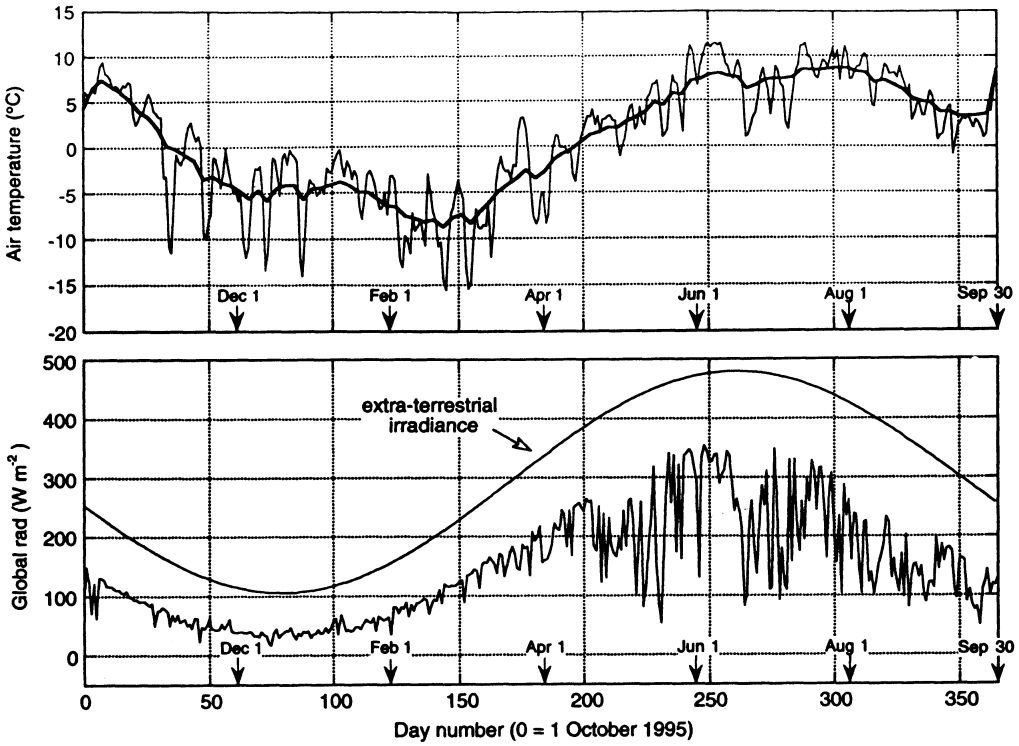



***Figure 2.3 – Daily mean values of air temperature (upper panel, smoothed curve also shown) and global radiation (lower panel) (Oerlemans and Knap, 1998).***

Figure 2.5 schematically shows the synchronicity and phase relationships of diurnal energy flows that control the net radiation balance. In a glacial / nival environment ground temperature and, therefore, net longwave radiation losses will probably represent a smaller proportion of the flux relative to net shortwave radiation gain, when surface temperatures at or near 0°C. Figure 2.6 shows how actual data exhibits a typical diurnal pattern of surface energy budget components under clear sky conditions at high elevation (2560m) in the Austrian Tirol. Between 06:00hrs and 18:00hrs (i.e. hours of daylight) net radiation dominates the energy balance with a near symmetric increase and decrease either side of solar noon. When the sun disappears below the horizon sensible and latent heat fluxes become the dominant influence over melt, although this influence is a fraction (less than one thirtieth) of the maximum daily energy input from solar radiation.

This inverse relationship over a diurnal cycle is caused by physical mechanisms that inter-relate the radiative components of the net radiation energy budget with sensible and latent heat fluxes.

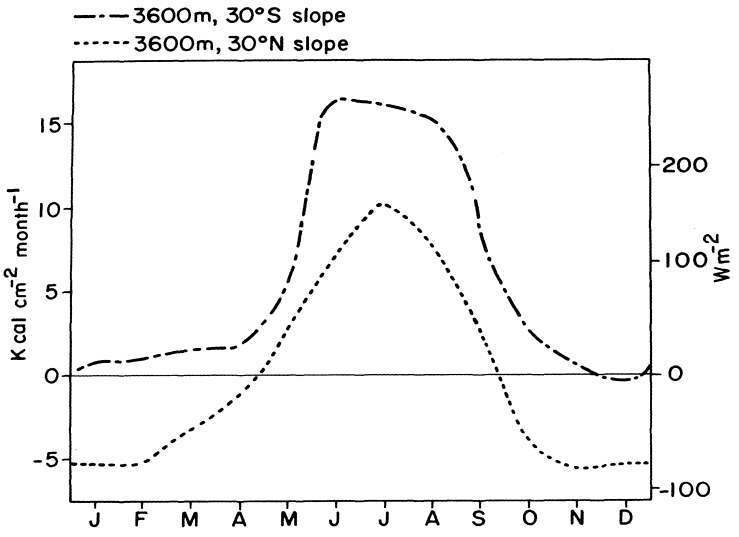



***Figure 2.4 – Calculated net radiation on north- and south-facing slopes of 30° in the Caucasus at 3600m (modified from Barry, 1992).***

To accurately evaluate temporal variation in melt rates of snow and ice at the catchment scale, it is essential to interpret energy changes as a system, including the interpretation of interconnections and feedback effects that component parts of the energy budget equation have on each other. Paterson (1994) describes one such example of a feedback effect where incoming shortwave radiation causes a rise in surface temperature and an increase in saturated vapour pressure. Instead of converting this energy input directly into melt, energy is lost through long wave radiation from the warmer ice surface, causing an increase in the evaporation rate and a decrease in the surface temperature, thus damping expected increase in melt rates. Although complications from such feedback systems exist, general trends and phase relations of net

radiation over a diurnal timescale can be established and sensible and latent heat fluxes can be estimated from meteorological data (see Table 2.2.). Inter-annual variability of energy budget components can be large, especially due to the influence of turbulent energy transfer on the sensible heat component. Lundquist (1982) showed at Nigardsbreen, Norway, over two consecutive years (1973 to 1974) the absolute radiative energy transfer remained stable but as a component of the total energy budget it increased by 30% due to lower turbulent energy transfers in the summer of 1974. Wallen (1948) illustrates similar variations but of intra-annual variability where convection and condensation (i.e. sensible and latent heat fluxes) as components of total ablation increase by approximately 30% and 10% respectively between May and August at the expense of radiative energy transfer.

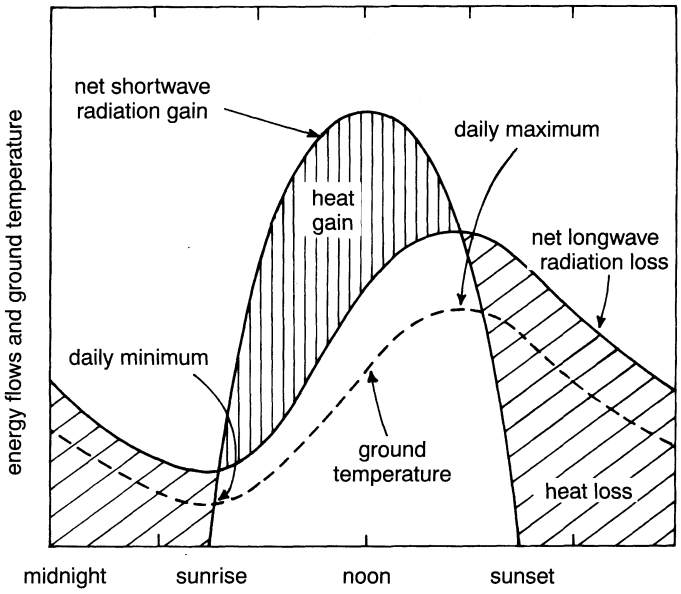



***Figure 2.5- Typical variations of radiation input and loss at ground level (Linacre and Geerts, 1997).***

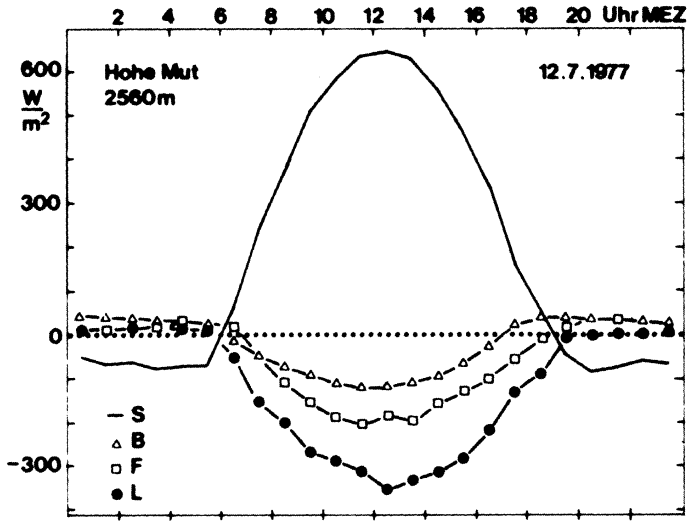



***Figure 2.6 – Hourly values of energy budget components, 12 July 1997, Hohe Mut (2560m), Austrian Tirol (Rott 1979 in Barry 1992). S = net radiation; B = soil heat flux; F = sensible heat flux; L = latent heat flux; MEZ = Central European Time.***

The importance of estimating the energy balance accurately is made apparent when considering effects of future climate change predictions on glacier melt rates. Impact on glacier melt rates can be modelled in terms of movement of snow line elevation, implications of which increase or decrease snow free proportions of the glacier surface that, in turn, increase or decrease melt rates during the ablation season. Oerlemans (1991/1992) imposed scenarios of greenhouse warming on a fictive glacier using this approach to calculate effects of increasing snow line elevation due to a potential increase in air temperature and decrease in cloudiness and albedo which resulted in an increase of 36 days in the ablation season of a glacier at 2400m by 2025 AD. Therefore, subtle changes at each stage in the parameterisation of the melt model can, therefore, have big implications when considering future projections of surface balances of glaciers and ice masses.

## 2.4 Theory of drainage in temperate Alpine glaciers

The basic equations that describe water flow in a glacier (Paterson, 1994; Shreve, 1972) rely on the fact that, "water flow is governed by variations in hydraulic potential, a measure of the

available energy at a particular time and place", (Benn and Evans 1998, pg99). Although, on the glacier surface the potential for water flow is dependent solely on differences in elevation of the point in question ($z$), the hydraulic potential ( ) for water flow within a glacier also relies on water pressure ($P_w$) and a constant describing the shape and size of the conduit ( $_0$):

$$\phi = \phi_0 + \rho_w + \rho_w g z$$

$$\rho_w = \text{density of water} (1000 \text{ kg m}^{-1})$$
$$g = \text{gravitational acceleration} (9.81 \text{ ms}^{-1})$$

***Equation 2.11***

Within and beneath a glacier water pressure ($P_w$) can fluctuate between atmospheric pressure and cryostatic pressure ($P_i$) which is the product of the weight and depth of overlying ice:

$$P_i = \rho_i g (z_s - z)$$

$$\rho_i = \text{density of ice} (\sim 920 \text{ kg m}^{-3})$$
$$z_s = \text{elevation of the glacier surface}$$

***Equation 2.12***

In a water filled sub- or englacial passage, when water is 'closed' from the atmosphere and therefore at cryostatic pressure (i.e. when $P_w = P_i$), the hydraulic potential is:

$$\phi = \phi_0 + \rho_i g z_s + g z (\rho_w - \rho_i)$$

***Equation 2.13***

Although the hydrostatic pressure as defined above is confined only to conduits it is conceptually useful to consider it as acting throughout the whole glacier (Paterson, 1994). Water will move from areas of high to low potential hydraulic pressure along the steepest hydraulic gradient ( ):

$$\nabla \phi = \rho_i \, g(\nabla z_s + 0.09 z_b)$$

***Equation 2.14***

Equation 2.14 shows that the slope of the glacier surface exerts a greater influence over the size of the hydraulic gradient than the slope of the bed by approximately a factor of ten. As a consequence the gradient of equipotential surfaces (planes connecting points of equal hydraulic potential) within the glacier will rise as the surface gradient increases towards the glacier snout (Figure 2.7). This influences the direction of water movement, which in a freely conducting body of inter-granular englacial conduits, will flow at an angle perpendicular to the equipotential surface. Water movement continues in this direction until it meets the bed, whereupon it will flow towards the snout in a direction determined by intersection of equipotential surfaces at the bed / ice interface (Benn and Evans, 1998).

In reality glaciers do not allow completely free internal movement of meltwater. Rates and absolute volumes of water that flow through a glacial hydrological system can be classified by the permeability of the medium through which it flows. Drainage can be broadly sub-divided into mediums of primary and secondary permeability. Primary permeability includes intact bodies of snow, ice and sediment whereas secondary permeability refers to tunnels and passageways created along discontinuities and fractures in similar materials. Primary permeability is concerned with small-scale movement of water through pores, capillary tubes, veins and small pipes that accounts for a large percentage of the total volume of liquid water in the glacial system. However, as the transit times for water movement through such routes are long, such small-scale movement has a negligible affect on diurnal and sub-seasonal variations in total discharge during the ablation season. Secondary permeability describes larger-scale movement of water through channels and conduits in the glacial system, which are further discussed in sections 2.4.2 and

2.4.3. Although this is likely to affect a lower proportion of the total liquid water content of the glacier it is the dominant control over diurnal and sub-seasonal variations in total discharge as it controls the rapid transfer of surface runoff during the ablation season.

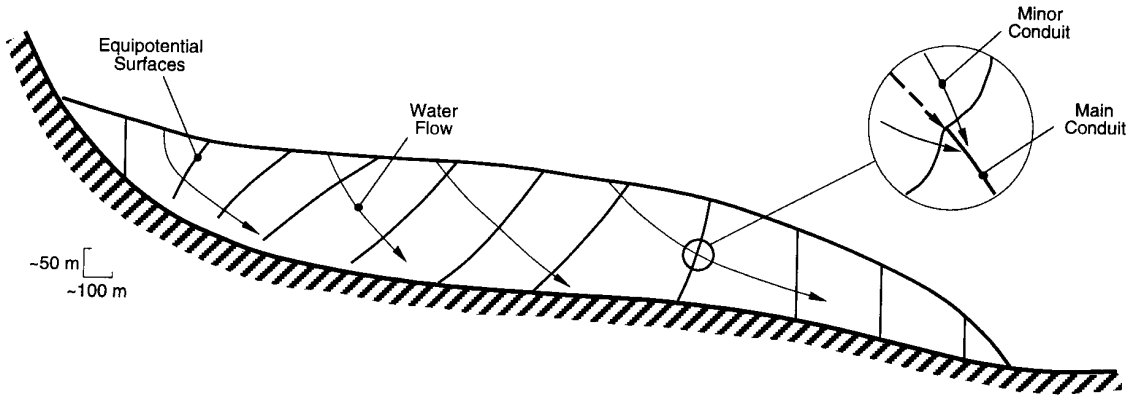



***Figure 2.7 – Schematic diagram of englacial equipotential surfaces that control direction of water movement (Lawson, 1993 after Hooke, 1989 and Shreve, 1972).***

Figure 2.8 shows movement of water through mediums of primary and secondary permeability varies in concentration and spatial extent throughout the glacial environment. Primary permeability is almost ubiquitous through veins and pores in both ice and sediment but, even at micro-scale levels of flow, water is concentrated as a product of pressure melting at interfaces between mediums of substantially different permeability. Figure 2.9 shows a conceptual interpretation of how a cross-section of a glacier in the ablation zone is separated into different layers of ice, sediment and bedrock. Although Menzies (1995) has used the diagram to illustrate active interfaces of net-melting it can equally be used to spatially delimit glacial drainage systems. Causes and mechanisms of such water flow will be discussed further in section 2.4.1. Secondary permeability tends to exploit such interfaces as well as discontinuities within mediums of uniform permeability. Moulins, fed by surface streams, channel water into the main body of the ice in a direction approximating to right angles to equipotential surfaces. When englacial channels reach layers of mobile and immobile sediments (if they are present), flowing water will either run along the interface or through the sediment depending on the energy of the flow

relative to the internal shear strength of the sediment. Similar principles exist if flowing water reaches the interface between sediment and bedrock. Theoretical formations and permanence of flow networks and channel sizes, shapes and dimensions are manifold and will be discussed further in section 2.6.

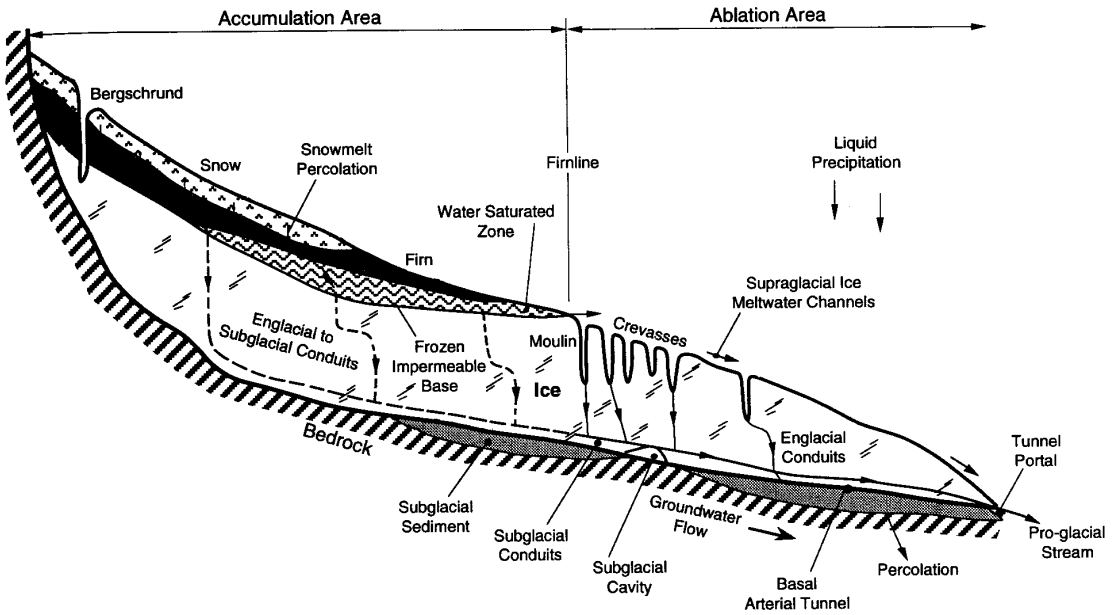



***Figure 2.8 – Schematic long-section of hydrological pathways through a temperate glacier (Lawson, 1993 modified from Collins, 1988).***

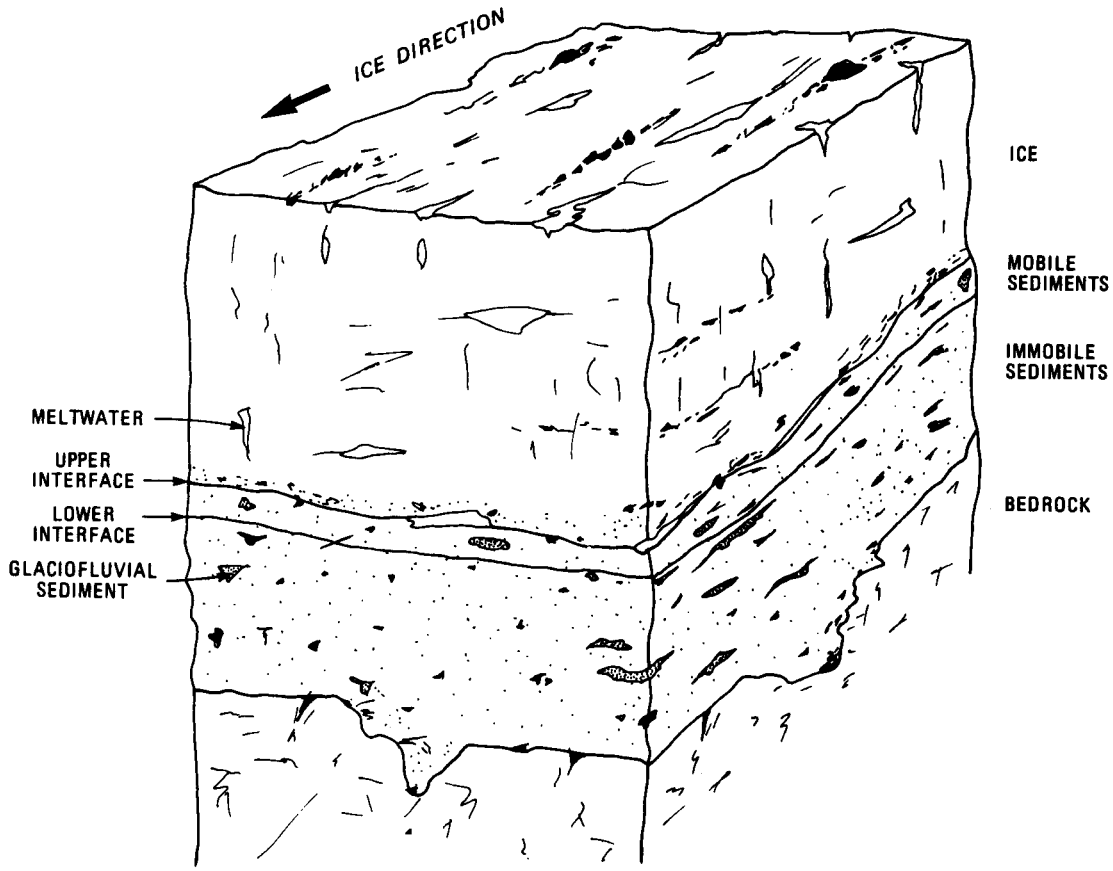



***Figure 2.9 – Model of possible active interfaces within an active net-melting subglacial environment (Menzies, 1995).***

### 2.4.1 Inter-granular water flow

#### 2.4.1.1 Inter-granular water flow through ice

Small-scale water movement within upper layers of glacier ice occurs at points where three ice crystals intersect creating triangular shaped veins. At intersections of four ice crystals such veins can join forming an upward branching network of capillary tubes (Nye and Frank, 1973). Evidence of this type of arborescent drainage structure, consisting of linked capillary veins approximately 25 m across, has been shown to exist in ice cores up to 60 m deep from Blue Glacier, Washington (Raymond and Harrison, 1975). The homogeneity of such drainage

structures in glacier ice depends on the coarseness of ice crystals, internal fracturing within the ice and the degree to which larger capillaries capture smaller capillaries at points of coalescence.

As the existence of capillary structures is dependent on three-crystal boundaries fine-grained ice will develop denser capillary drainage structures per unit volume than coarse-grained ice. Estimated rates of water transfer by intergranular water flux per unit area range between ~1 mm $a^{-1}$ (Raymond and Harrison, 1975) to 1 m $a^{-1}$ (Nye and Frank, 1973) for coarse and fine-grained ice respectively. Capillary veins may grow in size if the heat energy, generated by friction from water movement, melts the ice walls of the veins rather than being dissipated though the ice. As heat energy generated is proportional to the water flux, larger capillaries have a larger flux per unit area of capillary wall and will preferentially increase in size at the expense of smaller tributary capillaries to become millimetre-scale tubes short distances below the surface (Hooke, 1998). The degree to which such drainage pathways form a continuous network is uncertain due to constriction or blocking of veins by ice deformation, recrystallization or trapped air bubbles (Lliboutry, 1971). As *in situ* determination of vein size and network continuity is not possible, the rates of water flow suggested by Raymond and Harrison (1975) are considered as upper limits.

#### 2.4.1.2 Inter-granular water flow through consolidated sediment

Small-scale water movement within layers of subglacial sediment (or till) has a significant effect on both the total volume of water and rates of movement in the glacial hydrological system. Local hydraulic gradients and differences in permeability govern water flow within and between layers of subglacial sediment in a similar manner to capillary flow through ice. However, till is a more complex material than ice with uncertain relationships between applied stress and rates of deformation making conclusions from theoretical analysis of water flow through and over till

equally as uncertain (Paterson, 1994). Despite such uncertainty, movement of water in saturated sediment can broadly be separated into bulk movement and Darcian flow (Murray, 1997). Both types of water movement occur in mobile sediment layers whereas immobile sediment layers are restricted to Darcian flow. Darcian flow laws govern water flow through permeable sediment that is driven by a hydaulic gradient:

$$Q = -KA\frac{dh}{dx}$$

Q = Discharge across area A
K = Hydraulic conductivity of the sediment
A = total cross - sectional area including the space occupied by the sediment
H = piezometric head

***Equation 2.15***

The intrinsic permeability 'k' of a sediment represents the mean grain diameter of the particles 'd' combined with a shape factor 'C' associated with packing, size distribution and other factors:

$$k = Cd^2$$

***Equation 2.16***

To find the hydraulic conductivity 'K' of a sediment the intrinsic permeability, the specific weight of water ' ' and its dynamic viscosity at a known temperature ' ' are taken into account:

$$K = \frac{k\gamma}{\mu}$$

***Equation 2.17***

Permeability of glacial sediment is generally low as the grain size distribution consists of fractions ranging from clays to gravels that have a hydraulic conductivity of between $<10^{-9}$ and $10^{0}$ (Freeze and Cherry, 1979). Hydraulic properties of subglacial sediment are unlikely to be

ubiquitous. Sediment layers between basal ice and bedrock are variable in mobility and thickness (dependent on underlying bedrock topography and lithology) and they may be anisotropic, i.e. the permeability changes depending on the direction of water flow (Viessman and Lewis, 1996). Although the heteorogenous nature of sediment creates uncertainty in defining the values in equations Equation 2.16 and Equation 2.17 it is clear that even water movement by Darcian flow through rigid, undeformable sediment requires a high hydraulic gradient to maintain porewater flow. As this is an inefficient method of meltwater discharge it is unlikely it will solely be able to maintain sufficient fluxes to account for the rates of observed meltwater drainage under ice masses (Alley, 1989). Other mechanisms of small-scale water flow in sediment rich subglacial areas focus on concentration of flow between the interface of sediment and ice and advection of water within a matrix of mobile sediment.

A critical hydraulic gradient is set up if a rapid increase in porewater pressure of subglacial sediment equals or exceeds the downward confining pressure of overlying ice. This creates fluidisation of the sediment layer and causes water to move upwards, out of the sediment, collecting at the ice-sediment interface (see Figure 2.9) whereupon it may flow in more concentrated drainage routes such as in sheets or channels. However, if the process of meltwater infiltration into the sediment occurs at a slower rate it is possible that stresses from overlying ice can force sediment to deform or move as a slurry (Alley *et al.*, 1986)

#### 2.4.1.3 Inter-granular water flow through deformable sediment

Increasing porewater content from basal ice melt decreases inter-granular contact within the sediment matrix until a critical threshold is reached forcing sediment to behave as a slurry-like material. To maintain a slurry-like state, porewater pressures need to be greater than the critical threshold for advection but not too great as to increase sediment thickness so that more meltwater

is produced by pressure melting than is possible to be removed by advection within the sediment. If sediment becomes oversaturated due to a consistently higher rate of pressure melting than rate of meltwater removal by advection, fluidisation will occur and flow will be concentrated at the ice–sediment interface. Viscosity and permeability of the sediment control the velocity of water movement by advection. The Kozney-Carmen relation indicates that the permeability of sediment is inversely proportional to its viscosity, both of which are affected by responses of the sediment's rheology to external stresses applied by overlying ice (Murray, 1997).

A granular material such as subglacial sediment has a yield strength, or critical threshold described by the Mohr-Coulomb relation (Equation 2.18), which when exceeded causes the material to fail. Higher stresses are required to cause deformation, i.e. failure within a sediment matrix, as average particle size within sediment decreases. If sediment consists of very fine sized particles, i.e. clay-sized particle of less than 2 μm, particles may deform plastically. However, the proportion of clay-sized particles in glacial sediments is commonly low (~5%) due to the absence of subaerial weathering processes and frequently consist of minerals other than clays such as quartz particles (Iverson unpublished in Hooke 1998, pg107-8). Cohesion, which acts to arrest deformation within a confined sediment matrix, generally increases as the water content within sediment decreases. However, possible increased cohesion between clay minerals due to electrostatic charges at saturation levels is not significant in glacial sediment due to low abundance of such minerals. If air filled pores exist in a sediment matrix of larger sand-sized particles cohesion increases as surface tension is created through a thin film of water at the air-water interface of sand–sized particles, although when sediment becomes fully saturated any enhanced cohesion is lost.

$$s = c + N_e \tan\varphi$$

$s$ = yield strength
$c$ = cohesion
$N_e$ = effective normal pressure
$\varphi$ = angle of internal friction

***Equation 2.18***

If a sediment is saturated and over-consolidated, i.e. when sediment is compacted by a load greater than its own weight, deformation takes place through dilation and compaction, depending on the size distribution of particles, allowing individual grains to slide past one another locally at a rate limiting factor dependent on inter-granular frictional forces that act against sliding. Deformation, or shearing, of a granular material at a constant rate does not require the application of a constant mean shear stress. Initially shear stress is required to increase in a rapid linear manner until the yield strength of the material is attained (Figure 2.10). As subglacial sediment is over-consolidated the final value of shear stress that is needed to maintain a constant rate of deformation decreases from the peak yield strength to a residual strength, a decrease of the order of 10% from peak yield strength in sediments with low (<10%) clay content, which is a consequence of dilation taking place within sediment (Figure 2.10). Once the yield strength is exceeded the relation between stress and strain rates is of the form described by Equation 2.19

$$\dot{\varepsilon} \propto e^{\gamma\tau}$$

$\dot{\varepsilon}$ = strain rate
$\gamma$ = constant dependent of strength and granulometry of a material
$\tau$ = mean shear stress

***Equation 2.19***

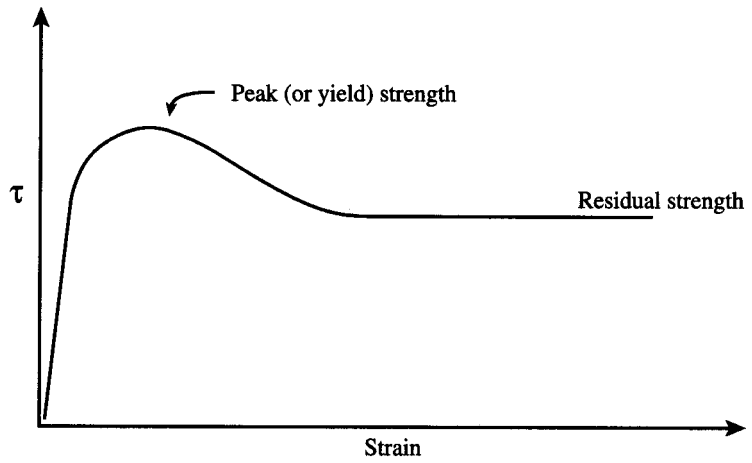



***Figure 2.10 – Schematic diagram showing variation of mean shear stress (τ) as a function of time (or displacement) in a granular medium that is sheared at a constant rate (Hooke, 1998).***

At smaller spatial scales, alignment of particles within a sediment matrix that affects the rate of shear that in Figure 2.10 was considered spatially constant throughout. Consequently, particle alignment to form three-dimensional arrangements of grain-bridges, formations of which are hypothesised by Hooke and Iverson (1995) in Figure 2.11, and subsequent failure due to shear stresses can provide a rate limiting factor increasing deformation that is stochastic in space and time. Strain rates are likely to decrease with depth in subglacial sediment in a non-linear manner as increasing rates of normal effective pressure with depth exceed that of the mean local shear stress required to cause deformation. A reduction in strain rates with depth may be more rapid near the ice-sediment interface as water from pressure melting increases the gradient of effective normal pressure nearer the interface as hydraulic head decreases with sediment depth. Deformation may actually cease deep in thick subglacial sediment layers if applied stress either no longer exceeds sediment strength or falls below a critical strain rate where sediment is no longer dilated (Alley, 1989). Consequently, although deformation is likely to be pervasive throughout sediment near the glacier sole, deformation may occur in spatially localised shear zones at increasing depth (Boulton and Hindmarsh, 1987).

Low effective normal stress and high water pressures near the glacier bed can cause decoupling between basal glacier ice and underlying sediment. The spatial extent of decoupling is uncertain although it is more likely in valley glaciers that have diurnally varying subglacial water pressures and high surface velocities, which show an inverse relationship with both normal effective pressure and shear strain rates in subglacial sediments (Iverson *et al.*, 1995).

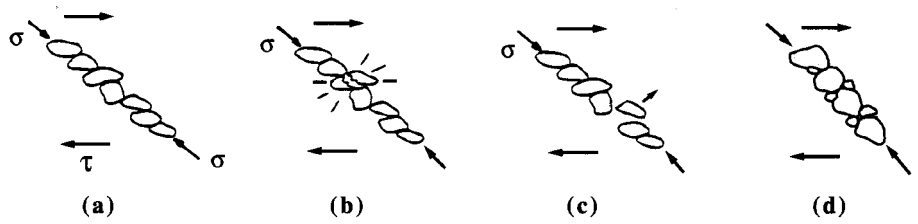



***Figure 2.11 – Hypothesised formation of grain bridges. Large arrows show shear stress applied to material, short arrows indicate component of this stress along grain bridges (Hooke and Iverson, 1995). (a) standard grain bridge; (b) grain fracture; (c) slip between grains; (d) reduction of stress at grain contact points due to additional material.***

### 2.4.2 Englacial drainage

Primary drainage pathways allowing concentrated water flow through the glacier from the glacier surface exploit cracks in ice caused when tensile stresses within the ice become greater than the tensile strength of the material. Tensile stresses consist of a combination of normal stresses acting at right angles to a surface and shear stresses that act in a parallel direction to a surface. As stress increases, the strain rate (the change in shape and size of a material due to stress) also increases. If the increase in magnitude of stress is small the strain may be elastic, i.e. the shape and size of a material is recoverable, whereas if the stress is large enough to surpass a critical threshold the strain may cause permanent deformation or failure. Elastic deformation of ice, where the glacier can adjust its shape fast enough to compensate for increasing strain rates is a consequence of the process of ice creep. Ice creep occurs due to micro-scale movement between individual ice crystals and rates of creep are, therefore, controlled by orientation of ice crystals

within the ice and the presence of impurities, i.e. solutes, gas bubbles and particulates. Flow laws describing the response of ice to stress vary depending on the nature of the ice crystal fabric and spatial distribution of impurities, although one of the most widely used, Glen's flow law (see Equation 2.20), indicates that strain rate is proportional to the cube of the shear stress as the empirically derived flow law exponent is usually close to three (Benn and Evans, 1998, pg 148).

$$\varepsilon = A\tau^n$$

$\varepsilon$ = effective strain rate
$A$ = viscosity parameter
$\tau$ = effective shear stress
$n$ = flow law exponent (empirically derived)

***Equation 2.20***

When rates of ice creep are insufficient to allow glacial ice to adjust in both shape and volume as a response to stress, ice will fracture as it is pulled apart by tensile stresses causing crevasses at the surface. Location of tensile stresses within a valley glacier are a product of difference in horizontal ice velocity both with increasing depth and throughout a long-section due to variations in slope angle of bedrock. Figure 2.12 shows ice velocity profiles within an unconfined ice mass show a distinctive form where velocity is almost independent of increasing ice depth in upper sections of the glacier and then decreases rapidly towards the bed. In a valley glacier constrained by topography, increased resistance to ice flow is provided by valley walls causing a two-dimensional pattern of ice flow. Raymond (1971) showed that in an alpine valley glacier (Athabasca Glacier in the Canadian Rocky Mountains) this increased resistance caused larger lateral gradients in basal ice velocity, attributed to reduced water pressures at the ice / bedock interface, than were predicted by theoretical calculations for glaciers with semicircular valley cross sections (Nye, 1965) (Figure 2.13). Consequently, as creep rates increase with depth, ice will flow faster and is more likely to deform without splitting as a response to increased stress.

Hence fractures are more likely in ice near the surface that moves at higher velocities and is less likely to internally deform. The viscosity parameter in Glen's flow law (Equation 2.20) also indicates that in temperate ice, deformation rates will be higher and fractures are less likely and of smaller relative size, than in colder polar ice.

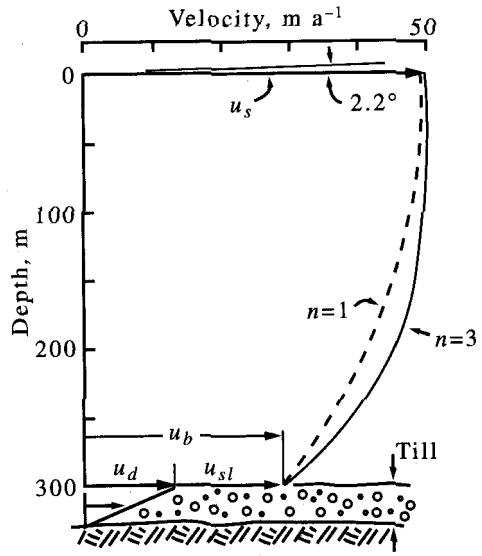



***Figure 2.12 – Velocity profile for an ice sheet (surface slope of 2.2 °, flow law exponent (n) = 3, viscosity parameter = 0.2 MPa $a^{1/n}$). A comparative profile (dashed line) for a linearly viscous material is shown for comparison and the thickness of the till is greatly exaggerated. Surface velocity = $u_s$, basal velocity due to sliding = $u_{sl}$, basal velocity due to deformation of till = $u_d$. (Hooke, 1998).***

The location of fractures in glacial ice, due to either tensile or compressive stresses, is heavily influenced by variations in the resistance of bedrock topography to movement caused by mass balance. Figure 2.14 shows how an increase in resistance to flow from an increase in gradient of bedrock (relative to the down-glacier direction of flow) causes compression of ice, whereas a decrease in gradient causes extension of ice. Both mechanisms can cause fractures. Fractures in compressive ice flow form along a shear plane where faster blocks of ice thrust above slower moving blocks in a manner analogous to tectonic movement, whereas fractures in extensive ice flow result from tensile stresses splitting ice apart. Figure 2.15 shows that fractures in upper layers of ice are near perpendicular to the surface as the orientation of the principal stress deviator

is parallel to the surface. However, with increasing depth shear stresses near the glacier base cause an increase in the down-slope inclination of the angle of orientation of the principal stress deviator under the influence of local stress fields (Paterson, 1994; Röthlisberger and Lang, 1987) (Figure 2.15 and Figure 2.16).

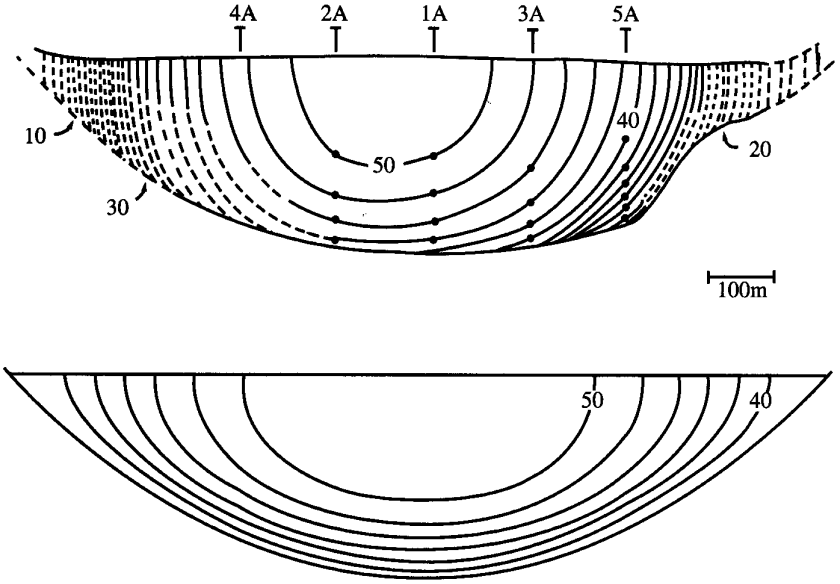



***Figure 2.13 – (Upper) Longitudinal velocity distribution ($ma^{-1}$) on Athabasca Glacier (dots indicate points of measurement, dashed contours are extrapolated). (Lower) theoretical distribution of longitudinal velocity in a parabolic channel, scaled to cover approximately the observed range of velocities (Raymond, 1971).***

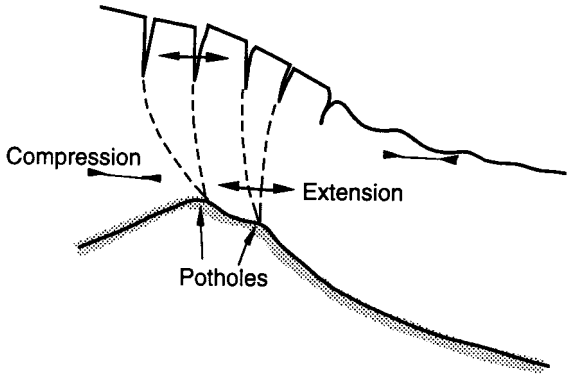



***Figure 2.14 – Hypothetical relationship between the position of potholes and the stress field in the glacier (Röthlisberger and Lang, 1987).***

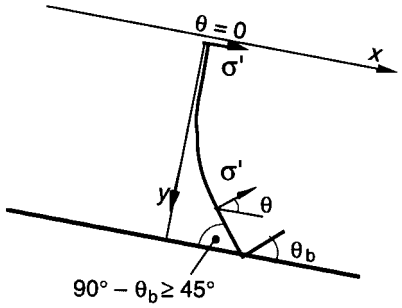



***Figure 2.15 – Orientation of the principal stress deviator (σ') as a function of depth (y) in the glacier (Röthlisberger and Lang, 1987).***

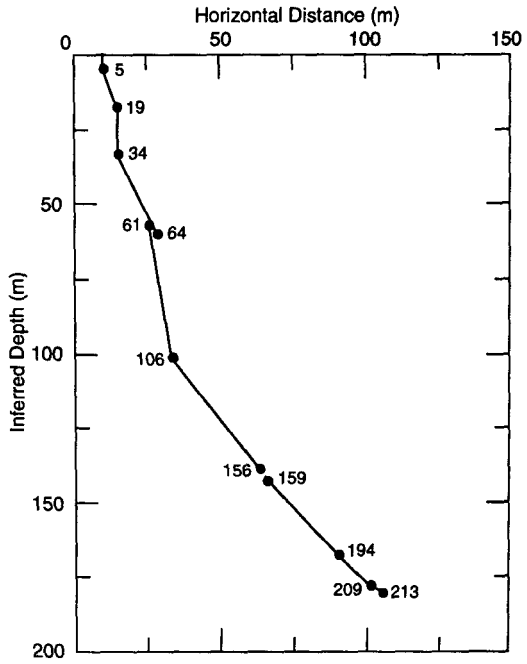



***Figure 2.16 – Approximate slope of a moulin conduit, White Glacier, Axel Heiberg Island, Canadian Arctic (Müller and Iken, 1973).***

As supraglacial streams flow into fractures in the ice surface (moulins), the increased temperature of water with respect to ice and the pressure of falling water combine to enlarge the crevasse through a combination of thermal and mechanical crack propagation. Consequently, unlike small diameter englacial channels less than 3 to 4mm in diameter (Hooke, 1984), inclination of moulins

are not necessarily perpendicular to equipotential surfaces. Instead, they are influenced by the crevasse from which it formed and a faster rate of melt in the moulin channel on the gravitationally lowest side through mechanical energy and dissipation of viscous heat.

The exact nature of the active englacial drainage system is unknown and can be partially measured from visual observations e.g. of Storglaciären (Holmlund, 1988), and inferred from proglacial meltwater hydrochemistry (Behrens *et al.*, 1975; Collins, 1977) and dye tracing of parcels of meltwater entering moulins from supraglacial streams to proglacial rivers (Nienow *et al.*, 1996a; Seaberg *et al.*, 1988; Stenborg, 1969; Willis *et al.*, 1991/1992b). Variation in transit times of such water parcels infer changes in sub- and englacial routing and storage of water within the glacial hydrological system. Temporal stability of the inclination and diameter of the moulin throughout the ablation season is, therefore, dependent on rates of internal deformation. This is controlled by rates of ice creep and variation in local sliding velocities that may cause further fracture of ice, which may either increase or decrease hydraulic connectivity of the englacial drainage network.

### 2.4.3 Subglacial water flow

Figure 2.8 illustrates that gravitationally controlled downward water flow through englacial conduits of varying size is impeded by the ice / bedrock interface creating a subglacial drainage system that either flows in discrete or distributed pathways. Consideration of subglacial flow pathways remains mainly theoretical due to lack of access for direct observation. Direct access to the glacier base through excavation of tunnels both in and under basal ice exists in only a few glaciers worldwide. Semi-permanent tunnels through basal ice in Urumqi Glacier No.1, Tianshan, China (Huang and Wang, 1987), extended up to 90m under the sub-polar type glacier at its maximum in 1981, allowing observations of ice temperature, glacier flow, ice displacement,

strain rate and basal sliding although research conducted in such environments will unavoidably disrupt natural stress and temperature fields within the ice. Permanent subglacial tunnels through rock under the glacier, constructed to capture water for hydro-electric power purposes from Engabreen (a valley glacier draining from the Western Svartisen ice cap in Norway), allow similar measurements to those at Urumqi glacier No.1. These can be taken from access points within the tunnel that open directly at the ice-bed interface (Cohen *et al.*, 2000). They also have a potential for tracing experiments to study the subglacial hydrology (Jackson, 2000). However, tunnels only provide highly limited spatial access to the glacier subsole and are not ideal for monitoring temporal variations in water pressure in concentrated subglacial drainage due to issues of safety. Consequently, most field and laboratory evidence used to support theoretical structures of subglacial flow pathways is inferred from changing transit times of parcels of water through the system, from borehole measurements (albeit highly spatially limited). They can also be inferred from laboratory-based porosity and deformation rates experiments of ice and sediments, from geomorphic evidence in front of the glacier terminus as the glacier retreats, e.g. channels or cavities incised into bedrock, and from the morphology of the ice itself at points accessible to portals at ice margins.

#### 2.4.3.1 Concentrated subglacial drainage

Field and laboratory evidence allows theoretical drainage structures that can be broadly classified into discrete and distributed structures. Concentrated water flow in a discrete drainage system, illustrated as (4) in Figure 2.17, provide efficient drainage through a dendritic network of interconnected tunnels either solely through ice or partially incised into sediment and bedrock. All theoretical treatments of water flow in channels are based on the principal that the size and permanency of subglacial channels are a result of water pressures in subglacial channels acting against ice overburden pressure. Channels can increase in size if high water pressures are greater

than ice overburden pressures allowing water flow through the channel to melt channel sides due to viscous dissipation of heat from frictional resistance at the water-ice interface. However, channels will decrease in size if water pressures are lower than ice overburden pressures causing plastic deformation of ice into the channel.

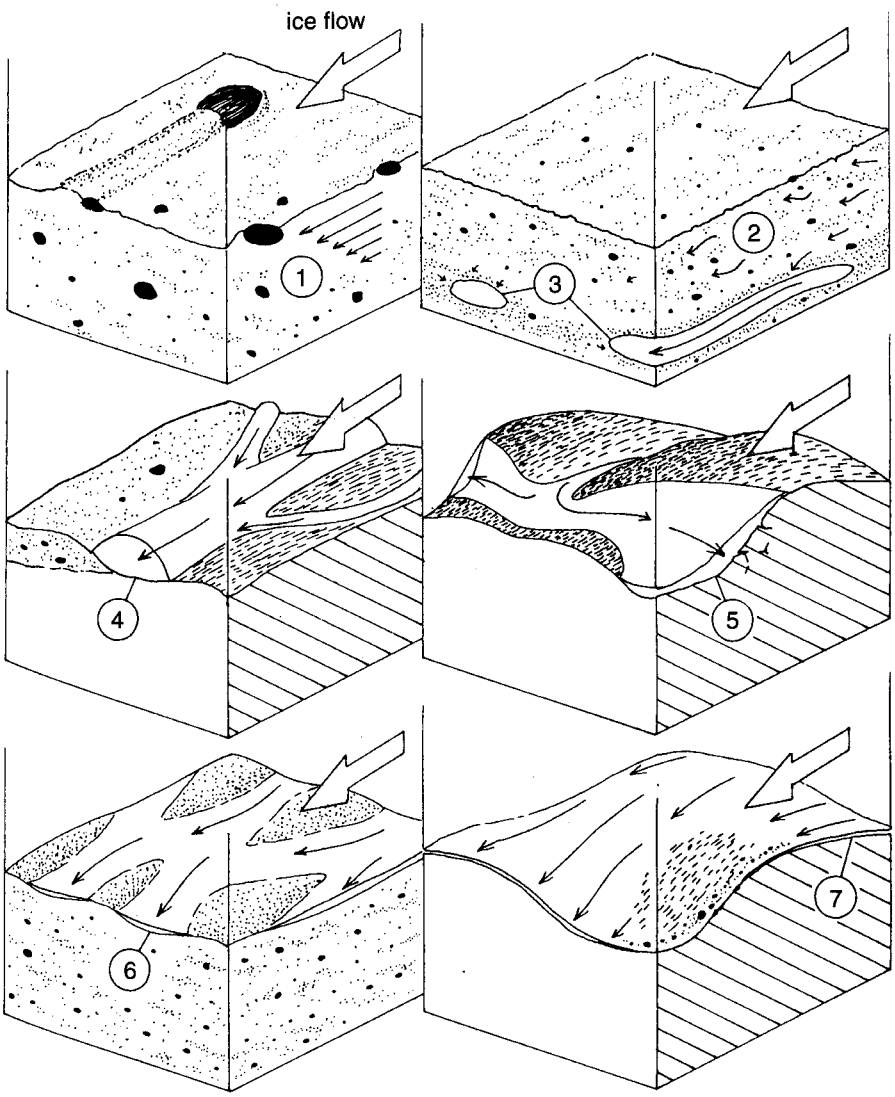



***Figure 2.17 – Different types of subglacial drainage system. (1) bulk water movement with deforming till; (2) Darcian porewater flow; (3) pipe flow; (4) dendritic channel network; (5) linked cavity system; (6) braided canal network; (7) thin film at ice-rock interface (Benn and Evans, 1998).***

Cylindrical ice walled channels, which are referred to as R-channels after Röthlisberger (1972), provide a basis for the theoretical treatment of channels of concentrated subglacial water flow from which there are many variations in shape (Hooke *et al.*, 1990) and subglacial location (Nye, 1973). R-channels assume steady state conditions, i.e. rates of deformation closing a channel are equal to rates of melt of channel walls by heat transfer (see Figure 2.18), i.e where $\dot{r} = P_c = 0$ in Equation 2.21 and Equation 2.22 (Hooke, 1998), where a channel along a unit length (*ds*) remains at a given size and pressure.

$$\dot{r} = \dot{m} - u$$

$\dot{r}$ = net rate of increase in channel size
$\dot{m}$ = melt rate
$u$ = rate of closure of channel by creep of ice

***Equation 2.21***

$$P_c = P_i - P_w$$

$P_i$ = ice overburden pressure
$P_w$ = channel water pressure
$P_c$ = pressure causing creep closure

***Equation 2.22***

$$\frac{u}{r} = \left( \frac{P_c}{nA} \right)^n$$

$r$ = radius of cylindrical channel
$n$ = empirically determined constant ($\sim 3$)
$A$ = viscosity parameter

***Equation 2.23***

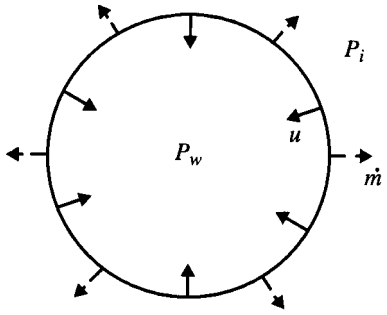



***Figure 2.18 – Idealised sketch of effects of ice deformation pressure and channel water pressure within a cylindrical ice walled conduit (in relation to Equation 2.21 and Equation 2.22, u and $P_i$ are defined as positive inward and $\dot{m}$ and $P_w$ are defined as positive outward (Hooke, 1998).***

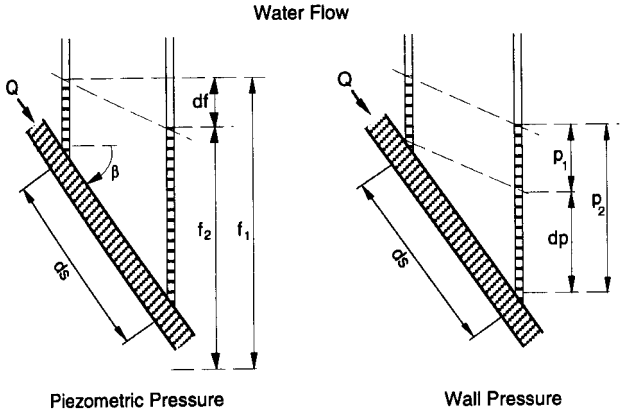



***Figure 2.19 – Differential elements for computation of water pressure in cylindrical ice walled conduits (Röthlisberger and Lang, 1987).***

Assuming steady state conditions, Figure 2.19 illustrates an inclined channel of length (*ds*), where channel slope angle ($\beta$), frictional pressure loss along the channel indicated by a change in piezometric level (*df*) and change in local water pressure within the channel (*dp*) are used within a coordinate axis (*s*) aligned to the axis of the channel in the direction of water flow (conduit slopes upwards in the positive direction of *s*) to calculate the change in channel water pressure (Equation 2.24 - Hooke, 1998).

$$-dp = -df + ds \sin \beta$$

***Equation 2.24***

The physical basis for interrelationships that control rates of channel expansion and closure in Figure 2.19, i.e. $\dot{m}$ and $u$ in Equation 2.21, as a consequence of channel water pressure, ice overburden pressure and gain or loss in energy as water adjusts to the pressure dependent melting point are described in a series of equations from Equation 2.25 to Equation 2.28 (Röthlisberger and Lang, 1987) with reference to physical constants of ice and water listed in Table 2.3. Channel discharge ($Q$) varies depending on whether flow in the channel is considered as turbulent or laminar but if $Q$ is considered as a known variable the rate of channel closure by creep (Equation 2.28) can be calculated using exponents $q$ and $m$, which are less than unity and are dependent on the type of water flow, and a parameter ($C$) which as well as being dependent on the mode of water flow, incorporates channel roughness and ice flow parameters (Röthlisberger and Lang, 1987).

$$\dot{m} = \dot{m}_f + \dot{m}_p$$
$$u = \dot{m}_c$$

$\dot{m}_f$ = frictional melt rate by volume in channel section $ds$
$\dot{m}_p$ = rate of melting (or freezing) that occurs when water flowing through channel section $ds$ adjusts to a new pressure melting point
$\dot{m}_c$ = rate of channel closure by creep of ice

***Equation 2.25***

$$\dot{m}_f = c_m^{-1} \rho_i^{-1} \rho_w g Q \left( -\frac{df}{ds} \right) ds$$

***Equation 2.26***

$$\dot{m}_p = c_t c_w c_m^{-1} \rho_w^2 \rho_i^{-1} g Q \left( -\frac{dp}{ds} \right) ds$$

***Equation 2.27***

$$\dot{m}_c = C Q^q \left( P_i - P_w \right)^n \left( -\frac{df}{ds} \right)^m ds$$

***Equation 2.28***

| Symbol | Property | Quantity | Unit |
|---|---|---|---|
| $g$ | Acceleration due to gravity | 9.807 | m $s^{-2}$ |
| $\rho_w$ | Density of water | 999.8 | kg $m^{-3}$ |
| $\rho_i$ | Density of ice | 916 | kg $m^{-3}$ |
| $c_w$ | Specific heat of water | 4.217 x $10^3$ | J $kg^{-1}$ $K^{-1}$ |
| $c_m$ | Energy of fusion | 3.34 x $10^5$ | J $kg^{-1}$ |
| $c_{t,0}$ | Change of pressure-melting point with pressure (pure water) | -7.4 x $10^{-8}$ | K $Pa^{-1}$ |
| $c_{t,s}$ | Change of pressure-melting point with pressure (air-saturated water) | -9.8 x $10^{-8}$ | K $Pa^{-1}$ |
| $\eta$ | Viscosity of water | 1.787 x $10^{-3}$ | kg $s^{-1}$ $m^{-1}$ |
| ***A*** | Ice deformation coefficient: | | |
| | Paterson (1981) | 0.167 | $bar^{-3}$ $a^{-1}$ |
| | Hooke (1984) | 0.244 | $bar^{-3}$ $a^{-1}$ |
| | Lliboutry (1983) | 0.232 | $bar^{-3}$ $a^{-1}$ |
| | Röthlisberger (1972) | 1.00 | $bar^{-3}$ $a^{-1}$ |
| $n$ | Exponent in the power law of ice defomation | 3.00 | |
| $k$ | Hydraulic roughness parameter for various channels: | | |
| | Smooth | 100 | $m^{1/3}$ $s^{-1}$ |
| | Medium | 50 | $m^{1/3}$ $s^{-1}$ |
| | Very rough (torrent) | 10 | $m^{1/3}$ $s^{-1}$ |

***Table 2.3 – Physical constants of ice and water at 0 ℃ and related properties (Röthlisberger and Lang, 1987).***

Röthlisberger (1972) used these relationships to predict increases in water pressure within a glacier (indicated by hydraulic grade lines in Figure 2.20) at increasing distances from the snout (starting at atmospheric pressure at the snout) using different values of channel roughness coefficient and variations of the exponent in the ice flow law. Hooke (1998), after Röthlisberger

(1972), suggest two major implications for channel water pressures in such cylindrical channels under steady-state conditions:

1. Water pressure in R-channels increases as the ice deformation parameter ($A$) decreases. Lower values of $A$ mean ice is more deformable, therefore, higher water pressures are needed to reduce closure rates, i.e. so that $u = \dot{m}$ .
2. As channel discharge decreases water pressure increases. Hooke (1998) describes this slightly counterintuitive relationship by considering an example where discharge is halved, causing a similar reduction in $\dot{m}$ . Consequently, cross sectional area of the channel decreases as a function of $r^2$, but the rate of channel closure only decreases as a function of $r$ (Equation 2.23). Therefore, when $r$ has decreased sufficiently to halve $u$ (to equal the new value of $\dot{m}$ ) the cross sectional area would have undergone a greater proportional decrease forcing an increase in water pressure.

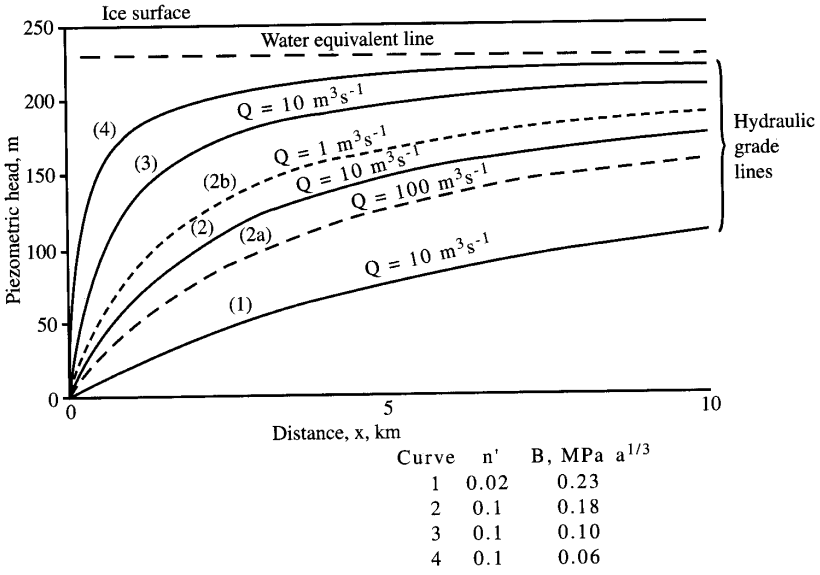



***Figure 2.20 – Hydraulic grade lines for a circular horizontal channel under ice of 250m thickness (B = ice flow / deformation parameter (B is the same as A in Table 2.3), n' = Manning roughness coefficient, x = distance from glacier snout) (from Hooke, 1998 after Röthlisberger and Lang, 1987).***

However, in reality, the inversely proportional relationship between discharge and water pressures in subglacial channels under steady-state conditions is rarely exhibited due to diurnal oscillations in meltwater input, which are reflected by diurnal changes in water pressure as the geometry of the channel does not change accordingly at the same rate. Only over yearly time periods can subglacial drainage channels approximate to a steady state system (Röthlisberger and Lang, 1987) as in reality daily water pressure varies in-phase with discharge.

Direct implementation of Röthlisberger's model is inappropriate for spatial prediction of water pressure throughout a long-section of a glacier over short (hourly and inter-daily) timescales. The physical basis for equations describing subglacial channel expansion and contraction and the influence of non-physically based parameters of channel efficiency and both ice and water flow is fundamental to understanding variations in subglacial water storage and release. Shape and efficiency of subglacial channels are affected by hydraulic channel roughness and factors governing ice flow and heat transfer. Hydraulic roughness in channels can increase by a factor of ten between a smooth ice-walled pipe and a rough boulder-strewn bed illustrating the influence of channel location within basal ice (Röthlisberger and Lang, 1987). Enhanced deformation can occur due to a low viscosity of basal ice with a high water content, especially in 'soft' temperate ice, when not supported by high water pressures. As diurnal oscillations exist in water pressure, rates of ice deformation at times of low water pressure throughout the diurnal cycle are proportionally greater, due to the power law of deformation, than periods within the diurnal cycle of average or low water pressure. Rough bedrock topography that provides obstacles to ice flow will further enhance total rates of deformation as increased deformation using the power law on the up-glacier side of obstructions are not compensated for in areas down-glacier of obstructions where deformation does not take place (Lliboutry, 1983). Although difficult to measure, increases (or possible decreases) in heat energy from groundwater sources and subsequent losses

of thermal energy from the system as water is discharged from the glacier influence melt rates of subglacial channel sides and, therefore, water pressures throughout the glacier (Lliboutry, 1983).

Specific predictions of subglacial water pressure using a dendritic pattern of R-channels as the principal means of subglacial drainage have been tested in the field without great agreement (Hooke, 1998). Poor agreement may be caused by many violations of the model by reality such as lack of steady state conditions, possible atmospheric (or near atmospheric) subglacial water pressures and variations in channel gradient due to channels following overdeepenings in topography. Also as indicated in Figure 2.9 preferential flow pathways at active interfaces within basal ice, or variations irrespective of basal topography altogether are possible contributors. Consequently, alternative channel shapes, e.g. broad low subglacial conduits (Hooke *et al.*, 1990), and locations, e.g N-channels incised into bedrock (Nye and Frank, 1973), within a framework of a concentrated subglacial drainage system have been hypothesised to improve the fit between predicted and observed water pressures.

Lliboutry (1983) suggested that increased 'softness' of ice around cylindrical channels, caused by enhanced closure rates on the stoss sides of bedrock irregularities that doubled the difference between ice and water pressure, may account for the difference between predicted and observed water pressures at Gornergletscher, Switzerland. However, an alternative mechanism proposed by Hooke *et al.* (1990) is that channels are broad and low (Figure 2.21) rather than circular or semi-circular. This would provide an alternative physical basis for calculation of water pressures instead of reducing the ice-viscosity parameter way below that value of ~1.6 bar $a^{1/3}$ that is widely accepted for temperate ice. Figure 2.22 shows the relationship between the angle of the arc, which is subtended by a chord to form a low broad channel, and the factor by which the ice-viscosity parameter must be reduced to produce similar water pressures. This illustrates principles of equifinality that are relevant to theoretical forms of subglacial drainage.

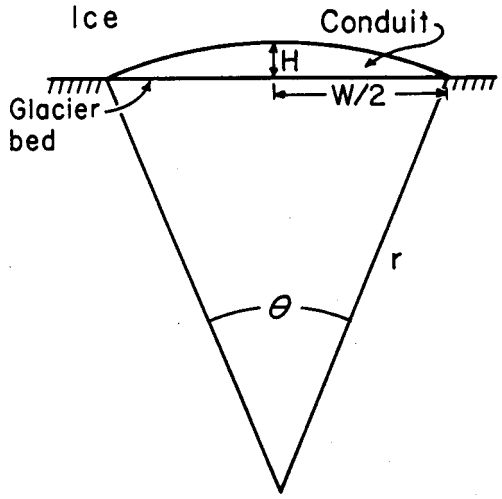



***Figure 2.21 – Geometry of an idealised broad, low subglacial conduit (Hooke et al., 1990).***

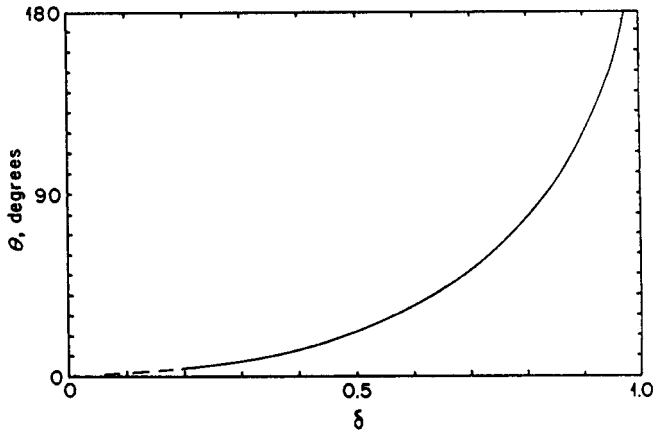



***Figure 2.22 – Relationship between angle (θ) controlling the length of arc and the factor (δ) by which the ice-viscosity parameter must be reduced to obtain the same piezometric pressures (Hooke et al., 1990).***

Alternatively, Nye (1973) suggested that bedrock protrusions into basal glacier ice will cause discontinuities in subglacial channels as ice flows across obstacles and proposed channels that are incised into the substratum. Incised channels would allow subglacial discharge of water from the ice surface whilst simultaneously permitting a thin film of water derived from pressure melting at the glacier base that enables ice movement over fine-scale obstacles to flow. Evidence for such

channels can be seen in bedrock as ice retreats and is more probable in areas of stepped bedrock topography that provides a dominant control over hydraulic gradient focusing subglacial water flow along a consistent axis.

If concentrated subglacial water flow exists at the interface between basal ice and a sediment substrate, the size and stability of steady-state R- and N-channels incised into consolidated or deformable sediment incorporates the rate at which sediment deforms into a channel relative to the rate at which sediment is eroded by channel water flow. Deformation and erosion of sediment is an additional influence on channel stability along with both channel water and ice overburden pressures that control stability in solely ice-walled channels. The stability of R-channels of radii between 0.001m and 10m incised into beds of diamicton (clay to gravel sized particles) were investigated by Alley (1989). A variety of parameters for subglacial water flow and sediment parameters were used and it was concluded that only sediment with a very high yield strength was capable of maintaining channel stability against closure by deformation of sediment into the channel. N-channels in deformable substrate, which tend to be more deeply incised into and enclosed by sediment than R-channels, are even more dependent on the yield strength of the sediment for channel initiation and maintenance. As subglacial water pressure increases, water pressure within sediment also increases until a critical stress governed by the yield strength of the material is exceeded (see Equation 2.18). Figure 2.10 shows that it is at this point the shear stress reduces, the sediment is dilated and liquefied allowing water to coalesce forming pipe-flow. With further increases in water pressures and discharge through pipes, ultimately N-channels may propagate in an up-glacier direction influencing drainage of water from surrounding sediment.

As well as the influx of water from sediment into the channel by porewater flow, influenced by the pressure gradient and hydraulic conductivity of the substrate, incised channels have an important influence on drainage of water as a result of pressure melting held at or near the basal

ice-sediment interface. Alley (1989) suggests the upper limit of spatial influence at which water can drain to the channel is $10^4$ times as wide as the radius (see Equation 2.29).

$$Q_x = 10^4 r\dot{m}$$

$Q_x$ = channel water influx
$r$ = radius of channel
$\dot{m}$ = basal ice melt rate

***Equation 2.29***

Much uncertainty exists in theoretical consideration of fluvio-glacial sediment transport systems and rheology of sediment in subglacial environments (Alley, 1989), e.g. erosion rates differ between laminar and turbulent flow and spatial variation of particle size distribution and particle alignment, restricting theory to qualitative assessments of drainage systems. Iterative predictions of such drainage systems under different conditions suggest when channel water pressures are high ice flow into the channel is reduced then flow of sediment into the channel increases, and vice versa for low water pressures (Walder and Fowler, 1994). Walder and Fowler (1994) indicate that closure rates of channels by the flows of ice and sediment are approximately equal when $P_i$ - $P_w \approx 0.8$ MPa, although this incorporates large uncertainty (Hooke, 1998). Steady-state channel geometries under valley glaciers will be controlled more by the inward flux of ice, rather than influx of sediment, into the channel. Characteristic steep surface gradients, causing high potential gradients, enhance melt rates and consequently reduce channel water pressures. However, where ice surface gradients are low and inward fluxes of sediment into a channel dominate inward fluxes of ice, channel water pressures increase as channel discharge increases, in an inverse manner to solely ice-walled channels. Walder and Fowler (1994) attribute this to the nature of the subglacial material within constrained channels. Phase relationships between channel water pressure and discharge are independent of channel width despite that fact that the

width of unconstrained river channels are a major controlling influence on the capacity of a channel to discharge (Parker, 1979). Consequently, where sediment influx dominates channel closure, pressure gradients force water from large to small channels maintaining a distributed drainage system, rather than from small to large channels in a dendritic more concentrated drainage system.

#### 2.4.3.2 Distributed subglacial drainage

Figure 2.23 shows that water flow across a more spatially distributed area of the ice-bedrock interface is described by a linked-cavity system (Kamb, 1987), where cavities in undulating bedrock topography are joined by small interconnecting channels in tortuous down-glacier hydrological pathways. Cavities exist at the ice-bedrock interface on the lee side of bedrock obstructions that protrude into basal ice, as ice pressures on the lee side are lower than on stoss sides of obstructions. Cavities become filled with water derived from pressure melting, which remain hydrologically isolated unless water pressure increases to such an extent that it exceeds localised ice overburden pressure forcing a link between adjacent cavities. Consequently for such a linked-cavity drainage system to be present undulating bedrock topography must exist over a wide spatial area, and both high sliding velocities and water pressures need to be maintained. As illustrated in Figure 2.24 formation of cavities, broadly subdivided into step or wave cavities and their hybrids, require a rapid decrease in gradient to force an ice bedrock separation. High sliding velocities, to limit infilling of cavities through deformation of ice, and high water pressures, which provide resistance to ice overburden pressure, are required in combination to maintain the size of cavities (Kamb, 1987).

Kamb's (1987) models of morphologies of subglacial linked-cavities clearly demonstrate that the geometry of the orifice ($l$ and $L_o$ in Figure 2.25) provides a rate limiting factor to water flow and

that cavities act as reservoirs of temporary storage. Dimensions of cavities have been hypothesised as ranging from up to 1m in height and from decimetres to metres in length whilst an orifice connecting two cavities is likely to be much smaller in height, approximately 0.1m, and highly variable in dimensions (Hallet and Anderson, 1980; Kamb, 1987; Walder and Hallet, 1979; Walder, 1986). As the capacity of a linked-cavity system to either store or release water is dependent on the geometry of orifice, increases in the capacity of an orifice to discharge water temporarily stored in cavities requires melting of orifice roofs. The ability of water fluxes to increase the orifice volume by ice melt is modelled using a dimensionless parameter of ice melt stability (Kamb, 1987), which when altered changes the roof profile in steady state configurations of step and wave orifices. A larger melt stability parameter reflects increasing ease of ice melt, causing evolution of orifice geometry that produces greater elongation of the orifice length relative to increase in its height in step orifice roof profiles, and vice versa in wave orifice roof profiles (Figure 2.26).

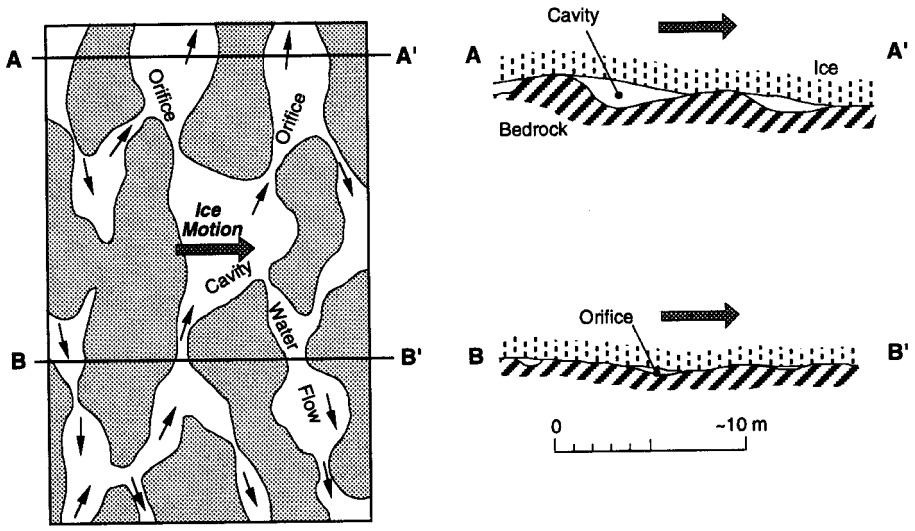



***Figure 2.23 – Schematic diagram of linked-cavity network. Plan view (left) has areas of ice contact with bed shaded and areas of ice-bed separation are blank. Vertical cross-sections (right) along axis AA' and BB' indicate water filled cavities and linking channels (Kamb, 1987).***

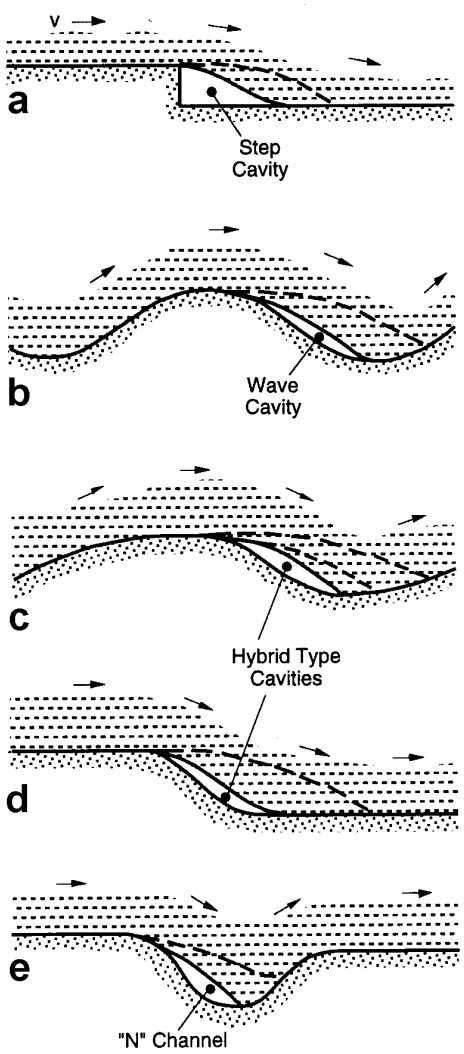



***Figure 2.24 – Idealised configurations for cavities in the linked-cavity model; (a) modelled step(Kamb, 1987); (b) wave cavities; (c) bedrock surface; (d) rounded bedrock step; (e) N channel of (Weertman, 1972).***

Unlike R-channels, where channels instantaneously adjust to variation in channel inputs through enlargement caused by dissipation of frictional heat or contraction caused by deformation of ice, the relationships between water pressures and channel discharge in linked-cavity systems are directly proportional to each other. Decreasing discharge through the orifices of linked-cavities has a small effect on the ice melt stability parameter as orifice stability is enhanced by the

physical effects of the bedrock step propping open the steady-state configuration of orifice roof (Hooke, 1998). Figure 2.27 shows that lower water flux through an orifice is, therefore, a response to lower water pressures in the linked-cavity system although water pressures may not necessarily vary with portal discharge due to the tortuous nature of the flow path. Kamb (1987) suggested that at channel discharges in excess of ~0.1 $m^3s^{-1}$ for step-orifice roof profiles (slightly less for wave-orifice roof profiles) higher subglacial water pressures are needed to maintain the orifice size. This results in consistently higher water pressures and a lower water flux in linked-cavity systems than in systems dominated by R-channels ('tunnels' in Figure 2.27) with implications for glacier sliding.

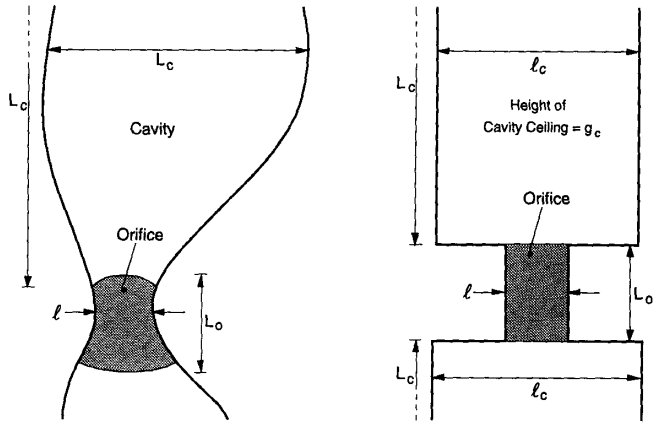



***Figure 2.25 – Plan views of actual (left) and modelled (right) subglacial morphologies of linked-cavities, showing modelled parameters (Kamb, 1987).***

Other forms of distributed subglacial drainage, illustrated in Figure 2.17, contribute to proglacial discharge such as bulk movement through deforming till (1) and porewater flow (2) – see sections 2.4.1.2 and 2.4.1.3; pipe flow (3) – see section 2.4.3.1; braided canal networks (6) and thin film flow (7). All of these subglacial drainage systems involve interactions of water flow with sediment (or till) between the basal ice layer and the bedrock, which has previously not been a consideration of linked-cavity or R-channel systems. As can be seen from Figure 2.9, due to the erosive power of glacier ice and the non-ubiquitous nature of the subglacial hydrological system preventing evacuation of eroded material, sediment is likely to accumulate beneath basal ice.

This can become an active component of the subglacial drainage network. Darcian porewater flow through sediments of low permeability and movement of deformable till as slurry are discussed in section 2.4.1. Total porewater flow and bulk water movement may account for movement of a large proportion of the total volume of subglacial water where rates of water movement are very low relative to linked-cavity and R-channel drainage systems. Although absolute rates of water flow through and within subglacial sediment are low, hydraulic connectivity between porewater in sediment and water pressure variations in more concentrated networks of subglacial drainage is shown to exist by diurnal oscillations of water levels in boreholes that terminate in subglacial sediment. Potential movement of water into and out of sediment adjacent to subglacial channels of concentrated water flow at times of maximum and minimum daily water pressure may well supplement discharge and temporary water storage, as well as providing implications for flushing small sized fine sediments from within the sediment matrix.

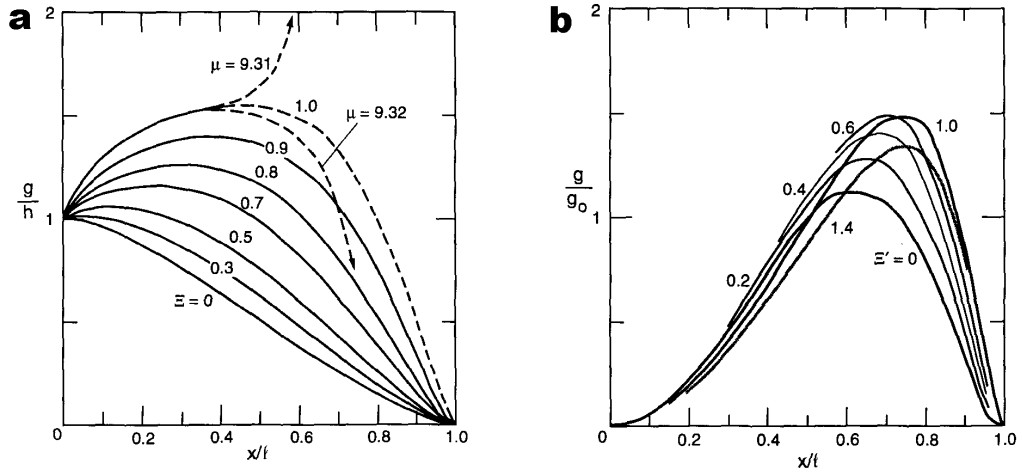



***Figure 2.26 – (a) Steady-state configurations of step orifice roof profile values for varying values of melt stability parameter (Ξ) where gap height (g(x)) is shown in terms of g/h as a function of dimensionless longitudinal coordinate x/l, where l is the gap length (Kamb, 1987). (b) Steady state configurations of wave orifice roof profile values for varying values of melt stability parameter (Ξ') where the gap height (g(x)) is shown in terms of the ratio g/$g_o$, where $g_o$ is the height midway along the length of the gap (x = ½) in the absence of roof melting (Ξ' = 0). The longitudinal coordinate x is scaled by the gap length l (Kamb, 1987).***

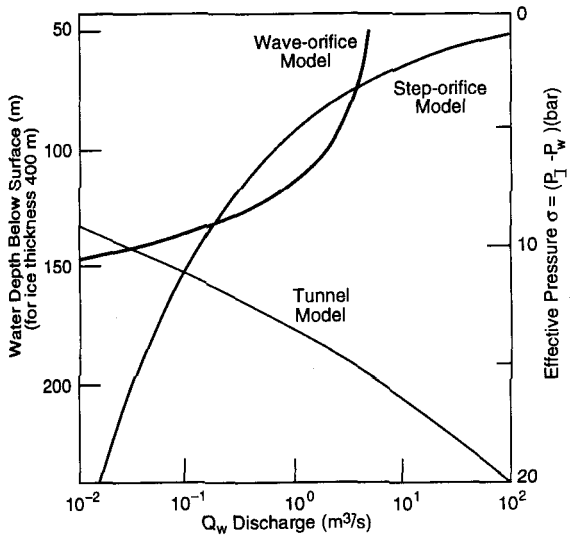



***Figure 2.27 – Comparison of effective confining pressure vs. discharge relationship for linked-cavity and channel-tunnel models (using an ice thickness of 400m) (Kamb, 1987).***

In Figure 2.9 we see how films of water at high pressure can accumulate at the ice-bedrock interface (Weertman, 1972), or other active interfaces within the basal ice zone due to pressure melting caused by the weight of overlying ice. Spatial homogeneity of water films may be enhanced by geothermal heat and bedrock topography, protrusions of which into basal ice will cause both pressure melting on the stoss side and regulation (re-freezing) on the lee side of any obstruction. Thickness of water films, which are unlikely to exceed a depth of a few millimetres (Walder, 1982), are determined by an interrelated combination of the normal effective pressure and bed roughness. Bed roughness is related to grain size, which controls cavitation and hence the potential for subglacial concentration of water films (Weertman, 1972).

Variations in thickness of water films caused as a result of pressure melting in basal ice, dependent on undulations in bedrock topography to regulate the rate of pressure melting, will prevent a spatially uniform water film from developing. This is likely to allow areas of water storage in films across bedrock to become spatially isolated from diurnal water pressure variations, which is indicated by constant, high water levels in boreholes terminating in such

areas. Thin film water flow is impossible to measure directly *in situ* without causing disturbance. Its existence is mainly justified by implicit evidence. Substantiation of thin film flow is derived from loss of fine fractions, typically less than 50μm in sediment matrices (Hallet, 1979; Vivian, 1975), which have been exposed as the glacier retreats. Fine fractions are removed by entrainment and transportation at very low velocities and can be seen as depositional features within calcite lenses that have precipitated from slow flowing subglacial waters over areas of former glacial beds (Hallet, 1979). Water film thickness is unlikely to become greater than 1mm, estimates are of approximately 0.2mm (Vivian, 1975), or else water will preferentially coalesce into small channels. Rates of subglacial drainage in films of this order of thickness will have a very low hydraulic efficiency due to high frictional resistance causing very low discharges.

As volumes of surface inputs to basal sediment layers increase the capacity for systems of water flow to discharge inputs as thin films at ice-sediment or ice-bedrock interfaces or as Darcian porewater flow within sedimentary material are exceeded. Resulting increases in subglacial water pressure as inputs increase cause coalescence, which forms branching, relatively low-pressure channels that are incised into the sediment (Boulton and Hindmarsh, 1987). Walder and Fowler (1994) suggest that such a drainage system requires a very rigid sediment, whereas if the sediment is saturated and subject to deformation it is likely water under pressure will collect at the ice-sediment interface and flow in a widespread interconnected system of low broad canals. In a similar manner to linked-cavity systems water pressure decreases proportionally with discharge, allowing a canal system incised into sediment to remain distributed over the glacier bed throughout oscillations in water pressure. Evidence of braided canal systems are also implicitly derived from broad lenses of sorted till that are exposed by retreating glaciers (rather than eskers resulting from concentrated drainage) as direct measurements without disturbance of the drainage system is not possible.

## 2.5 Influence of subglacial water pressure on glacier sliding and uplift

Hydraulic influences on rates of glacier sliding and uplift depend on basal topography and the nature of the substrate-bedrock interface with glacier ice. Increased subglacial water pressure can enhance rates of sliding in both hard bedded (Fowler, 1987; Haefeli, 1970; Lliboutry, 1968; Lliboutry, 1987; Schweizer and Iken, 1992; Weertman, 1964) and soft bedded areas (Boulton and Hindmarsh, 1987; Ng, 2000; Shoemaker, 1986) of a glacier as increased water pressures can cause decreased net effective pressures, hydraulic jacking and enhanced deformation of sediment. Although different mechanisms may operate simultaneously in spatially separate areas of the glacier bed, all will contribute to total rates of glacier sliding in conjunction with longitudinal stress gradients caused by forces of compression and extension within the glacier ice itself (Willis, 1995). Subglacial hydraulic mechanisms, especially increases in water pressure, can also combine with compressive longitudinal stresses to cause fluctuations of vertical movement of glacier ice (Iken *et al.*, 1983).

Temporally distinct cycles of increased velocities have been observed in virtually all glaciers within annual cycles (Willis, 1995), and at least intermittently over weekly (Harrison *et al.*, 1986; Hooke *et al.*, 1983) and diurnal timescales (Iken and Bindschadler, 1986). Increases in sliding velocities at each timescale result from increased surface inputs interacting with configurations of subglacial drainage that restrict flow and increase water pressures at the ice-bedrock interface or within deformable substrate. Consequently, sliding velocities tend to be higher in spring-summer than autumn-winter, higher during late afternoon than in early morning and higher during periods of enhanced melt from warm frontal weather systems. Relationships between variations in water pressure and sliding velocities are not consistent. Some glaciers predominantly show a relationship, some only at seasonally specific times and others not at all (Eschelmeyer and Harrison, 1990) inferring that the lack of temporal and spatial uniformity in sliding velocity has

connotations for evolution of drainage systems (Willis, 1995). Spatial and temporal patterns of low pressure tunnel-conduit systems usurping relatively high pressure distributed systems during seasonal evolution of subglacial drainage and vice versa towards the end of the ablation season and throughout the winter (when channel closure has implications for subglacial trapping of water), help identify causal mechanisms between water pressures and sliding velocities.

Willis (1995) suggests early season waves of basal motion may propagate up-glacier as high subglacial water pressures are first experienced towards the glacier terminus. Here water pressures continue to increase in an up-glacier direction as a response to retreat up-glacier of the transient snowline as air temperatures rise above 0°C at increasing elevations. Increases in the speed with which water is routed from the glacier surface to the bed also increases throughout the ablation season at progressively further distances up-glacier as a result of snow line retreat. This causes the amplitude of diurnal cycles of basal motion to be initiated and become more coherent at further distances up-glacier from the glacier terminus as summer progresses. Differences between daily maximum and minimum velocities decrease with increasing distance up-glacier, depending on how surface runoff is translated into subglacial water pressures as a proportion of the ice overburden pressure (Willis, 1995). Ice thickness tends to increase up-glacier (at least up to the equilibrium line altitude) increasing the absolute subglacial water pressures needed to trigger mechanisms of localised floatation or hydraulic jacking that are associated with rapid glacier movement. Such high pressures occur when a period of increasing water balance combines with low hydraulic transmissivity of a drainage network, e.g. linked cavity networks, so that only short periods of further increases in water pressures are necessary to exceed pressure thresholds that cause rapid cavity growth or till shearing required to increase rates of sliding. Multiple events of this kind may happen if subglacial drainage configurations and water pressures are maintained close to the threshold for glacier sliding. Maintenance of water pressures close to this threshold is aided at the beginning of ablation seasons if water that has become trapped in

subglacial cavities as the drainage system deteriorated at the end previous ablation season becomes re-integrated into subglacial drainage. Consequently, down-glacier 'mini-surges' resulting from multiple sliding events are more likely in the early part of the ablation season. As the season progresses low pressure tunnel-conduit systems redevelop, which diminishes both the spatial coherency and propagation of down-glacier velocity waves through distributed drainage systems.

Over shorter timescales localised cavity formation or enhanced deformation of subglacial sediment increases glacier sliding depending on the local basal topography. However, 'sticky spots' may exist where basal friction exceeds the local driving stress causing resistance to movement (Fischer *et al.*, 1999). Localised negative or reverse motion of glaciers is also possible when water pressures drop in areas where cavity formation is high causing cavity closure as glacial ice drops back into the unpressurised cavities (Willis, 1991).

## 2.6 Permanency of sub-glacial drainage structures in temperate Alpine glaciers

Sources of water in glacierised catchments are primarily supra-glacial, i.e. rainfall, ice- and snow-melt; or sub-glacial, i.e. pressure melt of basal ice, geothermal heat causing melt and groundwater flow. Temperate glaciers in the Swiss Alps are unaffected by geothermal activity. Hydrometeorological conditions causing supraglacial runoff dominate water sources within the catchment. Massive outburst flooding or jökulhlaups in glacial environments are a result of sudden collapse of either ice dammed lakes, which tend to be highly localised topographically controlled events, or subglacial reservoirs, which are usually but not exclusively formed by geothermal melting at the glacier bed. Consequently, due to the highly localised and sporadic nature of jökulhlaups a more general discussion of rates of water movement through glacierised

catchments is presented in temperate Alpine glaciers that are predominantly influenced by the capacity of:

1. a glacier to drain surface runoff englacially
2. subglacial drainage to store water from englacial channels
3. subglacial drainage to discharge stored water

The degree of structural permanency or variation in each of the three potential rate limiting sections (indicated above) to water flow through a glacierised catchment will be considered over inter-annual to sub-seasonal timescales. Figure 2.28 shows that over an annual cycle, runoff within the catchment occurs during the ablation season, i.e. from between approximately mid-May to mid-October, and is minimal for the rest of the year.

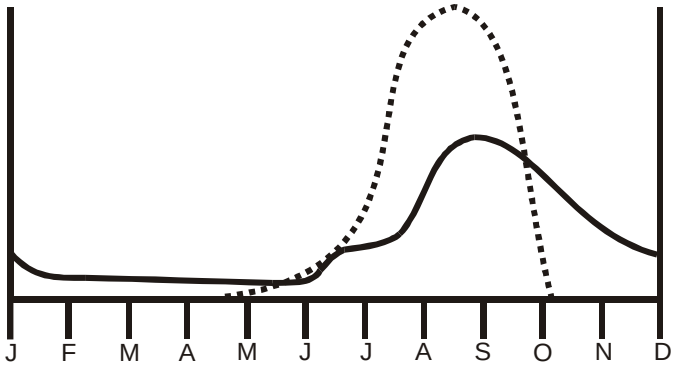



***Figure 2.28 - Schematic diagram to show relative changes in volume of surface runoff (dashed) and capacity to discharge runoff (solid) throughout an annual cycle in a temperate Alpine glacier.***

As runoff increases at the beginning of the ablation season the initial capacity for water to drain through the glacier is a function of how spatially well developed and efficient drainage was the previous year. It also depends on the degree to which channel closure due to ice overburden pressure and glacier sliding has occurred during the winter when surface runoff and channel water pressures are negligible. Relict channel features within glacier ice undoubtedly persist to a

certain extent inter-annually, especially in upper ice where lower overburden pressures cause a lower rate of ice deformation into channels created by previous englacial water pathways; in comparison with high deformation rates in basal ice. Inter-annual persistence of moulins can develop ice cave systems combining relict and contemporary englacial drainage networks in upper levels of glacier ice (Figure 2.29). Röthlisberger (1996) suggests moulins that develop in a top to bottom direction will initially follow the simple stress induced curve shape, indicated in Figure 2.16, independently of older 'abandoned' moulins that are located in a down-glacier direction. However, sub-surface persistence of abandoned moulins that developed during previous ablation seasons create englacial channels that run approximately parallel to the glacier surface, which may intersect and capture water from newer moulins as they curve with depth (Figure 2.29). Consequently, downward propagation of the new crevasse is halted and the point of intersection with the subglacial drainage network is still controlled by the previous englacial system developed by thermal and mechanical erosion of meltwater from now abandoned moulins. Inter-seasonal perpetuation of englacial drainage in near-surface ice may be globally limited as it is more applicable to non-temperate glaciers where ice is well below 0°C, rather than 'soft ice' in temperate glaciers which is more likely to deform or collapse. However, this type of englacial channel configuration demonstrates the capability of persistence within the glacial hydrological system.

If new conduits that open up inter-annually coalesce with older well developed englacial pathways, rather than having to create completely new englacial channels to connect with the subglacial drainage system, the capacity to drain volumes of meltwater englacially at the beginning of the ablation season will be high and not act as a rate limiting factor to water movement within the catchment. Alternatively, if new moulins are isolated from previous englacial channels, a sudden increase in surface runoff may cause water to pond and overflow in

the moulin as inputs to the moulin exceed its capacity to discharge. Surface relief of the glacier will, therefore, concentrate water overflowing from the moulin entrance in either lateral or medial supraglacial streams depending on whether the surface is concave or converse respectively.

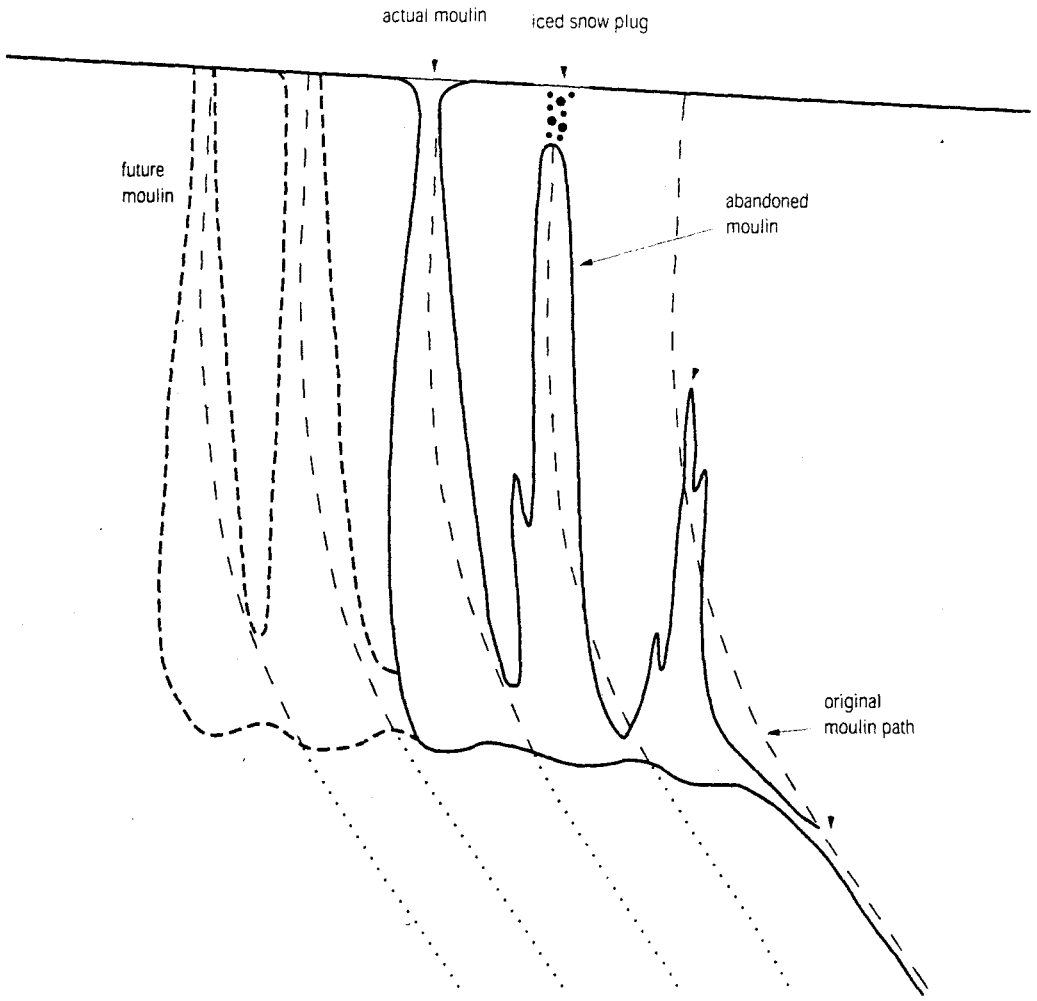



***Figure 2.29 - Schematic development of a cave system. Future moulins (short dash), course of crevasses due to water pressure (long dash) and potential course of crevasses (dotted) (Röthlisberger, 1996).***

Similar principles of drainage system permanence or deterioration are used when describing inter-annual and inter-seasonal changes in the capacity of the subglacial drainage system to discharge variable volumes of inputs. Without particular reference to any theoretical modes of water movement, seasonal changes in the overall ability of the subglacial system to store and

subsequently discharge water are described by Figure 2.28. Subglacial drainage systems undergo annual cycles of evolution, when the system becomes more hydraulically efficient, and deterioration, where efficiency decreases primarily as a response to a reduction in supraglacial inputs. Figure 2.28 indicates there is a lag between seasonal increase in efficiency, i.e. an increase in capacity to discharge, in response to an increase in surface runoff. The lag time is dependent on the degree to which both size and spatial extent of the subglacial drainage system from the previous year has deteriorated over the winter period when surface runoff is minimal, i.e. early October to mid-April. Deterioration refers to any disruption of subglacial areas that were previously hydraulically connected, i.e. closure of channels or conduits, disconnection of cavities or spatial isolation of thin film flow. Deterioration of subglacial drainage is caused either as a result of ice or sediment deformation into channels when ice and sediment pressures exceed channel water pressure or internal failure of ice resulting from spatial variation in sliding velocities relative to changes in bedrock topography. The rates and spatial extent at which such deterioration of the subglacial hydrological system affects the capacity of the glacier to discharge englacially routed inputs is uncertain and is approximated by the curve between September to May in Figure 2.28. Consequently, lag times between increased rates of surface runoff and evolution of subglacial drainage during the following ablation season are initially controlled by the extent to which hydrological pathways within ice and sediment of the former ablation season can be re-established. Re-establishment of former pathways by pressurised water is an easier, more rapid way of increasing the capacity to discharge at the start of the ablation season rather than having to carve out brand new pathways through consolidated ice and sediment.

### 2.6.1 Seasonal evolution and deterioration

Evolution of subglacial drainage will first occur slowly as water pressures gradually increase but as inputs rise further during the spring melt increasing subglacial water pressures may transcend

critical thresholds of stability in subglacial drainage. Water that backs-up in englacial channels, leading to ponding in temporary supraglacial lakes causes very high subglacial pressures. Rapid release of temporarily stored pressurised water can force one, or a combination of, hydro-fracturing within the main body of glacier ice. Hydraulic jacking causes detachment between basal ice and the substrate and exponential expansion of small channels within ice due to frictional heat resulting from rapidly increasing channel water velocities. Such flushing or 'spring' events are associated with large scale sediment evacuation from beneath the glacier, e.g. draining of the Gornersee at Gornergletscher, Switzerland (Collins, 1982b); rapid increase in both vertical and horizontal surface velocities, e.g. Unteraargletscher, Switzerland (Iken *et al.*, 1983) and temporary supra-glacial emergence of pressurised water due to englacial hydro-fracturing, e.g. John Evans Glacier, Ellesmere Island, Canada (Nienow, 2001). Hence, as shown in Figure 2.28 spring melt events have a major impact on subglacial drainage evolution causing a rapid increase in hydraulic efficiency of the system during the beginning of the ablation season.

After the effects of the spring melt event have increased subglacial hydraulic connectivity, rates at which the system can store and discharge water increase steadily to approach rates at which supra-glacial inputs enter the englacial system shortly after seasonal maximum surface runoff. Efficient transfer of water within a glacier is not necessarily the immediate, unrestricted discharge of water through the system; rather it is the capacity to discharge the total surface runoff over a 24-hour diurnal cycle within the same 24-hour period. Efficient transfer, therefore, allows for temporary sub- and englacial storage at times of peak surface runoff throughout the diurnal cycle, as long as temporary storage can be fully discharged within the same 24-hours.

Different types of subglacial drainage, principally either concentrated or distributed, may contribute to efficient transfer as defined above. A distributed system may be able to discharge

large inputs of water if the spatial area is great enough as although transit times through such networks are long, the wide spatial distribution of the network will limit back-up of water that causes temporary storage. Transit times of water through a concentrated drainage network will be much shorter than through a distributed system, although as such drainage is spatially limited, a greater percentage of the total discharge will be routed through only a few channels. At times of peak surface runoff during a 24-hour period a relatively large proportion of total daily water input may temporarily back-up in channels and be discharged at a rate dependent on the dimensions of the channel. Consequently, it is theoretically possible that both systems could discharge all surface runoff over a 24-hour period, i.e. be equally efficient, if increased transit times for water flow through many small channels in a distributed system are equal to the delay to discharge caused by back-up of water in a few large channels in a concentrated system.

Although theoretically separate systems can allow similar total discharges over a 24-hour period, diurnal cycles of increasing and decreasing discharge, which are almost in-phase with fluctuations in surface runoff (in response to hydrometeorological conditions), indicate concentrated drainage exists. This allows for short transit times (of the order of a few hours) for water flow through the glacial hydrological system. Distributed drainage that causes characteristically long transit times through tortuous channel networks cannot, therefore, be the only type of drainage involved in the subglacial system. Consequently, at daily maximum discharge the proportion of water that has flowed through tunnel-conduit systems is high, whereas at minimum daily discharge the proportion of water that has flowed through distributed linked cavity drainage is much higher. The absolute proportion of water from linked cavity systems at low flow is dependent on the dilution effect of delayed drainage of water from tunnel-conduit systems that was backed-up when maximum daily inputs exceeded the capacity to discharge.

Increasing supra-glacial inputs of surface runoff into the sub- and englacial hydrological system during the ablation season causes an increase in the capacity of the whole glacial hydrological system to store or discharge increasing volumes of inputs. Subsequently, both distributed and concentrated forms of drainage systems within the entire subglacial network exhibit different responses to consecutive days of increasing maximum daily surface runoff.

When considered under steady state conditions, water pressures in tunnels or conduits (concentrated drainage networks) vary inversely with channel discharge. Consequently, during periods of rising discharge large tunnels, generally parallel to the direction of ice flow, expand at the expense of smaller adjoining conduits. Drainage evolution occurs within a conduit-tunnel network as larger tunnels expand due to proportionally higher discharges and lower water pressures than in tributaries, increasing the hydraulic gradient and consequently capturing flow from smaller channels with higher water pressure. Subglacial water flow is likely to become highly concentrated through this positive feedback mechanism of water capture causing hydraulic efficiency and mean flow rates to be higher than in distributed linked cavity drainage systems (Walder, 1986). Increasing the proportion of total glacier discharge that flows through a tunnel-conduit system enables a reduction in average transit times of water through a glacier. Also a reduction in the proportion of daily runoff temporarily backed-up in channels will also reduce glacier sliding velocities. Reduction of sliding velocities is primarily due to tunnel-conduit systems preventing surface runoff from influencing a wide spatial area of the glacier subsole, thereby increasing frictional forces at the ice-subsole interface and reducing the likelihood of widespread hydraulic jacking.

A distributed drainage system of linked cavities, in which water pressure varies proportionally with discharge, is more stable than a conduit-tunnel system so long as sliding velocities are high

enough to maintain cavitation between basal ice and subglacial topography. Greater stability is maintained as cavity and orifice walls consist partly of bedrock providing extra support to cavitation. If water pressures are reduced cross-sectional areas of cavities and orifices are reduced by a proportionally smaller factor than if walls consisted completely of deformable ice (Walder, 1986). Such enhanced mechanical stability means linked cavity systems can adjust to lower water pressures under steady state conditions creating proportionally higher discharges at low water pressures compared to discharges at higher water pressures. Linked cavity systems, although inherently more stable than tunnel-conduit systems, may become unstable under very high water pressures. Instability may then lead to combined conditions of increased viscous melting of both cavity and orifice roofs and increased basal sliding, which could result in the growth of larger, more continuous channels (Kamb, 1987). As cavities may have multiple connections between each other, flowing water will have multiple pathways allowing dispersion of water pressure over much wider spatial areas of the glacier subsole than conduit-tunnel systems. Stability of linked cavities may almost even be independent of melting by viscous dissipation of heat in favour of control by geometric configuration and seasonally changing system parameters (Kamb, 1987). Rapid changes in water pressure are, therefore, likely to be influenced by increased glacier sliding velocities which heavily influence cavitation rather than rapid variation in discharge (Iken and Bindschadler, 1986; Kamb *et al.*, 1985). Under steady state conditions such stability allows water pressures in linked cavity systems, beyond a certain threshold of discharge, to potentially be greater than pressures in conduit-tunnel systems (Kamb *et al.*, 1985; Walder, 1986) although such stability means linked cavity systems are less likely to evolve spatially over the ablation season than tunnel-conduit systems (Walder, 1986).

Distributed drainage over a potentially wide subglacial area but with low rates of water movement occurs within sediment, either through consolidated sediment or as slurry through

deforming till. Seasonal water movement within sediment is relatively slow in comparison to all other forms of drainage. However, over a diurnal timescale, sediment adjacent to channels can act as a temporary reservoir that receives water when channel water pressures are high and releases water when water pressures are low. An increase in distributed drainage, both through linked cavities and within sediment, as a part of seasonal evolution, will increase average transit times and spatial distribution of water flow beneath basal ice.

In tunnel-conduit systems, due to inequalities between ice-melt by viscous dissipation of heat and channel closure by deformation of ice by overburden pressure there are no truly steady state conditions and fixed hydraulic gradients. Consequently, tunnel-cavity systems are more likely to evolve than distributed linked-cavity systems. They are also more likely to deteriorate in response to perturbations in discharge, either very high or very low discharges, especially in the late ablation season when very low discharges ($<0.5$ $ms^{-1}$ in mid-October) and water pressures (near atmospheric) are likely due to reduced surface runoff (Fowler, 1987; Kamb, 1987). However, linked cavity systems that are able to maintain stability at low water pressures (unless discharge or sliding velocity is negligible) are more likely to become unstable and deteriorate into more coherent tunnels at very high discharge and water pressures, i.e. flood discharges, which cause unstable orifice growth (Walder, 1986).

As evolution of the tunnel-conduit system concentrates water flow in only a few large channels, constriction or collapse of such channels will have a large impact on total glacier discharge and a major influence on spatial routing of water through remaining subglacial pathways. Relative effects of deterioration in linked cavity systems on total glacier discharge are less certain due to numerous combinations of flow pathways. It is likely that deterioration of linked cavity systems will result in increasing temporary water storage within spatially specific areas of the subglacial

drainage network due to decreasing hydraulic efficiency. However, spatial variation in the rate at which the entire subglacial drainage network deteriorates is far from certain due to localised bedrock topography, ice thickness, subglacial sediment availability and most importantly the effect that different formations of subglacial drainage have on each other.

### 2.6.2 Coexistence of multiple drainage systems

Coexistence of both concentrated tunnel-conduit and distributed linked cavity systems may theoretically occur where water pressures in cavities and tunnels are equal and unperturbed under steady state conditions. For such coexistence to occur glacier sliding velocities must be above the threshold that maintains cavitation in linked cavity systems, but must be lower than the threshold that will cause deterioration of tunnel-conduit systems. If the distributed and concentrated drainage systems are hydraulically connected, high water pressures in a conduit-tunnel drainage system can force water into cavities. This will ultimately increase both orifice and cavity size. An increase in discharge through linked cavities as a result of changes in preferential subglacial hydrological routing is unlikely to affect the stability of distributed drainage unless increased water flow is catastrophic, i.e. complete collapse of a tunnel or conduit causing total re-routing of water flow. If water pressures decrease in the tunnel-conduit system the hydraulic gradient may reverse causing water flow back from cavities into a tunnel-conduit system. Spatial variation of preferential water flow pathways throughout the subglacial hydrological system could conceivably operate in this manner over a diurnal timescale.

Evidence for switching subglacial hydrological pathways is indirectly gained from monitoring variations in surface runoff, discharge and glacier sliding velocities. Increased water pressures and possibly increases in the proportion of the glacier subsole accessed by subglacial drainage

will reduce frictional resistance to glacier sliding, dependent on bedrock topography and distribution of subglacial sediment. Consequently, if increasing surface runoff into the glacier is associated with increased surface velocity, and if discharge appears attenuated, it is possible that the hydraulic gradient is forcing water out of concentrated drainage systems and into distributed drainage. However, for this scenario to accurately indicate switching of hydrological pathways, increased subglacial water pressures in distributed drainage systems need to have a substantial influence on ice velocity. These are complicated by multiple factors thought to affect sliding velocities within a glacier (see section 2.5). Misinterpretation is possible as water may be simply backing-up in tunnels in concentrated drainage systems whilst glacier velocity increases for reasons unconnected to drainage system switching. Other evidence or suggestion for coexistence of concentrated and distributed drainage systems consist of geomorphic evidence on the glacier bed after a glacier has retreated (Walder and Hallet, 1979) and theoretical verification (Fowler, 1987; Walder, 1986).

As there is some ambiguity in evidence justifying linked cavity systems coexisting with tunnel-conduit systems Hock and Hooke (1993) suggested a multibranched arborescent drainage system that incorporates characteristics of both concentrated and distributed systems. Dye tracer studies at Storglaciären, Sweden, indicated water velocities were too low to suggest subglacial drainage exists solely through a tunnel-conduit system. However, models of subglacial drainage appeared to fit well if the tunnel-conduit drainage system bifurcated a number of times until the highest order tributary accounted for ~3% of the total discharge at the terminus. Coupled with multiple peaks in dye return curves the conceptual description was initiated by subglacial water movement through a network of low, broad conduits each of which are individually braided (Hock and Hooke, 1993). The drainage network pattern forms a dendritic pattern. A large number of high order tributaries could drain water from within numerous moulins in the heavily crevassed up-

glacier surface. Such a network would leave no part of the bed far from a conduit and is consistent with relatively uniform water pressures measured across the bed that are common in distributed linked cavity systems. The multibranched arborescent system is an attempt to combine concentrated drainage through R-channels, as water pressure in the arborescent system is suggested to vary inversely with discharge, with a degree of turbulent, tortuous flow in braided channels that influence a wider subglacial area.

### 2.6.3 Influence of outburst flooding

Outburst drainage and flood routing of water that is suddenly released from temporary storage in supra- and englacial reservoirs can exert a large influence on both the evolution and deterioration of subglacial drainage systems. Possible physical mechanisms that initiate outburst flooding are numerous, e.g. through breaching an ice dammed lake, siphoning, breach widening and the Glen mechanism (Tweed and Russell, 1999), or sudden high magnitude input from a large meteorological event that mobilises water trapped in subglacial cavities (Walder and Driedger, 1995). Flooding from high magnitude input events indicate that the physical presence of an ice-dammed lake is not necessarily a prerequisite for outburst flood events.

Analysis of outburst floods or jökulhlaups are herein limited to those in which drainage is routed through an existing subglacial hydrological system, regardless of the initial trigger mechanism. Rates of water drainage are a function of the initial hydraulic efficiency of the drainage network and the rate at which it can change to accommodate a rapid increase of inputs. Hydraulic efficiency during outburst flood events is dependent on the geometry and tortuosity of subglacial drainage systems. These result from a balance between forces exerted by water pressure and ice overburden pressure as well as the influence of substrate type and topography, basal sliding and

enhanced lateral ice compression if subglacial pathways run perpendicular to ice flow (Jones *et al.*, 1985).

Slow rates of drainage from reservoirs of temporarily stored water are maintained if water percolates through a layer of deformable sediment that is unbounded by ice. However, where flowing water from a reservoir is in contact with ice, melt widening of channels and orifices in either discrete or distributed drainage systems causes a rapid increase in subglacial hydraulic efficiency. Exploitation of the existing drainage system requires access to the initial position of leakage from the reservoir. A distributed drainage network is consequently more likely to connect with initial leakage from a reservoir than a tunnel-conduit system that is relatively spatially isolated. If water flow from a reservoir connects directly to a spatially discrete tunnel-conduit system water will be rapidly evacuated as melt widening (which also contributes to volumes of water flow) and mechanical tunnel enlargement combine to increase the capacity of the system to discharge. If water flow from a reservoir connects with a distributed drainage network of linked cavities such a system will be destabilised as very high subglacial water pressures, due to high water inputs and low hydraulic efficiency of the drainage system, will cause melt widening, mechanical erosion and possible localised ice floatation. Consequently, high water inputs from a reservoir into a distributed system will result in a switch to a concentrated system of drainage (Walder and Driedger, 1995).

Flood routing and resulting changes in subglacial drainage influence estimation of peak discharge, often the most destructive stage of an outburst event, which can be approximated well using empirical relationships (Clague and Mathews, 1973). The exact nature of the discharge hydrograph is dependent on whether water is routed through single or multiple channels and whether those channels are regularly used or unused by non-outburst flow (Tweed and Russell,

1999). Walder and Costa (1996) used hydrograph shape to distinguish between flood routing through distributed (non-tunnelled) and concentrated (tunnelled) drainage systems. Flood routing through distributed drainage indicates a rapid rise to peak discharge, as the system is quickly destabilised, which terminates abruptly producing a flashy hydrograph. Routing through concentrated drainage produces a hydrograph characterised by a prolonged approach to peak discharge, reflecting progressive enlargement of conduits, followed by a rapid decrease in flow.

## 2.7 Field instrumentation and methodology

Much information can be ascertained about glaciohydrological processes by observing and monitoring hydrometeorological surface inputs and proglacial outputs (combining fluvial processes and resultant geomorphic landforms). Black-box modelling, only using input and output data to the glacial system, needs to be complemented by identification of rates at which the physical processes that control water movement interact within englacial and subglacial environments. The location of sub- and englacial water pathways and sediment configurations may be identified 'passively' using ground penetrating radar. However, the technique of drilling boreholes, from the glacier surface to the bedrock (or at least into the basal ice zone) is a more established and documented technique used to gain direct access to the internal glacial system.

### 2.7.1 Boreholes

Boreholes drilled through ice allow direct access to, and *in situ* measurements to be made of, the englacial and subglacial environment. The use of pressurised hot water has increased the ease with which boreholes can be drilled; therefore, rapid creation of multiple borehole arrays allows temporal and spatial variations of measurements to be made within a glacier or an ice sheet. Boreholes are used to verify the existence of water, sediment and ice along a vertical profile

through a glacier. Measurement of rates of ice creep, sediment deformation and water flow within and beneath boreholes allows direct access to contemporary glacier systems whilst minimising disturbance to the systems being measured.

The use of boreholes as a means with which to investigate the character and behaviour of subglacial drainage systems rely on the assumption that changes in water volume and water quality within a borehole are representative of variations of subglacial drainage (Barrett and Collins, 1997; Cutler, 1998; Engelhardt, 1978; Engelhardt and Kamb, 1997; Fountain, 1994; Gordon *et al.*, 1998; Gordon *et al.*, 2001; Hanson *et al.*, 1998; Hantz and Lliboutry, 1983; Hodge, 1976; Hodge, 1979; Hooke, 1984; Hubbard *et al.*, 1995; Iken and Bindschadler, 1986; Iken *et al.*, 1996; Iken and Truffer, 1997; Kamb *et al.*, 1985; Kavanaugh and Clarke, 2000; Murray and Clarke, 1995; Röthlisberger *et al.*, 1979; Stone and Clarke, 1996). However, both the quantity and quality of water in a borehole is also affected by water flow directly from surface runoff, though microscopic veins in ice (especially in near surface ice) and intersection with englacial conduits (evidenced by rapid falls in water level during borehole drilling before the substrate is reached).

Changes in borehole water levels and chemical composition are dependent on both sub- and englacial hydraulic connectivity and the nature of connections. As boreholes may also be completely hydraulically unconnected there are multiple resulting combinations of sub- and englacial hydrological influences on water in boreholes. Gordon *et al.* (2001) classified hydraulic connections to boreholes as either connected, whose physical properties respond to the glacial drainage system, or unconnected, whose properties remain static. Unconnected boreholes are then subdivided into those that terminate englacially, referred to as blind, and those that terminate basally but fail to respond to the drainage system which are referred to as apparently unconnected. Connected boreholes can be subdivided into either englacially connected, basally

connected or a combination of both, multiply connected. Finally, Gordon further subdivides both connected and disconnected boreholes into those that intersect an englacial cavity that itself is unconnected to the drainage network, referred to as complex, and boreholes that have no intersections of this kind, which are termed simple. Further classification using stratification of EC or turbidity profiles within water columns in boreholes is a feature of a borehole that is subglacially connected, providing a sediment source and highly concentrated meltwaters. The extent of stratification within the borehole has a more temporally variable basis than previous classifications based on hydraulic 'plumbing' connections.

When a borehole taps into a subglacial drainage system water levels in the borehole reflect changes in water pressure instantaneously within the system if the local drainage system has sufficient capacity to fill and drain boreholes so that water can enter and leave boreholes rapidly enough (Hubbard *et al.*, 1995). If a borehole makes a direct intersection with a subglacial channel, once the channel is full water will be forced up the borehole providing there is a further increase in pressure in the subglacial channel (caused by a greater rate of meltwater input to the section of channel relative to the rate at which it can discharge). Open boreholes (i.e. those that are not frozen shut at the glacier surface) act like manometers if the quantity of water entering and leaving a borehole is negligible compared to the total subglacial throughput of water. Consequently, for the condition that water pressure in the channel is greater than atmospheric pressure, the height of a water column in a borehole is proportional to the water pressure in the channel.

Pathways of concentrated water flow may be small in their spatial extent relative to the total surface area of the ice-bedrock interface reducing the chance of a borehole directly intersecting a drainage route that has the capacity to instantaneously reflect changes in subglacial water pressure. If the chance of an englacial connection is excluded it is likely that the base of a

borehole reaches either bedrock (unconnected), a subglacial layer of sediment (either connected or apparently unconnected depending on the hydraulic conductivity of the sediment) or that it terminates before reaching the bed (blind). Of these three options only connection of the borehole with a subglacial layer of sediment may produce changes in borehole water levels, albeit not immediate, which are caused by water pressure variations in subglacial drainage. The delay with which variations of subglacial water pressure in a sedimentary substrate are reflected in borehole water levels depends on the distance between the base of the borehole and the nearest major drainage channel, and the quantity and uniformity of the sediment's hydraulic properties.

Changes in the quantity and quality of water in boreholes are typically measured by pressure transducers, commonly sharing a single wire with 'hydrology units' that incorporate EC cells and turbidity sensors (Stone and Clarke, 1996). Pressure transducers are located within the borehole close to the glacier bed, ~2m above the bed (Kavanaugh and Clarke, 2000), or at an optimum level below the mean water level to maximise measurement resolution of diurnal variations (Barrett and Collins, 1997). Inaccuracies in measurement of borehole water levels occur as absolute error, during installation of the transducer within the borehole, and relative error, limited by the sampling resolution of the transducer (Kavanaugh and Clarke, 2000). Relative error of water levels is an order of magnitude smaller than absolute error, ~0.15m absolute error during installation compared to ~0.02m relative error (Kavanaugh and Clarke, 2000). Limiting relative error is more important than limiting absolute error as borehole water levels are interpreted in conjunction with relative fluctuations in other hydrometeorological and glaciological variables.

Studies of borehole water levels in glaciers have been able to demarcate subglacial areas of homogeneous and heterogeneous water pressures, as well as identifying links with glacier sliding velocity (Harbor *et al.*, 1997; Meier *et al.*, 1994), allowing their development into integrated glacier discharge models (Clarke, 1996; Richards *et al.*, 1996). Smart (1996) used nearest

neighbour analysis of water levels in a network of adjacent boreholes at Small River Glacier, Canada, to demonstrate boreholes could delimit spatial connectivity or non-connectivity of subglacial drainage, indicating spatial coherency and integrity of the system where it existed (Hubbard *et al.*, 1995). This helped justify the physically based interpretation and demarcation of spatial variation in subglacial drainage using diurnal maximums, minimums and ranges in borehole water levels. Concentrated tunnel-conduit style drainage is evident where borehole water levels have large diurnal ranges. They can have low minimums in comparison to surrounding boreholes, as for example a linear zone of low minimum water pressures defined the path and area around a channel at Haut Glacier d'Arolla, Switzerland, termed a variable pressure axis (Hubbard *et al.*, 1995). A broad low pressure zone around boreholes containing high standing water levels at South Cascade Glacier, USA, was interpreted by (Fountain, 1994) to be a subglacial conduit draining a large area of sedimentary substrate. Fountain (1994) calculated the hydraulic conductivity of the substrate decreased throughout the season, ranging between $10^{-4}$ to $10^{-7}$ $ms^{-1}$, causing water levels to rise as subglacial flow pathways through the sediment filled with fine abrasion particles. Murray and Clarke (1995) identified high spatial heterogeneity in subglacial drainage at Trapridge Glacier, Canada, using force and response (F-R) plots of water levels in boreholes. High local pressure gradients between the base of adjacent boreholes, which were closed to the atmosphere at the surface, showed the response of borehole water levels to water pressure variations in the subglacial drainage system were different over very short distances of 5m. Mathematical modelling of F-R plots was attempted using non-linear differential equations to replicate trends within often highly complex hysteresis loops.

Direct access to the subglacial sedimentary substrate at the base of a borehole allows insertion of mechanical sensors into the substrate or at the ice-till interface. Tilt cells are used at the ice-till interface to measure change in inclination (Gudmundsson *et al.*, 1999; Iverson *et al.*, 1999; Truffer *et al.*, 2000). Penetrometers allow minimum depth estimates of sediment layers (Hooke

*et al.*, 1997) ploughmeters or load bolts determine sediment strength and deformation rates (Fischer and Clarke, 1994; Fischer *et al.*, 1998; Iverson *et al.*, 1994) and slidometers or dragspools allow measurement of glacier sliding (Blake *et al.*, 1994). Retrieval of till samples from the base of boreholes in alpine glaciers (Truffer *et al.*, 1999) and ice streams (Engelhardt *et al.*, 1990) has allowed laboratory analysis of till porosity, strength and deformation etc. However, retrieval inevitably causes disruption of the sediment matrix through removal of confining pressure amongst many other factors. *In situ* testing of the hydraulic properties of the subglacial substrate is achieved by response testing (also known as impulse or slug testing). Response testing involves artificial displacement of borehole water levels (Stone *et al.*, 1993; Stone *et al.*, 1997; Waddington and Clarke, 1995), whether through insertion and removal of a solid cylinder (slug tests) in open boreholes or release of air pressure (packer tests) in closed boreholes by breaking the surface ice seal (Hubbard and Nienow, 1997). Monitoring of water level recovery after the artificial displacement, in the form of a series of dampened oscillations indicate the hydraulic character of the substrate although interpretations may be limited due to numerous uncontrolled sub- and englacial hydrological interactions, especially with a sedimentary substrate (Hubbard and Nienow, 1997). Intra-decadal monitoring of borehole water levels as part of a large scale monitoring programme at Findelengletscher, Switzerland, in 1982, 1985 and 1994 indicated changes in seasonal development of the type and spatial extent of subglacial drainage (Iken and Bindschadler, 1986; Iken and Truffer, 1997). Links between water pressure and sliding were made to illustrate that ice velocity was more insensitive to variations in water pressure in 1994, when fewer boreholes connected with the subglacial drainage system, than in 1982 or 1985. Consequently, water pressure variations in 1994 affected a smaller area of the glacier bed than in 1982 or 1985 suggesting drainage had become less distributed and developed into a predominately conduit-tunnel system more rapidly throughout the ablation season.

Variation in hydrostratigraphy of boreholes have been measured using bulk EC (Smart and Ketterling, 1997) along with variations in the individual ionic composition of basal water (Lamb *et al.*, 1995; Tranter *et al.*, 1997) at Haut Glacier d'Arolla, Switzerland. Hydrochemical measurements of water in boreholes that have not drained are complicated by standing water within the borehole being predominantly of supraglacial origin as a by-product of the hot water drilling process. Temporal variations in the hydrostratigraphic record require profiling up to every 30 minutes for hydraulically dynamic boreholes (Smart and Ketterling, 1997) allowing identification of the influence of englacial and subglacial connections. As relative comparison over a time series with other glacio-hydrological parameters are required, rather than simply using temporally specific absolute values of individual ionic concentrations in basal waters in boreholes, repeated borehole profiling is necessary. Smart and Ketterling (1997) concluded that adequate monitoring of dynamic profiles of more than a few boreholes in a close area has many practical limitations which makes acquisition of a large series of measurements presently impossible.

Other techniques for hydrological investigation include artificial mineralisation of water in boreholes, which allows electrical resistivity imaging of englacial drainage pathways in the ice between boreholes (Hubbard *et al.*, 1998). Tracer injections directly into the base of boreholes are used in conjunction with tracers in moulins to identify spatial difference in subglacial drainage. For example, observed tracer return curves from dye injections made into the base of boreholes at Aletschergletscher, Switzerland were found to have multiple peaks (Hock *et al.*, 1999), which inferred the borehole drained into a drainage system with significant long-term storage that released pulses of labelled water in-phase with diurnal water pressure cycles.

Boreholes provide englacial access for glaciological investigation that impact on hydrology. Thermal structure of ice can be determined using borehole thermometry (Haeberli and Funk,

1991; Jania *et al.*, 1996) and are allied with ground penetrating radar data to measure internal heat fluxes and delineate layering of cold and warm glacier ice (Hodgkins *et al.*, 1999; Moore *et al.*, 1999; Odegard *et al.*, 1992). Rates of motion within glacier ice, primarily caused by deformation or fracture, are studied using measurements of borehole inclinometry (measurement of long axis geometry). Repeated measurement of multiple boreholes allows investigation of ice deformation (Cuffey *et al.*, 2000; Harper *et al.*, 2001; Hooke *et al.*, 1992) and when magnetometers are incorporated into inclinometers, compass bearings enable exact locations within a glacier to be identified for emplacement of sub-surface sensors (Blake and Clarke, 1992). Emplacement of stress tensor sensors in ice allow variation in vertical strain throughout a borehole profile (Harrison *et al.*, 1993) measuring internal ice compression and extension (Copland *et al.*, 1997a; Pfeffer *et al.*, 2000). Spatial variation in the nature of sub- and englacial ice and sediment layers, which affect the internal strength of a glacier, can also be observed in boreholes that have drained using borehole cameras (Koerner *et al.*, 1981) borehole video (Copland *et al.*, 1997b; Harper and Humphrey, 1995; Pohjola, 1994; Pohjola, 1993) and more recently acoustic televiewer logging (Morin *et al.*, 2000) to help differentiate between clear and bubbly ice in water filled boreholes. Direct observations in this manner are used to corroborate indirect, remotely sensed data of sub- and englacial hydrological, glaciological and sedimentological structures.

### 2.7.2 Proglacial solute and suspended sediment fluxes

Analysis of water quantity and quality in proglacial rivers provide remote techniques for investigating seasonal evolution and deterioration of water drainage through a glacierised catchment. Analysis of the hydrochemistry of proglacial discharge in terms of bulk meltwater discharge and specific ionic composition, as well as calculation of suspended sediment fluxes, allow conclusions to be drawn regarding the character and variations in subglacial drainage.

#### 2.7.2.1 Solute fluxes

Electrical conductivity (EC) is used as a surrogate for solute concentration of bulk meltwaters, allowing variations in solute fluxes to be interpreted in terms of combinations of 'parcels' of water that have different flow pathways through the subglacial drainage network. As flow pathways differ in efficiency and size different transit times of water flow through, or residence times within, the drainage system will influence the solute concentration of the water parcels. When parcels of water from different pathways meet at or near the glacier terminus the solute flux within proglacial discharge will be a result of the mix of water from the different pathways. Different flow pathways can conceptually be regarded as separate reservoirs of varying transit times within a glacier, therefore, a hydrochemical glacial mixing model is the combination of solute fluxes from each reservoir. Collins (1979) crudely split the subglacial drainage network into two reservoirs, one that allows fast transit times, i.e. describing concentrated tunnel-conduit systems, and the other that causes slow transit times, i.e. describing distributed drainage within small pipes in a tortuous network. Solute content of water is dependent on availability of reactants, i.e. intersection of drainage pathways with subglacial comminution debris, residence time of water and reaction kinetics. Concentration levels of solutes when water is initially under-saturated increase in a quasi-exponential manner until a finite point of saturation is reached. Consequently, in a subglacial environment parcels of water flowing through reservoirs with fast transit times will typically have lower solute concentrations (low EC) than water through reservoirs with low transit times (high EC). In this model, surface runoff is assumed to be ionically dilute as contact with reactive debris in the supraglacial environment is considered highly limited. Efficient subglacial flow (quick -flow) of such ionically dilute water through the subglacial drainage network remains dilute due to short residence times, whereas inefficient flow (delayed-flow) has much higher residence times in the reactant rich (e.g. $Ca^{2+}$, $Mg^{2+}$ and $SO_4^{2-}$) subglacial environment and increases in concentration at a rate dictated by the Nernst curve.

Reconstruction of temporal variations in components of subglacial drainage, assuming constant EC values for quick-flow (~$10^0$ μS $cm^{-1}$) and delayed-flow (~$10^1$ μS $cm^{-1}$) (Hubbard and Nienow, 1997), allows mixing models to be used in conjunction with hydrograph separation (Lecce, 1993) and in particular analysis of breaks of slope in daily discharge recession curves (Collins, 1982b).

The two-component chemically based mixing model is used as a basis for increasing hydrochemical analysis of supraglacial, proglacial and *in situ* subglacial discharge, sampled in boreholes (Stone and Clarke, 1996; Tranter *et al.*, 1997). However, it is likely that flow pathways are not discrete, are more numerous than just the two reservoirs within the glacial hydrological system (Gurnell, 1993) and that the EC of water flowing through each reservoir is not constant or chemically uniform (Sharp *et al.*, 1995b; Tranter *et al.*, 1997). An increasingly physically based approach to meltwater hydrochemistry, to interpret the impact of post mixing chemical reactions on bulk meltwater chemistry (Brown *et al.*, 1994) and individual ionic interactions (Hodgkins *et al.*, 1998; Tranter and Raiswell, 1991) allows contrasts to be made between polar and temperate glaciers in terrestrial and maritime conditions (Collins, 1999; Skidmore and Sharp, 1999; Tranter *et al.*, 1996; Wadham *et al.*, 1998). A physically based analysis has increased understanding of acid hydrolysis reactions within the glacial hydrological system; usually carbonate, silicate or aluminosilicate hydrolysis (Hubbard and Nienow, 1997). Analysis of acid hydrolysis reactions and partial pressures of $CO_2$ in solution in meltwaters allow rates of chemical denudation and atmospheric $CO_2$ sequestration to be compared in different glacial environments. The relationship between supply of protons and their consumption due to weathering reactions allows characterisation of bulk meltwaters into open or closed systems in a subdivision of meltwaters similar to that by EC. Open systems occur when the rate of proton consumption by chemical reactions is not limited by proton supply, primarily by dissolution of $CO_2$ from the atmosphere although supply also possibly increases due to acidic snowmelt, gas expulsion due to meltwater freezing, neutralisation of acidic meltwater by carbonate dissolution or oxidation of sulphides

amongst other meltwater parameters (Fairchild *et al.*, 1994; Raiswell, 1984; Sharp, 1996; Tranter *et al.*, 1993). Conversely, closed systems occur when the rate of proton supply and consumption are mismatched. Subglacial drainage characteristics and rates can, therefore, be inferred from both individual and bulk ionic analysis of different glacial environments and their importance to net consumption of $CO_2$ from the atmosphere can be assessed (Hodson *et al.*, 2000; Sharp *et al.*, 1995a).

#### 2.7.2.2 Suspended sediment fluxes

Sediment fluxes in Alpine proglacial rivers are a function of interactions between sediment both in basal ice and at the ice-bedrock interface and the capacity of the subglacial drainage network to erode and transport the available sediment. Sediment fluxes may, therefore, be considered as either supply limited (restricted subglacial sediment availability) or transport limited (restricted spatial extent or erosive power of subglacial drainage). Long term records of sediment fluxes (Collins, 1989b) show that seasonal patterns of fluxes are related directly to development of subglacial drainage. During winter the rate of glacier erosion is much greater than the rate of subglacial sediment evacuation as surface runoff is negligible. Products of glacier erosion accumulate over the winter at the ice-bedrock interface until increasing surface runoff at the beginning of the ablation season allows fluvial erosion and transport of accumulated sediment. As the subglacial drainage network is re-established or relocated sediment is progressively but episodically evacuated. After early season 'flushing' by surface runoff of subglacial sediment built up during winter time erosion of the substrate by glacier ice, the volume of sediment discharged varies directly, though not synchronously, with flow discharge where sediment supplies are available (Fenn, 1987). However, as available sediments are formed in a spatially non-uniform, temporally discontinuous manner the relationship between quantity of sediment discharged and flow discharge will vary accordingly. Variation in the volume of sediment that is

evacuated will be dependent on variations in the size, course and channel capacity of the subglacial network in response to increasing surface water inputs. It is likely that most movement and evolution of channels is achieved by numerous small, unstable tributary channels (perhaps at the periphery of the network) that can shift course more readily and frequently than the main channels (Collins, 1979c).

The type of drainage network, which characterise the spatial extent, water pressures, direction and stability of hydrological pathways in the subglacial environment; all combine to have a large influence on the timing and magnitude of sediment evacuations. Whether the glacier rests on a substrate of either solid bedrock or deformable sediment, will determine the ease with which seasonal evolution and deterioration of a drainage network will affect rates of sediment evacuation. Bedrock substrates provide a large primary source of potentially erodable material but a rapidly exhaustible secondary source, or temporary store, of erosional by-products. Sedimentary substrates will provide a more or less constant source of erosional by-products that will take less energy to erode and entrain.

Erosion of subglacially available sediment by flowing water occurs at greater rates than sediment can be produced by erosion of bedrock by ice, causing temporary subglacial sediment stores to become depleted (Østrem, 1975) to the point of exhaustion throughout the ablation season (Collins, 1989b). Seasonal evolution of the drainage network provides a major control over the extent of sediment exhaustion throughout the ablation season and the possibility of transient expansion of the network as a response to high water pressures. If the drainage network evolves into an efficient tunnel-conduit formation the spatial extent of meltwater interaction with subglacial sediment becomes increasingly limited, even in response to increases in subglacial water pressures, and hence seasonal exhaustion becomes more likely, whether or not the substrate is bedrock or a sediment layer (Collins, 1996). However, if subglacial drainage is more spatially

distributed, such as a linked cavity network which is maintained despite variations in water pressures (Fowler, 1987), transient expansion is possible at times of very high water pressure, e.g. under conditions of glacier surging (Humphrey *et al.*, 1986; Humphrey and Raymond, 1994), providing access to previously inaccessible stores of subglacial sediment. Spatial stability of subglacial drainage networks and sediment storage depend on localised factors, e.g. bed roughness, topography and geotechnical properties of sediment. These cause increased subglacial water pressures to change the pathways of water movement from film flow through temporarily stored subglacial sediment to more concentrated tunnel-conduit flow, hence increasing the volumes of sediment that can be discharged (Alley, 1989; Lawson, 1993).

As highly variable temporal and spatial conditions influence sediment production, storage and evacuation, there are no universal rating relationships between suspended sediment concentration (SSC) and discharge. Instead, SSC in relation to a series of diurnally rising and falling discharge limbs indicate hysteresis patterns over diurnal and seasonal timescales (Fenn, 1989; Østrem, 1975). The strongest rating relationships between discharge and SSC in alpine, warm-based glaciers occur when sediment fluxes are transport limited at the beginning of the ablation season (Gurnell *et al.*, 1994) after which exhaustion, and both erratic evolution and deterioration of the drainage network, can cause clockwise and anti-clockwise hysteresis loops. In arctic, cold-based or polythermal glaciers seasonal exhaustion does not occur, therefore, SSC varies as a direct function of discharge (Gurnell *et al.*, 1994; Hodgkins, 1996). Diurnal lag and lead times of SSC and discharge correspond to a SSC lead if hysteresis is clockwise and a discharge lead if hysteresis is anti-clockwise. Seasonal trends of diurnal lags and leads of cold-based or polythermal glaciers in Svalbard, which decrease in diurnal SSC, lead over discharge exhibiting clockwise hysteresis (Hodgkins, 1996) and contrast with temperate alpine glaciers in which SSC and discharge vary almost synchronously with each other throughout the season (Gurnell *et al.*, 1994). Consequently, hysteresis generating processes of sediment exhaustion in temperate

glaciers are offset by the process of up-glacier migration and exploitation of subglacial sediment sources relative to the increasing supraglacial surface area contributing to meltwater production; a process which is far less pronounced in non-temperate glaciers (Gurnell *et al.*, 1994).

Temporal variability of seasonal increases and exhaustion of sediment fluxes from glaciers of different thermal regimes is hard to predict. Analysis and modelling concentrates on multiple regression and time series techniques to identify similarities in sub-seasonal sediment flux patterns and major pulses of sediment that are isolated as large positive residuals within regressions (Willis *et al.*, 1996). Statistical explanations of SSC are improved upon by using multiple regression techniques where discharge is supplemented by other predictors acting as surrogates for variability in sediment supply (Hodson and Ferguson, 1999). However, as such improvements in statistical analysis still need to account for additional stochastic elements, conceptual models of drainage evolution in relation to sediment evacuation are equally appropriate. Collins (1996) suggested a physically based conceptual model that delimits the glacier subsole in a grid-square pattern through which water spreads, integrating the subsole with water flow as a function of discharge. As sediment is abraded at a uniform rate in cells not interacting with water and is redistributed to the margin of the wetted area by deformation in two directions, the model allows investigation of relationships between the spatial pattern of the subglacial drainage network, suspended sediment flux and discharge

### 2.7.3 Tracer studies

Tracers have been widely used in tests on the internal drainage system of glaciers (Burkimsher, 1983; Collins, 1995; Fountain, 1993; Hock and Hooke, 1993; Krimmel *et al.*, 1973; Moeri and Leibundgut, 1986; Nienow *et al.*, 1996a; Nienow *et al.*, 1996b; Seaberg *et al.*, 1988; Stenborg, 1969). Parcels of water that flow through the glacial hydrological system, entering as

supraglacial surface runoff into moulins and exiting at the glacier portal as highly turbid water, are best labelled using brines or fluorescent dyes, e.g. salt, uranine, fluorescein, tinopal CBS-X, rhodamine-B or rhodamine-WT. Such tracers are identified within bulk proglacial meltwaters as return curves using EC, if brines are used, or dye concentration of any of the fluorescent dyes. Return curves (or breakthrough curves) primarily allow analysis of transit times (time between dye insertion and peak dye concentration at the detection site), minimum estimates of mean flow velocity, dispersion and mean cross-sectional area of sub- and englacial drainage systems (Nienow *et al.*, 1996b). The magnitude and shape of return curves, relative to the amount of dye injected, depend on levels of dye dispersion throughout the hydrological system and recovery of dye at the measurement site in the proglacial river. Less than 100% of the dye injected will be recovered if water is temporarily stored within the glacier or dyed water is diluted to such an extent that the fluorescence per unit volume drops below natural background levels. However, return curves primarily indicate the transit time of a parcel of water, which is the difference between the time of injection and time of peak dye concentration in the proglacial river. Dispersion of the water parcel is indicated by the time between the first detection of dye at the proglacial measuring site and the time at which fluorescence drops back to natural background levels (Collins, 1995). Calculation of flow velocity-discharge rating relationships (Equation 2.30) for individual hydrological pathways may be calculated using experimental data to calculate the appropriate parameter ($k$) and exponent ($m$).

$$V = kQ^m$$

***Equation 2.30***

Dispersion of a dye cloud through a single flow pathway may be due to water being delayed by stable eddies (especially at low discharges), adsorption of dye onto sediment and flow through restrictive small subglacial channels that have lower flow velocities than surface flow (Seaberg *et*

*al.*, 1988). Subdivision of a single dyed parcel of water by branching channels within sub- and englacial networks causes different transit times of each subdivided volume of water that was supraglacially dyed as a homogenous unit. Return curves of a water parcel subdivided in this manner will show multiple peaks rather than a smooth increase and decrease in dye concentration over time.

Variation in return curves of repeated dye injections into a single supraglacial stream flowing into a moulin, or multiple dye injections into a number of spatially separate supraglacial streams, over both seasonal and diurnal timescales can give indications of the structure, functioning and seasonal evolution of sub- and englacial pathways e.g. (Seaberg *et al.*, 1988; Stenborg, 1969). Dye tracers in a number of moulins, sometimes injected simultaneously when using different dyes that do not interfere with each other e.g. tinopal CBS-X and rhodamine WT (Fountain, 1993), may show different transit times that allows spatial delimitation of multiple forms of drainage within the overall hydrological network (Burkimsher, 1983; Fountain, 1993; Moeri and Leibundgut, 1986).

Diurnal examination of discharge-velocity relationships reveals transit times decrease with increasing stage (or discharge), e.g. at Findelengletscher (Collins, 1995); that hysteresis loops occur suggesting non-uniformity in meltwater routing, e.g. at Haut Glacier d'Arolla (Nienow *et al.*, 1996b); and specifically in the degree of braiding in multibranched arborescent channels, e.g. at Storglaciären (Hock and Hooke, 1993). Over the entire ablation season, repeated dye traces down a number of moulins can indicate temporal switching of subglacial pathways as a result of changing inputs (Nienow *et al.*, 1996b). Estimates of channel geometry, flow path length, depth and velocity, can be made as a result of dye tracing allowing indications to be made of the types of channels that control the rates of drainage, i.e. the relative width, depth and sinuosity of channels (Fountain, 1993), primarily either contrasting differences between channelised and

distributed drainage systems (Burkimsher, 1983; Iken and Bindschadler, 1986; Nienow *et al.*, 1996b); with combinations of both systems (Hock and Hooke, 1993; Seaberg *et al.*, 1988).

## 2.8 Summary

An extensive review of processes that control rates of surface runoff and rates of water flow through a temperate glacier has been presented. The advantages and limitations of monitoring techniques commonly used to investigate these rates of input and throughput have also been discussed. It has been shown that hydrometeorological inputs (meltwater and precipitation) and glaciological processes (basal sliding and ice deformation) interact throughout the ablation season to produce a subglacial drainage network that is spatially and temporally variable in its capacity to modify water flow through a catchment. Therefore, to investigate the interrelationships between subglacial water storage and the capacity of the glacial hydrological system to transfer volumes of surface runoff there is a requirement to make temporally and spatially distributed measurements of not only inputs and outputs but also glacier movement.

Though boreholes provide the best means of making spatially distributed measurements of subglacial water pressures, there are numerous factors that influence water levels within the boreholes other than just water pressures in subglacial channels. There is, therefore, a requirement to develop methods for interpreting the links between borehole water levels and the glacial hydrological system, furthering recent progress made by Gordon *et al.* (2001) and Kavanaugh and Clarke (2000).

With respect to understanding flood events, concentration of all measurements towards the end of the ablation season is required. This is because during the early ablation season the rate of surface runoff increases faster than the rate at which the subglacial hydrological network can

discharge. Increasing summer air temperatures and net radiation produces increased rates of runoff from the glacier surface. In turn, this causes a rapid rate of increase in elevation of the transient snow line (TSL), which results in greater runoff from the snow-free proportion of the glacier surface. However, the rate of increase in the capacity of the subglacial drainage system to discharge lags behind increased volumes of runoff. The lag is due to the time taken for increased runoff to enlarge subglacial channels as a result of higher subglacial flow velocities.

Conversely, towards the end of the ablation season when air temperatures and net radiation are declining, a reduction in the volume of inputs causes a decrease in the capacity of the subglacial drainage system to discharge. This is caused by an increase in net effective pressure, forcing ice to deform into previously enlarged subglacial channels. However, until the TSL permanently decreases in elevation for the duration of the winter, the potential for large runoff events is still high, for example from a late season high intensity rainfall event. Potential for large runoff is due to the high proportion of the glacier that is snow-free, over which runoff is rapid.

# 3 AIMS AND OBJECTIVES

As stated in chapter 1, the general aim of this thesis is to investigate the impact of subglacial water storage and release mechanisms on the capacity of a glacial hydrological system to transfer surface runoff during the late ablation season. Processes controlling storage and release of water within a temperate Alpine glacier will be considered in detail.

To achieve this aim the water balance must first be quantified. This can be achieved using 'black box' modelling techniques that only require knowledge of inputs to and outputs from the glacial hydrological system. Consequently, the following objectives must be achieved:

- To model surface runoff.
- To monitor discharge.

Further understanding of the processes that cause subglacially-routed water to be temporarily stored and then released will be gained by analysing temporal and spatial variations in the subglacial drainage structure. This will be achieved by:

- Monitoring a distributed network of boreholes that hydraulically connects with subglacial drainage.
- Monitoring a distributed network of stakes that reflects motion of the glacier surface.

These measurements will allow:

- Description of the hydraulic character and spatial extent of the subglacial drainage network.
- Identification of processes causing changes in hydraulic connectivity within the subglacial drainage structure.

- Identification of the dominant factors controlling changes in subglacial drainage that influence water storage.

A subsidiary aim is to improve the methodological basis for interpretation of subglacial water pressures at diurnal and seasonal timescales. Therefore, in addition to making temporally and spatially distributed measurements of water pressures there is also a requirement to:

- Develop conceptual models of relationships between subglacial water pressure and borehole water levels.

# SECTION II - FIELD METHODS, SURFACE RUNOFF MODELS AND THEORETICAL DEVELOPMENT OF SUBGLACIAL WATER STORAGE

# 4 RESEARCH DESIGN AND FIELD METHODS

## 4.1 Introduction

Chapter 4 defines the field methods used for analysis of water storage in a temperate Alpine glacier. The location of the study site is outlined and justified in sections 4.2 and 4.3. Description of the field techniques used are presented in section 4.4. This describes the development of an integrated research programme that incorporates measurements of ten separate environmental variables at locations throughout the catchment. This section only presents the practical aspects of the field methodology as the theory behind the use of instrumentation has been previously outlined in chapter 2.

Section 4.5 identifies problems of both faulty and missing data in borehole water level records. Missing borehole water level data were caused by water pressures exceeding the design capacity of the pressure sensor during the day and borehole water levels dropping below the pressure sensor at night. This provided a problem for analysis of phase relationships between inputs, throughputs and outputs within the glacial hydrological system that were used to investigate water storage in section III. Consequently, a justifiable protocol was established that identified when data were faulty. Statistically robust methods, including a worked example, were also developed to reconstruct periods of missing data. As these problems have not been explicitly dealt with in previous borehole studies sections 4.5.1 and 4.5.2 are part of original work by the author.

## 4.2 Location of study site

Findelengletscher is a valley glacier situated in the Upper Rhône basin, Pennine Alps, Canton Valais, Switzerland (Figure 4.1). The catchment incorporating Findelengletscher covers 24.9 km$^2$ (76.7 % of which is glacierised) covering a basin elevation range of 2500 – 4199 m a.s.l. (Collins, 1998a). The longitudinal axis of Findelengletscher is aligned approximately east-west in a down-glacier direction bounded by mountain ridges to the north and east, with the southern boundary comprising a rock ridge between Gornergrat and Stockhorn and a division within the ice-field that feeds both Findelengletscher and adjoining Gornergletscher. The stream draining from Triftjigletscher (a component of the Findelenbach catchment) is diverted by the southern lateral moraine bounding Findelengletscher but is captured by a hydroelectric adduction gallery that joins the stream draining Findelengletscher immediately upstream of the gauge (Collins, 1998a).

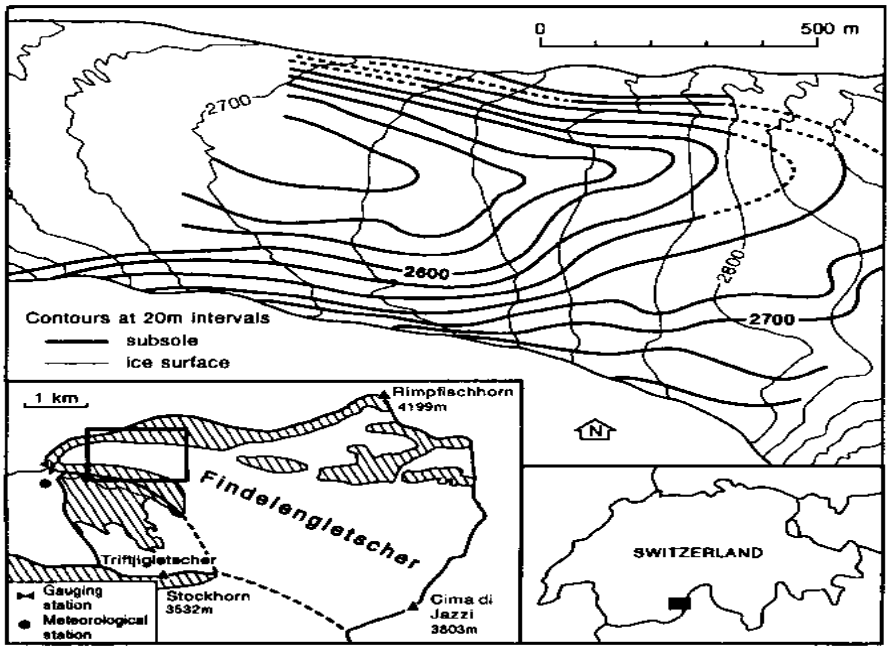



***Figure 4.1 - Location map of the study area, Findelengletscher, Switzerland (Barrett and Collins, 1997).***

The Eurasian-African plate boundary runs across the Findelenbach basin (Bearth, 1953) creating a mix of rock types of continental and oceanic origins. The greatest proportion of the basin is

derived from metamorphosis of Mesozoic sediments such as amphibolite, ophiolite and other ultrabasic rocks (Bearth, 1953) and to a lesser degree contains granites and gneiss. Traces of gypsum and dolomite can be found in thin strips beyond the terminus of Findelengletscher. The rocks underlying Findelengletscher provide a predominantly impermeable surface, other than in discrete areas of exposed jointing. Seismic soundings of the glacier bed have revealed two reflecting horizons (Süsstrunk, 1959) ranging from 10 to 60m apart between the south and north sides of the subglacial area. Although interpretations of the difference in height are uncertain it is possible it indicates a dirt layer within and beneath basal ice, which is corroborated by borehole drilling records (Iken and Bindschadler, 1986). Consequently, a subglacial sediment layer is suggested to exist although its spatial extent and connectivity is highly uncertain.

Findelengletscher is located 46°01' N, 7°50' W where meteorological conditions at summit level (~4200m) are dominated by south-westerly frontal air masses that have picked up hot moist tropical air from across the Atlantic (Barry, 1992). However, much of the moisture from south-westerly frontal movement of air masses across the Alps is deposited as precipitation over the French Alps. Consequently, the Zermatt / Taschaulp valleys are in a semi-arid region where mean annual precipitation (measured at 220m a.s.l.) is only 60cm (Bezinge, 1987).

Microclimates within the Zermatt valley have an important influence on the climatic regime influencing Findelengletscher. Mean annual runoff is used to give an indication of mean annual precipitation after evaporation and mass balance have been taken into account (Kasser, 1973). Consequently, comparison of mean annual runoff of individual upland catchments within the Zermatt valley shows very low flow indices for west-facing, right bank basins (of which Findelengletscher is one) in comparison to east-facing glaciers, despite all catchments in the comparison being highly glacierised and at high elevation (Bezinge, 1987).

## 4.3 Selection of study site

Findelengletscher was deemed suitable for the study for many reasons. Firstly, major logistical support was available from the hydroelectric power company Grande Dixence S.A. enabling helicopter transport of heavy scientific equipment and permanent river gauging infrastructure. Other amenities such as an electrical power point, drinking water and emergency shelter were also provided by Grand Dixence S.A. This allowed long-term habitation and the ability to run an integrated research programme in an otherwise remote environment. Secondly, much previous work has been carried out at Findelengletscher. The Swiss Glacier Commission has monitored the position of the glacier terminus since 1923 and Grande Dixence S.A. (a hydroelectric power company) has recorded hourly resolution discharge of the stream draining from Findelengletscher since 1974. In addition, many workers have investigated subglacial hydrological pathways and glaciological responses to water flow within the catchment using solutes (Collins, 1979b), dye tracing (Moeri and Leibundgut, 1986) and boreholes (Barrett and Collins, 1997; Iken and Bindschadler, 1986; Iken and Truffer, 1997). Finally, much field experience and unpublished data exists and has been made available through the Alpine Glacier Project, which has maintained a continuous series of discharge and water quality measurements throughout the ablation seasons at this site since 1977.

## 4.4 Field Methods

Two fieldwork campaigns were accomplished between June and September in 1998 and 1999 at Findelengletscher. Data collected during the 1998 ablation season was subsequently used as a pilot study whereas the bulk of the data presented in this thesis was collected in 1999. A successful measurement programme collected data describing hydrometeorological inputs (air temperature, incoming solar radiation and precipitation), hydrological throughputs within the

glacier (borehole water levels and dye tracing) and hydrological outputs (discharge and dissolved load) from the glacial system.

### 4.4.1 Hydrometeorological

Hydrometeorological data were measured at two sites within the catchment. One site was temporary and located on the glacier surface at 2750m a.s.l. (meteorological station 1 in Figure 4.2), whilst the other site was permanent and located on bare rock adjacent to the glacier at approximately 2510m a.s.l. (meteorological station 2 in Figure 4.2).

Air temperature, incoming solar radiation (short-wave) and precipitation data were collected from the weather station sited on the glacier surface at 2750m a.s.l. Air temperature was recorded using a Campbell Instruments screened thermometer attached to a tripod so that it was positioned 130cm above the glacier surface. Incoming short-wave radiation was measured using a Kipp and Zonen pyrometer positioned 250cm above the ice surface. Precipitation was recorded using a Casella tipping bucket rain gauge, calibrated at 0.2mm per tip, which was sited on the ice surface. All instrumentation was automatically logged at ten-minute intervals on a Campbell CR10 datalogger.

Air temperature data were also acquired from a weather station sited off-glacier at 2510m a.s.l. that was maintained by Grande Dixence S.A (meteorological station 1 in Figure 4.2). Although air temperature measurements were collected and logged on similar equipment to the on-glacier weather station, data were recorded at an hourly resolution.

Two measurement sites were used, as air temperature measurements on the glacier were significantly influenced by a boundary layer microclimate dominated by an ice surface permanently at or below 0°C (Oke, 1995). Consequently, off-glacier temperature measurements were useful to corroborate or discount anomalous air temperatures recorded on the glacier and were likely to be more representative of air temperatures within the surrounding valley.

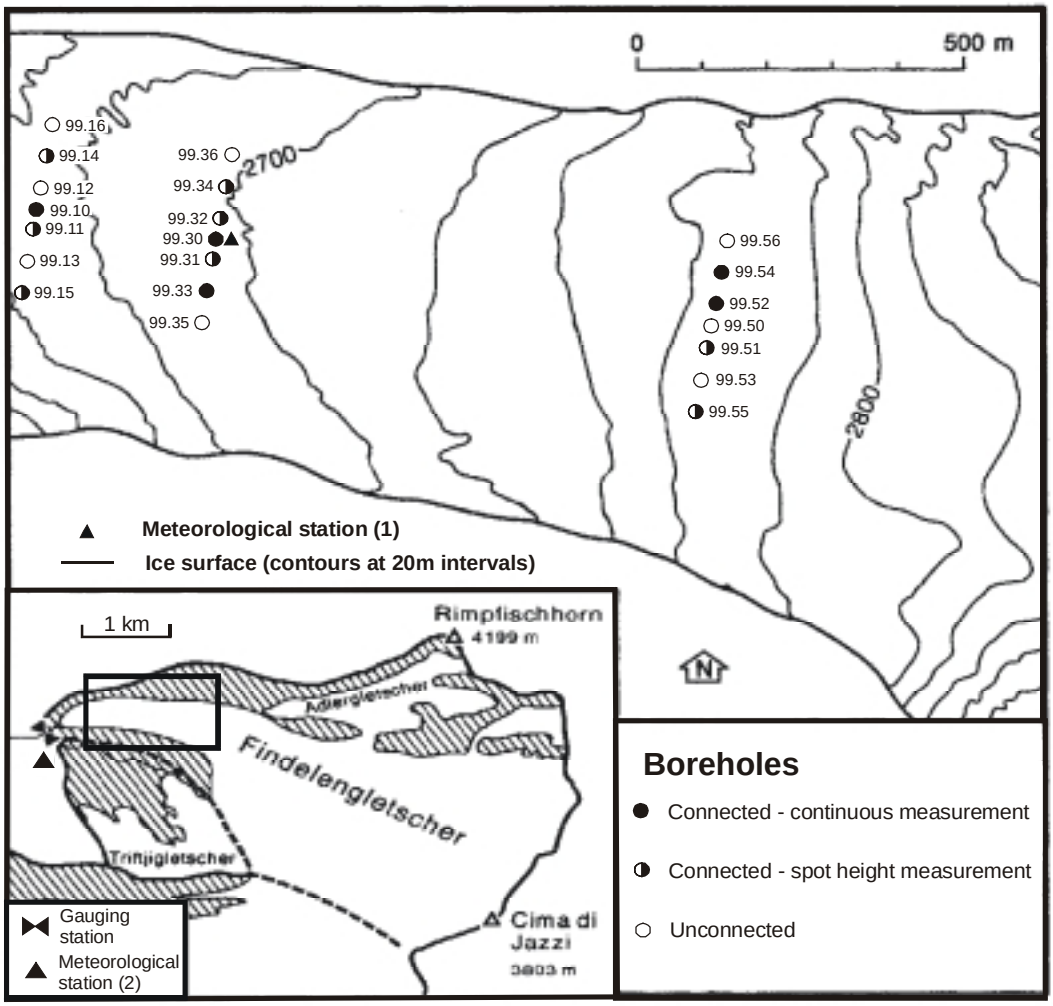



***Figure 4.2 - Map of meteorological stations and borehole locations at Findelengletscher, including type of borehole connectivity with the subglacial hydrological system, during 1999.***

### 4.4.2 Borehole drilling

During the pilot study in 1998 fourteen boreholes were drilled from the surface to the base of Findelengletscher, using a hot-water drill. Twenty-one boreholes were drilled in 1999 following the same procedure.

Drilling was conducted in the ablation zone approximately between 2660m and 2780m a.s.l (Figure 4.2) because previous studies have shown potential for a variety of types of subglacial drainage systems in this area (Barrett and Collins, 1997; Iken and Truffer, 1997). For examination of different drainage types the study location is optimal as it is situated between down-glacier areas that are likely to be characterised solely by conduits and up-glacier areas where drainage is liable to become more distributed (Iken and Truffer, 1997). Chances of the subglacial drainage network in the study area exhibiting varied drainage conditions, such as a confluence of channels linking distributed and concentrated areas of drainage, are increased as a result.

Boreholes were drilled in three structured arrays, each of seven boreholes, which run laterally across the width of Findelengletscher to provide a spatial understanding of changing conditions in subglacial water pressures (see Figure 4.2). Identification of boreholes followed a numbering convention previously instigated for mass balance measurements (Østrem and Brugman, 1991). All boreholes were prefixed by the year in which they were drilled followed by an identification number, i.e. borehole number ten drilled in 1999 would be 99.10. Moving up-glacier along the fall line, boreholes were numbered in increments of twenty, i.e. 99.10, 99.30 and 99.50. Boreholes across the arrays in a up-glacier direction transverse to the direction of ice flow were labelled with even numbers if they were located to the left of the fall line, i.e. 99.12, 99.14 and 99.16, and odd numbers if located to the right, i.e. 99.11, 99.13 and 99.15. The location of the

fourteen boreholes that were drilled during the pilot study in 1998 occupied similar positions to those of boreholes 99.10 through to 99.36. Boreholes adjacent to the central borehole within an array were sited 30m either side. For example, boreholes 99.11 and 99.12 were sited 30m either side of 99.10. Further holes in each array were sited in 50m increments in both directions to create seven holes in each lateral array. For example, borehole 99.13 and 99.14 were located 50m away from boreholes 99.11 and 99.12 respectively. Variable distances between boreholes within an array were used to act as a compromise between gaining extensive spatial coverage of the subglacial drainage network whilst focussing drilling in areas most likely to represent concentrated subglacial drainage, which were determined from the pilot study in 1998.

Boreholes were drilled using pressurised hot water. Water was extracted from diurnally ephemeral supraglacial streams, using a petrol fuelled Honda WB10 pump, and heated by a diesel fired boiler in a modified Kärcher HDS 1000 BE industrial steam cleaner. Water pumped into the Kärcher unit was heated to between 60 and 90 °C and then compressed, which forced it through a variable number of 100m sections of 25mm diameter reinforced PVC Gates HK408 hoses at approximately 5 MPa. Connected sections of reinforced hosing terminated in a 2m long 25mm diameter steel drill stem that culminated in a brass nozzle with a 2.8mm diameter aperture, which acted as the drilling bit. Hosing was threaded through a wheel, supported by a 2.5m high tripod, which supported the drill stem in each borehole. Increased friction created by threading hosing through the wheel allowed the drill operator greater control over the descent of the drill stem as hot, pressurised water cut through the ice. Control over the descent of the drill stem was important to help maintain verticality of boreholes whilst drilling. This allowed the drill stem to hang from the supporting wheel, thereby utilising gravitational forces to control the direction of the incision into surface ice, which initiated the vertical direction of a borehole. As drilling continued, care was taken to prevent the nozzle and stem from resting on the ever-descending cutting face of the borehole, which would have altered the angle of descent through the glacier.

During drilling special attention was paid to water exiting the surface of the borehole. Observations were noted of any increase in suspended sediment or rapid draining or expulsion of water due to the intersection of a borehole with an englacial channel or pressurised englacial water pocket. Such events helped construct ideas of possible englacial and subglacial hydrological conditions in drilling areas. Drilling at each borehole was concluded when there was no significant downward movement over a period of one hour of continual drilling. At this point either the glacier base or an impassable object within basal ice layers was assumed to have been reached. The depths of boreholes drilled in 1999 ranged between 98m and 183m and typically took between three and eight hours to drill.

### 4.4.3 Borehole water level monitoring

In 1999 water levels in five boreholes could be monitored continuously and provided the bulk of the data for this study. Boreholes that connected hydraulically, but were unable to be measured continuously, had manual spot height measurements taken wherever possible using a borehole camera connected by optical cable to a Sony GV-S50E Video Recorder / Monitor. The same equipment provided confirmation of water levels in boreholes that were continuously monitored.

Boreholes that have direct hydraulic connections with the subglacial drainage network act as piezometers and, therefore, the height of the water level in the borehole will be proportional to the pressure at the base of the borehole (Barrett and Collins, 1997). Boreholes connecting hydraulically with the drainage network were monitored continuously using either Druck or Gems TransInstrument pressure transducers submerged in the water column. Gems TransInstrument pressure transducers, designed to measure over a range of 0-40m, were used in boreholes 99.10, 99.33, 99.52 and 99.54. A Druck transducer, designed to measure over a range of 0-160m, was used in borehole 99.30 (see section 11.2 for further information on data loggers

and calibration of transducers). Pressure transducers were installed at optimum heights within the boreholes to maximise overlap between the measurement range of the transducer and the diurnal range in borehole water level. Diurnal variations in borehole water levels frequently exceeded the 0-40m measurement range of the Gems TransInstrument pressure transducers. Attempts were made where possible to maintain continuity of water level data by raising or lowering the pressure transducer within the borehole in response to variation in the elevations of the diurnal range in borehole water levels. However, the pressure transducer units and wire connecting them to the dataloggers on the glacier surface were prone to freezing into the side of the boreholes and subsequently were unable to be moved. Consequently, the ability to maintain a continuous record of borehole water levels proved very difficult, as suggested in the pilot study during 1998 and previous borehole studies (Fountain, 1994; Gordon *et al.*, 1998; Hodge, 1979; Hubbard *et al.*, 1995; Stone and Clarke, 1996).

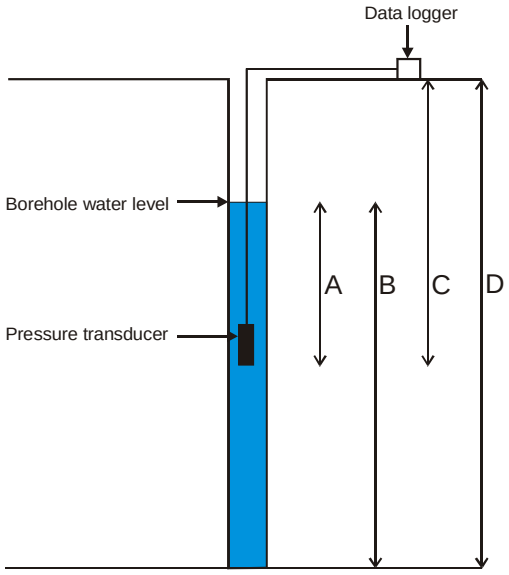



***Figure 4.3 - Calculation of borehole water levels***

Borehole water levels are calculated relative to the glacier surface (Figure 4.3) and are then converted into absolute elevations. Although calculation of water levels uses the glacier surface

as a reference elevation, ablation throughout the measurement period is not incorporated into measurements. Ablation is considered to have a negligible affect on the absolute transducer elevation as freezing of the transducer unit and connecting wire to the side of the borehole has a greater influence.

Data continuity was limited, primarily due to movement of borehole water levels out of the measurement range of the pressure transducers and also because of sporadic equipment failure. In combination with discontinuities in hydrometeorological and proglacial discharge data, despite two years of effort, only frustratingly short discrete sequences in the time-series show simultaneous measurements of all variables. In an attempt to increase the amount of continuous borehole water level data available for analysis, reconstruction of missing data has been carried out, where possible, using methods described in 4.5.2.

### 4.4.4 Dye tracing

Rhodamine- B was used as a tracer to determine transit times of water flow through the glacial hydrological system. Dye injections involved manual flushing of a 6g parcel of dye into the supraglacial stream that flowed into the largest moulin in the glacier, which was located close to the fall line 75m downglacier of borehole 99.10. This moulin was the dominant conduit for supraglacial inputs into the glacier during both 1998 and 1999. Personal communications from other members of the Alpine Glacier Project suggested that this moulin had inter-annual permanence since at least 1996. Dye injections were made in mid-afternoon when supraglacial inputs were estimated to be at diurnal maximums. Analysis of dye return curves focussed solely on the time between dye injection and peak dye concentration at the detection site.

Dye emergence was detected by continuous flow fluorometry at a position ~20m upstream of the gauging station on the proglacial river. At the gauging station Grande Dixence S.A measured hourly averages of proglacial river discharge, which incorporated all waters (other than groundwater) draining from the catchment, including water draining from Triftjigletscher. Discharge was measured continuously to an accuracy of two decimal places ($m^3s^{-1}$) as water flowed through an adduction gallery of known dimensions.

### 4.4.5 Solute load

Electrical conductivity is used as a surrogate for solute concentration in conjunction with discharge data to calculate solute load in the proglacial river. A Campbell 247 conductivity probe, calibrated with 0.01M KCl under standard conditions, was submerged within the adduction gallery of the gauging station. The probe was attached to a Tinylog logger via a pHOX box.

### 4.4.6 Surface velocity and vertical displacement

Surface velocity and vertical displacement were measured using a Global Positioning System. Trimble 4000SSE Geodetic System Surveyors were used to measure vertical and horizontal surface motion. This had an advantage over optical methods as surveying was not affected by adverse weather conditions blocking the line of sight or by refraction errors commonly experienced over ice surfaces.

The study area in 1999 comprised five hollow aluminium stakes (illustrated in Figure 4.4) within an overall network of eleven. Each stake was positioned at approximately 50m intervals along the glacier fall line. Each stake was ~2m long, 35mm in diameter and was hand drilled into the

ice surface to a depth of 1.8m. Periodic re-drilling took place throughout the measurement programme when stakes became unstable due to ablation of surrounding ice. Ice melt at the base of the stakes was limited by using rubber bungs to seal the base, which restricted the amount of heat conducted from the exposed section of the stake into the ice. Furthermore, two holes were drilled near the base of each stake to prevent the stake from floating in any holes that were waterlogged. Both of these modifications helped maintain the accuracy of vertical motion measurements. A numbered flag, following the numbering convention of Østrem and Brugman (1991), was used to identify each stake in a similar manner to that used when numbering the boreholes.

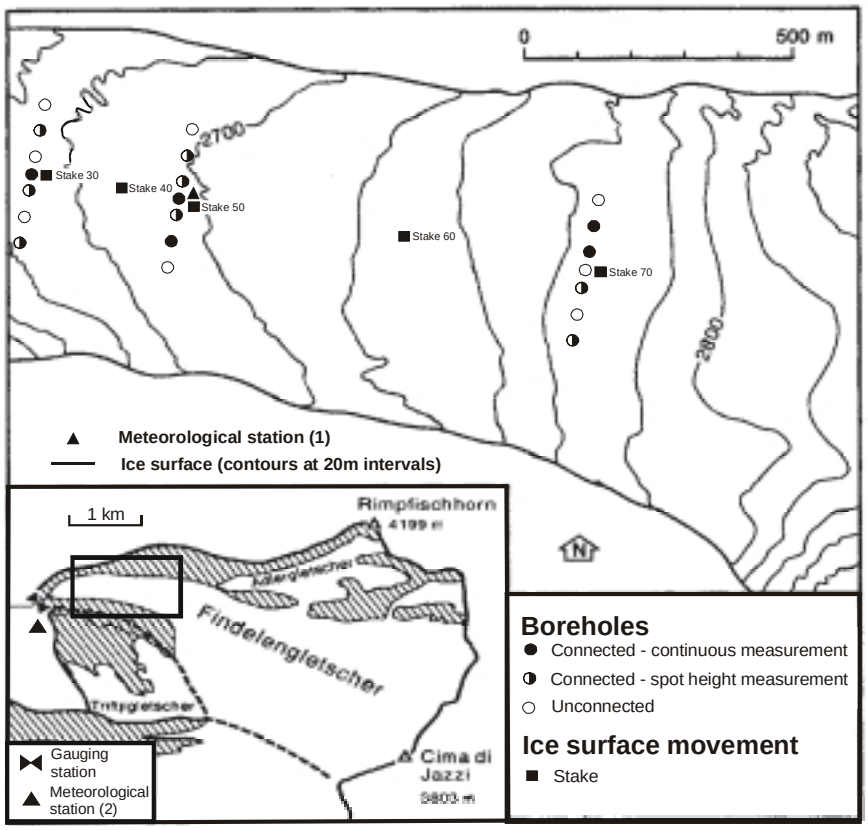



***Figure 4.4 - Positions of stakes used to determine ice surface movement relative to the positions of boreholes.***

Surveying equipment primarily consisted of two self-calibrating 4000SSE receiver units, measuring rods and geodetic L1 / L2 antenna. The units received L1 and L2 signals from the US NAVSTAR network of twenty-four satellites, up to nine of which could be tracked simultaneously by the receivers. When sufficient data from four or more satellites was available the GPSurvey® v2.3 post processing software was capable of computing a horizontal accuracy of positions to 5mm + 1 ppm x baseline length and vertical accuracy to 10mm + 1 ppm x baselength.

Faststatic surveys were carried out relative to two known reference points that were previously fixed by reproducible six-hour static surveys. Differential positioning used L1 and L2 signals to calculate the position of one receiver relative to a known and fixed other. This was used to correct any errors unavoidably introduced into the measurements. Errors included environmental errors such as tropospheric delays or human induced errors such as selective availability, which was introduced by the US Department of Defence to degrade navigation accuracy. Surveys used a roving antenna fixed to the top of each stake in sequence within the stake network relative to the base antenna at a fixed, known position. Results have been modified to account for the tilt and re-drilling of individual stakes and are presented in terms of XYZ coordinates relative to the base station.

Although no electrical interference was observed throughout the surveying procedure the surrounding topography, particularly the peaks directly to the north of Findelengletscher such as Oberrothorn (3414m), occasionally caused signal disturbance by masking a proportion of the sky. A minimum of four satellites in good geometric positions were required to be electronically visible at any one time to make accurate measurements. This is achievable 24-hours a day at any latitude if elevation masks are less than 15°. However, as the surrounding topography caused masks of up to 20°, occasionally lines of sight to satellites which were evenly distributed

throughout six different non-stationary twelve hour circular orbits, were blocked and surveying had to temporarily cease.

## 4.5 Data Management

Conventional data management procedures for downloading and processing field data were followed (see section 11.1), except for post-processing of GPS data which utilised GPSurvey® v2.3 software. Where necessary field calibration of instruments were also completed, the results of which are outlined in section 11.2.

Initial analysis of borehole water level data quickly shows that periods of continuous measurements are short in comparison to the total duration of monitoring and that periods exist within field data where measurements were considered faulty. This required a separate data management strategy that is rarely evident in previous borehole studies. Previous studies may have either encountered similar problems and treated the presented data without explanation. Alternatively, previous studies have concentrated analysis in the short time periods where data has been both accurate and continuous. However, no glaciological studies other than Kavanaugh and Clarke (2000), have explicitly dealt with interpretation of output from pressure transducers after water pressures have exceeded the design capacity of the sensor.

It was important to thoroughly address the problems of both faulty and missing data. Attempts to find the best means of reconstruction were essential as sections of borehole water level data that were missing or faulty tended to occur around extremes in the diurnal ranges. This meant that many daily maximum and minimum values of borehole water levels were missing, which were central to the analysis of phase relationships between inputs, throughputs and outputs within the glacial hydrological system. Consequently, there is a need to create a justifiable protocol that

identified when data were faulty, which required an understanding of how pressure transducers work. Furthermore, there is a need to develop a statistically robust method with which to estimate maximum and minimum values where data were missing or were removed after being identified as faulty. Sections 4.5.1 and 4.5.2 describe in detail the methodological developments created to address problems of faulty and missing data.

### 4.5.1 Identification of faulty data

Filtering faulty data from the raw data set firstly eliminates recorded data that is far above the intended operating range and then eliminates data interpreted as 'faulty' within the operating range. Figure 4.5 shows an example of faulty borehole water level data. Faulty data tends to have an erratic diurnal signal, usually in combination with an inversion in the output when peaks are expected due to defects in the silicon sensor caused by prior periods of high overburden pressure (see section 11.3).

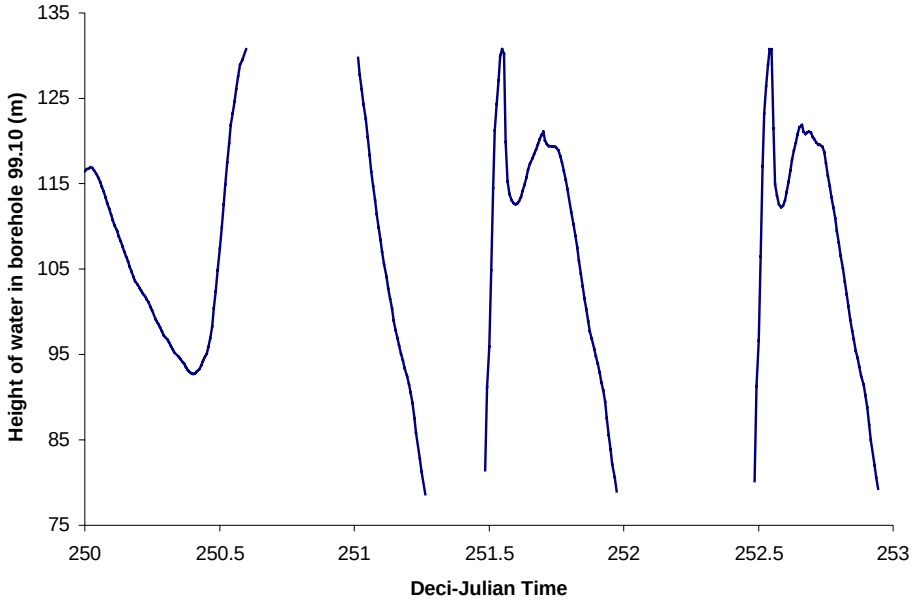



***Figure 4.5 - Faulty borehole water level data from borehole 99.10***

Figure 4.5 exhibits this type of fault over three days of borehole water level data from borehole 99.10 at Findelengletscher. The transducer, located at approximately 77m above the base of the 133m deep borehole, was overburdened by rising water levels late on Julian Day (JD) 250 affecting the ability of the sensor to reflect water pressures at the high end of the intended measurement range, which can be seen as an inversion at the expected time of peak on JD 251 and JD 252 respectively. Determination of the quality, or credibility, of electronic output from pressure transducers relies on a degree of subjectivity to categorise faulty and accurate data. The subjective element to the filtering technique is justified by using basic shape analysis from data prior to the high magnitude overburden event that shows single peaks in the daily cycle (Figure 4.6). This indicates subglacial water pressures exhibit a relatively smooth diurnal cycle. A possible physical explanation for the major deviation in the diurnal pattern is that a high basal water pressure event late on JD 250 changed the subglacial hydraulic connection between the base of the borehole and the subglacial hydrological network to such an extent that a sharp increase in water pressure during the morning of JD 251 caused failure in a sub- or en-glacial hydraulic connection to the borehole. However, this is unlikely due to the repetitive nature of the pattern in further successive diurnal cycles and lack of corroborating evidence for diurnally repetitive ice or sediment failure in previous glacial borehole studies. This reasoning supports the use of subjective filtering. Consequently, it is less likely that false conclusions will be drawn from filtered data than if data regarded as faulty were included in the final record used for interpretation.

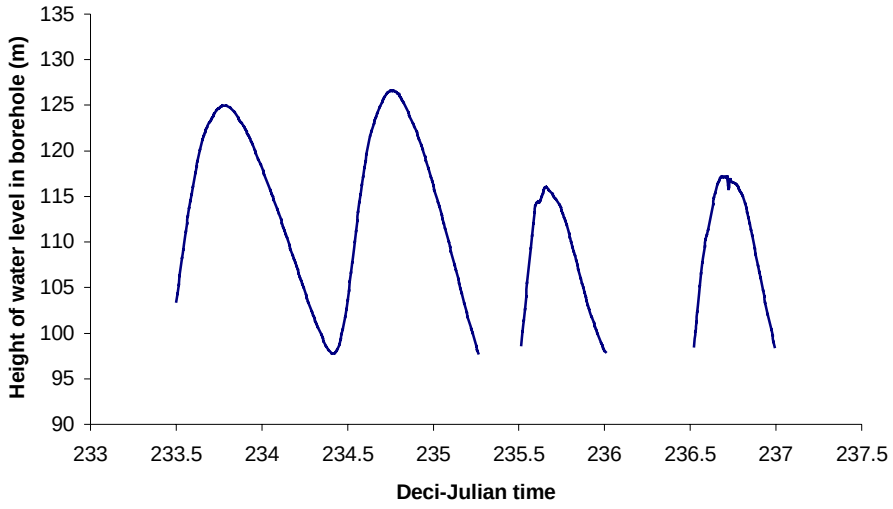



***Figure 4.6 – Peaks in diurnal cycles before overburden pressures affect the pressure transducer in borehole 99.10 (n.b. water levels drop below that of the transducer at night).***

### 4.5.2 Reconstruction of missing data

Periods of missing data occur due to electrical and physical failure in the measurement system (i.e. failure of the sensor, logger or intermediate connecting equipment), failure during recording, downloading and transfer of measured data and failure due to limitations in the measurement range of both sensors and logging equipment. Failure of measurement equipment is exacerbated by cold, wet and dusty glacial environments, which reduce battery life and can damage relatively delicate electrical connections and computing equipment.

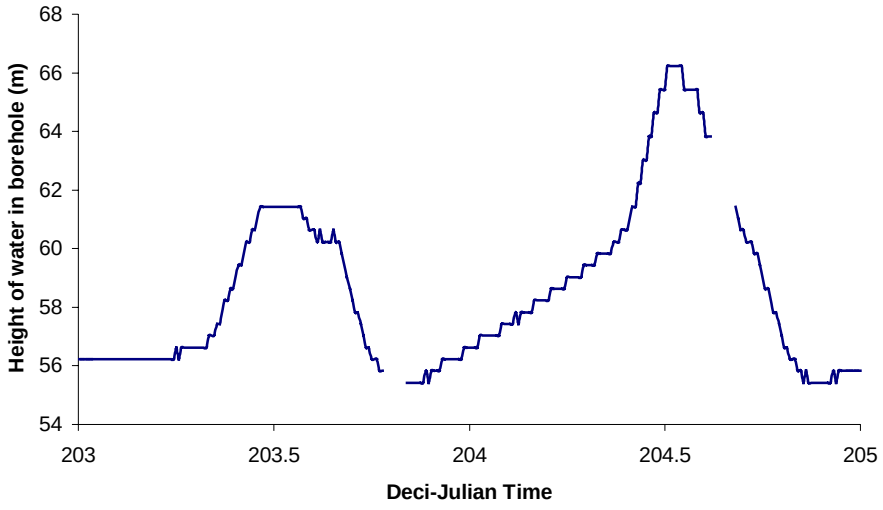



***Figure 4.7 – Low resolution measurements of borehole water level data***

The magnitude of diurnal variations in borehole water levels are affected by variations in water pressure in subglacial drainage channels and by both the distance and hydraulic nature of the connection between the base of the borehole and the subglacial hydrological system. As such influences are both highly spatially and temporally variable, prediction of the diurnal range of borehole water levels required to be measured by pressure transducers is reduced to an estimation. Knowledge of ice thickness at the drill site (~80 to ~190m) provides an upper boundary limit to possible ranges, probably only applicable if the borehole makes a direct connection with a main channel in a well developed drainage system. However, lower boundary estimates are much harder to be made due to such variable subglacial hydraulic influences. Choice of measurement range required of the pressure transducer, therefore, becomes a balance between the resolution and accuracy of data required. A transducer that measures over a range of 0-160m (attached to a logger that measures between 4-20mA) can be placed at the base of a borehole and will detect change in water levels anywhere within the hole. However, as it operates at a relatively low level of resolution (i.e. a 1m change in water level equating to a

variation in output of 0.1mA) it provides a less accurate interpretation of water level movement (see Figure 4.7) than if it were monitored by a transducer attached to the same logger at a higher level of resolution over a smaller measurement range. The detraction to using transducers that are calibrated at a higher resolution for use over a smaller measurement range is that the diurnal range and the median position of the range within the hole can change both progressively or suddenly throughout the ablation season. This can cause diurnal variations to either drop below the level of the measurement sensor (see Figure 4.6) or above the measurement range, which can cause permanent damage to the sensor (see Figure 4.5). Transducers that output at a high resolution over a large measurement range are prohibitively expensive. Transducers have a tendency to freeze into the borehole, thus preventing removal and reclamation. Hence, a balance between costs, resolution, accuracy and the loss of data must be accepted.

Where missing data exists, attempts are commonly made to interpolate between known points, for example during flood events (Barrett and Collins, 1997). As periods of missing data increase relative to the size of the data sets used as a basis for reconstruction, the accuracy and confidence limits of reconstructed data diminishes. An arbitrary limit of twelve hours of missing data in any time-series was used as a maximum limit for data reconstruction to reduce the risk of making false conclusions from reconstructed data. After removal of observed but potentially faulty data, reconstruction of borehole water level data in this manner was only valid for boreholes 99.10 and 99.33.

Methods of reconstruction focussed on regression curve fitting. Best fit is obtained by using the least squares method that minimises the sum of the squares of deviations between data and a fitted curve (Equation 4.1). The goodness of fit is represented by $R^2$ (Equation 4.2). Choice of the regression curve function is largely dependent on physically based prior assumptions. The purpose of the function is to predict a stationary point in a region of missing data, whilst making

fewest possible assumptions regarding the data. It is important for the function to estimate the experimental error within observed data and not to just fit a line through all the observed data points. The simplest fitting function is that obtained by extrapolating two separate linear regression lines through ascending and descending limbs of observed data, and then predicting the maximum or minimum value at their point of intersection. However, this method causes over prediction of the maximum or minimum values and does not make any attempt to account for the smoothness of the previously observed peaks and troughs. A quadratic function takes all the data of both limbs into account but would produce a curve that is symmetric around the stationary point. Previous data normally showed asymmetry. A cubic function, therefore, provides the best function to fit to observed data as it is the least order polynomial that takes into account all observed data, is both smooth and asymmetric around stationary points and allows the maximum error to be calculated.

$$\text{minimum} = \sum_{i=1}^{n} \left( \hat{Y}_i - Y_i \right)^2$$

$$Y = \text{observed value of } y$$
$$\hat{Y} = \text{estimated value of } y \text{ on fitted curve}$$

***Equation 4.1 (Davis, 1986)***

$$R^2 = \frac{SS_R}{SS_T}$$

$$SS_R = \sum_{i=1}^{n} \hat{Y}_i^2 - \frac{\left(\sum_{i=1}^{n} \hat{Y}_i\right)^2}{n}$$

$$SS_T = \sum_{i=1}^{n} Y_i^2 - \frac{\left(\sum_{i=1}^{n} Y_i\right)^2}{n}$$

$R^2 = \text{goodness of fit}$
$SS_R = \text{sum of the squares due to regression}$
$SS_T = \text{total sum of the squares}$
$Y = \text{observed value of } y$
$\hat{Y} = \text{estimated value of } y \text{ on fitted curve}$
$n = \text{number of observations}$

***Equation 4.2 (Davis, 1986)***

A high value of the goodness of fit ($R^2$ approaching 1) suggests a good fit between the observed data and the regression curve, and provides an adequate reconstruction (Figure 4.8). Estimates of physical error from transducers are likely to be severe underestimates of the total error in reconstruction compared to experimental error in observed data, requiring estimates of error of reconstructed data. The mean values of $Y_i$ are the same as the mean values of $\hat{Y}_i$ due to the least squares fit, but the variances are unknown. Assuming the set of twenty observed data points act as a sample from a normally distributed population then this sample can be represented by a Student's t-distribution that acts as a probability density function and is, therefore, useful for establishing the confidence limits on the value of the peak. Critical values of the Student's t-distribution can be read from standard statistical tables that represent integrals under the curve of the distribution. Probability in the distribution is expressed as the number of standard deviations from the mean, at nineteen degrees of freedom (as n = 20). One percent of the area under the curve lies at a distance greater than 2.539 standard deviations (see Equation 4.3) away from the mean. The standard deviation, therefore, gives an estimate of the experimental errors, under

minimum reasonable assumptions of the data set. Consequently, confidence limits of 99% can be derived from the regression curve by displacing the points by this value. This allows an estimate of the uncertainty in the position of the stationary point. A worked example of this procedure can be found in section 11.4.

$$s = \sqrt{\left( \frac{\sum_{i=1}^{n} \left( Y_i - \hat{Y}_i \right)^2}{n(n-1)} \right)}$$

$s$ = standard deviation of the sample
$n$ = number of observations
$Y$ = observed value of $y$
$\hat{Y}$ = estimated value of $y$ on fitted curve

***Equation 4.3 (Sivia, 1996)***

Sensitivity testing of the number of observations used to fit a regression function was carried out. Ten data points either side of the missing period were used to represent properties of the descending and ascending diurnal limbs. Occasionally, observed data points on the ascending and descending limbs furthest away from missing data were removed from the regression calculation where they inhibited the reconstruction.

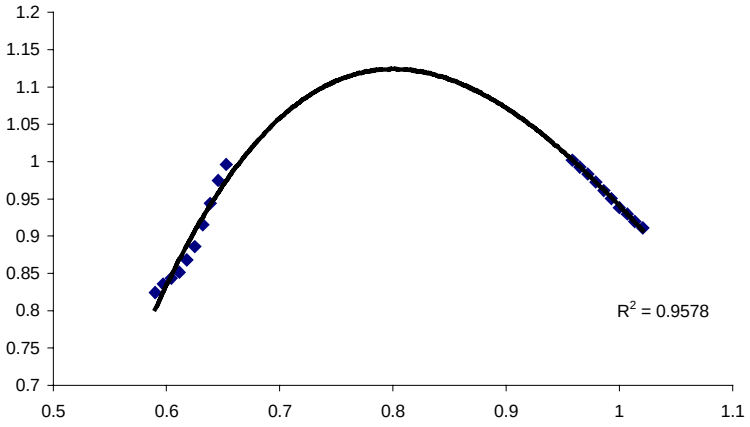



***Figure 4.8 - Regression analysis used to reconstruct data.***

# 5 SURFACE RUNOFF MODEL DEVELOPMENT

## 5.1 Introduction

Calculation of water storage requires estimates to be made of volumes of surface runoff from the glacierised proportion of the catchment. This chapter explains how a surface runoff model was constructed in accordance with the aims and objectives outlined in chapter 3.

In section 5.2 a brief discussion is presented of energy balance and temperature-index models and their synthesis to create the model used to calculate runoff at Findelengletscher, which is an adaptation of a model created by Hock (1999). The necessary spatial and temporal resolution criteria required by the surface runoff model are then outlined. An explanation is also presented of the physical basis required of the model as well as its limitations.

Sections 5.2.1 and 5.2.2 explain how individual components of the model equation are mathematically derived. Then in section 5.2.1 the volume of runoff is calculated at a single position on the glacier surface and in section 5.2.2 runoff is calculated across the entire glacier surface. Application of the surface runoff model to Findelengletscher is considered in section 5.3. Problems inherent in model validation are then discussed and optimisation of the only non-physically based parameter in the model equation is performed and justified.

## 5.2 Model development

Previous studies that calculate surface melt of ice or snow can be broadly split into either temperature index models or energy balance models. Temperature index models are based on assumed relationships between air temperature and ablation. This method lumps all energy exchanges into one or two parameters depending on the number of degree-day factors used to describe the surface of a catchment (see Equation 5.1).

$$M = \frac{1}{n} DDF_{snow/ice} T$$

$M$ = melt rate ($mm\ hr^{-1}$)
$n$ = time steps ($n = 24$)
$DDF$ = degree day factor for snow or ice ($mm\ d^{-1}\ °C^{-1}$)
$T$ = Positive air temperature (°C)

***Equation 5.1 - (Hock, 1999)***

$$Q_N + Q_H + Q_L + Q_G + Q_R + Q_M = 0$$

$Q_N$ = net radiation
$Q_H$ = sensible heat flux
$Q_L$ = latent heat flux
$Q_G$ = change of heat in a vertical column from the surface to the depth at which vertical heat transfer is negligible
$Q_R$ = sensible heat flux from rain
$Q_M$ = energy for melt

***Equation 5.2 - (Hock, 1998)***

Energy balance models involve the assessment of energy fluxes into and out of the snow or ice surface under investigation. This method is much more descriptive of the physical processes involved in causing melt than the temperature index model. However, there is much uncertainty in many of the physical processes involved in energy exchange requiring parameterisation and assumptions, many of which are violated by reality. Equation 5.2 shows an energy balance equation where the surface is assumed to be at 0°C and any surplus energy is immediately used for melting. Melt rates are calculated by dividing the energy available for melt by the density of water and the latent heat of fusion. For further information Hock (1998) provides a thorough assessment of both types of model and presents a comprehensive review of previous work.

Both types of model provide a physical basis to calculations of surface runoff. Consequently, the choice of model is essentially dependent on availability of data and the heterogeneity of the catchment. As valley glaciers such as Findelengletscher are highly heterogeneous, the amount of meteorological and background topographic data required of a detailed energy balance model is large (Arnold *et al.*, 1996). However, meteorological data available to this study is limited to air temperature, incoming solar radiation and precipitation. This would cause an increase in parameterisation of many processes that cause melt and consequently reduces the appeal of a complex energy balance model. Accordingly, the surface runoff model required to provide volumes of inputs with which to analyse water storage in section III should be a semi-distributed simple energy balance model, which attempts to accurately replicate variations in both timing and magnitude of surface runoff. The aim of the model is to produce an hourly time series of total surface runoff, including both melt and precipitation over the Findelen catchment upstream of the gauging station, which incorporates spatial differences in runoff intensity. Therefore, the objectives of the model are as follows:

1) Estimate volumes of meltwater runoff from variations in the timing and magnitude of total energy fluxes into the glacier as a function of incoming short-wave radiation and sensible heat.

2) Estimate the physical state of precipitation (rain or snow) and the volume of direct runoff produced.

3) Sub-divide the catchment into elevation bands to allow incorporation of spatial variation in intensity of precipitation and melt rates.

### 5.2.1 Temporal variation in surface runoff at a single point on the glacier surface

Total discharge in the proglacial river is the product of ice and snow melt, precipitation and any groundwater or pressurised sub-surface up-wellings (Lawson, 1993). Volumes of ground-water from up-wellings are hard to quantify accurately and are unlikely to account for a significant component of proglacial discharge in comparison to surface meltwater and precipitation. Consequently, total surface runoff into the glacial hydrological system is calculated by the addition of runoff from meltwater and precipitation. Meltwater runoff is calculated using an energy balance model (Equation 5.3) slightly adapted from Hock (1999) that uses short-wave radiation and air temperature data. Runoff from precipitation is calculated directly from spatial extrapolation of field data. All notations used in equations in this chapter are listed in Table 5.1. Although the basis for calculation of surface runoff has been taken from a previously published model (Equation 5.3) the assembly of constituent parts of the model have been completed solely by the author. Equally, construction of a computer code in FORTRAN90 to process data in the prescribed manner is the author's original work and can be seen for reference in section 11.7.

$$M = \begin{cases} \left( \frac{1}{n} MF + a_{snow/ice} I \frac{G_s}{I_s} \right) T : T > 0 \\ 0 \qquad\qquad\qquad : T < 0 \end{cases}$$

***Equation 5.3 - (Hock, 1999)***

| **NOTATION** | |
|---|---|
| $\phi$ | Angle of incidence between the normal to the surface and the solar beam |
| $\psi$ | Atmospheric clear sky transmissivity |
| A | Latitude |
| $a_{snow/ice}$ | Radiation coefficient (different for snow and ice surfaces) |
| az | Solar azimuth angle |
| b | Slope angle |
| d | Declination (degrees) |
| Ds | Diffuse radiant power ($Wm^{-2}$) |
| E | Value of the Equation of Time |
| $G_s$ | Measured global radiation at the ground surface ($Wm^{-2}$) |
| H | Hour angle |
| *I* | Direct short-wave incoming solar radiation (clear sky) ($Wm^{-2}$) |
| $I_0$ | Solar constant (~1368 $Wm^{-2}$) |
| $I_s$ | Potential clear sky direct solar radiation at the measurement point ($Wm^{-2}$) |
| L | Longitude |
| $L_0$ | Longitude of the standard meridian defining the local time zone |
| Lhf | Latent heat of fusion of water (0.334 MJ $kg^{-1}$) |
| m | Relative air mass |
| *M* | Melt rates (mm $hr^{-1}$) |
| MLT | Surface melt rate |
| *MF* | Melt factor |
| *n* | Number of time steps per day |
| Nm | Number of days since 21 March |
| P | Atmospheric pressure (Pa) |
| $P_0$ | Mean atmospheric pressure at sea level (Pa) |
| q | Transmission coefficient |
| qg | Transmission coefficient for air (dry and clean) |
| qw | Transmission coefficient for water vapour |
| qs | Transmission coefficient for aerosols |
| Qds | Direct irradiance of a sloping surface ($Wm^{-2}$) |
| Qd | Solar beam irradiance measured at ground level onto a surface facing the sun ($Wm^{-2}$) |
| *R* | Instantaneous Sun-Earth distance |
| *Rm* | Mean Sun-Earth distance |
| sa | Solar altitude (or solar elevation) |
| sz | Slope azimuth angle (i.e. aspect) |
| t | Transmissivity |
| T | Air temperature (°C) |
| Tlm | Value of *Tt* after subtraction of the Equation of Time correction |
| Tls | Local standard time |
| Tt | True solar time |
| Tu | Universal time |
| *Z* | Local zenith angle |

***Table 5.1 - Notation used in equations.***

Short-wave rather than long-wave radiation fluxes dominate the radiative energy component of 'global radiation' ($G_s$ in Equation 5.3) due to limitations of measurement equipment. Air temperature is used as a surrogate for sensible heat fluxes in calculations of melt rates in Equation 5.3. Complexities in energy transfer of sensible heat through interactions between surface topography and boundary layer atmospheric movement, which are discussed in section 2.3, have not been incorporated in melt estimates again due to limitations in measurement instrumentation.

$$I = I_0 \left( \frac{Rm}{R} \right)^2 \psi^{((P/P_0)/\cos Z)} \cos\phi$$

***Equation 5.4 - (Hock, 1999)***

Equation 5.4 provides the basis for computation of maximum potential short-wave radiation fluxes on a sloping surface on the earth. Following Equation 5.4, the following terms in Equation 5.5 require estimation. Equation 5.5 accounts for the position of the sun in the sky relative to the calculation point on the earth's surface at any point during the year. Equation 5.4 accounts for extra-terrestrial radiation at the edge of the atmosphere and both diffusion and reflection of the solar ray through the atmosphere. However, although Equation 5.4 incorporates a parameter ($\psi$) that describes the transmissivity of the atmosphere this does not account for separation of short-wave radiation received at the earth's surface into direct irradiance (*Qds*), see Equation 5.6 and diffuse irradiance (*Ds*), see Equation 5.7.

$$\cos\phi = \cos b.\sin sa + \sin b.\cos sa.\cos(az - sz)$$

$$sa = 90 - A + d$$

$$d = 23.45 \times \sin\left(\frac{360}{365} Nm\right)$$

$$\cos(az - sz) = \cos az.\cos sz - \sin az.\sin sz$$

$$\sin az = -\cos d \times \frac{\sin H}{\cos sa}$$

$$H = 15 \times (Tt - 12)$$

$$Tt = Tu - \frac{L}{15} + \frac{E}{60}$$

$$Tu = Tls + \frac{L_0}{15}$$

$$\cos az = \frac{(\sin d - (\sin A.\sin sa))}{(\cos A.\cos sa)}$$

***Equation 5.5 - (Linacre, 1992)***

$$Qds = Qd \times \cos\phi$$

$$Qd = I_0 \times q^m$$

$$m = \frac{P}{1013 \times \sin sa}$$

$$q = qg \times qw \times qs$$

***Equation 5.6 - (Linacre, 1992)***

$$Ds = 94(\sin sa)^2.(\cos(b/2))^2$$

***Equation 5.7 - (Linacre, 1992)***

Although inclusion of Equation 5.6 and Equation 5.7 would increase the physical basis for melt calculations, separation of the transmissivity parameter into diffuse and direct components, incorporating individual physical mechanisms that cause attenuation, are not included in calculation of total melt rates. Their inclusion would be unlikely to add to the accuracy of melt rate estimates and instead further error may be encountered in prediction of the coefficients themselves. Instead, the clear sky transmissivity parameter is estimated to be 0.75 (Hock, 1999) calculated from the mid-point of the range 0.6-0.9 of measured values from other studies (Oke, 1995).

The short-wave radiation component of Equation 5.3 is incorporated into the second term in parenthesis. The amount of short-wave radiation that reaches a sloping ground surface is found by scaling maximum potential short-wave radiation fluxes ($I$) for the desired calculation point on the earth's surface at a particular time, using a ratio of measured incoming radiation or 'global radiation' relative to the maximum potential radiation at the position of measurement ($\frac{G_s}{I_s}$). As the position of radiation measurement becomes nearer the point of calculation, the ratio will become more representative of changes in short-wave incoming radiation due to atmospheric attenuation. An albedo parameter ($a_{snow/ice}$) that describes reflectivity of the surface to incoming radiation is incorporated. The parameter is physically based using measured albedo values of snow and ice at Findelengletscher of 0.195 and 0.7 respectively (Bezinge, 1987). Actual values of the albedo parameters used in the melt model use the measured albedo scaled by $10^{-4}$ to increase the fit between the magnitudes of predicted and measured melt rates. However, the relative difference between reflectivity of different surfaces is maintained allowing spatial delimitation of melt rate intensities. The use of a physically based parameter is a departure from Hock's model that uses statistically optimised values rather than values linked to albedo.

Temporal resolution of melt rates are controlled by the time step increment ($n$) that is presented as a fraction of a daily cycle in the first term in parenthesis. Consequently, for hourly increments the value of $n$ = 24. This time step increment provides the denominator for the melt factor parameter, which is the only parameter ($MF$) in the model that is not physically based. The melt factor parameter describes conversion of sensible heat fluxes into meltwater and becomes dominant within the parenthesis when measured radiation is low. For example, using optimised parameter values derived by Hock (1999) over one hour time steps at a single point on Storglaciären, Sweden (Table 5.2), the first term within parenthesis dominates the melt rate equation when radiation drops below 87.5 $Wm^{-2}$ and 12.5 $Wm^{-2}$ for ice and snow surfaces respectively. Consequently, the first term in parenthesis and air temperature act in combination as a proxy for combined meteorological and terrestrial conditions that absorb incoming radiation and emit heat via conduction, which accounts for melt at night caused by sensible heat.

| Climatic input data | Melt-model parameters | Optimised values |
|---|---|---|
| Air temperature | Melt factor ($MF$) | 2.1 |
| Global radiation | Radiation factor for ice ($a_{ice}$) | 0.001 |
| | Radiation factor for snow ($a_{snow}$) | 0.0007 |

***Table 5.2 – Model parameters (MF is in mm $d^{-1}$ °$C^{-1}$ and radiation factors are in $m^2$ $W^{-1}$ mm $h^{-1}$ °$C^{-1}$) at Storglaciären, Sweden (Hock, 1999).***

In Equation 5.3 air temperature expresses the intensity of melt and is the dominant controlling influence in the model over the sum of both terms in parenthesis. Negative melt rates, produced in Equation 5.3 if air temperatures are negative, are avoided by the incorporation of a binary multiplier that reduces the melt rate to zero if air temperatures drop below a threshold of 0°C, thus maintaining conceptual correctness. Using example parameter values from Hock (1999), see Table 5.2, the importance of terms in and out of parenthesis for calculation of melt rates of an ice surface are shown to be equal in magnitude. Variation within the parenthesis is caused by radiation, theoretically ranging between 0 $Wm^{-2}$ and 1368 $Wm^{-2}$, which gives a product over

hourly time steps of between 0.0875 and 1.4555 (a difference in magnitude of order two). Variation outside the parenthesis is dependant solely on air temperature, which is measured to an accuracy of 0.1°C (on a scale where T > 0°C). In practice the difference in magnitude between maximum and minimum air temperatures used by the model is also of order two. Neither measured variable exhibits a variation that overwhelms the influence of the other, instead it allows observed variation in either of the measured data sets to control melt rate output.

Surface runoff derived from melt may be supplemented by rainfall, which occurs over discrete time intervals to produce the total volume of runoff at a particular point within the catchment. Air temperature thresholds dividing the physical state of precipitation have been found to be highly site specific, ranging around small positive values, typically 1.5°C and 2.8°C (Ersi *et al.*, 1995; Rohrer, 1989). However, in the model precipitation is separated into either snow or rain depending on an air temperature threshold of 0°C. This keeps the model conceptually correct despite not maintaining absolute accuracy. If precipitation coincides with an air temperature greater than 0°C infiltration rates into surface ice are assumed to be zero. Therefore, direct surface runoff is assumed at all measurement points within the catchment. Transfer of latent heat between liquid precipitation and ice due to rainfall refreezing or frictional melt resulting from running water over the ice surface are not considered. As methods of data collection were insufficient to quantify snowfall, any precipitation events when air temperatures are equal to or less than 0°C are not included as inputs to the hydrological system.

Hourly volumes of meltwater are calculated from the product of energy fluxes in Equation 5.3 that have been divided by the latent heat of fusion to produce a meltwater runoff volume in millimetres of water equivalent. Hourly volumes of precipitation are then added to calculated volumes of meltwater to produce the total surface runoff (TSR).

### 5.2.2 Runoff across the glacier surface

The purpose of the melt model is to reflect spatial as well as temporal variations of physical mechanisms controlling melt production and runoff from precipitation. Spatial extrapolation of total runoff from a single point, over the whole catchment requires sub-division of the catchment into units or grid-cells that act in a homogenous manner. An optimum level of catchment sub-division involves a grid-cell resolution that enables the model to be physically based, yet not so reductionistic that it requires a very high level of resolution to account for the heteorogeneity of variables controlling surface runoff. Consequently, grid-cells of 100m elevation bands across the catchment (including both glacierised and non-glacierised areas) are used to accommodate changes in air temperature and precipitation, which along with radiation, are the main inputs to the model.

Air temperature is measured at different elevations both on and off glacier. It is extrapolated across the catchment from the off-glacier measurement site at the lowest of the two elevations using a lapse rate applicable to the free atmosphere of 0.6°C $100m^{-1}$ (Barry, 1992). This requires an assumption that atmospheric structure in a mountain environment is laminar, approximating the free atmosphere. Although this is a departure from reality it is coherent with the idea of separating differences in air temperature into isotherms of similar elevation. Calculation of a lapse rate using the average difference in air temperatures between measurements at different elevations on and off glacier was rejected. It was rejected due to the affect of the glacier surface (maintained at or around 0°C) on the boundary layer microclimate relative to the off-glacier meteorological station sited above bare rock. The glacier surface microclimate exaggerated the decrease in air temperatures between measurement elevations on average by 2.1 °C $100m^{-1}$. This is calculated using differences between the two-day running averages of air temperature at each elevation, causing underestimations of energy inputs when extrapolated across the entire

catchment. Off-glacier measurements are used in preference to on-glacier measurements as the point from which air temperature is extrapolated because there are less anomalously low measurements than in the on-glacier record. Such anomalously low measurements are possibly caused by instrument error or highly localised meteorological conditions that do not accurately reflect fluctuations in air temperature over the whole catchment. Consequently, variations in calculated sensible heat fluxes rely solely on air temperature changes with elevation and do not take into account micro scale interactions between glacier surface topography (surface roughness), wind speed or turbulent movement of air in the boundary layer.

Incoming short-wave solar radiation received within a glacierised catchment varies due to glacier surface hypsometry and shading from surrounding topography. Over a diurnal cycle, incoming solar radiation at sunrise illuminates the glacier surface first at the highest elevation then last at the snout and vice versa at sunset. The increased length of time that higher elevations of the glacier surface are exposed to direct short-wave radiation, compared with lower elevations, will not have that great an effect on daily melt totals due to low intensities of the solar beam at extremities of daylight hours. Consequently, there is little advantage of incorporating diurnal differences in short-wave radiation into grid cells, delimited in 100m elevation bands, into the melt model. However, if topography surrounding the glacier rises steeply, which is common around valley glaciers such as Findelengletscher, the diurnally varying solar elevation needs to have a very high angle to avoid shading areas of glacier surface. Shaded areas will only receive diffuse radiation causing a reduction in melt rates. Incorporation into melt model calculations of diurnal variations in glacier surface shading, by subdivision of the maximum potential short-wave radiation into a direct and diffuse component, needs a detailed digital elevation model of the entire catchment and a high resolution of grid-cell size. Incorporation of spatial differences in surface shading propagating from south to north across Findelengletscher, would substantially increase realism into the physical basis of the melt model (Arnold *et al.*, 1996; Hock, 1999).

However, the grid cell resolution required to accurately describe shading would require sub-division of the presently homogenous grid-cells of similar elevation (every 100m). This would require a greater resolution of other variables, such as slope angle for which data is not available, in order to make the model consistent. However, some of the affects of topographically induced shading may be incorporated into some measurements of global radiation ($G_s$) made at meteorological station 1, which is located at 2738m on the glacier surface. Other attenuating affects on radiation, such as cloud cover, are also incorporated into $G_s$ and are then extrapolated spatially across the catchment without any alteration for differences in elevation.

Topographic influences on absorption of incoming short-wave radiation are controlled by surface albedo and the angle that the ice surface makes with the solar beam (Linacre, 1992). Maximum intensities of radiative energy input from incoming solar radiation per unit of surface area, occur when the solar beam is perpendicular to the ice surface. As glacier surface slope angle varies widely in three dimensions causing dispersion or concentration of the solar beam, there is great heterogeneity in the amount of energy that is absorbed or reflected over all illuminated areas of the glacier surface at any one time. Slope angles for each grid cell are calculated by averaging transects in a down-glacier direction, within each 100m elevation band in glaciated sections of the catchment, which provide a single angle that reflects grid-cell location within the basin hypsometry. As the model is designed to predict spatial distribution in the production of combined volumes of meltwater and direct precipitation, rather than inclusion of any routing component describing the transit of water from location of production to the proglacial river, the effect of slope angle on velocity of surface runoff within a grid-cell is not considered.

Difference in glacier surface albedo, which is crudely divided into either snow or ice, is demarcated by the elevation of the transient snow line (TSL), describing the boundary position between ice and snow within the catchment. Seasonal variations in the elevation of the TSL are

traced using field observations to the nearest 100m, ensuring subdivision of a single grid-cell into either ice or snow that allows the application of the appropriate radiation coefficient ($a_{snow/ice}$) into Equation 5.3. Although more sophisticated methods for observing variations in the TSL have been developed at Findelengletscher using numerical modelling of the retreating snowpack (Turpin, 1998) field observations are sufficient to make accurate measurements of the TSL at 100m resolutions. Figure 5.1 illustrates interactions between the increased elevation of the TSL and glacier surface hypsometry, which causes a non-linear relationship to exist between increases in the TSL and changes in percentage of the glacier surface that is snow-free. Rates of increase in elevation of the TSL are linked to rapid rates of increase in air temperature with the onset of the ablation season. After an initial rapid increase, the elevation of the TSL then stabilises for the majority of the ablation season due to constraints imposed by the basin hypsometry (Collins and Lowe, 1997). However, if a rapid drop in the elevation of the 0°C isotherm coincides with a precipitation event, snowfall will cause a temporary drop in the TSL. Attempts to calculate the timing, magnitude and intensity of snow, either falling or melting, are not incorporated in the melt model due to limitations of measurement equipment. Instead, during periods where air temperatures are at or near 0°C, careful field observations are made of precipitation events allowing adjustment of the TSL in the model, at a daily temporal resolution, to account for changes in meltwater production.

Precipitation measured at meteorological station 1 on the glacier surface is assumed to have fallen ubiquitously over all glacierised areas of the catchment. However, estimates of direct runoff from rainfall are only spatially extrapolated over grid cells that are snow-free. If the cell is snow-covered (i.e. above the TSL) it is assumed that precipitation falling as a liquid will freeze as it percolates through the snowpack due to temporally variable sub-zero temperatures within the snow and firn (Singh, 1999) and consequently is not incorporated in calculations of direct runoff production. This is a relatively simple interpretation of water flow through snow, which may not

accurately reflect isothermal characteristics within the lowest elevations of the snowpack where refreezing is unlikely. Calculations of direct runoff are extrapolated spatially from the single measurement point at meteorological station 1, accounting for changes in intensity with elevation using a precipitation gradient. The precipitation gradient is calculated from estimates of 99mm/100m/annum made in Valais (Swiss Alps) from elevations between 1700m to 3810m by Lang (1985), which equates to a precipitation gradient of 0.0001301 mm/m/hr.

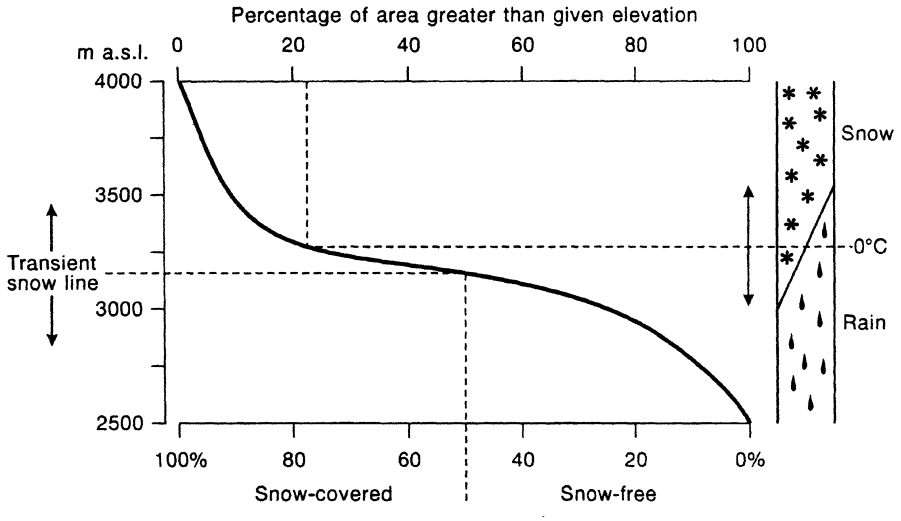



***Figure 5.1 - Interaction of vertical movements of the transient snow line with catchment basin hypsometry of Findelengletscher, Switzerland (Collins, 1998).***

## 5.3 Model application and parameter optimisation

The purpose of the model is to calculate temporal changes in total surface runoff from a combination of meltwater and direct precipitation in the Findelen catchment up-valley of the gauging station. The major benefits of using this model instead of just a time-series of individual meteorological variables are that it reflects spatial differences in the intensity of runoff across the catchment. Individual meteorological variables would only illustrate temporal differences at a single point within the catchment. Model outputs are then used to provide estimates of total surface runoff entering the glacial hydrological system. Changes within this time series of inputs to the hydrological system can then be contrasted relative to changes within the time series of outputs to estimate water storage.

Although construction of a physically based model has been achieved, verification and validation of both the magnitude and timing of fluctuations in modelled output remain. Verification of the model was achieved by numerically testing the code through step-wise calculations, using separate programming techniques, on a sample data set in a 3 by 2 matrix (three temporal units by two spatial units). Equality of the calculations at each stage allowed corroboration of the computational methods used.

Validation of the model concerns whether the simulation provides a good representation of reality (Viessman and Lewis, 1996). Total surface runoff, which is 'reality' in this situation, can be quantified using a combination of rain gauge and ablation measurements. Melt rates are measured using ablation stakes, the resolution of which are accurate to the daily scale at the highest resolution (Munro, 1990). Higher resolution measurements, for instance half hourly resolution using electric ablatometers (Lewkowicz, 1985), could not be made due to unavailability of equipment. However, modelled melt rates are calculated at an hourly temporal

resolution, which are much higher than the resolution of melt measurements using ablation stakes. As melt measurements using ablation stakes do not provide an accurate enough resolution with which to validate temporal fluctuations in model output at an hourly resolution, discharge measurements on proglacial rivers are commonly used to quantify fluctuations in total surface runoff (Arnold *et al.*, 1996; Richards *et al.*, 1996; Willis *et al.*, 1991/1992a). However, to allow accurate validation of modelled outputs a routing component, which reflects the transit time of surface runoff from the point of production through the glacial hydrological network to the point of discharge measurement, must be incorporated into the model. Hock (1999) coupled a discharge-routing model based on Baker et al (1982) and used by Hock and Noetzli (1997) on Storglaciären, Sweden, to the melt model outlined in Equation 5.3. The routing component assumes runoff flows through a series of three linked linear reservoirs (snow, firn and ice), each of which is assigned a parameter describing the velocity of water flow. Parameters of flow velocity (or storage) in the discharge-routing model vary for each reservoir but remain constant in time. Consequently, to validate the model using proglacial river discharge, assumptions must be made of the capacity of the glacial hydrological system to discharge inputs from surface runoff. Assumptions that reservoirs act as linear systems, where capacity to discharge is proportional to the volume of water in the reservoir, can be used as a means of comparison for the investigation of temporal change in subglacial channels (Richards *et al.*, 1996). However, if temporary changes occur within a reservoir, from a constriction or expansion in the pathway of water flow, further assumptions at increasing spatial resolution are necessary regarding the location of a perturbation within the system and the rate at which the capacity to discharge changes. The affect of flow perturbations on temporary storage and hydraulic efficiency will result in changes to the diurnal pattern of proglacial river discharge.

The diurnal pattern of modelled surface runoff is inherently different to that of proglacial river discharge. Surface runoff is considered as an instantaneous volume totalled across the entire area

of the catchment at any one point in time. Neither transit times to points of concentration nor rate limiting factors on water flow need to be considered as influences on the diurnal pattern. As surface storage is not a consideration, the diurnal pattern is likely to be much more responsive to fluctuations of input variables and is not 'dampened' by effects of temporary subglacial storage on proglacial discharge. Consequently, attempts to validate the modelled runoff data with proglacial discharge data by comparison of diurnal patterns will be flawed as both patterns are influenced by different physical mechanisms. Data from boreholes are used to increase the spatial resolution at which temporal changes of storage within the subglacial drainage system can be monitored. Therefore, it is inappropriate to make assumptions of discharge routing using linear reservoirs with constant storage parameters for purposes of model validation.

Validation of model output cannot be made using ablation measurements, due to incompatibility of the temporal resolution. As extra assumptions of subglacial flow conditions that are needed in a discharge routing model to compare melt inputs against hourly measurements of proglacial river discharge are inappropriate an alternative theoretical approach is required.

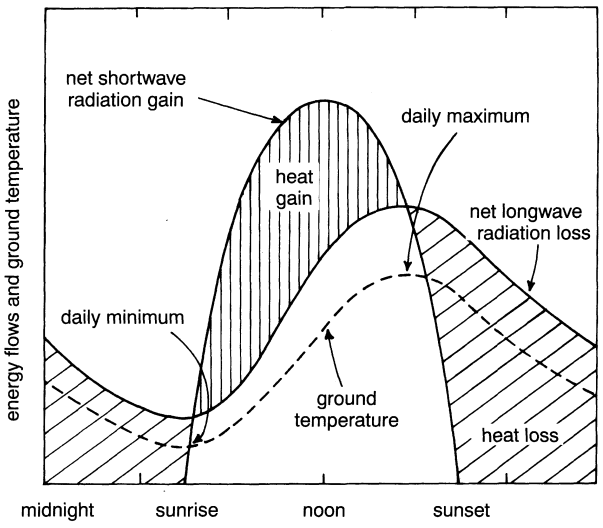



***Figure 5.2 - Typical variations of radiation input and loss at ground level (Linacre and Geerts, 1997).***

A more qualitative method of validation can be performed by comparing modelled output with the timing of diurnal maximums and minimums of theoretical variations in energy fluxes. Maximum radiative energy fluxes will occur at solar noon. Figure 5.2 illustrates an idealised situation at a longitude of 0° using Greenwich Mean Time (GMT) under a cloudless sky. The timing of solar noon varies with longitude, daylight saving time and a seasonal correction described by the equation of time. At a longitude of 7° East, the longitude of the Findelen catchment, timing of solar noon during June to September will fluctuate (dependent on the equation of time) around 13:28 (BST) or 14:28 (CET). In reality, timing of peak melt rates incorporate a lag that accounts for change in the physical state of water from solid to liquid and the influence of sensible heat. Diurnal fluctuations in sensible heat are controlled by long-wave radiation loss that tends to peak later in the diurnal cycle, indicated by ground temperature in Figure 5.2.

Timing of diurnal troughs in glacier melt are more stable and occur just before sunrise when both incoming short-wave radiative energy and long-wave radiation loss are at a minimum. Timing of peaks and troughs in meltwater runoff relative to similar points in the daily pattern of proglacial river discharge can be used to help indicate the validity of the model. Both peaks and troughs in meltwater runoff should occur before peaks and troughs in discharge.

Transit times of meltwater runoff from the glacier surface to the gauging station were measured using dye tracing techniques showing an average transit time of approximately two hours at times of high diurnal flow. Thus, peaks in meltwater production should occur approximately two hours before peaks in proglacial discharge. Troughs in surface runoff are much harder to demarcate in this manner, as the timing of troughs in discharge will depend on antecedent conditions that influence the amount of temporary storage (over successive diurnal cycles) and, therefore, the velocity of water flow through the hydrological system. However, lag times between the onset of

melt at sunrise and the start of the ascending limb of the diurnal discharge hydrograph are greater and more uncertain than lags between peak melt and peak proglacial discharge. Uncertainty is caused as the velocity of water flow through the glacier is more variable. Comparison of relative differences in lags between peaks and troughs in surface runoff and proglacial river discharge acts as a qualitative method of model validation. Surface runoff caused by direct precipitation superimposes short-term peaks of varying magnitude onto cycles of meltwater production. Timing of peaks in precipitation can be validated by comparison with the precipitation time series that should be of similar duration.

Whereas the timing of variations in modelled surface runoff are dependent on data arrays read into the melt model, magnitudes of modelled surface runoff are dependent on values given to the melt factor parameter (*MF*) (see Figure 5.3). The melt factor is the only parameter that is not physically based and affects the magnitude and amplitude, through extension or compression, of the diurnal pattern of meltwater output. Changes in the melt factor alter the shape of the diurnal meltwater output rather than just implementing a scalar increase or decrease in the magnitude.

As part of the validation process, optimisation of the melt factor parameter relies on the ability to compare simulated with observed data. Although, comparison of hourly increments of proglacial river discharge data with predicted volumes of total surface runoff fail to compare like with like, optimisation of the melt factor was attempted using curve fitting between simulated runoff and measured discharge patterns at varying values of *MF*. Following Hock (1999), goodness of fit *($R^2$)* was expressed by an efficiency criterion from Nash and Sutcliffe (1970) (Equation 5.8). The efficiency coefficient was optimised when the melt factor was 3.35, producing a $R^2$ value of 0.22 (see Figure 5.4). Further improvement of the fit primarily requires a change in timing of predicted total surface runoff to account for transit times of supra-glacial water to the proglacial

river. Table 5.3 shows that a delay of around 2 to 3 hours in surface runoff would optimise the fit, to a far greater extent than any achieved by manipulation of the amplitude of the diurnal cycle.

$$R^2 = 1 - \frac{\sum_{i=1}^{n}(Q_m - Q_s)^2}{\sum_{i=1}^{n}(Q_m - \overline{Q_m})^2}$$

$Q_m$ = measured discharge in the pro - glacial river
$Q_s$ = simulated volumes of total surface runoff

***Equation 5.8 - (Nash and Sutcliffe, 1970)***

| Delay to total surface runoff (hours) | $R^2$ (from Nash and Sutcliffe 1970) |
|---|---|
| 0 | 0.222 |
| 1 | 0.373 |
| 2 | 0.457 |
| 3 | 0.457 |
| 4 | 0.387 |
| 5 | 0.264 |

***Table 5.3 – Comparison of $R^2$ values with increasing delay in the timing of the modelled total surface runoff.***

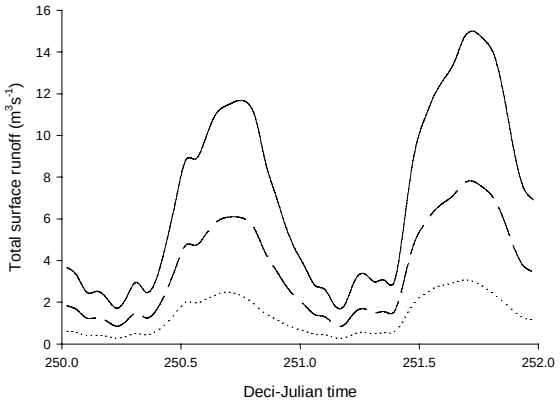



***Figure 5.3 – Extension and compression effects on modelled total surface runoff of variations in the melt factor (MF) parameter (MF = 1.0 pecked line, MF = 3.0 dashed line, MF = 6.0 solid line).***

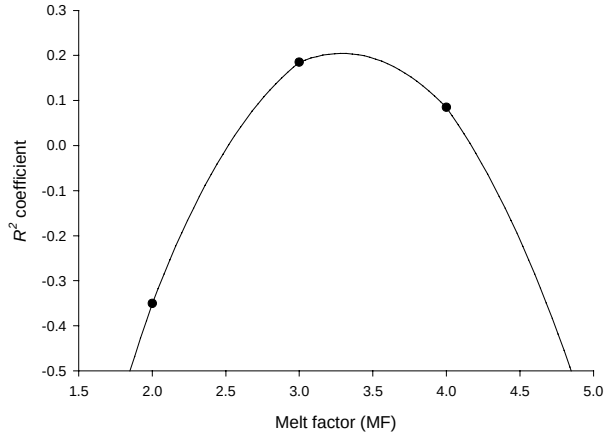



***Figure 5.4 – Optimised values of $R^2$ coefficients derived from comparison of hourly values of modelled total surface runoff and proglacial river discharge using the Nash and Sutcliffe (1970) measure of efficiency.***

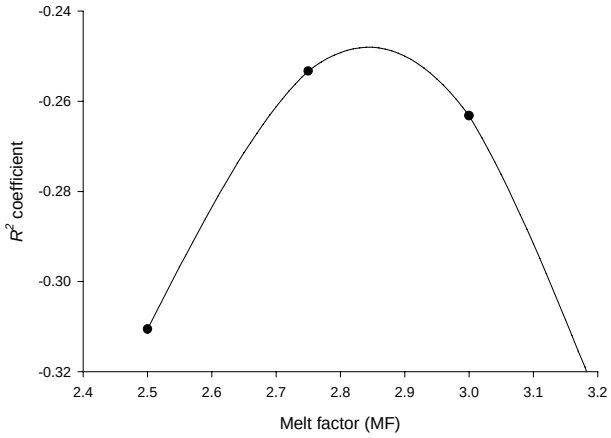



***Figure 5.5 - Optimised values of $R^2$ coefficients derived from comparison of daily range values of modelled total surface runoff and proglacial river discharge using the Nash and Sutcliffe (1970) measure of efficiency.***

However, incorporation of such a delay in modelled runoff would not be consistent with the desired use of the model to only represent inputs, so a different method of optimisation is required. As the model is used to compare variations within separate time series of inputs and outputs rather than direct comparison, an alternative approach of comparison of diurnal ranges was used. The efficiency coefficient derived from comparison of diurnal ranges using the same method (Nash and Sutcliffe, 1970) was optimised using a melt factor of 2.85 producing a $R^2$ factor of –0.248 (see Figure 5.5). This alternative approach was attempted to reduce the influence of the time lag between total surface runoff and proglacial discharge by comparison of the difference in variation between each data set, highlighted in Table 5.3. However, such a change in the type of data used for comparison (i.e. range rather than point data) decreased the resolution of variation from hourly to daily intervals and consequently the number of observations involved, which combined to produce a lower $R^2$ coefficient than comparison of hourly data. Consequently, the melt factor coefficient of 3.35, which was derived from hourly resolution measurements was preferred.

Although optimisation of the melt factor using the Nash and Sutcliffe (1970) method on hourly data was satisfactory, sensitivity analysis was conducted to compare distributions of hourly discharge and total surface runoff data. Histograms of each data set show non-parametric distributions that are positively skewed (see Figure 5.6). As the number of observations is high, n=1128, it is acceptable to use the Student's t-test to compare the means of both distributions despite the data being non-parametric (Blalock, 1979). The Student's t-test is preferable to the Mann-Whitney U-test or the Kolmogorov-Smirnov test as it compares mean values that provide a representative measure of central tendency of each distribution. Comparison using the Student's t-test of modelled total surface runoff and measured proglacial discharge were made against a critical value of the t-statistic of 1.961, for a two tailed test at a level of significance of 0.001, with n=1128 and assuming distributions of unequal variance (Davis, 1986). If the calculated t-

statistic is above this critical value the null hypothesis can be rejected, which means that there is a probability of less than 0.05 that the data sets are significantly similar.

| Value of melt factor used in calculation of total surface runoff | t-statistic (Student's t-test) |
|---|---|
| 1.35 | 35.15 |
| 2.35 | 18.12 |
| 3.35 | 4.23 |
| 4.35 | 6.52 |

***Table 5.4 – t-statistics for Student's t-tests between hourly proglacial discharge and modelled total surface runoff, calculated using variations in the melt factor parameter.***

Table 5.4 shows that all calculated t-statistics are greater than the critical value. Hence, this means characterising distributions of total surface runoff (using four different melt factor values at or near the previously optimised value of 3.35) are significantly different to the means that describes discharge data. Although the comparison may not be statistically significant using the Student's t-test, possibly influenced by the very high number of observations, the total surface runoff derived using a melt factor of 3.35 provides the best possible statistical fit to measured discharge data. Figure 5.7 demonstrates that the distributions of total surface runoff and measured discharge are most similar with a melt factor of 3.35 and shows the changes in sensitivity of the spread and magnitude of each distribution with variations in melt factor values.

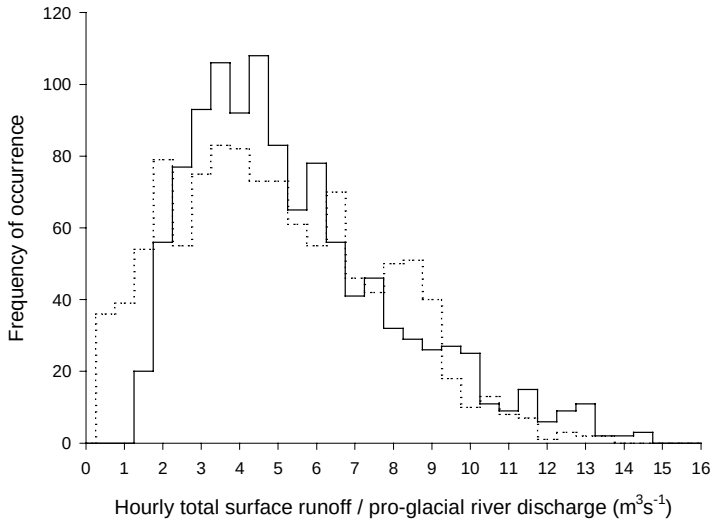



***Figure 5.6 – Histograms of hourly values of proglacial river discharge (solid line) and modelled total surface runoff model output (pecked line) using a melt factor value of 3.35, between 31 July and 16 September 1999.***

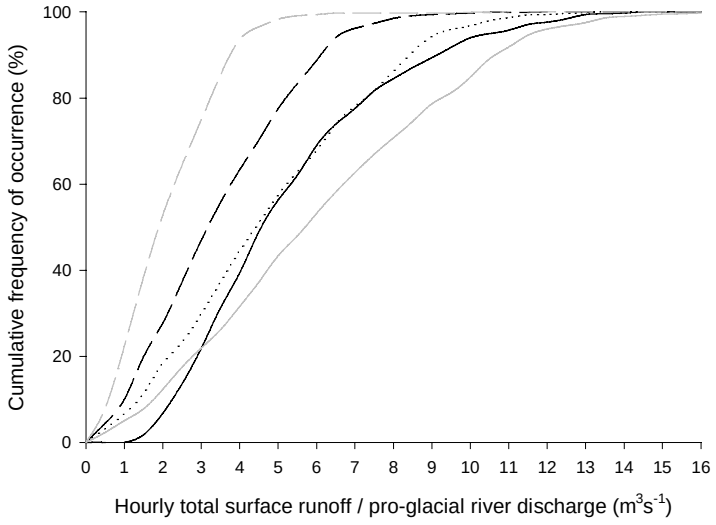



***Figure 5.7 – Cumulative frequency plot of hourly values of proglacial river discharge (solid back line) and modelled total surface runoff using various values for the melt factor parameter (dashed grey line = 1.35, dashed black line = 2.35, pecked line = 3.35 and solid grey line = 4.35), between 31 July and 16 September 1999.***

## 5.4 Summary

Chapter 5 describes the construction and validation of a semi-distributed simple energy balance model of surface runoff at Findelenglescher. Air temperature, incoming solar radiation, precipitation, transient snow line and topographic data are used to accurately replicate variations in both timing and magnitude of surface runoff. The model has an hourly resolution, incorporates spatial differences in runoff intensity and includes only one non-physically based parameter. A computer code has been created in FORTRAN90 (see section 11.7), which processes the aforementioned data and produces volumes of inputs to the glacial hydrological system that are used in section III to analyse water storage.

# 6 THEORETICAL DEVELOPMENT OF SUBGLACIAL WATER STORAGE USING BOREHOLES

## 6.1 Introduction

The purpose of this chapter is to develop a protocol for interpretation of water level variations in boreholes that connect hydraulically with the subglacial drainage system. This is necessary to facilitate advancement in semi-quantitative analysis of subglacial water storage that is performed in chapters 7 and 8. Analysis compares phase relationships and synchroneity of variables describing throughputs of subglacially routed runoff with inputs to and outputs from the glacial hydrological system.

Section 6.2 provides a brief explanation of standard ways to quantitatively analyse and explain water flow through a glacier. It shows that for analysis of water storage over diurnal timescales, with the purpose of interpreting subglacial hydrological processes, current quantitative methods that rely on linear discharge models or use steady state conditions are insufficient. Consequently, it is necessary to develop more detailed conceptual models than are presently available as a means of interpreting the physical processes that cause variations in borehole water levels.

Sections 6.3 and 6.4 develop conceptual models that consider water levels in boreholes that directly intersect subglacial channels. This takes into account the affect of temporary obstructions in subglacial channels and the size of the channel orifice, which determines a channel's capacity to discharge. Section 6.5 develops conceptual models that consider water levels variations in boreholes that do not directly intersect subglacial channels. Instead, these boreholes terminate in a layer of subglacial sediment that acts as a medium for hydraulic communication with subglacial channels located some distance away.

## 6.2 Conceptualisation of the glacial hydrological network

A common method of conceptualising the glacial hydrological system is by treating the glacier as a single store or reservoir. Figure 6.1 illustrates this concept with the combined total of runoff from ablation and precipitation acting as the single rate of inputs to the store and the diameter of the exit hole, representing the orifice size of the subglacial channel, acting as the single rate of outputs. Dimensions of the store are reduced by rates of ice deformation inwards and are increased as frictional heat from flowing water at the ice-water interface causes ice to melt. Consequently, water balance in the store is a direct result of the rate of inputs relative to the rate of outputs.

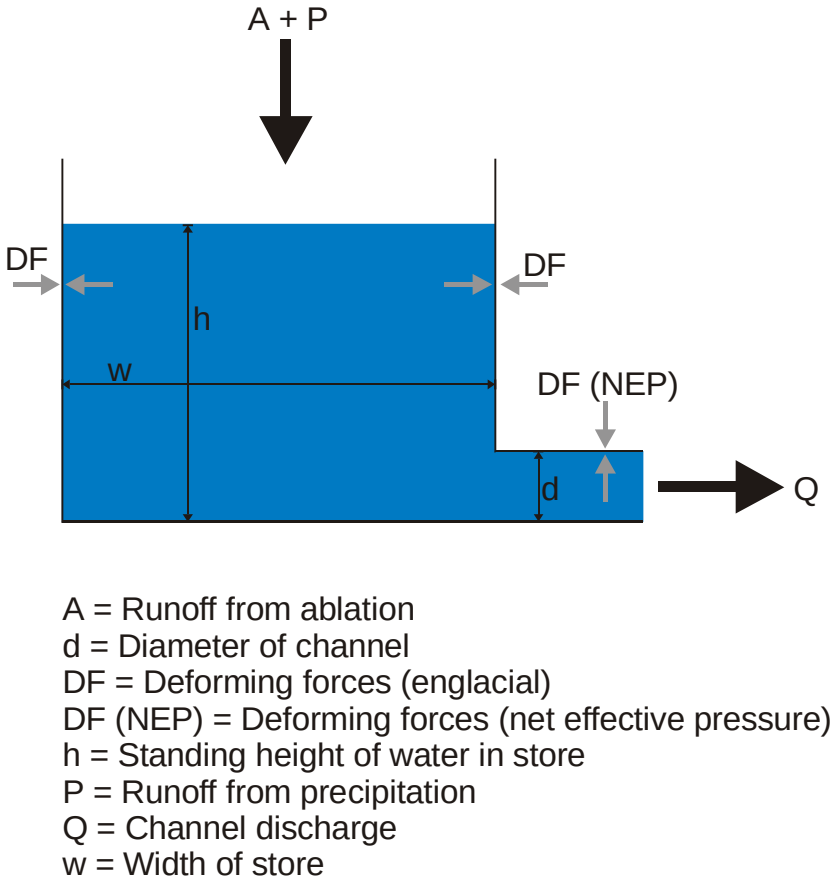



***Figure 6.1 – Conceptual model of the glacial hydrological system as a single store (or reservoir).***

Numerical modelling of runoff from glacierised catchments uses any number of linked stores to describe the subglacial hydrological system (Baker *et al.*, 1982; Lundquist, 1982; Mader and Kaser, 1994). Calculated meltwater production is then routed through the stores, each with a storage parameter that does not necessarily have a physical basis. The resulting hydrographs can then be compared with measured hydrographs and analysis of the residuals between the two recession curves can refine the storage parameters. However, Gurnell (1993) suggests there may be a great deal of ambiguity when deciding on the number of stores that make up the subglacial network and when apportioning a storage parameter to each one. Ambiguity also exists regarding the number of interconnections between each store, whether stores are in series or parallel to each other and the proportion of the total discharge that flows through each one.

Where the sole interest of an investigation is the accuracy of discharge from an operational model, the linked reservoir approach to modelling the subglacial hydrological network is perfectly valid. However, more spatial and temporal flexibility is required to understand changes in the subglacial drainage network that result from hydrometeorological inputs or internal glaciological movements. Timescales over which these changes can occur range from sub-diurnal timescales, for example the rapid collapse of cavity systems due to a change in sliding velocity (Kamb, 1987; Lliboutry, 1968), to seasonal patterns within annual cycles (Iken and Truffer, 1997). Consequently, temporary obstructions in subglacial channels and changes in preferential subglacial pathways linking different areas of drainage would need a multitude of linked stores representing every constriction and component of frictional resistance that the internal glacial hydrological system presents.

Linked reservoir models have to simplify the glacial hydrological system to such an extent that they do not allow the temporal and spatial flexibility needed to adequately examine the processes responsible for increasing or decreasing water storage. These methods require prior assumptions

about the state of the drainage network that may have little physical basis. Consequently, this investigation requires conceptual models that directly reflect subglacial processes, have the flexibility to react to rapid changes in different parts of the drainage network and are controlled by *in situ* measurements of subglacial water pressure.

The use of borehole water levels in conceptual models to investigate the subglacial hydrological system is evident in previous studies. Murray and Clarke (1995) used conceptual models to categorise boreholes into those that were connected, unconnected or had alternating connections with the subglacial hydrological system. Simple models have been used to describe hydraulic connections through a subglacial sediment layer. Barrett and Collins (1997) and Fountain (1994) have used these models to explain how boreholes that do not intersect subglacial channels can reflect changes in water pressures in channels elsewhere through a subglacial sediment layer. Stone and Clarke (1993) amongst others use such a conceptual model of hydraulic connection through subglacial sediment to investigate the physical properties of the substrate using borehole-response tests.

However, development of conceptual models that link analysis of subglacial processes controlling water storage with phase relationships and synchroneity of water pressures in separate areas of subglacial drainage is not explicitly evident in previous research. To fulfil this requirement, sections 6.3 to section 6.5 present the development of conceptual models analysing the cause of variations in borehole water levels over both seasonal and diurnal timescales, which are the result of original work by the author.

## 6.3 Diurnal variations of water levels in boreholes directly intersecting a subglacial channel

Figure 6.2 to Figure 6.10 illustrates the situation (albeit unlikely) that boreholes have been drilled directly into a major subglacial channel with constant dimensions that runs along steeply sloping basal topography. Boreholes are assumed to remain vertical, to be of uniform diameter throughout and not to be intersected by englacial conduits. For the purpose of theoretical discussion surface runoff is assumed to drain instantaneously and vertically through macropores in glacier ice from the point of production on the surface to the base of the glacier. Changes in borehole water level act as a surrogate for changes in subglacial channel water pressure, validating the use of boreholes as manometers if the borehole directly intersects the channel. The quantity of water moving in and out of the borehole is very small in respect to the quantity of water moving through the channel. This prevents the borehole from having a significant influence on temporary storage of subglacial water. It may be convenient to think of subglacial channels as cylindrical (Röthlisberger, 1972), therefore, knowledge of changes in diameter would accurately reflect the ability to discharge. However, due to uncertainties over subglacial channel size and shape (Fowler and Walder, 1993; Iken and Bindschadler, 1986; Nye, 1973; Walder, 1986; Weertman, 1972) the channel size, shape, and hydraulic efficiency will be collectively referred to as the channel orifice (as in Kamb, 1987). If a channel has a fixed orifice size, changes in water pressure reflect the amount of water that is stored (or backed-up) in the channel network. In practice, water pressure is not necessarily a reflection of absolute channel discharge as it is a result of both channel orifice size and water pressure acting in combination (see Table 6.1).

In reality the channel orifice size is unknown at every position along the subglacial drainage network due to highly limited spatial accessibility (Hodge, 1979; Kamb *et al.*, 1979) and temporal

variation throughout the entire year (Gordon *et al.*, 1998; Iken and Truffer, 1997). Consequently, absolute estimates of subglacial channel discharge can not be accurately calculated and instead relative changes are used to determine variation in the capacity of the system to discharge.

| Channel orifice | | Water pressure | | Channel discharge |
|---|---|---|---|---|
| Large | + | High | = | High |
| Large | + | Low | = | Medium |
| Small | + | High | = | Medium |
| Small | + | Low | = | Low |

***Table 6.1 – Theoretical inter-relations between subglacial channel size, water pressure and channel discharge.***

Caution must be exercised if interpreting daily variations in borehole water levels in a similar manner to pro-glacial river discharge hydrographs. Hydrographs of pro-glacial river discharge are a product of four interacting parameters: incoming solar radiation, air temperature, position of the transient snow in relation to basin hypsometry and the capacity and extent of the sub- and englacial drainage network (Collins, 1982a). In practice a change in the diurnal hydrograph is a product of all these inter-related parameters and the exact effect of each cannot be isolated individually. However, variations in the diurnal pattern of borehole water levels predominantly reflects changes in the capacity of a drainage system to discharge, especially in periods where diurnal cycles of hydrometeorological parameters of melt are approximately constant.

### 6.3.1 Connection with an unobstructed channel

Figure 6.2 to Figure 6.4 illustrates a theoretical situation through a long section of the glacier where three boreholes, which are drilled at increasing elevations up-glacier, directly intersect a straight subglacial conduit running along the glacier bed. Diurnal cycles of radiated energy fluxes and terrestrial mechanisms such as surface albedo, which control rates of meltwater production, are considered to be constant over the glacier. Air temperature decreases uniformly

with increasing elevation and precipitation is zero. Figure 6.3 shows a situation where during the daytime, surface meltwater inputs are high causing water levels in boreholes 1, 2 and 3 to rise to similar absolute elevations, providing an indication of the piezometric surface of hydraulic water head within the glacier (Hubbard *et al.*, 1995; Röthlisberger *et al.*, 1979). Equality in elevation of borehole water levels are maintained due to increasing water pressure at the base of boreholes further down-glacier. This is caused by water backing up in subglacial channels as temporary storage. Overnight, a drop in inputs through lack of surface melt will cause a drop in borehole water levels (see Figure 6.2) which, if the subglacial system communicates perfectly, may cause water to almost drain out of borehole 3 altogether. Diurnal variation in borehole water levels (Figure 6.4) are a response to changes in water pressure in the subglacial drainage system, caused by diurnal variations in volumes of surface runoff flowing through channels, which are considered in Figure 6.2 and Figure 6.3 as having a fixed radius. Over a 24 hour cycle the range and pattern of water level movement in boreholes 1, 2 and 3 over a diurnal cycle are perfectly synchronous, but as the borehole water level movement is illustrated in Figure 6.4 as the height of the water column in the borehole ($h$) instead of an absolute elevation, water levels will fluctuate lower down within boreholes drilled at higher elevations.

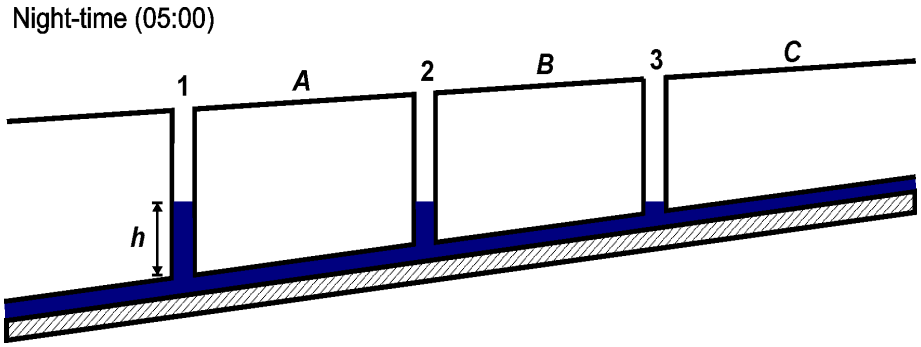



*Figure 6.2 – Water levels at night in boreholes directly intersecting an unobstructed subglacial channel where, h, represents the depth of water columns in each borehole.*

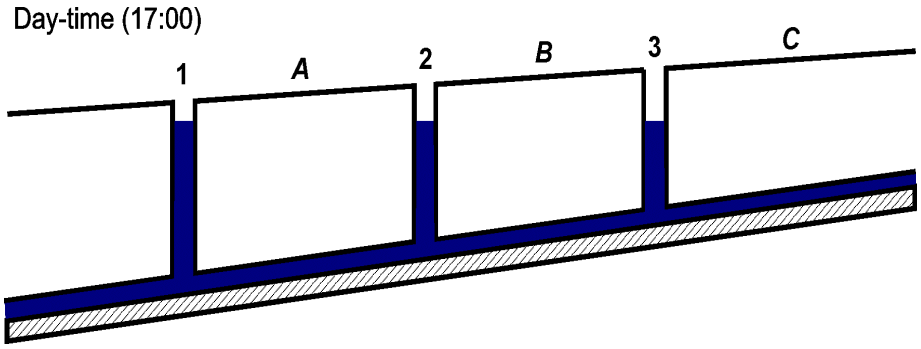



*Figure 6.3 - Water levels during the day in boreholes directly intersecting an unobstructed subglacial channel.*

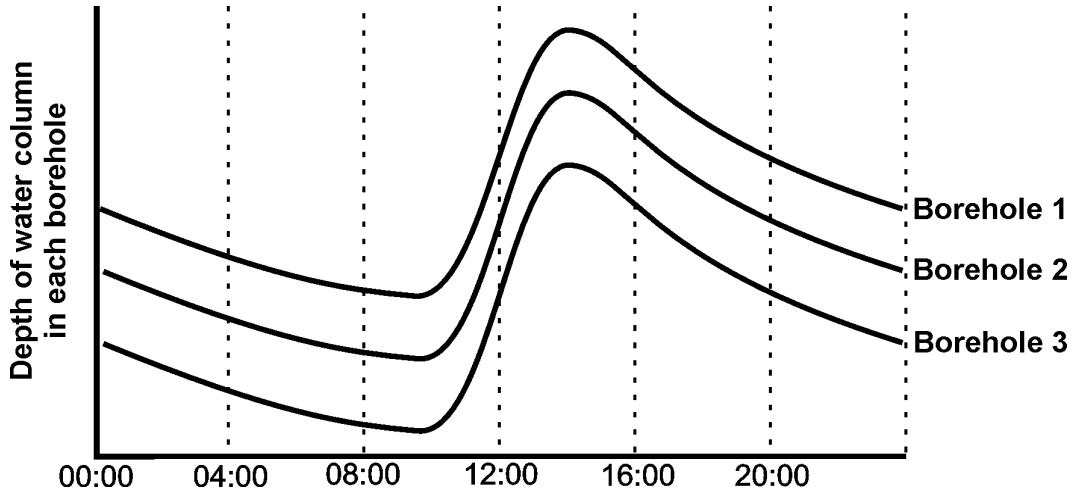



*Figure 6.4 – Diurnal time series of water levels in boreholes at different elevations directly intersecting an unobstructed subglacial channel.*

### 6.3.2 Connection with an obstructed channel

#### 6.3.2.1 Down-glacier obstruction

In reality the subglacial hydraulic system will not communicate perfectly. This is conceptually described as a temporary obstruction or constriction in the channel providing spatial variations in restriction and resistance to water flow. The influence of hydraulic efficiency of subglacial channels on patterns of borehole water levels are superimposed on diurnal cycles driven by surface input. A subglacial channel constriction acts as a rate limiting factor on water flow from the drainage network up-glacier from the point of constriction. Constrictions affect the water pressure and consequently the height of water levels in boreholes, which is illustrated in Figure 6.5 as a constriction in the drainage network between boreholes 1 and 2, creating temporary water storage up-glacier that is reflected by increased daily maximum and minimum water levels in boreholes 2 and 3. Conversely, the constriction will cause a decrease in maximum and minimum water levels in borehole 1 as the rate of water supply from up-glacier stores has been reduced. Variation in differences between diurnal maximum and minimum water levels in borehole 1 and boreholes 2 and 3 (the difference between *a* and *b* in Figure 6.5 and Figure 6.6) will be accentuated at night when meltwater inputs are at or near to zero. Higher rates of meltwater runoff are experienced during the daytime over area *A* rather than areas *B* or *C* (see Figure 6.5), as intensities of melt are higher at lower elevations due to higher air temperatures. They partly compensate for increased rates of drainage below the constriction and thereby reduce the potential difference between *a* and *b*. Diurnal patterns of borehole water levels vary depending on the position of the channel constriction in relation to the base of the borehole and whether there is a restriction of water flow from up-glacier or restriction in drainage down-glacier (see a summary in Table 6.2). In Figure 6.7 water levels in boreholes 2 and 3, over a single diurnal cycle, will increase faster and decrease more slowly than in Figure 6.4 as the decrease in channel orifice size down-glacier will cause a more rapid backup with the onset of daily melt and a more

gradual release of the diurnally stored water. Consequently, in Figure 6.7 water levels in borehole 1 will increase more slowly and decrease faster than in Figure 6.4 as the rate of water release from the channel section around the base of borehole 1 is now considerably greater relative to the rate of input.

The timing of maximum and minimum values in Figure 6.7 are no longer the same as in Figure 6.4. In Figure 6.7 water levels in boreholes 2 and 3 will reach a diurnal minimum and then begin to rise earlier than in borehole 1 as the rate of meltwater input, which remains unaltered, will exceed the reduced rate of output earlier. However, water levels in boreholes 2 and 3 will peak at the same time as in Figure 6.4 as there has been no alteration to the inputs. Unless water drains completely from borehole 1, whereupon channel water pressure becomes equal to atmospheric pressure, the diurnal minimum will occur at the same time as in Figure 6.4. If atmospheric pressure is reached there will be a delay to the start of the ascending limb until the channel becomes full, exceeds atmospheric pressure and begins to force water up the borehole. However, although the rate of output is unchanged, the rate of input which was previously dominated by supply of water from the up-glacier drainage network, will be increasingly influenced by the transit time and rate of meltwater from surface *A* relative to reduced rates of input from surfaces *B* and *C* caused by the subglacial channel constriction. Timing of the daily maximum water level in borehole 1 in Figure 6.7 relative to the maximum in Figure 6.4 is likely to remain the same if the dominant inputs to the channel are still routed from the up-glacier subglacial drainage network from sources areas *B* and *C*. However, daily maximum borehole water levels will occur earlier if the dominant inputs are derived from surface *A* which has a more rapid, partially unconstrained route to the channel at the base of borehole 1.

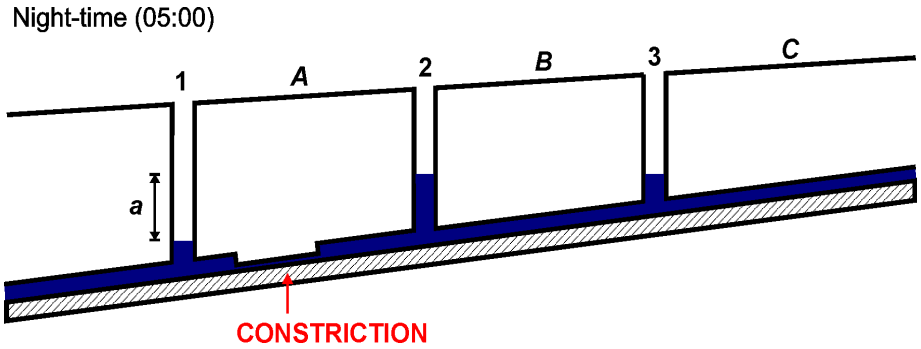



*Figure 6.5 - Water levels at night in boreholes directly intersecting a subglacial channel that has a temporary obstruction in a down-glacier section where, a, represents the difference between the height of the water level in borehole 1 relative to other boreholes.*

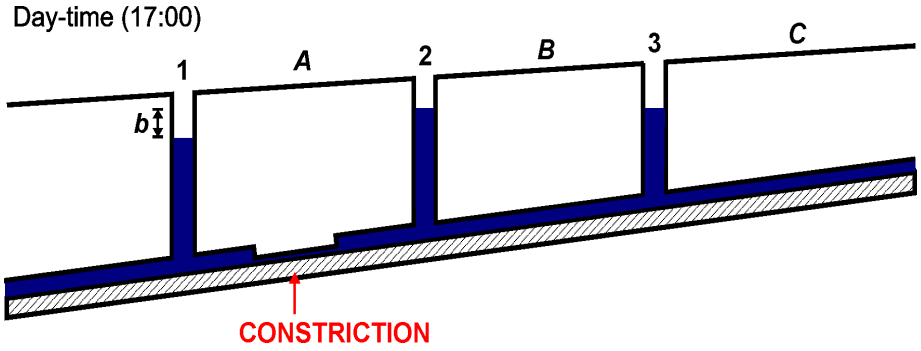



*Figure 6.6 - Water levels during the day in boreholes directly intersecting a subglacial channel that has a temporary obstruction in a down-glacier section where, b, represents the difference between the height of the water level in borehole 1 relative to other boreholes.*

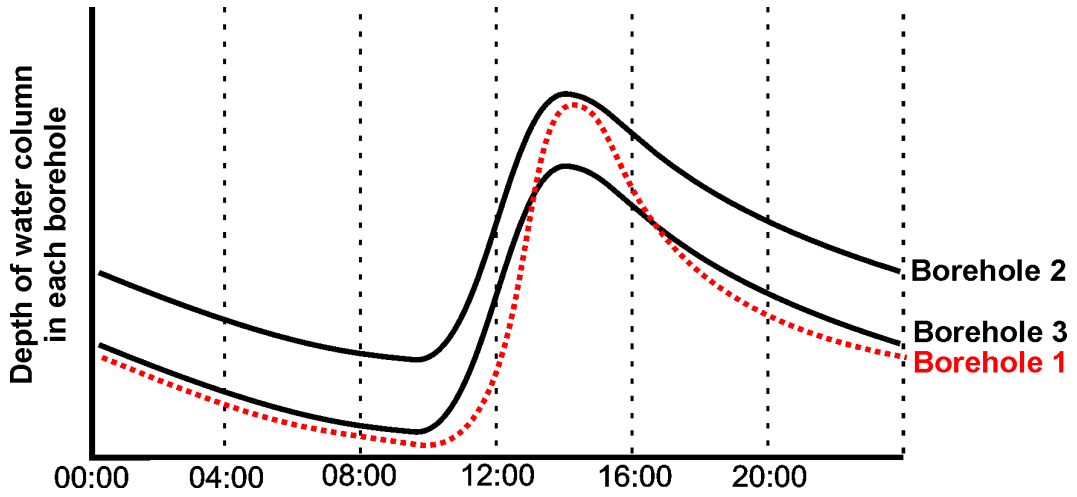



*Figure 6.7 - Diurnal time series of water levels in boreholes at different elevations directly intersecting a subglacial channel that has a temporary obstruction in a down-glacier section.*

| |
|---|
| ***Descending limb:*** <br> $\frac{d(h)}{dt}$ of borehole 1 $\rangle$ $\frac{d(h)}{dt}$ of boreholes 2 and 3 |
| ***Ascending limb:*** <br> $\frac{d(h)}{dt}$ of boreholes 2 and 3 $\rangle$ $\frac{d(h)}{dt}$ of borehole 1 |
| ***Variation in difference between water levels in borehole 1 and boreholes 2 and 3 at diurnal maximum (a) and minimum (b):*** <br> $a \rangle b$ as $\frac{d(I)}{dt}$ of surface $A \rangle$ $\frac{d(I)}{dt}$ of surfaces $B$ and $C$ |

***Table 6.2 - Summary table for borehole water levels where an obstruction in the subglacial channel exists between boreholes 1 and 2 (see Figure 6.5 and Figure 6.6). Where, h, represents the height of the water columns in each borehole and, I, represents the volume of surface runoff over an ice surface.***

#### 6.3.2.2 Up-glacier obstruction

The position of the constriction changes in Figure 6.8 and Figure 6.9 so that it is situated between boreholes 2 and 3. Comparison of rates of change in borehole water levels in Figure 6.10 with Figure 6.4, summarised in Table 6.3, follow the same principles as the previous comparison with Figure 6.7 where water levels rise faster and drop slower above the constriction (borehole 3) and vice versa below the constriction. Increased intensities of daytime melt on the combined surfaces *A* and *B* will have a greater compensating effect on potential difference between diurnal maximum and minimum water levels in boreholes 1 and 2 and borehole 3. Therefore, *a* and *b* in Figure 6.8 and Figure 6.9 are less than *a* and *b* in Figure 6.5 and Figure 6.6. Synchroneity of diurnal maximum and minimum borehole water levels in Figure 6.10 relative to Figure 6.4 follow similar principles of an earlier rise and the same peak time for boreholes up-glacier of the constriction and the possibility of later starts and earlier peaks down-glacier. The possibility of a delay in minimum water levels in boreholes down-glacier of the constriction in Figure 6.10 is less likely than in Figure 6.7 as there is a larger surface area (combined areas *A* and *B*) that contributes more intensely to meltwater runoff due to changes in air temperature with respect to elevation. Timing of the diurnal peak in boreholes down-glacier of the constriction are also more likely to

be controlled by the volume of surface runoff from areas *A* and *B,* as it has become a more dominant component of total surface meltwater runoff.

| |
|---|
| ***Descending limb:*** <br> $\frac{d(h)}{dt}$ of boreholes 1 and 2 $\rangle$ $\frac{d(h)}{dt}$ of borehole 3 |
| ***Ascending limb:*** <br> $\frac{d(h)}{dt}$ of borehole 3 $\rangle$ $\frac{d(h)}{dt}$ of boreholes 1 and 2 |
| ***Variation in difference between water levels in borehole 1 and 2, and borehole 3 at diurnal maximum (b) and minimum (a):*** <br> $a \rangle b$ as $\frac{d(I)}{dt}$ of surfaces $A$ and $B \rangle$ $\frac{d(I)}{dt}$ of surface $C$ <br> $\left[ \begin{array}{l} \text{where there is an up-glacier constriction both } a \text{ and } b \text{ are likely to be less than} \\ a \text{ and } b \text{ where there is a down-glacier constriction as:} \\ \frac{d(I)}{dt} \text{ of surface } A \rangle \frac{d(I)}{dt} \text{ of surface } B \rangle \frac{d(I)}{dt} \text{ of surface } C \end{array} \right]$ |

***Table 6.3 - Summary table for borehole water levels where an obstruction in the subglacial channel exists between boreholes 2 and 3 (see Figure 6.8 and Figure 6.9). Where, h, represents the height of the water columns in each borehole and, I, represents the volume of surface runoff over an ice surface.***

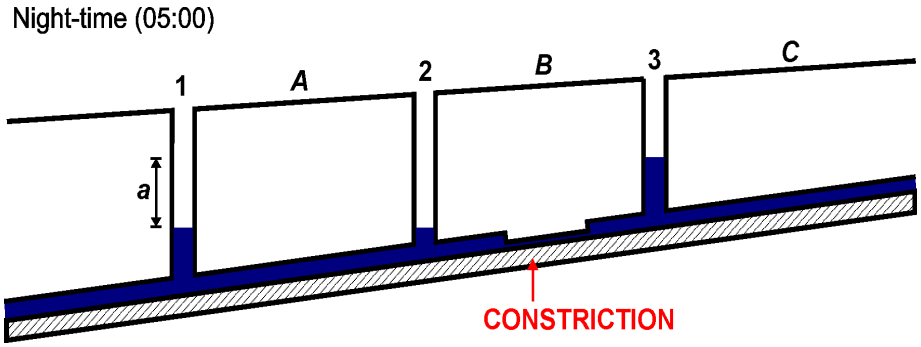



*Figure 6.8 - Water levels at night in boreholes directly intersecting a subglacial channel that has a temporary obstruction in an up-glacier section where, a, represents the difference between the height of the water level in borehole 3 relative to other boreholes.*

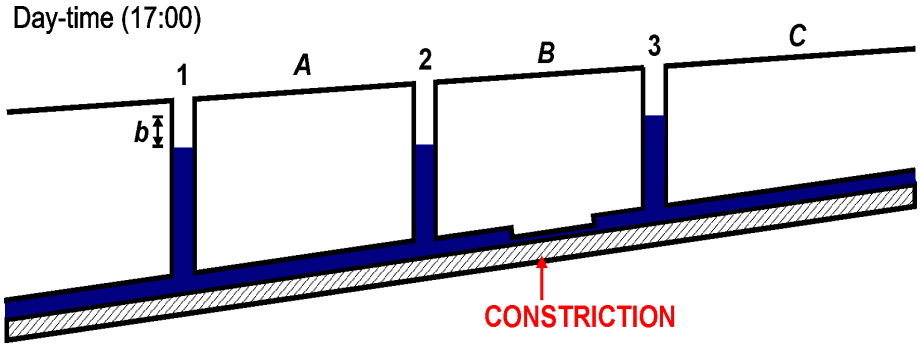



*Figure 6.9 - Water levels during the day in boreholes directly intersecting a subglacial channel that has a temporary obstruction in an up-glacier section where, b, represents the difference between the height of the water level in borehole 3 relative to other boreholes.*

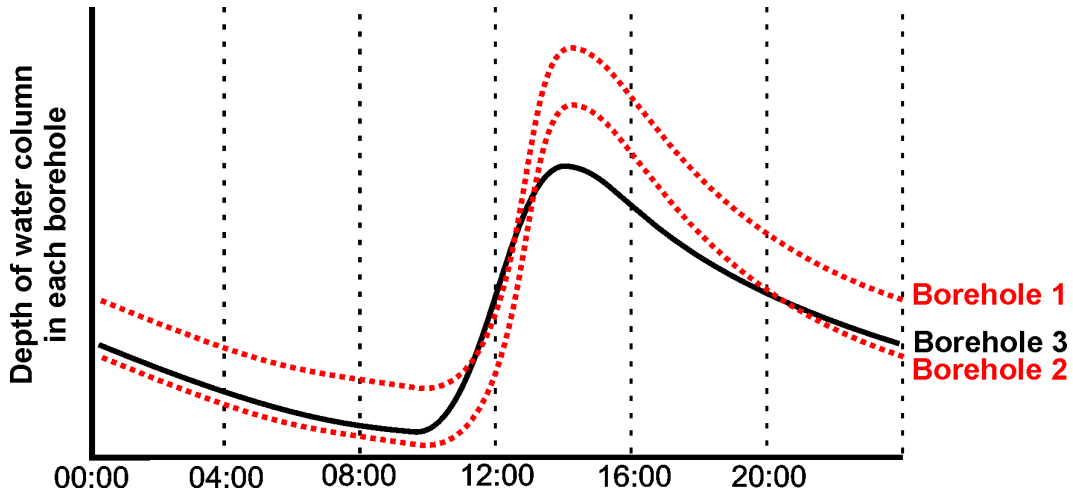



*Figure 6.10 - Diurnal time series of water levels in boreholes at different elevations directly intersecting a subglacial channel that has a temporary obstruction in an up-glacier section.*

## 6.4 Affect of subglacial channel size on borehole water levels

Channel orifice describes the size, shape and hydraulic efficiency of a sub- or englacial channel. For the purpose of theoretical development, intersection between the base of the borehole and the subglacial channel was assumed not to have a localised affect on the channel orifice dimensions, although in reality this is unlikely to be the case. Consequently, it is the net effective water pressure in the channel that controls the rate of increase or decrease in channel size and geometry at the point of borehole intersection. Net effective pressure is the difference between water pressure and ice pressure acting against each other in a subglacial conduit. Figure 6.11 shows these pressures acting on a cylindrical ice-walled conduit. Subglacial conduits may also be bounded by sediment and bedrock that provide localised differences in the resistive forces impacting on channel water pressure. In reality, even if the orifice of the channel or cavity has been enlarged whilst forcing a connection during hot water drilling of boreholes, the first section of unaffected channel up-glacier of the intersection will provide a rate limiting factor to water flow into the enlarged cavity that accurately reflects the unaltered state of the conduit. Consequently, as long as the conduit section at the point of borehole intersection remains full, the localised change in orifice dimensions will not affect the borehole water level's representation of subglacial water pressures.

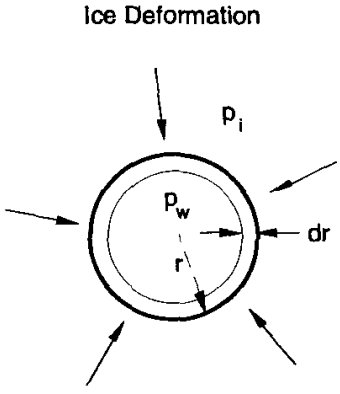



***Figure 6.11 – Idealised diagram of influences in computation of net effective pressure in an ice walled, cylindrical conduit ($P_w$ = water pressure, $P_i$ = ice overburden pressure) after (Röthlisberger and Lang, 1987).***

### 6.4.1 Diurnal variations

Effects of relative difference in channel orifice size on borehole water levels are illustrated in Figure 6.12 to Figure 6.14. Similar volumes of water moving through subglacial channels with small and large sized orifices over a diurnal cycle will cause fluctuations in borehole water levels that are greater and more rapid if connected to a channel with a small, rather than large sized orifice. Timing of daily maximums and minimums in boreholes 1 and 2 are synchronous with each other (see Figure 6.14), although the form of the diurnal pattern between maximum and minimum points is controlled by volumes of water interacting with the relative geometry of the channels.

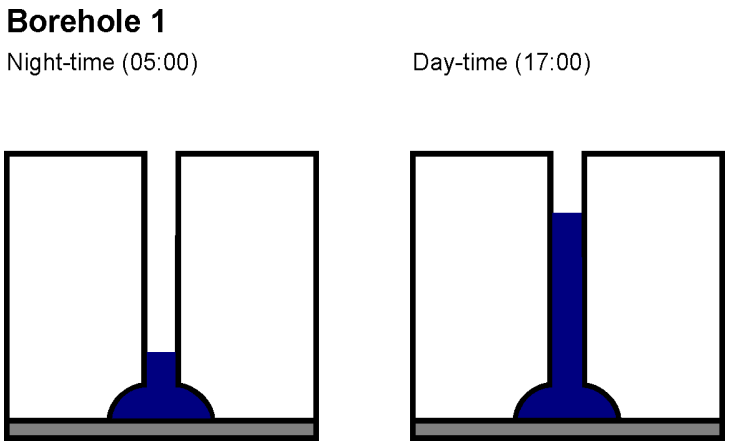



***Figure 6.12 –Affects of a small sub-glacial channel orifice on diurnal changes in borehole water levels.***

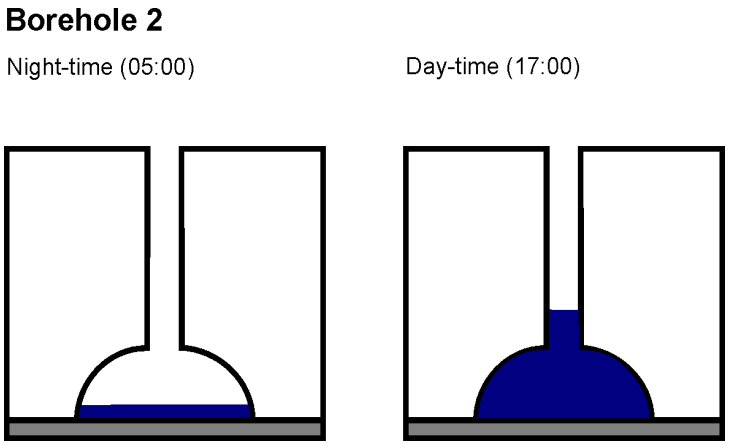



***Figure 6.13 - Affects of a large sub-glacial channel orifice on diurnal changes in borehole water levels.***

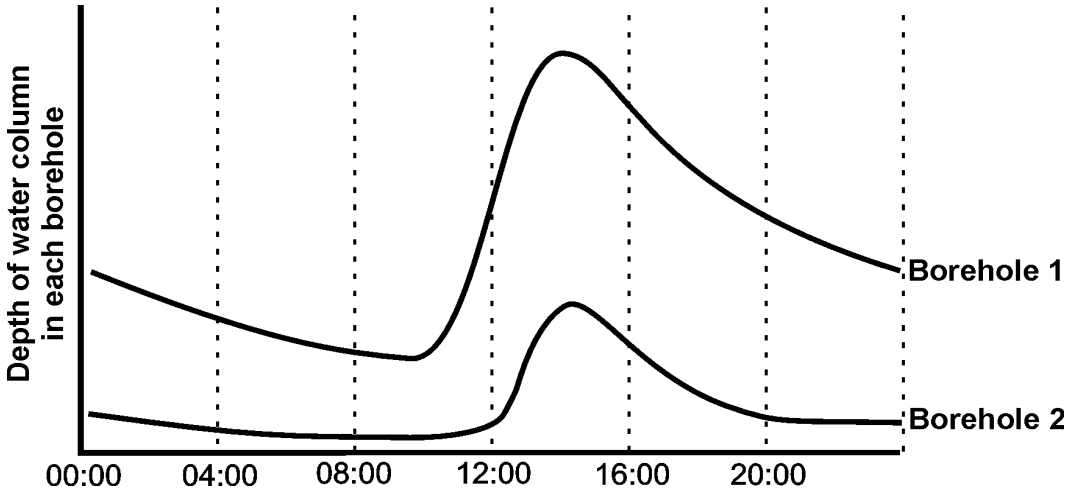



***Figure 6.14 - Diurnal time series of water levels in boreholes drilled into sub-glacial channels with small (Figure 6.12) and large (Figure 6.13) sized orifices that receive similar volumes of surface runoff.***

### 6.4.2 Seasonal variations

Although absolute water pressures in specific subglacial channels are unknown, estimates of changing water pressures in channels of varying orifice size throughout the ablation season in the European Alps from May to October can be made to illustrate expected relationships. In reality, it is possible for both small and large channels to co-exist simultaneously in the subglacial drainage network, possibly in close proximity. Figure 6.15, Figure 6.16 and Figure 6.17 show the seasonal development and inter-relationships between channels with both large and small sized orifices. Due to very low subglacial water pressures during winter (November to April) the effective pressure in the channel is dominated by the ice overburden pressure causing creep closure that reduces the channel size. It is unlikely that large channels, relative to a channel's maximum potential to increase over an annual cycle, will exist and in May / June. Consequently, low meltwater inputs will cause diurnal patterns of borehole water levels as exhibited in Figure 6.15.

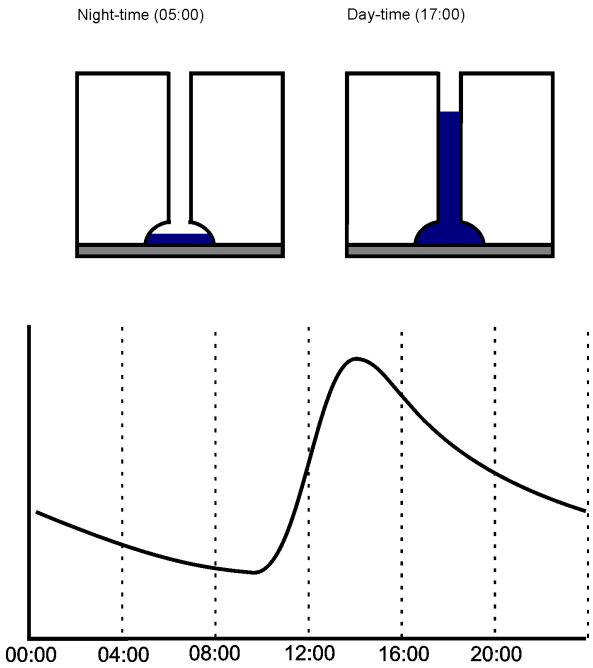



***Figure 6.15 – Diurnal variations in borehole water levels in the early ablation season (May / June) when runoff is low. Boreholes directly intersect sub-glacial channels with a low capacity to discharge (small orifice size).***

In July / August meltwater input is high due to an increased intensity of incoming short-wave solar radiation and sensible heat fluxes. Increased water pressures that accompany large volumes of meltwater flowing through small subglacial channels cause higher velocities, which in turn, increase the orifice size due to greater frictional melt and sediment evacuation. High night-time water pressures are maintained by temporary storage of water in up-glacier channels that has backed-up during the daytime when rates of inputs far exceed rates of channel outputs. Therefore, effective pressure in channels is continuously acting against adjacent ice and sediment throughout the diurnal cycle preventing the effect of creep closure due to ice overburden pressure. Growth of the channel orifice throughout the year reaches a maximum during peak pro-glacial river discharge in mid-summer. An increase in channel orifice size provides a range of possible water pressures and borehole water levels, dependant on orifice size and efficiency (see Figure 6.16).

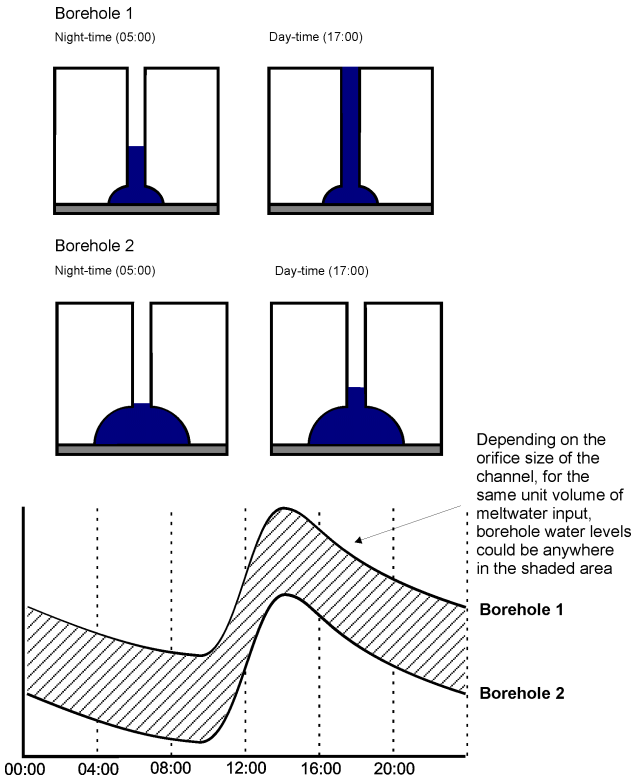



***Figure 6.16 - Diurnal variations in borehole water levels in the mid-ablation season (July / August) when runoff is high. Boreholes directly intersect sub-glacial channels with a high capacity to discharge (large orifice size).***

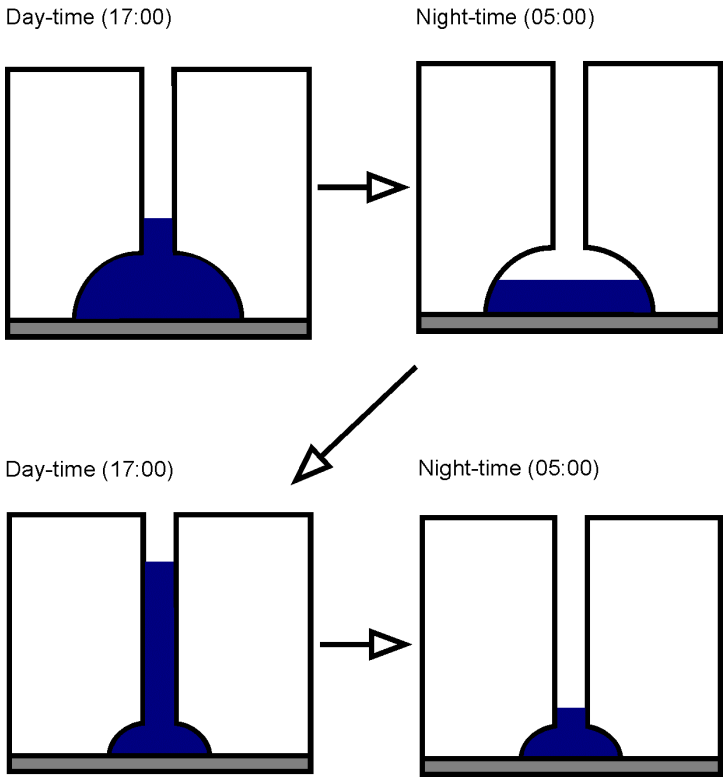



***Figure 6.17 - Schematic diagrams of decrease in the capacity of subglacial channels to discharge (decreasing orifice size) in the late ablation season (September / October) when runoff is decreasing. Boreholes directly intersect subglacial channels.***

In September / October, decline in channel orifice size is caused by an inverse mechanism to channel orifice enlargement. Meltwater inputs may vary greatly during this period as the seasonally high elevation of the transient snow line is subject to temporary drops in elevation due to lower air temperatures and short periods of sporadic snowfall. A temporary increase in snow cover, which is likely to coincide with low air temperatures and high cloud cover, will reduce the surface runoff. During September / October a series of sharp, temporary declines may occur in the total glacial melt rate. However, melt rates can be quickly reinstated by a rise in air temperature (although possibly not fully to previous melt rates), which may allow ice overburden pressure to exceed dominant effective channel water pressure for a proportion of the daily cycle great enough to allow channel closure. Schematic illustration of channel closure is shown in the

form of a flow diagram in Figure 6.17. During this period diurnal variations in borehole water levels will depend specifically on inter-relations between orifice size and meltwater input, i.e. not just either influence considered in isolation. The trend of variations in borehole water levels over this period may well be erratic, depending on variations in the rate of channel orifice closure relative to meltwater inputs. Consequently, although the timing of peaks and troughs of this superimposed signal are diurnally controlled, the magnitude of daily maximums and minimums are not uniform in their graduation reflecting a great degree of spatial heterogeneity in the reduction of channel orifice size throughout the subglacial drainage network. Uncertainty exists regarding the timing of physical mechanisms that cause this graduation, providing a focus for this research.

Interpretation of rates of water flow through the drainage network during this period describes limitations to flow as temporally variable constrictions in the orifice of one or many of the subglacial channels in the drainage network. A sudden constriction in any one of the channels will cause water to back-up through an otherwise well developed drainage network with a high capacity to discharge, unless there is an alternative pathway. Assuming the high discharges of July and August have developed the most efficient drainage pathway at the expense of all other subglacial routes, large amounts of temporarily stored water will rapidly increase the water pressure behind any constriction. High water pressures will either cause exponentially increasing discharges due to increasing rates of frictional melt around the wetted perimeter of the constricted orifice or the ice overburden pressure may be exceeded over a wide enough spatial area to cause localised floatation of overlying ice and catastrophic release of the stored water.

## 6.5 Diurnal variations of water levels in boreholes hydraulically connected to a subglacial channel through subglacial sediment

Boreholes that do not directly intersect subglacial channels at their base will terminate either at bedrock or in a basal sediment layer. Boreholes that terminate directly at bedrock are very likely to remain unconnected from the subglacial hydrological system. Volumes of water in unconnected boreholes exist as a remnant from the hot water drilling process and will stand in the borehole at a stationary level below the surface depending on the displacement of water as the hose is removed when drilling is finished (excluding any water level increase caused by surface input from melt or internal ice deformation). Water levels in bedrock-based boreholes will not show any significant variation diurnally or seasonally. The following scenarios indicate the affects of changing three properties of subglacial sediment, which provides a medium of hydraulic communication between boreholes and a subglacial channel. The properties include saturation, hydraulic conductivity and spatial confinement of sediment and will each be considered in turn.

### 6.5.1 Confined, saturated sediment of constant hydraulic conductivity

Figure 6.18 shows two boreholes terminating in uniformly distributed, confined sediment that underlies adjacent subglacial channels of different sizes. As the sediment is saturated and has a uniform hydraulic conductivity, pressure changes in the channel are reflected perfectly throughout the sediment. However, for the same unit volume of meltwater inputs, channels with a small orifice (Figure 6.18) will create higher daytime water pressures, as more water is forced out of the channel and into the sediment, which is reflected by higher daytime borehole water levels than those with a larger channel orifice.

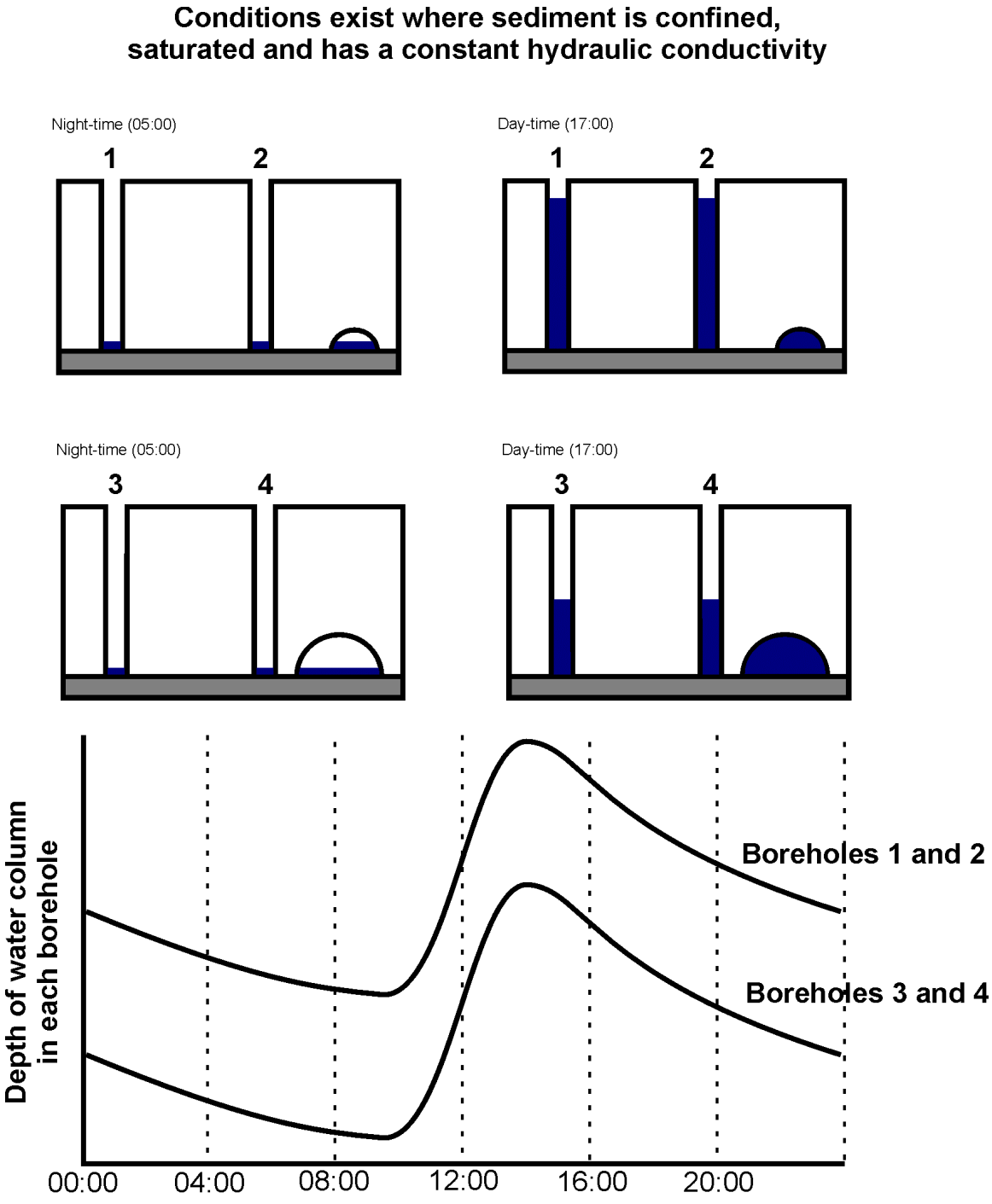
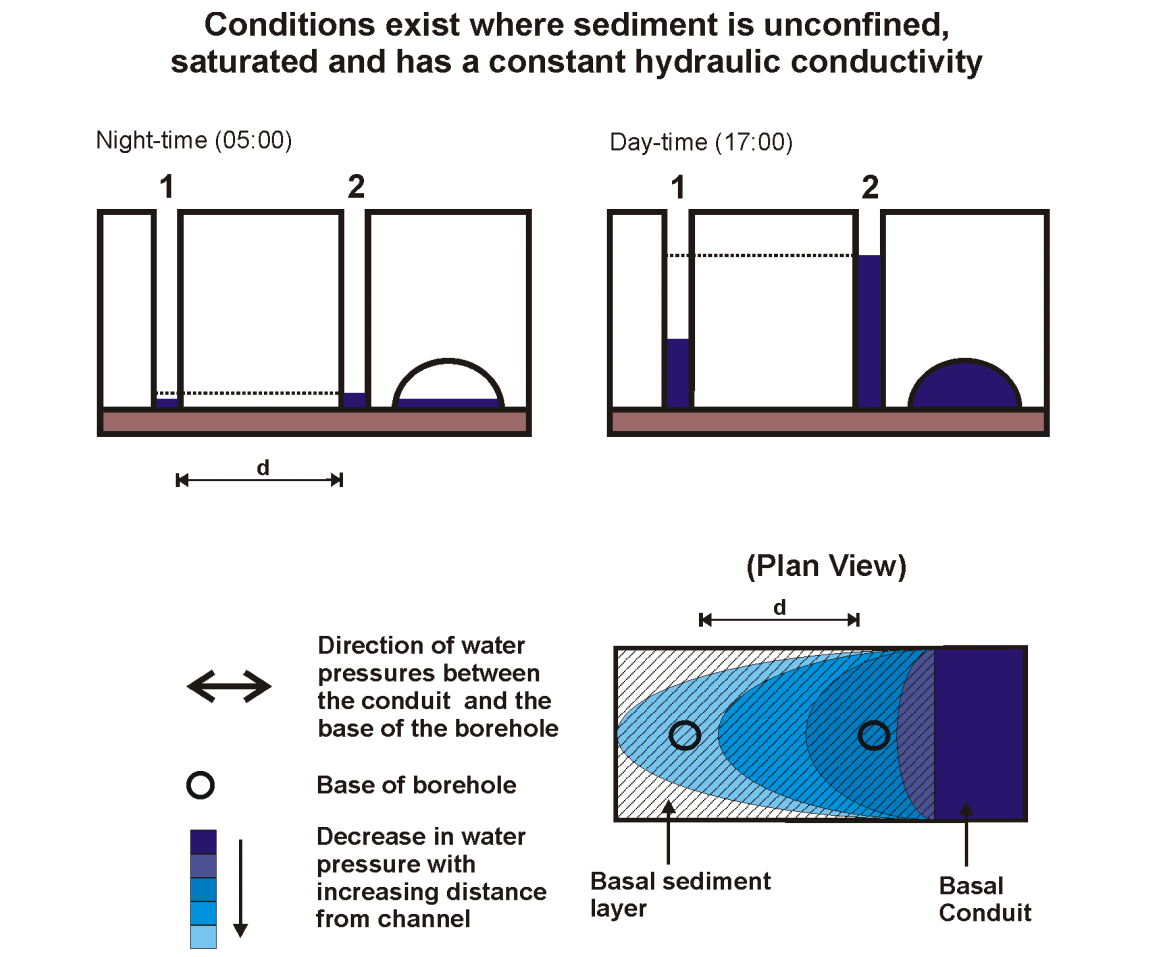



***Figure 6.18 – Diurnal variations in water levels of boreholes hydraulically connected to subglacial channels through a sediment layer.***

### 6.5.2 Unconfined sediment

Figure 6.19 illustrates a similar situation as Figure 6.18 shows, except the saturated sediment layer is not confined, and therefore incorporates a distance decay function of pressure wave magnitudes that emanate from the channel. Diurnal water level maximums in boreholes 1 and 2 will be similar in timing but lower in magnitude ($I_1$) further away from the channel as the pressure wave propagates through saturated sediment during a diurnal cycle. This differs to the ubiquitous, instantaneous change in pressure that occurs in a confined, saturated sediment layer. Distance between the channel and the borehole base is the controlling variable over the magnitude of the decay function, as pressure waves will diminish in magnitude with distance travelled.



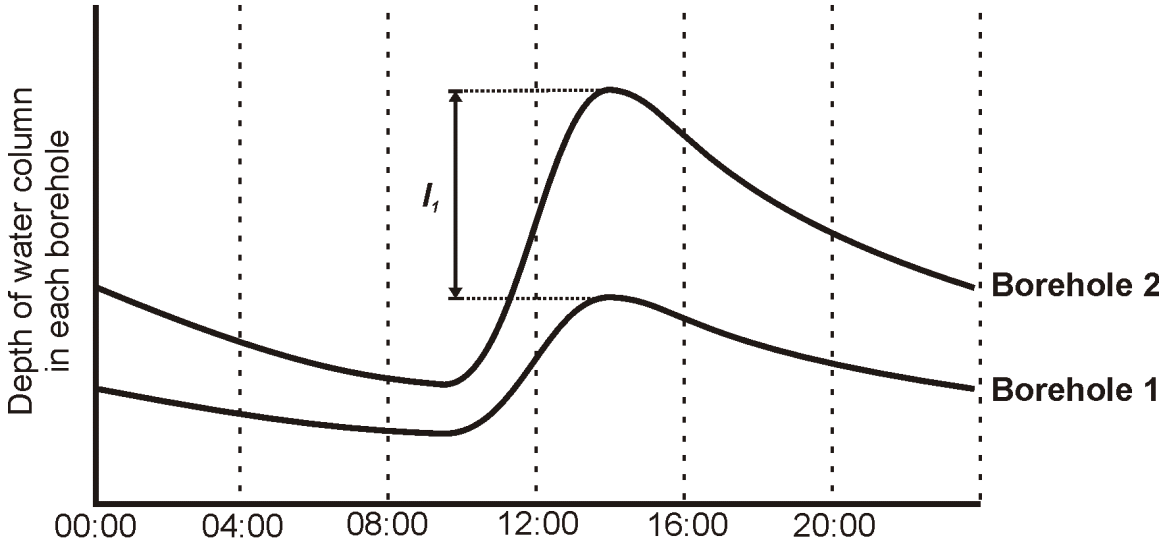




***Figure 6.19 – Diurnal variations in water levels of boreholes hydraulically connected to subglacial channels through a sediment layer. Where, $I_1$, represents the difference in magnitude of daily maximum water levels between boreholes.***

### 6.5.3 Unsaturated sediment

Figure 6.20 shows a similar scenario except that the sediment becomes unsaturated, causes greater spatial difference in propagation of water pressure waves from the channel. This is due to water having to physically flow through voids in the sediment rather than transfer a pressure wave by inter-molecular contact. More energy is used to transfer pressure through the physical movement of water as it has to overcome hydrostatic resistance of empty voids in sediment. This accentuates the magnitude of difference in maximum borehole water levels between boreholes located at different distances along an axis moving away from the channel. Not only will the height of the water column in boreholes be lower further away from the channel but also the respective ascending and descending limbs of diurnal borehole water level variations will start later ($I_2$) and finish earlier. However, the timing of maximum borehole water levels will still be the same regardless of the distance from the channel.

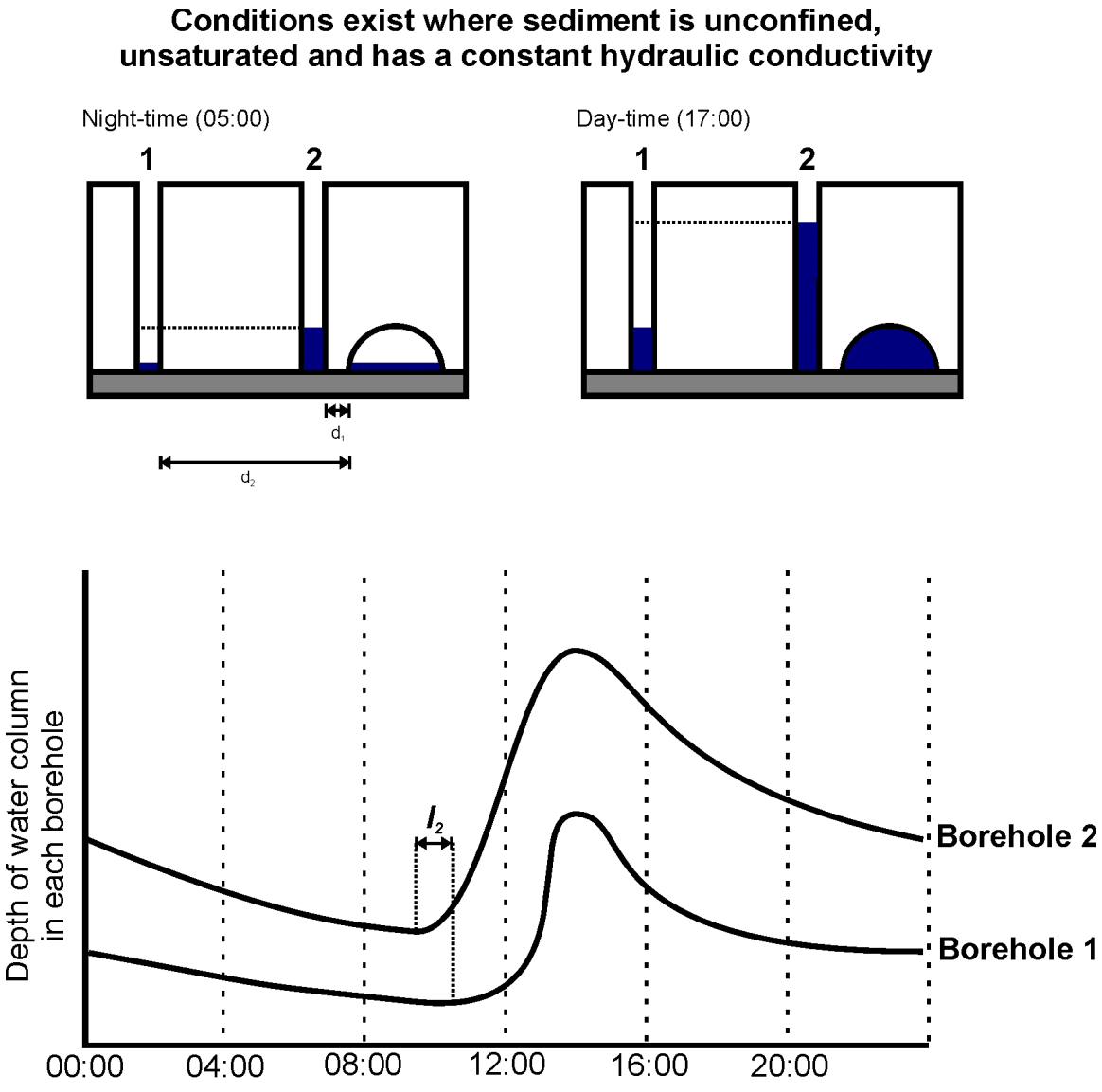



***Figure 6.20 - Diurnal variations in water levels of boreholes hydraulically connected to subglacial channels through a sediment layer. Where, $I_2$, represents the lag time between daily minimum borehole water levels.***

### 6.5.4 Variable hydraulic conductivity of sediment

Figure 6.21 shows the final theoretical situation, which most closely approximates reality where sediment is neither confined nor uniform in hydraulic conductivity or saturation. Variable hydraulic conductivity of the sediment incorporates greater unpredictability into the lag times of daily maximum and minimum borehole water levels, and the form of daily ascending and descending limbs. Figure 6.21 illustrates subglacial conditions after successive diurnal movements of water from the channel through sediments have preferentially washed out fines within the sediment matrix nearer the channel. This creates a hydraulic conductivity gradient in sediment that decreases with distance away from the channel. Consequently, the pattern of water level variation in borehole 2 shows a rapid increase and decrease due to greater efficiency in transfer of water pressure and movement of water. Daily maximum and minimum water pressures occur later in borehole 1 ($I_3$), which has a more attenuated diurnal pattern, due to increased transit times of water movement and dispersion of pressure waves in areas of unsaturated sediment. Water levels in boreholes nearer the channel respond more rapidly to changes in channel pressure than boreholes further away, causing the sign of the gradient of the piezometric surface to alter over a diurnal timescale.

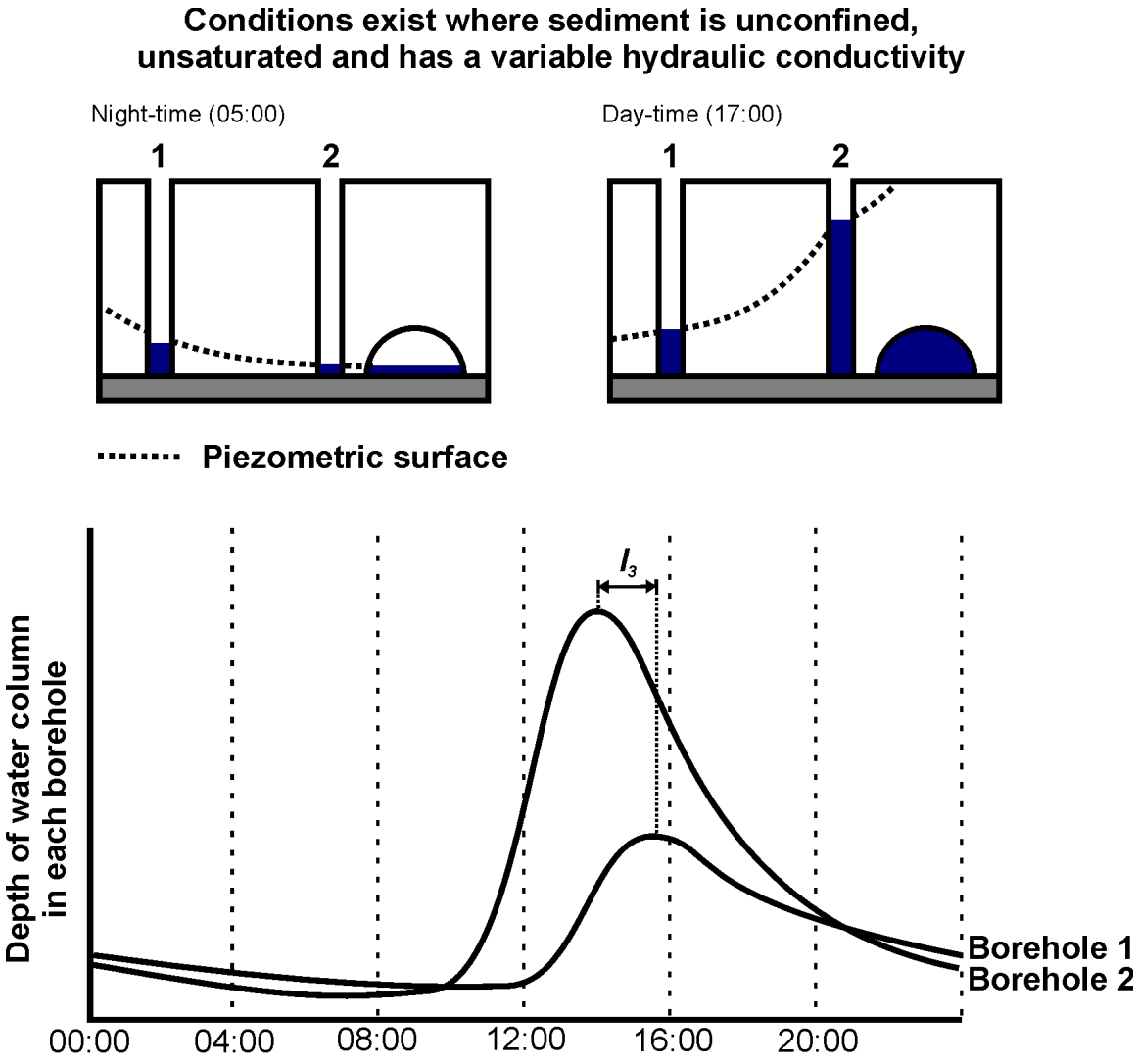



***Figure 6.21 - Diurnal variations in water levels of boreholes hydraulically connected to subglacial channels through a sediment layer. Where, $I_3$, represents the lag time between daily maximum borehole water levels.***

## 6.6 Summary

Development of conceptual models have demonstrated that although the subglacial environment is a complex system, major glaciological change in the subglacial drainage network may be observed in borehole water levels over both diurnal and seasonal timescales. When combined with surface runoff and proglacial discharge data, causes of changes in the subglacial drainage network that influence water storage can be identified and explained with greater confidence using *in situ* measurements of borehole water levels.

These conceptual models also provide a means to interpret a data series that is largely discontinuous in nature. Worthwhile statistical analysis of borehole water levels, such as cross-correlation techniques (Gordon *et al.*, 1998), force-response plots (Murray and Clarke, 1995) or nearest-neighbour analysis (Smart, 1996), requires periods of continuous borehole water level data. As has been outlined in chapter 4, despite every effort to reconstruct periods where there is missing data, continuous borehole water level data in this study is limited in availability.

Conceptual analysis demonstrates that great caution must be used when interpreting borehole water levels. Even if boreholes have only one simple basal hydraulic connection (Gordon *et al.*, 2001) interpretation of borehole water levels is fraught with uncertainty concerning hydraulic connections of boreholes with the subglacial drainage network. Therefore previous scenarios, although simplistic, best identify how perturbations of subglacial drainage can be evaluated in a semi-quantitative analysis. Other studies involving borehole water levels, such as the identification of a variable pressure axis at Haut Glacier d'Arolla (Hubbard *et al.*, 1995), have also restricted interpretations to a semi-quantitative analysis. To exceed this would create too much doubt over the validity of interpretations of variations in borehole water levels, which has recently been demonstrated by analysis of boreholes with more than one hydraulic connection

(Gordon *et al.*, 2001). Consequently, section III will go on to use such a semi-quantitative approach to elucidate changes in the glacial hydrological system as recognised from detailed treatment of water storage.

# SECTION III - RESULTS AND SYNTHESIS

Section III presents data collected during the monitoring programme and its subsequent analysis. Chapter 7 calculates and analyses water storage using 'black box' modelling techniques. The water balance is calculated within the glacial hydrological system by using modelled surface runoff (chapter 5) as inputs to the system and proglacial river discharge as outputs. Causes of changes in the capacity to discharge of the drainage network, here considered as a single reservoir, are examined chronologically throughout the ablation season and possible drainage structures are then discussed.

Spatial resolution of the analysis of water flow within the subglacial drainage system is increased in chapter 8. A distributed network of boreholes and surface velocity stakes are used to analyse spatial as well as temporal variations in subglacial water pressures and ice motion. These measurements allow a more detailed analysis of the processes that cause changes in the capacity to discharge within the subglacial drainage network and their affect on water storage. As processes that affect storage in chapter 7 are being considered at increasing spatial scales in chapter 8, chronological interpretation over the same time periods causes some repetition in the discussion. However, no apologies are made for this unavoidable repetition as the effectiveness of hydro-glaciological processes in changing the capacity to discharge of the subglacial drainage system are dependent on antecedent conditions. These are best analysed in a chronological manner. Despite the occasional annoyance of repetition, this method of analysis at least guarantees a thorough analysis of all available data.

Chapter 9 provides a synthesis of the conclusions made in chapters 7 and 8. Hydro-glaciological processes that affect water storage and the use of borehole water levels as a method of interpreting changes in subglacial drainage are discussed in relation to conceptual models created in chapter 6. Conclusions are then made regarding the structure of the subglacial drainage system.

# 7 WATER STORAGE

## 7.1 Introduction

Chapter 7 presents data describing surface runoff into and discharge from the glacial hydrological system at Findelengletscher. Using this data water storage is calculated and implications are made about the nature of the subglacial hydrological system in terms of its capacity to discharge surface inputs throughout the ablation season.

Section 7.2 compares the output of modelled surface runoff (the product of chapter 5) with meltwater equivalent derived from ablation measurements and proglacial river discharge. Cumulative total daily volumes of runoff using each method of estimation and their sub-seasonal trends are then contrasted.

Variations in the water balance are presented in Section 7.3. Trends in the water balance are identified and compared with trends previously highlighted in proglacial discharge. The water balance time series is then demarcated into periods of increasing and decreasing water balance (each period consists of an increasing followed by a decreasing trend in the water balance). Section 7.4 presents more detailed observations of each water balance period and proposes implications for the capacity of subglacial drainage system to discharge surface runoff.

Section 7.5 examines how changes in subglacial drainage affect the water balance and the discharge hydrograph throughout the entire ablation season. Suggestions are made about the nature of the mechanisms that cause temporary storage and subsequent release of subglacially routed water within a chronologically ordered discussion of each water balance period.

## 7.2 Comparison of modelled surface runoff and proglacial discharge

Figure 7.1 shows how estimated total surface runoff combines the effects of four meteorological and glaciological variables on rates of surface melt and direct runoff from liquid precipitation during the period Julian Day (JD) 212 to JD 259 in 1999. Variations in air temperature provide the main control over both seasonal and diurnal fluctuations in surface runoff. Trends in TSR over synoptic timescales are a reflection of variations in air temperature controlled by frontal weather systems in the mid-latitudes of Western Europe. For example, cold fronts and associated precipitation occur on JD 223 to JD 225 and JD 246 to JD 248, both of which are followed by warmer air masses. Trends of global radiation have little influence on TSR estimates over synoptic timescales although diurnal fluctuations in global radiation have a large influence on TSR over diurnal timescales. Increases in global radiation cause boundary layer air temperatures to increase, the rates of which are mainly dependent on the albedo of the surface. Daily variations in radiation caused by cloud cover are replicated in the time series of air temperature, such as distinct double peaks on JD 223 and JD 240. Intensity and duration of rainfall events, only interpolated over the snow-free area of the glacier, are reflected directly in TSR as spikes of runoff superimposed on volumes of meltwater, e.g. JD 228, JD 232 and JD 250. The effect of precipitation falling as snow on JD 224 and 247 reduces the elevation of the transient snow line (TSL) dramatically, effectively reducing rates of ice melt to zero if the TSL drops to an elevation below that of the glacier snout. As the TSL is estimated visually at a daily resolution and volumes of snow are not converted into meltwater when the elevation of the TSL subsequently increases, it is likely that hourly resolution TSR is underestimated. Due to the daily resolution of TSL assessment, such underestimation is unavoidable despite maintaining a conceptually correct physical basis to the model. However, Figure 7.1 shows over all forty-seven days, modelled TSR provides a good representation of variations in timing and relative magnitudes of expected variations in supra-glacial runoff.

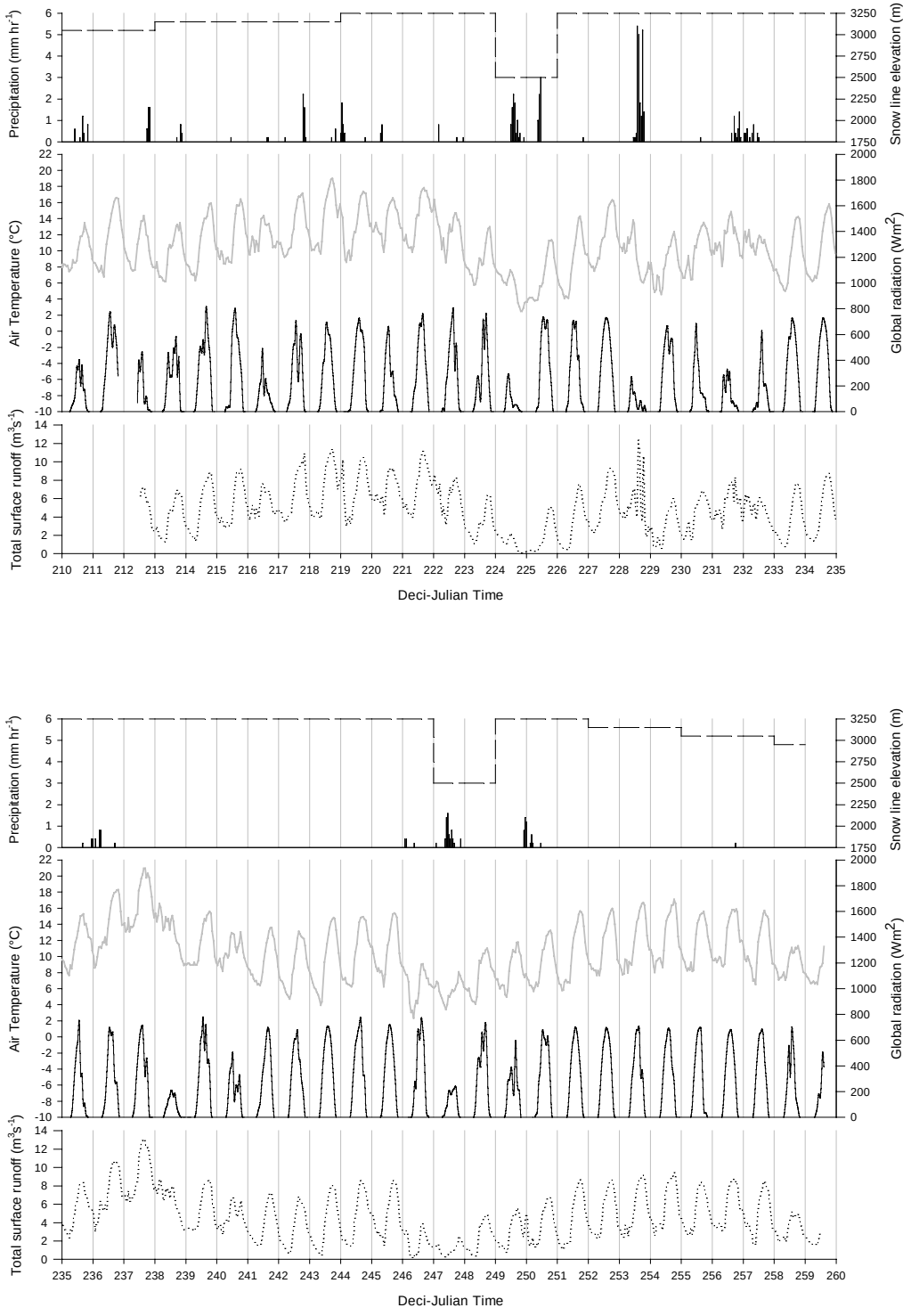



***Figure 7.1 - Hourly total precipitation (bars), diurnal variation of air temperature (grey solid), incoming solar radiation (black solid), modelled total surface runoff (pecked) and daily estimates of snow line elevation (dashed) at Findelengletscher, 29 July-17 September, 1999.***

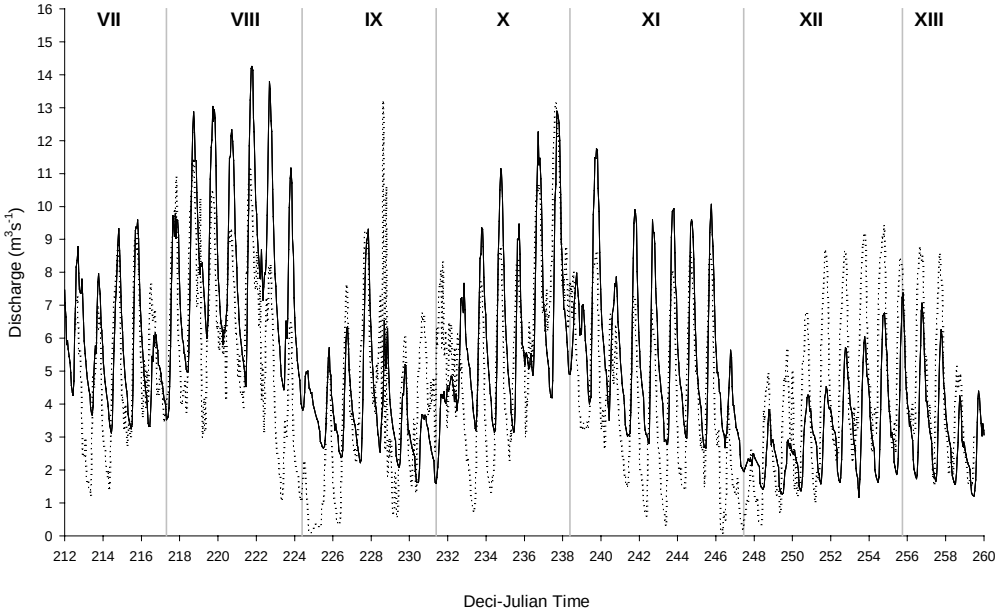



***Figure 7.2 - Hourly discharge (solid line) and modelled total surface runoff (pecked line).***

Comparison of modelled TSR with pro-glacial discharge does not compare like with like as TSR does not account for transit times of water through the glacial hydrological system nor temporary storage of water within the glacier. Consequently, underestimation of TSR in comparison with absolute values of minimum daily discharge is expected when glacier surface melt rates drop rapidly due to lack of global radiation at night. Also, possible overestimation is expected of maximum daily values, relative to discharge, as attenuating effects of temporary englacial storage are not incorporated. Despite such a physical basis for disparity between absolute measurements, values of TSR and discharge are within the same absolute range between 0–15 $m^3s^{-1}$ (see Figure 7.2).

Figure 7.3 demonstrates cumulative hourly TSR is consistently lower than cumulative hourly discharge between JD 213 and JD 260. Cold air temperatures and a drop in the TSL on JD 224

and 247 heavily influence consistent under-prediction of cumulative volumes. The influence of daily measurement resolution of TSL on hourly variations of TSR, relative to hourly measurements of discharge, causes a quicker reduction in rates of increase of cumulative TSR for a longer duration than hourly discharge. Thus, TSR and discharge both incorporate and respond more rapidly to volumes of released snow melt and indicate an earlier increase in rates of ice melt.

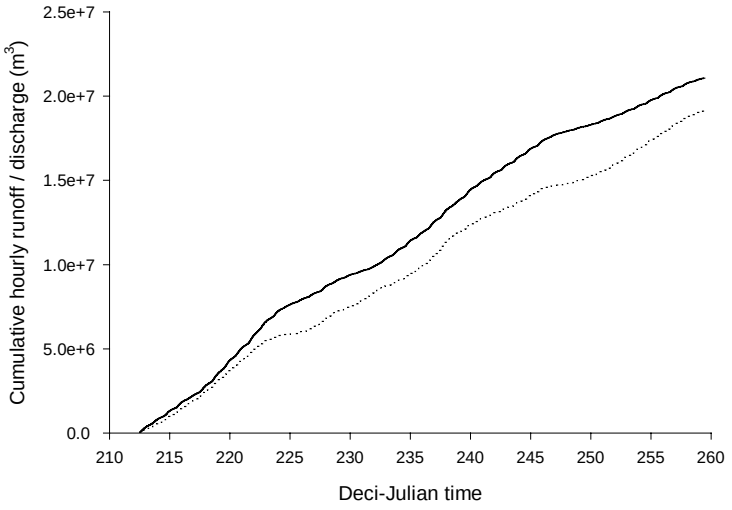



***Figure 7.3 - Cumulative total hourly runoff predicted over 30 consecutive days in 1999 using measurements from discharge in the pro-glacial river (solid line) and modelled estimates of total surface runoff (pecked line).***

Figure 7.4 shows how sub-seasonal trends in discharge throughout the ablation season are split into fourteen hydrological episodes, each of which are delimited by changing trends in proglacial discharge. In Figure 7.2 both daily maximums and minimums of TSR during hydrological episodes VII to XI tend to be less than that of discharge, unless meltwater is supplemented by high intensity precipitation (JD 228 and JD 321). Whereas, later in the ablation season (hydrological episodes XII and XIII) daily maximum TSR is consistently greater than discharge and minimums become approximately equal to or greater than discharge.

Timing of daily maximum and minimum discharge lags behind that of TSR throughout the monitoring period. Lag times of discharge behind TSR, using an hourly measurement resolution, are consistently 1-2 hours behind diurnal maximums and 3-5 hours behind diurnal minimums. Lag times between daily peaks in TSR and discharge of approximately two hours are corroborated by dye tracing experiments (see Table 7.1). An average transit time of parcels of water through the glacial hydrological system of 125 minutes was calculated by dye tracing parcels of water when river discharges were at or near daily maximums, which were routed from the glacier surface at approximately 2650m to the gauging station on the Findelenbach at 2500m.

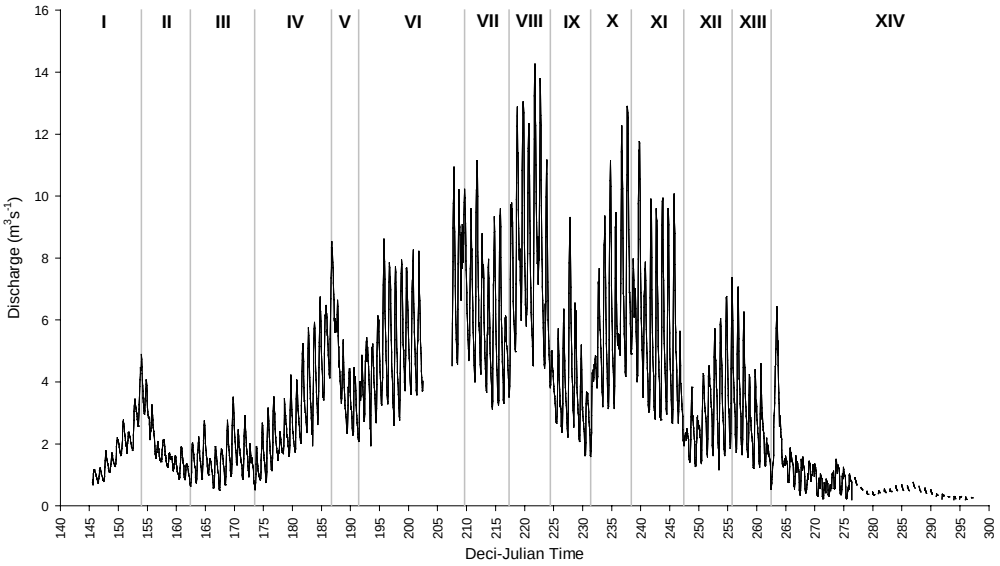



***Figure 7.4 - Hourly pro-glacial river discharge in the Findelenbach, 20 May - 27 October 1999. Vertical bars separate hydrological episodes (I - XIV) into distinct hydrological periods.***

| **Date** | **Time of dye dump (deci-julian time)** | **Transit time to peak (minutes)** | **River discharge at dye concentration peak ($m^3s^{-1}$) *(% of maximum daily discharge)*** |
|---|---|---|---|
| 23 Aug | 235.795 | 95 | 11.43 *(88%)* |
| 25 Aug | 237.741 | 125 | 9.76 *(99%)* |
| 27 Aug | 239.758 | 150 | 8.60 *(90%)* |
| 30 Aug | 242.849 | 133 | 6.64 *(88%)* |
| 1 Sept | 244.821 | 117 | 6.13 *(82%)* |
| 3 Sept | 246.850 | 129 | 9.13 *(100%)* |

***Table 7.1 – Summary table of six dye traces of parcels of water from runoff at 2650m of the glacier surface to the gauging station at 2500m on the Findelenbach, 1998.***

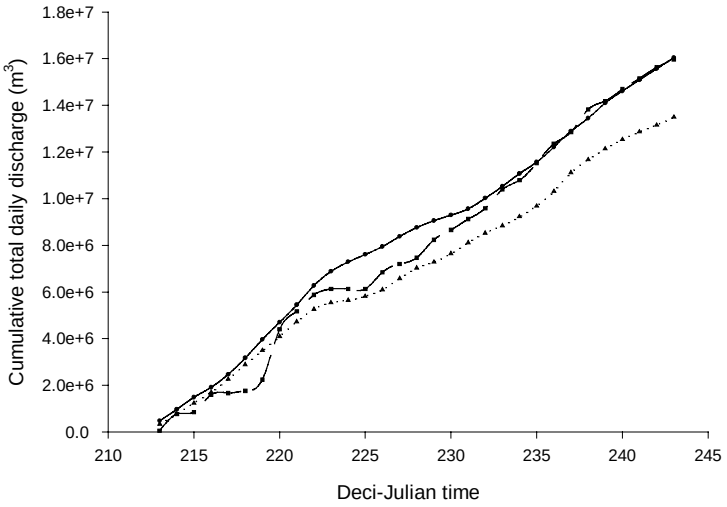



***Figure 7.5 – Cumulative total daily runoff from Findelengletscher 1–31 August 1999, using measurements from ablation stakes (dashed), discharge in the Findelenbach (solid) and modelled estimates of total surface runoff (pecked).***

Trends in ablation were measured at a daily resolution between JD 213 and JD 243, a shorter period than modelled TSR. Figure 7.5 compares cumulative modelled TSR and proglacial discharge with cumulative surface runoff calculated using ablation measurements. Cumulative runoff from ablation measurements provides a less accurate comparison to proglacial discharge than modelled TSR until JD 220, after which the comparison becomes more accurate (especially

after JD 233) until JD 243. Rates of increase in cumulative runoff calculated using ablation measurements drop twice between JD 216 to JD 219 and JD 222 to JD 225. The first reduction between JD 216 and JD 219 is followed by a sharp increase and is due to a combination of low measurement resolution and possible manual error in measurement between JD 217 to JD 219 that was accounted for by the measurement on JD 220. The second drop between JD 222 and JD 225 reflects the effect of cold air temperatures and a drop in elevation of the TSL that is replicated in modelled TSR. In comparison to measured discharge, variations in estimates of surface runoff using ablation measurements are more erratic than modelled TSR. Consequently, TSR reflects more accurately the relative changes in volumes of water draining from the glacier if not absolute amounts of discharge.

## 7.3 Variations in the water balance

Figure 7.6 show variations in water balance within Findelengletscher that are estimated from JD 212 to JD 259 by subtracting measured hourly discharge in the Findelenbach from modelled estimates of TSR. Water balance measurements are restricted to this portion of the ablation season due to a lack of meteorological and discharge data at other times. Although Figure 7.3 shows an overall trend in water draining from Findelengletscher, the hourly water balance indicates within this trend there are cycles of both storage and release of water within and from the sub- and englacial hydrological system. An approximate 5-day cycle of storage and release running from JD 214 to JD 244 is followed by a longer period of storage until JD 254, which is slowly released until the end of the monitoring period. It is unlikely that there is much significance to the temporal characteristic of 5-day cycles other than providing evidence that the subglacial hydraulic system does respond to changes in hydrometeorological conditions influencing both the absolute quantity and the rate of inputs and throughputs respectively.

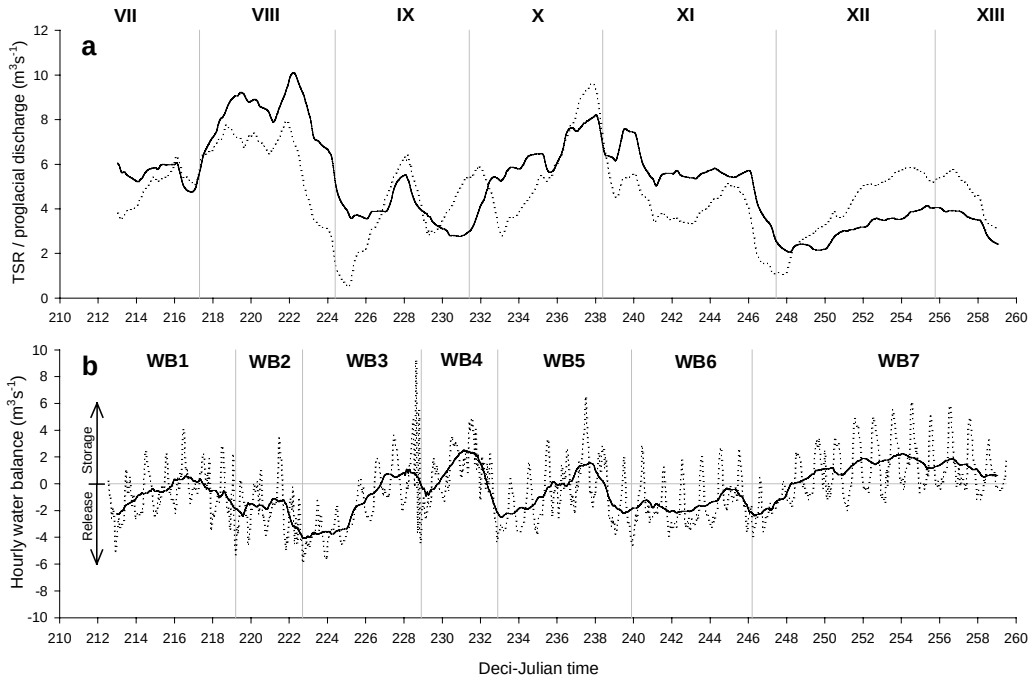



***Figure 7.6 - (a) 24-hour running average of total surface runoff (pecked) and proglacial discharge in the Findelenbach (solid) demarcated into hydrological periods, (b) hourly water balance (pecked) and 24 hour running average (solid) demarcated into periods of rising and falling water balance at Findelengletscher, 31 July - 16 September 1999.***

A clear diurnal signal of temporary daytime storage is exhibited (Figure 7.6) when inputs become backed-up in channels as volumes of inputs exceed the capacity to discharge (CTD), followed by release of backed-up water at night. The daily pattern of water balance, which is controlled by both shape and gradient of ascending and descending limbs of discharge and TSR, reflect the capacity of the glacial hydrological system to discharge runoff over a diurnal cycle. As over hourly timescales the subglacial drainage network does not act as a steady state system, variations in daily maximum and minimum values of discharge and TSR over consecutive days infer changes in lag times taken for the CTD to adjust to hydrometeorological inputs. Changes in CTD are evident if either consecutive daily maximum or minimum TSR and discharge fluctuate out of phase with each other. A decrease in the overall subglacial CTD occurs if TSR increases simultaneously with decreasing discharge, causing increasing rates of storage of subglacially

routed water. Conversely, CTD increases if TSR decreases simultaneously with increasing discharge causing increasing rates of release of subglacially stored water. Any other in-phase variations of TSR with discharge, including maximums and minimums that are equal on consecutive days, do not provide conclusive indications of variations in the CTD of the entire subglacial drainage network but may provide indications of trends in CTD over longer timescales. For reference, a detailed explanation of a channel's CTD using conceptual models and the affect that variation in the CTD has on temporary water storage throughout the ablation season can be found in sections 6.3 and 6.4.

Figure 7.6 shows broad sub-seasonal trends in TSR, proglacial discharge and water balance are identified using twenty-four hour running averages. Identification of increasing and decreasing trends in water balance allow demarcation into periods where the glacial hydrological system first stores and then releases water. Figure 7.6 shows clearly that unlike demarcation of hydrological episodes both the increase and subsequent decrease in water balance are together considered as one water balance period. In Figure 7.6 water balance periods are compared with the discharge hydrograph previously demarcated into periods of rising and falling discharge to contrast hydrometeorological and glaciological influences controlling water flow through Findelengletscher. Comparison of twenty-four hour running averages of TSR and discharge are used to highlight the cause of trends in water balance. When TSR and discharge vary are out of phase with each other trends in water balance vary rapidly, or if both variables fluctuate in-phase with each other but at different rates trends in water balance vary slowly. Twenty-four hour running averages of TSR and discharge are generally in phase with each other for the duration of the monitoring period (JD 212 to JD 259) other than on JD 229 to 230 (Figure 7.6). Until JD 229, increase and decrease in water balance results from differences in rates of change of predominantly in-phase fluctuations in trends of TSR and discharge. Trends of TSR and discharge are similar until this point with TSR leading discharge throughout.

Hourly changes in the water balance are slowly affected by differences in the rate of TSR and discharge when in-phase, and rapidly affected by differences between variables when they are out of phase. Although rates of change in water balance are greatest when both variables are out of phase with each other, the duration of such periods are dependent on relatively short lag times, which generally occur between the start of diurnally ascending TSR and discharge limbs. As a result, change in water balance is mainly a function of the relative differences in gradient of in-phase variables throughout the majority of the time series, for example the decrease in water balance at 13:30 on JD 221.

Throughout the ablation season, cycles of increasing and decreasing water balance indicate that the glacial hydrological system responds to changes in TSR. When volumes of surface runoff exceed the CTD of the subglacial drainage system higher subglacial water pressures cause frictional heat energy from larger flow velocities (as a consequence of increased water pressure) to melt ice walled channels, thus increasing the overall CTD of the drainage system. Timescales over which change in CTD occurs are hard to quantify exactly. Increases in CTD may happen relatively smoothly if channels consist of a single well consolidated material (generally either ice or sediment). A faster change in CTD may occur if channel walls are not well consolidated. Either increased flow velocities at high water pressures or removal of hydraulic support at low water pressures can exploit weaknesses in the mechanical structure of a channel wall causing a more abrupt failure. As changes in CTD can only be determined by the response of the glacial hydrological system, identification of changes are made through comparison of maximum or minimum TSR and discharge values before and after the event.

This section has identified the changing water balance at Findelengletscher. In doing so, it is clear that changes in the water balance are not easily derived simply from analysis of proglacial

outputs using an 'inverse approach.' (Richards *et al.*, 1996). Consequently, the integration of inputs (TSR) and outputs (proglacial discharge) is clearly justified for the identification of changes in CTD. The following section examines the impact of changes in CTD upon water storage in detail.

## 7.4 Detailed observations of water storage

The first water balance period (WB1) begins with successive days of increasing maximum daily TSR from JD 213 up to and including JD 218, which are only interrupted by low daily maximum TSR and discharge on JD 216. Increasing TSR creates increased water storage within the glacier up to and including the start of JD 217 as daily minimum TSR increases whilst CTD remains unchanged. Increasing maximum and minimum discharge on JD 218 to JD 221 suggests an increase in CTD within the whole drainage network. Figure 7.7 shows that at approximately 19:30 on JD 217 there is a sudden decrease in water balance, signifying a change in trend from an increasing to a decreasing water balance. A declining trend in water balance continues after a rainfall induced peak in TSR at 01:30 on JD 219, causing increasing daily minimum discharge later that day. Daily maximum TSR decreases on JD 219 compared with JD 218 whilst daily maximum discharge on both days is approximately equal. This indicates CTD on JD 219 has increased causing the release of temporarily stored water that supplements TSR to maintain maximum daily discharge.

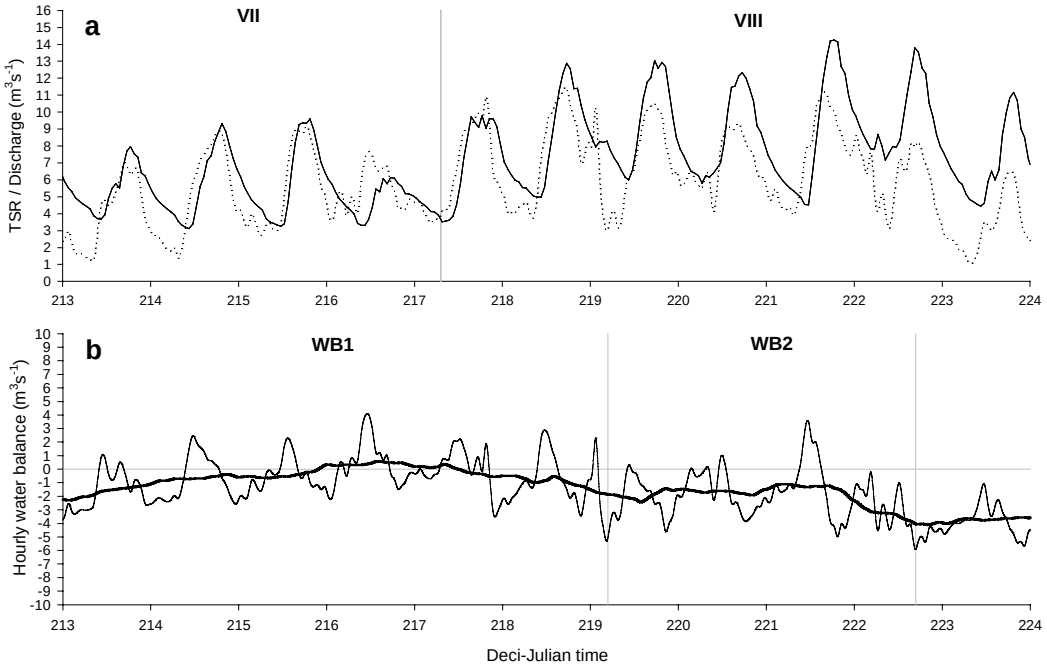



***Figure 7.7 - (a) Hourly total surface runoff (pecked) and proglacial discharge (solid), (b) hourly water balance (thin solid) and 24 hour running average (thick solid), Findelengletscher and Findelenbach 1–12 August 1999.***

Reduced daily maximum TSR on JD 219 and JD 220 affects discharge at the beginning of the second water balance period (WB2). Declining minimum daily discharge continues to be partially offset by release of water from temporary subglacial storage. Two consecutive days of seasonally high maximum daily discharges on JD 218 and JD 219 are consequences of high but declining daily maximum TSR in combination with released water from temporary storage as a function of increased CTD that increases overall efficiency of subglacial water throughput. Increased CTD reduces temporary storage of water from peak daily TSR backed-up in channels during the day and reduces the length of time backed-up water takes to discharge at night. This causes a substantial reduction in minimum discharge on JD 221. A further increase in CTD causes the water balance to decrease from 11:30 to 19:30 on JD 221 as a combination of subglacially stored water and increased daily maximum are discharged. Further release of water

from subglacial storage increases daily minimum discharge on JD 222 (the largest minimum discharge throughout the ablation season) and causes an increasingly negative water balance.

Maximum and minimum TSR continue to decline until JD 225 at the start of the third water balance period (WB3). The trend of decreasing water balance is arrested by a decline in TSR and the release of stored water on JD 222 to JD 223. This also causes a decline in daily maximum and minimum discharge during JD 223 and JD 224, which maintains a stable negative water balance. It is likely that CTD decreases between JD 223 and JD 225 as the high water pressures needed to maintain the increased channel orifice size through frictional melt do not occur during daily maximum discharges on previous days. Also, long periods of low (possibly atmospheric) channel water pressure will exist during diurnal cycles allowing channel orifice closure by ice creep when hydraulic support for the channel structure is unavailable. A decrease in elevation of the transient snow line causes very low TSR on JD 224 and JD 225, temporary exhaustion of subglacially stored water and a low discharge.

Daily minimum discharge drops slightly from 3.9 $m^3s^{-1}$ on JD 244 to 2.3 $m^3s^{-1}$ on JD 227 despite a higher daily maximum TSR on JD 226 than JD 223 indicating during the interim period there has been a reduction in CTD. Despite increasing maximum and minimum daily TSR between JD 225 and JD 228 causing an increase in the water balance minimum daily discharges exhibit a slight decreasing trend. This indicates TSR stored subglacially during the daytime, as peak TSR exceeds the CTD, are not released during the night. Prolonged increase in subglacial storage results. Maximum TSR on JD 228 is low, albeit interspersed by two large high intensity but low duration precipitation events, causing a temporary reduction in the water balance.

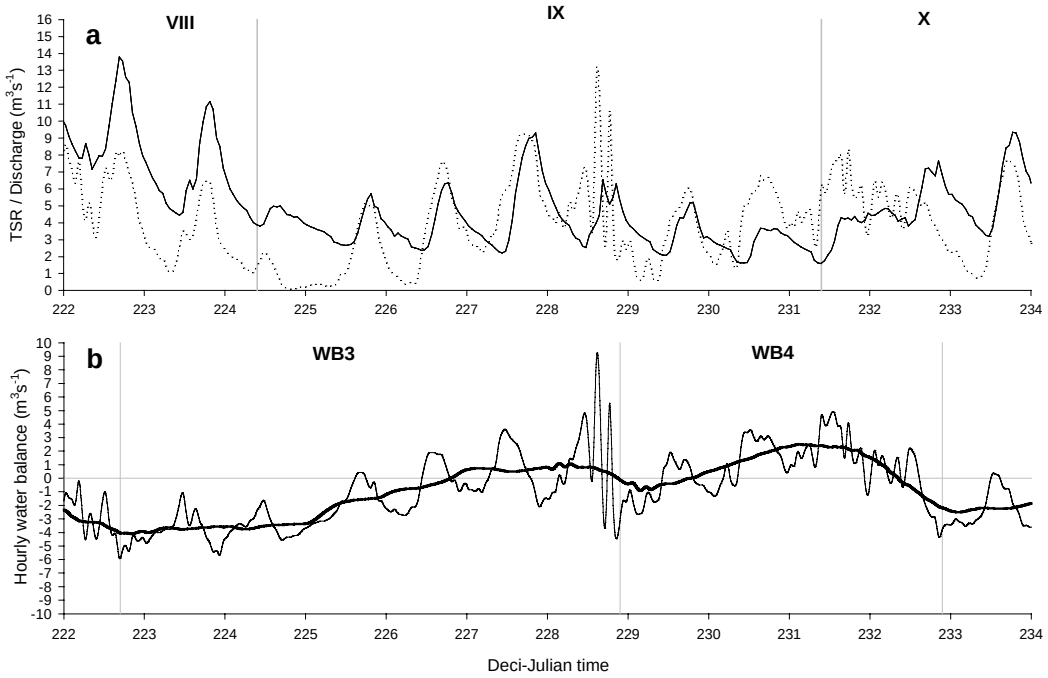



***Figure 7.8 - (a) Hourly total surface runoff (pecked) and proglacial discharge (solid), (b) hourly water balance (thin solid) and 24 hour running average (thick solid), Findelengletscher and Findelenbach 10–22 August 1999.***

An increasingly positive water balance at the beginning of the fourth water balance period (WB4) is a result of increasing maximum daily TSR between JD 229 and JD 231. Increasing TSR does not force an increase in CTD as daily maximum and minimum discharges remain low throughout. A further increase in daily maximum TSR on JD 231 is prolonged due to a high duration precipitation event that continues into the early hours on JD 232. The larger daily minimum discharge on JD 232, which is approximately equal to a continuation of maximum daily discharge on the previous day, is a combination of prolonged high TSR combining with release of subglacially stored water. Consequently, prolonged maximum discharge on JD 231, which is actually maintained for 19 hours, increases CTD so that TSR on JD 232 causes a peak in maximum daily discharge in conjunction with a rapidly decreasing water balance.

A decreasing trend in water balance on JD 232 is reversed on JD 233 at the beginning of the fifth water balance period (WB5). Despite the prior increase in CTD, increases in maximum daily discharge between JD 232 and JD 234 result from increasing maximum and minimum daily TSR. The increase in CTD between JD 231 and JD 232 is illustrated by comparison of daily maximum TSR and discharge before and after JD 231 and 233 respectively. Daily maximum TSR on both days are approximately equal yet daily maximum discharges increase from 4.3 $m^3s^{-1}$ to 9.3 $m^3s^{-1}$ as CTD is less restrictive to subglacial water flow. As daily minimum TSR between JD 233 and 236 increases faster than daily minimum discharge the increasing trend in water balance continues. Within this period of increasing water balance although daily maximum TSR on JD 235 is slightly less than on JD 234, daily maximum discharge on JD 235 is much lower in comparison to JD 234. This suggests CTD is slowly increasing in response to increasing water balance. Further increases in daily minimum TSR and discharge on JD 236, as increasing water balance is temporarily arrested, indicates CTD allows greater release of subglacially stored water. Water balance continues to increase on JD 237 despite increasing CTD as TSR has reached seasonally high daily maximum and minimum, therefore, causing increasing maximum and minimum discharge whilst still exceeding the CTD. An increasingly negative water balance from JD 238 up to JD 240 is a direct consequence of maximum and minimum discharge decreasing in-phase with TSR through an enlarged CTD.

Maximum and minimum discharge stop decreasing after JD 241 during the sixth water balance period (WB6), but the reasonably constant trend in negative water balance continues until JD 243 as daily maximum and minimum TSR continue to decrease. Release of subglacially stored water during JD 241 and JD 242 supplements volumes of TSR, therefore, daily maximum and minimum discharges are approximately equal to those on JD 244 and 245 despite having a lower daily TSR. As maximum discharges between JD 238 and JD 242 are lower than the potential maximum rates allowed by the CTD any reduction in CTD is slight if indeed altered at all until

JD 248. Consequently, a slight increase in water balance on JD 244 and JD 245 and a reduction on JD 246 are controlled solely by variations in TSR.

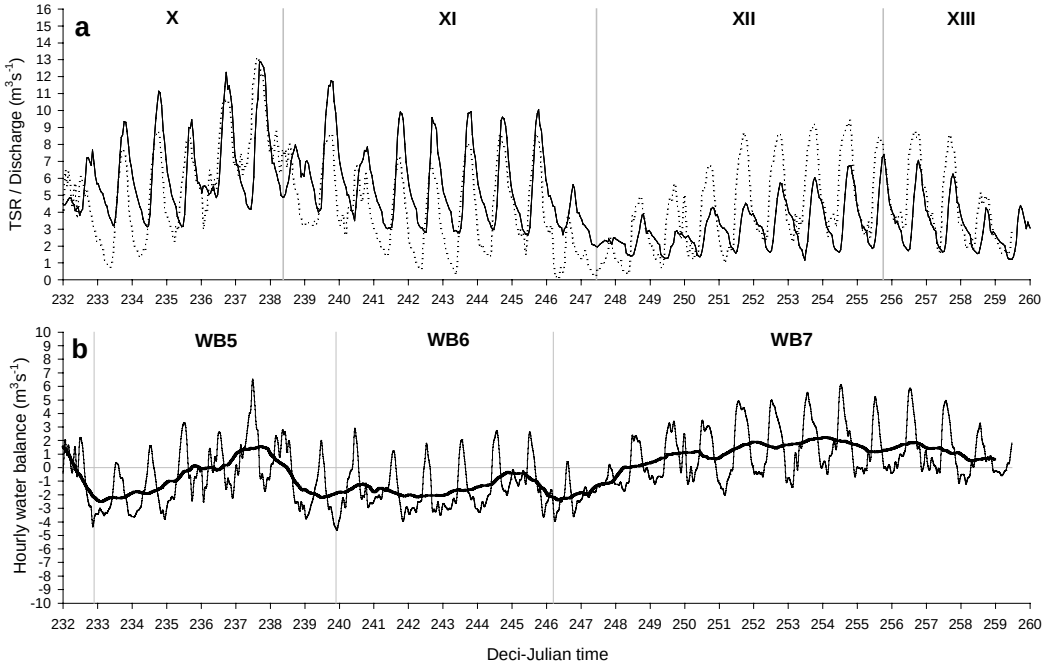



***Figure 7.9 - (a) Hourly total surface runoff (pecked) and proglacial discharge (solid), (b) hourly water balance (thin solid) and 24 hour running average (thick solid), Findelengletscher and Findelenbach 20 August - 17 September 1999.***

Two days of very low TSR on JD 246 and 247 at the beginning of the seventh water balance period (WB7), caused by a temporary descent in elevation of the snow line, are in-phase with a similar reduction in discharge. A reduction in CTD by JD 247 is illustrated by comparison of a greater daily maximum TSR on JD 248 than JD 246 creating a lower maximum daily discharge on JD 248 than JD 246. However, another reduction in CTD occurs early on JD 249 as again daily maximum TSR on JD 249 is greater than JD 248 whilst daily maximum discharge is less on JD 249 than JD 248. This decrease in CTD is shown in subsequent diurnal cycles on JD 250 and 251 where despite an increase in daily maximum TSR daily maximum discharge remains approximately constant. A lower CTD limits peak discharges and causes a more attenuated

hydrograph shape with a pronounced shoulder in the descending limb as TSR takes longer to discharge throughout the diurnal cycle. Although there is little variation in maximum daily TSR between JD 251 and JD 255 daily maximum discharge increases steadily as CTD gradually increases. As more water from daily inputs can be released at peak discharge the diurnal hydrograph becomes less attenuated throughout water balance period seven. Increasing water balance and CTD throughout the subglacial drainage network combine to allow increasing volumes of daily TSR to be discharged the same day, which maintains a similar minimum daily discharge between JD 249 and JD 255 and a positive water balance. Decrease in daily maximum and minimum TSR from JD 256 to JD 259 causes in-phase decline of discharge whilst maintaining a stable positive water balance.

## 7.5 Affect of seasonal variation in subglacial drainage on water storage

Analysis in section 7.4 shows a thorough examination of changes in the CTD of the subglacial drainage system as a whole. Due to the complex nature of the glacial hydrological system analysis of changes in CTD were conducted in isolation from an explanation of physical mechanisms describing their cause.

However, section 7.5 discusses why changes might occur in CTD, which have been highlighted in section 7.4, within the context of seasonal development of the subglacial drainage system. Consequently, the nature of mechanisms that cause temporary storage and subsequent release of subglacially routed water within the variable structure of subglacial drainage are presented in section 7.5. Evidence for seasonal development and interaction between hydraulically efficient and inefficient subglacial pathways is also presented in a chronologically ordered discussion of the entire ablation season.

### 7.5.1 Subglacial drainage in the early ablation season

Small peaks in discharge, which commonly punctuate the increasing seasonal trend of the Findelenbach, result from rapid evolution of the subglacial hydraulic system. Figure 7.4 shows two peaks or 'spring flood' events within the increasing trend, at the end of hydrological periods I and IV, are evident in the 1999 seasonal discharge hydrograph. The first peak, at the end of hydrological period I, is caused by initial seasonal snowmelt, the increasing rate of which is a result of interaction between the 0°C isotherm and glacier surface hypsometry that increases the elevation of the transient snow line.

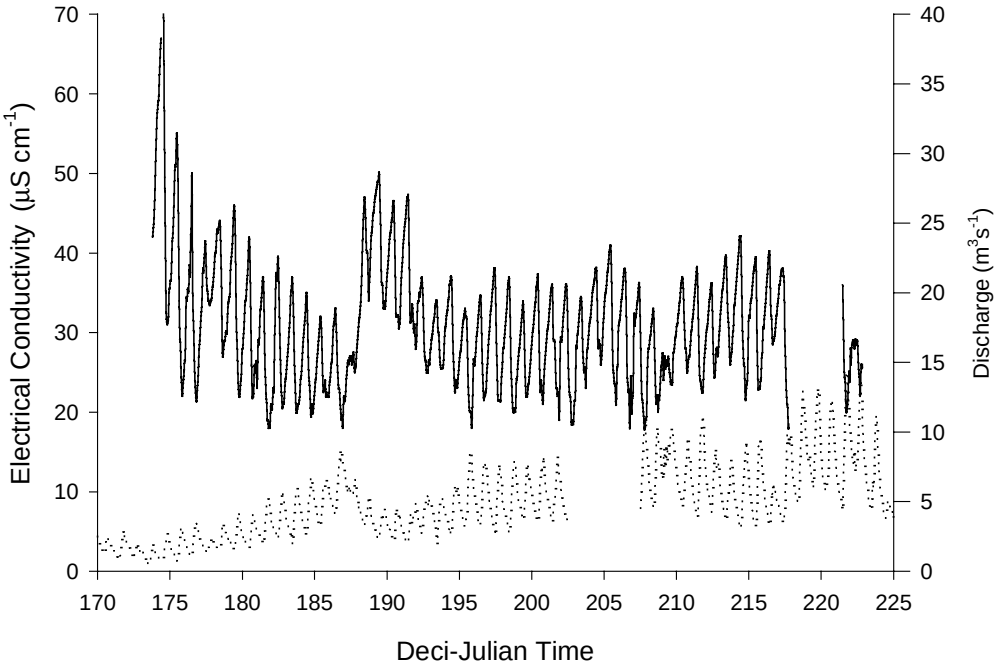



***Figure 7.10 - Hourly electrical conductivity (solid) and discharge (pecked) in the Findelenbach, 22 June -10 August 1999.***

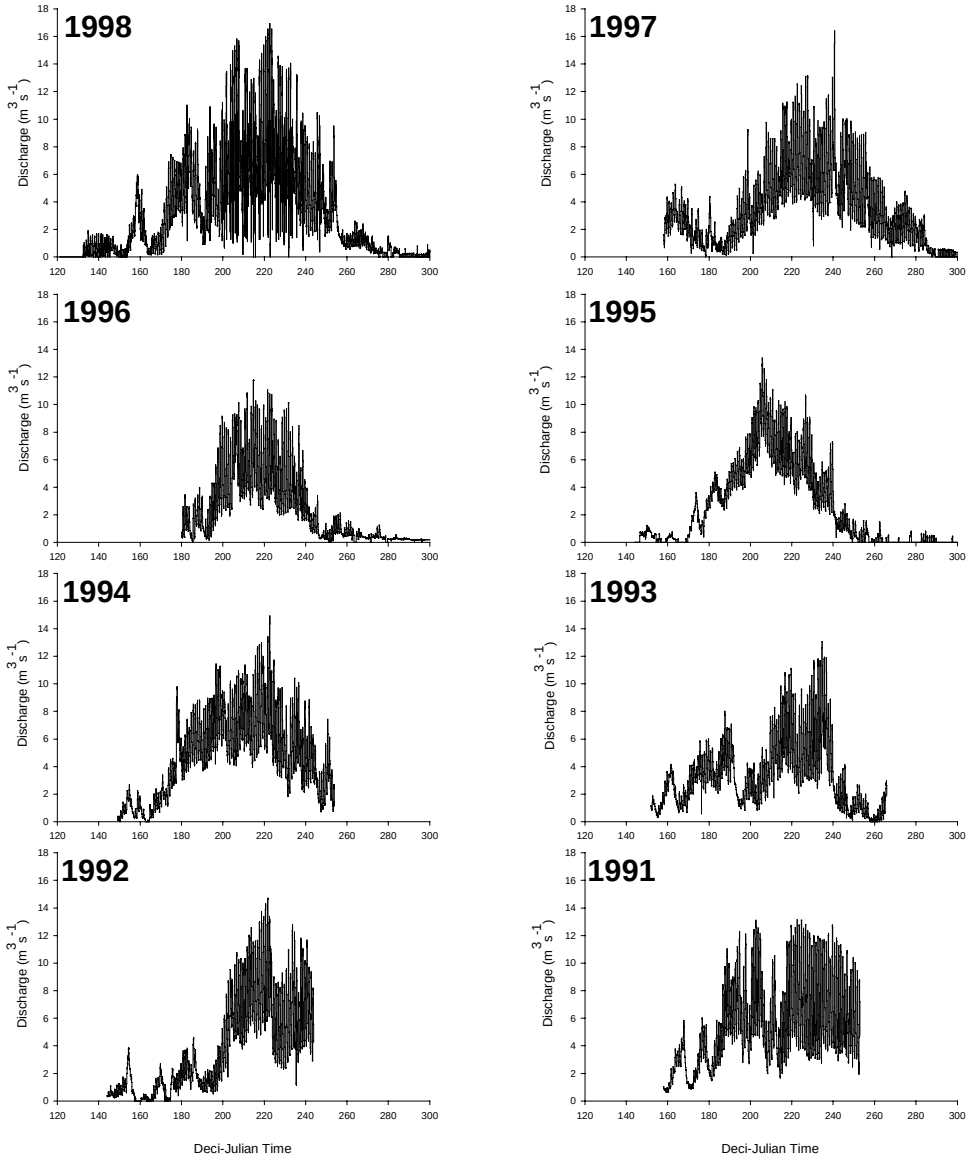



***Figure 7.11 - Annual discharge in the Findelenbach, 1991 - 1998 (Collins, Unpublished data).***

By the time of the second discharge peak at the end of period IV, comparison with bulk EC (used as a proxy for solute concentration) in the Findelenbach (Figure 7.10) indicates that the subglacial drainage system has become increasingly efficient at discharging surface inputs. An inverse

relationship between bulk EC and discharge exists from JD 173 to JD 195 suggesting that total discharge consists of a quick-flow component (low solute concentration) that dilutes a slow-flow component (high solute concentration) at times of high TSR. This inverse relationship both during and after a drop in discharge is maintained. It is in-phase with low TSR caused by low air temperature on JD 187 and suggests that by this point in the ablation season both distributed (slow-flow) and concentrated (quick-flow) drainage types coexist within the whole subglacial drainage network.

Comparison of the discharge hydrograph in the Findelenbach during the 1999 ablation season (Figure 7.4) with hydrographs (consisting of complete or near complete data) from the previous eight years (Figure 7.11) shows that single or multiple early season peaks are common within trends of increasing discharge. Early season peak discharges of this nature are highly significant to subglacial drainage evolution as they rapidly increase the CTD of the drainage system allowing subsequent increases in the daily discharge range, which are illustrated after the second peak in 1999. Increase in daily range is caused by a proportionally lower increase in daily minimums than daily maximums as less water is backed-up within the drainage system at times of peak TSR so that a greater proportion of total daily TSR is discharged through the glacier quickly during the day and not at night. Large ranges and low daily minimums, for example 1998 in Figure 7.11, indicate the drainage system has quickly evolved to efficiently discharge (in each twenty-four hour period) the total daily volumes of TSR generated by hydrometeorological conditions of a particular ablation season. Dye tracing experiments in 1998 (see Table 7.1) provide evidence that the subglacial drainage network at Findelengletscher can evolve at least partly into a highly efficient subglacial drainage system, indicating rapid transit times (~125 minutes) of water flow through the glacier at or near the time of peak daily discharge. Low diurnal ranges and high daily minimum discharges indicate either TSR is consistently high or transit times of peak TSR through the subglacial drainage network are low. Low transit times can be saused when peak daily TSR

becomes either backed-up in concentrated drainage systems without increasing the CTD routed through distributed drainage systems with long transit times. Low ranges and consistently high daily minimums, for example 1995 in Figure 7.11, indicate the whole drainage system has a smaller capacity to discharge relative to daily volumes of TSR. Maintenance of high daily minimums suggest water is routed through a more distributed drainage network of numerous small channels where longer transit times are maintained, as volumes of surface runoff do not exceed the CTD for a sufficient period of time each day to substantially increase the CTD and reduce transit times on subsequent days.

Comparison of hydrographs between 1991 and 1999 indicate that, subject to the idiosyncrasies of seasonal hydrometeoroloical weather conditions, for example sudden snowfalls on JD 224 and JD 247, the evolution and deterioration of subglacial drainage systems under Findelengletscher are inter-annually variable. Glaciological factors significantly influence the seasonal variation in daily maximum, minimum and range of discharge within an ablation season, although no clear inter-annual trends of glaciological controls over discharge are evident from the hydrographs alone. As shown in Figure 7.12, such inter-annual variation in subglacial drainage is in accordance with other recent studies at Findelengletscher. Iken and Truffer (1997) established that an arborescent subglacial channel system, which connected moulins to large R-channels, was destroyed by increases in glacier sliding velocities during the winter of 1979-80. Subsequently the proportion of distributed drainage increased, which seasonally evolved to feed smaller, more numerous R-channels that were independent of previous larger R-channels. As small R-channels were re-established, seasonal evolution during 1981-85 allowed redevelopment of the former arborescent drainage network consisting of fewer, larger R-channels.

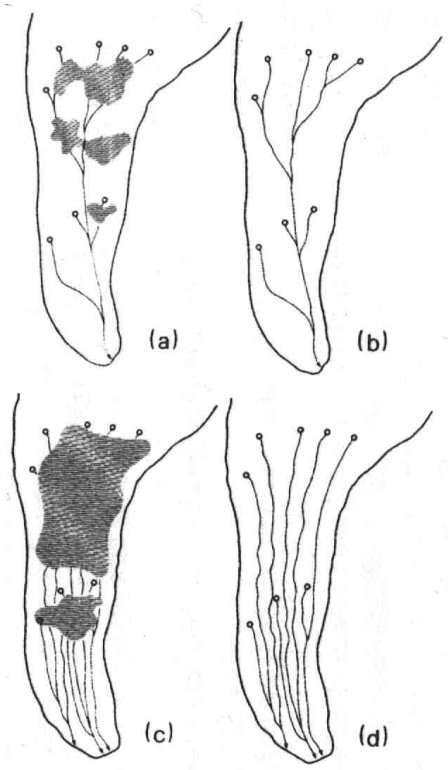



***Figure 7.12 - Scheme of presumed changes of subglacial drainage at Findelengletscher prior to and during an advance represented by moulins (circles), subglacial R-channels (lines) and zones of interconnected cavities (shaded). (a) and (b) are prior to the advance and (c) and (d) are during; (a) and (c) are early in the ablation season and (b) and (d) are late (Iken and Truffer, 1997).***

### 7.5.2 Subglacial drainage in the mid ablation season

As modelled TSR is likely to slightly underestimate actual TSR (see section 7.2) absolute variations in water balance are also likely to be underestimated causing the water balance to be negative for a greater amount of time than in reality. Consequently, the point at which TSR equals discharge (resulting in a water balance of zero) is used as a secondary approximate measure compared to the primary objective of identifying relative change within the water balance time series. As water balance incorporates differences in both TSR and discharge, diurnal patterns of water balance are more erratic than either TSR or discharge considered in isolation. Comparison of 24-hour running averages in Figure 7.6, shows the speed of increase or

decrease in water balance is more gradual when both TSR and discharge vary at different rates whilst in-phase with each other, for example WB6, whereas rapid change occurs when they vary out of phase with each other, for instance during WB4. Differences in diurnal phase relationships, usually as a function of the time lag between the start of diurnally ascending and descending limbs of TSR and discharge, cause erratic temporal fluctuations that are superimposed over a regular diurnal pattern of increase and decrease.

Demarcations of trends in water balance (WB1-WB7) are not in alignment with demarcation of hydrological periods (VII-XIII) of increasing and decreasing trends in discharge. As water balance is calculated from the difference between TSR and discharge, the disparity between demarcation of trends is a result of glaciological factors controlling subglacial storage and release of water and not solely hydrometeorological conditions dictating trends in discharge.

Within each demarcated water balance period the duration of increasing water balance tends to be longer than the more rapid decrease. Physical processes controlling temporary subglacial water storage, which either increase transit times through existing preferential subglacial pathways or re-route water towards previously less efficient pathways as a result of localised changes in the hydraulic gradient, take longer than processes causing reversal and consequent release of stored water. Both processes of temporary subglacial water storage and consequent release of stored water can operate when TSR is either increasing or decreasing. For example, an increase in water balance occurs when TSR is increasing during WB5 and when TSR is decreasing at the beginning of WB3. Decrease in water balance occurs when TSR is increasing during WB1 and when TSR is decreasing during WB6. This suggests subglacial routing of water that results in temporary storage can be caused by multiple subglacial hydraulic mechanisms that are dependent on antecedent glaciological conditions.

When maximum daily discharges are approaching or at the seasonal maximum at Findelengletscher, variations in water balance during WB1 and WB2 are primarily under the influence of variations in TSR as subglacial hydraulic conditions provide a secondary rate limiting factor to water flow. At this stage of the ablation season the subglacial hydrological system is likely to be operating at its maximum capacity with as large a proportion of daily TSR as possible being routed through the most efficient part of the system herein referred to as the tunnel-conduit system. Only a gradual increase in temporary storage of water within the subglacial hydrological system occurs before a low maximum daily TSR on JD 216 during WB1. Any water that may be held in temporary subglacial storage prior to JD 216 is not released during the period of low TSR, which provides an opportunity for temporarily stored water to supplement discharge. Instead, a precipitation event on JD 217 that sustains and increases peak TSR causes a release in subglacially stored water that is shown by a rapid decrease in the water balance.

Despite TSR increasing on JD 218 release of subglacially stored water continues and is exacerbated by another precipitation event that peaked at 01:30 on JD 219 causing a lower water balance than on JD 217. The CTD of the subglacial drainage network as a whole has been increased by sudden rainfall induced increases in TSR, which are superimposed on regular diurnal cycles, rather than gradual changes in response to in-phase fluctuations of TSR and discharge. It is more likely that the sudden nature of increases in CTD have resulted from increased connectivity of many small, relatively unstable (possibly distributed) drainage pathways rather than gradual enlargement of one or two major R-channel type conduits through melt from frictional heat. Sudden short duration increases of TSR, which are superimposed on diurnal cycles, increase inputs so that volumes and pressures of subglacial water exceed stability thresholds within small channels independent of the main tunnel-conduit system. As a result new, more efficient flow pathways are formed within areas of distributed drainage that can subsequently be enlarged by melt from frictional heat.

Increased efficiency within subglacial areas of distributed drainage allows water that is released from temporary storage to supplement maximum daily discharge despite declining TSR. This maintains a constant trend in negative water balance in WB2. As the proportion of temporarily stored water that contributes to TSR to create total discharge declines, an increase in water balance on JD 221 is caused by increasing transit times of TSR at the beginning of the daily ascending limb of the TSR cycle. Transit times have increased as less water is flowing through a drainage system with an enlarged CTD, causing reduced flow velocities due to a combination of lower water pressures and increased channel wetted perimeter producing greater frictional resistance. Lag times between commencement of ascending limbs of TSR and discharge on JD 221 are consequently greater.

However, despite an increase in daily maximum TSR a further reduction in the water balance occurs as more water is released from temporary subglacial storage to cause the maximum seasonal discharge. A sudden increase in the rate of release of water from temporary subglacial storage, in comparison to rates of release throughout the previous night that caused a decrease in minimum daily discharge, is most likely to be the result of low subglacial pressures in the tunnel-conduit section of the drainage network. Low channel water pressures at night in the tunnel-conduit system can cause reversal in the direction of hydraulic gradients. Hence, the potential direction of water flow is now from adjacent areas of distributed drainage where water is temporarily stored towards the tunnel-conduit system. Localised, relatively stochastic factors of ice shear strength, floatation and sediment cohesion will determine when temporarily stored water breaches ice-sediment barriers connecting the tunnel-conduit section of the drainage network with adjacent areas of distributed drainage in which water is temporarily stored. Increasing flow rates from areas of distributed drainage to the tunnel-conduit system that enlarge the CTD of hydraulic connections connecting the two systems are likely to persist for the rest of WB2, thereby creating

the largest daily minimum discharge of the ablation season and a further decrease in water balance.

Water draining from sources of temporary subglacial storage continues to supplement rapidly decreasing TSR maintaining a negative water balance in WB3. It is possible almost all water in temporary subglacial storage has been released after the cold period in WB3, which reduces TSR to the lowest daily maximum throughout the monitoring period on JD 224. After the entire subglacial drainage network has reached its highest CTD to date a combination of very low TSR and release of the majority of subglacially stored water from temporary storage causes low volumes and low water pressures within the network. Low water pressures allow creep closure of channels by ice overburden pressures, especially of hydraulic connections between the distributed and tunnel-conduit sections of the drainage network. These will reduce the capacity of the entire network to discharge over a period of 24 to 36 hours around JD 224. As a result of creep closure, subsequent TSR flows through a drainage system with a lower CTD cause greater rates of storage and an increase in water balance during WB3. It is likely most of the TSR that contributes to increased storage is once again being routed into areas of initially distributed subglacial drainage prior to JD 224 temporarily incorporated into the more efficient tunnel-conduit system. Increasing proportions of steadily rising TSR between JD 225 and JD 227 are routed through the main channel(s) in the tunnel-conduit section of the drainage network providing a regular shape to the diurnal hydrograph. However, it is unlikely that creep closure of channels in the main network causes TSR to back up over three consecutive days as daily minimum discharges remain virtually unchanged. This would not be the case if water stored temporarily in the tunnel-conduit system during the daytime was discharged at night. Instead, it is more likely that creep closure has affected the newly opened and most likely smaller sized orifices through which subglacially stored water was released into the tunnel-conduit channel network when precipitation induced increases of TSR caused water pressures to exceed subglacial stability thresholds. Consequently,

the connectivity of large areas of initially inefficient subglacial drainage pathways, which were previously hydraulically isolated from the tunnel-conduit system, may well be ephemeral requiring constant high inputs to force and maintain hydraulic connections.

Two high intensity precipitation events on JD 228 appear not to have had the same impact on the entire subglacial drainage network as previous precipitation events. Although there is a decrease in water balance the decrease is more likely to be caused by low rates of ice-melt due to heavy cloud cover. The two peaks in TSR are reflected rapidly by two distinct peaks in the discharge hydrograph, indicating rapid transit of precipitation derived TSR through the tunnel-conuit network. As throughput of precipitation derived TSR is not obstructed by water that could have been temporarily backed-up in the tunnel-conduit system, the increasing water balance of the previous three days is a consequence of significant proportions of daily TSR being routed into subglacial areas adjacent to the tunnel-conduit section of the network. Such adjacent areas, comprising of distributed style drainage act as reservoirs that are ephemerally connected to the tunnel-conduit section of the drainage network. The impact of precipitation derived TSR events on JD 228 on subsequent subglacial routing of TSR becomes apparent at the start of WB4 as the water balance increases when TSR increases out of phase with discharge. High magnitude precipitation induced peaks in TSR on JD 228, albeit each of low duration, appear to be large enough to transcend thresholds constraining the direction of subglacial water flow. This causes preferential routing of subsequent TSR into subglacial areas away from the tunnel-conduit section of the network. Glaciological rather than hydrometeorological controls become the dominant influence over water routing through the glacierised section of the catchment until precipitation prolongs TSR early on JD 231 and the daily maximum discharge is maintained throughout the night due to a combination of precipitation and release of subglacially stored water until the end of WB4.

An increasing water balance during WB5 is a consequence of areas of distributed subglacial drainage adjacent to the tunnel-conduit section of the drainage network filling with water whilst TSR increases in-phase with maximum discharge. Gradual recharge of these areas through storage of TSR, since the last major release of temporarily stored water during JD 232, is released on JD 236 when an increase in daily minimum discharge is again synchronous with a short precipitation event. Release of temporarily stored water on JD 236 is rapidly followed by further increases in TSR culminating on JD 237 with seasonally high maximum and minimum daily TSR. High volumes of TSR exploit hydraulic connections between the tunnel-conduit section of the drainage network and adjacent subglacial areas of distributed drainage. Increased hydraulic efficiency of these connections allows the whole subglacial drainage network to discharge TSR more quickly. Seasonal maximum TSR does not produce a seasonal maximum discharge as although both the CTD and TSR are high, the absolute volumes and rate of release of temporarily stored water that commenced on JD 236 are not large enough to continue supplementing discharge by JD 237. Consequently, a reduction in the water balance after the peak seasonal TSR is simply a result of a reduction in TSR that is unaffected by rates of subglacial water storage or release.

Low TSR through the daytime on JD 238 does not observe a recognisable diurnal cycle (after relatively high TSR the previous night due to warm air temperatures) and causes a double peak in the diurnal discharge cycle. The second peak is a result of one of two mechanisms. Water is either released from temporary storage when low water pressures in the tunnel-conduit section of the drainage network cause a reversal in the hydraulic gradient, initiating flow from adjacent areas of storage towards the tunnel-conduit section of the network. Alternatively, a substantial proportion of TSR during the previous night may be routed through hydraulic pathways adjacent to the tunnel-conduit network that have much longer transit times and contribute to the second diurnal peak. The lack of a recognisable diurnal cycle in TSR on JD 238 may have highlighted

constituent parts of the regular diurnal hydrograph. This separates the diurnal discharge cycle into components of quick-flow through the main tunnel-conduit network and slow-flow through a less efficient section of the total drainage network that is dominant in the recessional curve.

In WB6 after JD 240 similar maximum and minimum daily discharges are maintained by a combination of trends in release and storage of water within the subglacial network that are synchronous with trends of decreasing, then increasing TSR. Variations in trends of release and storage of subglacially routed water are consequently out of phase with decreasing and increasing TSR throughout WB6. This causes the release of temporarily stored water to compensate for decreasing TSR up to and including JD 242 and then increasing TSR compensates for decreasing rate of release of water from temporary storage until the end of WB6. The ability for the subglacial drainage system to compensate for variations in TSR through temporary storage and release is also illustrated over a shorter timescale when a double peak in TSR on JD 240, during a period of otherwise declining TSR at the beginning of WB6, is reflected by only one attenuated peak in discharge. Trends in TSR and trends in storage or release of subglacially routed water indicate that preferential pathways of subglacial water flow are dependent on water pressures and spatial connectivity within the drainage network. As TSR decreases, water pressures in the main tunnel-conduit part of the network should decrease faster than adjacent areas of less hydraulically efficient drainage. Consequently, the hydraulic gradient between the tunnel-conduit system and distributed drainage should become stronger towards the tunnel-conduit system. Maintenance of near constant maximum and minimum daily discharges indicate the subglacial drainage system has evolved over WB5 into an increasingly efficient system that can adjust to changes in inputs. It does so by rapid subglacial redistribution of water through spatial variation in water pressure, allowing temporary storage and release of water without requiring major changes in glacial hydraulic configurations.

Decreasing discharge at the beginning of WB7 is caused directly by a large drop in TSR on JD 246, the relative magnitude of which cannot be compensated for by release of subglacially stored water. Even lower TSR on JD 247 causes an increase in the water balance as low water pressures in the tunnel-conduit system cause increased transit times of what little TSR is flowing through the subglacial system. This acts in combination with a decrease in the CTD of channels connecting distributed and tunnel-conduit systems due to creep closure. An increasing trend of maximum daily TSR until JD 255 is in-phase with discharge other than on JD 249 when despite increasing maximum and minimum TSR, including an additional precipitation-induced input, the maximum daily discharge decreases. In comparison to the low discharge on JD 247 the low, attenuated discharge on JD 249 is a result of glaciological rather than hydrometeorological influences that have decreased the CTD of the subglacial drainage network. As a result of the second decrease in CTD within three days there is a further increase in subglacial water storage that is indicated by an increasing water balance on subsequent days.

### 7.5.3 Subglacial drainage in the late ablation season

A constant positive water balance continues throughout WB7 until the end of the period for which TSR can be calculated. Although lack of precipitation and radiation data after JD 260 prevents continued comparison of discharge with TSR, Figure 7.13 shows a comparison of air temperature with discharge and provides an indication of further variation in the water balance. A large increase in discharge on JD 263 is superimposed on an otherwise decreasing trend of maximum and minimum daily discharge. Air temperature also observes a general decreasing trend but the regular diurnal variations undergo severe perturbations as discharge increases on JD 262. Departure from the regular diurnal cycles in air temperature suggests the perturbations are caused by a period where there is heavy cloud cover and possibly precipitation. Although data does not exist to verify or disprove this hypothesis, the meteorological sequence of rising air

temperature associated with heavy rainfall, followed by a rapid decrease then increase in air temperature over a synoptic time scale, is consistent with the passage of a warm front over the glacierised catchment from JD 261 to JD 267. If precipitation and warm air temperatures do occur through the night between JD 262 and JD 263, as a result of frontal atmospheric movement and associated heavy cloud cover, the peak in discharge on JD 263 may result from increased precipitation induced TSR. This could be in combination with release of temporarily stored water in subglacial areas adjacent to the main tunnel-conduit network. A positive water balance for the majority of WB7 implies that a large proportion of total daily TSR has become stored within areas of the subglacial network that are either not contributing or contributing at very low rates to total daily discharge. Release of stored water on JD 263 through precipitation induced subglacial mechanisms would follow similar releases earlier in the ablation season on JD 219, JD 231 and JD 236.

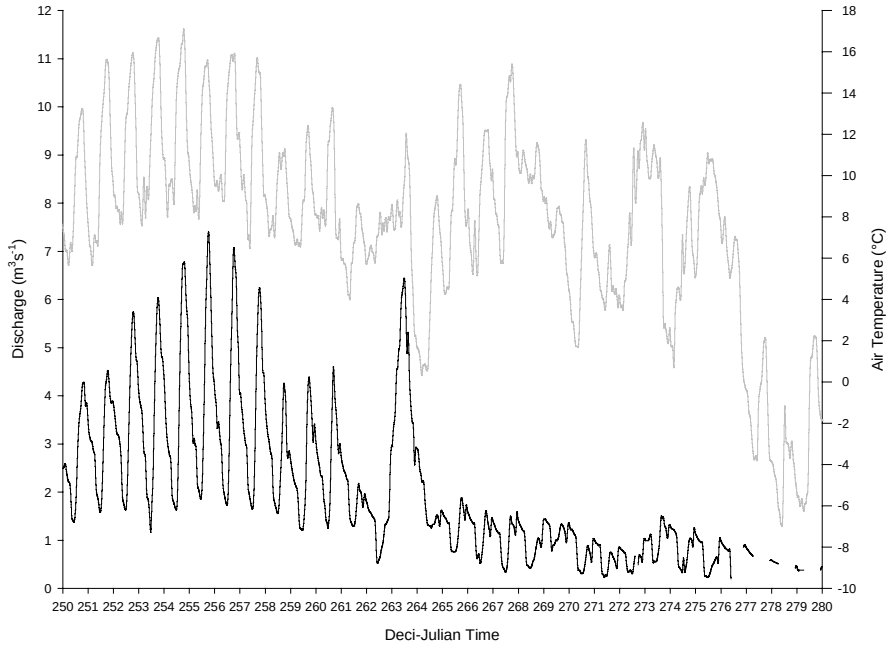



***Figure 7.13 - Hourly air temperature (grey solid) and pro-glacial discharge (black solid) in the Findelenbach, 7 September - 7 October 1999.***

## 7.6 Summary

Temporal variations in the water balance at Findelengletscher have been calculated. It has been clearly shown that integration of inputs (TSR) and outputs (proglacial discharge) is necessary for identification of changes in the CTD of the glacial hydrological system rather than using either inputs or outputs in isolation. Conceptual models developed in sections 6.3 and 6.4 have proved useful tools in understanding and analysing the affect of the CTD of subglacial channels on the overall water balance.

After the second spring peak discharge event at Findelengletscher on JD 186 in 1999, the subglacial drainage network is comprised of sections of hydraulically efficient (tunnel-conduit) and inefficient (distributed) drainage. Hydraulically efficient subglacial drainage is likely to consist of only a few large channels that may be cylindrical like R-channels (Röthlisberger, 1972) or broad and low (Hooke *et al.*, 1990), which are likely to have intra-annual persistence (Iken and Truffer, 1997). Hydraulically inefficient subglacial drainage, which consists of many small interconnected channels that are tortuous in nature such as linked-cavities (Kamb, 1987), is likely to coexist with and temporarily connect to the larger channels. Variations in the water balance are suggested to be a function of the CTD of hydraulically efficient and inefficient systems and the proportion of total daily TSR that is routed through each.

Analysis of seasonal variations in the water balance indicate three main mechanisms cause temporary subglacial water storage:

1. Increased transit times of water flow through the existing tunnel-conduit system. This results from low volumes of TSR flowing through channels previously enlarged by larger volumes of TSR.

2. TSR becomes backed-up within the tunnel-conduit system. This results from rates of water input to a channel section exceeding the capacity of the channel to discharge.
3. Re-routing of water from the tunnel-conduit system through less efficient subglacial pathways. This is due to localised changes in the hydraulic gradient that substantially increase subglacial residence times.

The first storage mechanism, when enlargement of channels increases transit times of subsequent throughflow of TSR, has a very short-term affect on water storage and is dependent on lag times between diurnally ascending limbs of TSR and discharge that are of the order of only a few hours. Lag times of discharge behind TSR have the affect of rapidly increasing the rate of subglacial water storage (or at least reducing the rate of release) during the diurnal water balance cycle and are sensitive to prevailing meteorological conditions that can be highly variable. Water storage resulting from the second mechanism will also be short-term and unlikely to exist for longer than a twenty-four hour cycle without changing the dimensions of the channel through which it is flowing or exploiting a different subglacial hydrological pathway.

Increasing water storage over timescales greater than twenty-four hours occurs via the third mechanism when TSR is re-routed from the tunnel-conduit section of the drainage network. Water can be re-routed supraglacially into moulins and crevasse fields that have different englacial hydrological connections with the subglacial drainage network. Otherwise subglacial re-routing of water occurs when the hydraulic gradient causes water to flow away from the tunnel-conduit section of the system and towards adjacent sections of the network. Adjacent sections consist of less efficient, distributed drainage systems such as linked cavities (Kamb, 1987), small multibranched arborescent networks (Hock and Hooke, 1993) or sedimentary layers beneath basal ice. The rate and duration of water transfer from the tunnel-conduit system into adjacent sections of distributed drainage are determined by a combination of diurnal variations of

water pressure in the tunnel-conduit system, the size of hydraulic connections between tunnel-conduit and distributed drainage (whether it be a channel orifice or hydraulic conductivity of sediment) as well as localised topographic factors.

Analysis of seasonal variations in the water balance shows that release of temporarily stored water is caused by large changes in the hydraulic gradient between areas of tunnel-conduit and distributed drainage within the subglacial drainage system. The two main mechanisms that cause a sufficient change in hydraulic gradient to cause release of water from temporary storage are:

1. Inputs from rainfall-induced TSR events increasing subglacial water pressures in areas of distributed drainage.
2. Very low daily TSR, caused by a temporary drop in elevation of the transient snow line, reducing subglacial water pressures in tunnel-conduit areas of drainage.

All these conclusions, which highlight spatial difference within the subglacial drainage system, support ideas of seasonal evolution at Findelengletscher made by (Iken and Truffer, 1997) and further substantiates the influence of rainfall at high elevation on release and transfer of water through Findelengletscher (Barrett and Collins, 1997; Collins, 1998a). However, as not all rainfall-derived TSR and low daily TSR events cause release of subglacially stored water, further analyses using in situ measurements of subglacial water pressure are necessary. Consequently, chapter 8 will provide the focus for investigation of temporal and spatial variations in the ephemeral nature of hydraulic connections, both between and within tunnel-conduit and adjacent sections of distributed drainage. Conceptual models developed in chapter 6 will be used to aid interpretation of borehole water levels, which reflect variations in subglacial water pressures caused by localised changes in the CTD of the subglacial drainage system.

# 8 HYDRO-GLACIOLOGICAL INFLUENCES ON SUBGLACIAL WATER STORAGE

## 8.1 Introduction

Chapter 8 increases the spatial resolution of water storage analysis within the subglacial drainage system. Data describing subglacial water pressures, glacier sliding velocity and vertical displacement are presented from a distributed network of boreholes and stakes drilled into the glacier surface.

Potential topographic influences that may restrict or enhance subglacial water flow are discussed in Section 8.2. Section 8.3 then presents borehole water level data as a surrogate measure of subglacial water pressures, bearing in mind limitations for interpretation that have been outlined during development of conceptual models in chapter 6. Detailed observations of borehole water levels are considered in relation to increasing and decreasing trends in the water balance using semi-quantitative analysis of phase relationships. Then interrelationships between the structure of the subglacial drainage system and variations in water pressures are discussed as causes of water storage during each water balance period.

Section 8.4 presents data describing fall-line velocities and vertical displacement of the glacier surface. Ice motion events are then discussed in relation to changes in subglacial water pressures and their affect on the water balance.

## 8.2 Topographic influences on subglacial drainage

Subglacial topography as well as surface topography will influence the spatial distribution of water beneath the glacier subsole. Gravitational forces primarily influence the direction of water flow within the catchment. However, subglacial water is likely to be at pressures greater than atmospheric pressure. Therefore, as the glacier is not a freely conducting body, water does not necessarily flow at an angle that is either perpendicular to the englacial equipotential surface or at the lowest possible subglacial elevation. This is illustrated in other temperate Alpine glaciers, for example the location of the variable pressure axis beneath Haut Glacier d'Arolla (Hubbard *et al.*, 1995), where subglacial channels are not present at the point of lowest elevation along a cross-section of the glacier bed.

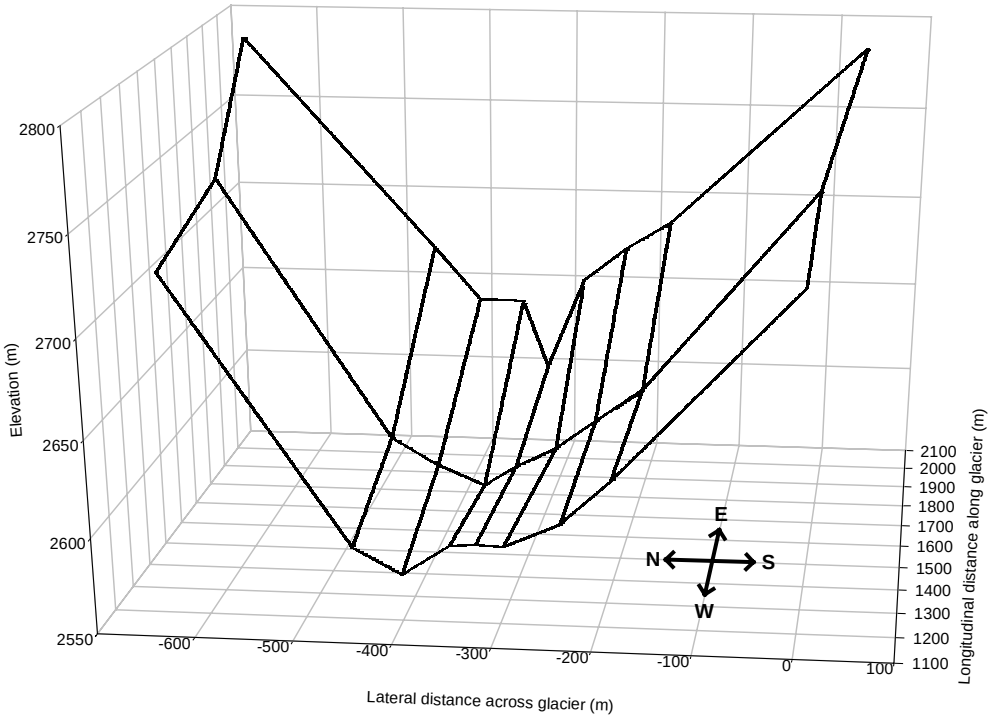



***Figure 8.1 - Three-dimensional estimate of a section of the subsole of Findelengletscher made from ice depth measurements in boreholes (exaggerated in the vertical axis).***

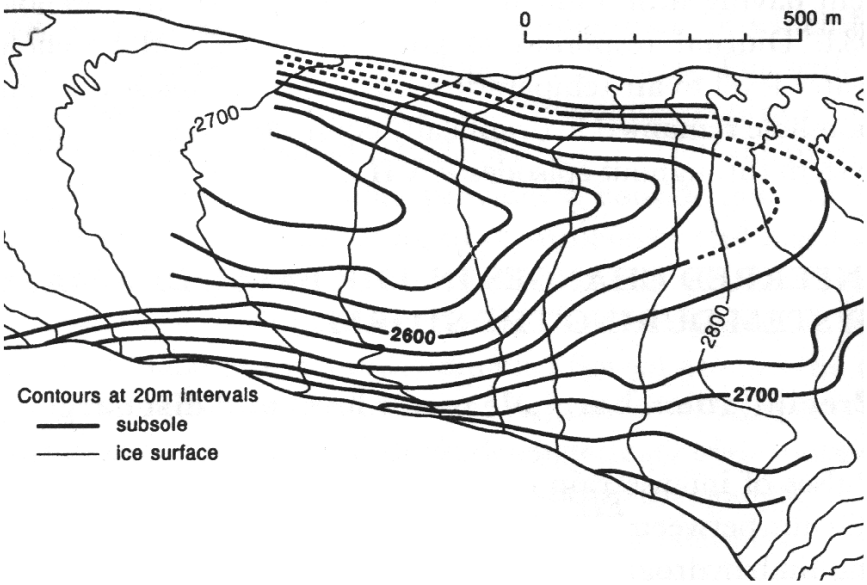



***Figure 8.2 - Map of ablation area of Findelengletscher, showing contours of ice surface and subsole (Modified from Iken and Bindschadler 1986; from radio-echo soundings by H. P. Wächter Unpublished).***

Figure 8.1 provides estimates of the subglacial topography under Findelengletscher that have been made using boreholes to provide twenty-one point measurements of ice depths. Previous studies have used radio echo soundings (Wächter, Unpublished), see Figure 8.2, and seismic soundings (Süsstrunk, 1959) to reconstruct subglacial topography over the area between the three borehole arrays (see Figure 8.4). The number of point measurements in Figure 8.1 is inadequate to give a reliable estimate of subglacial topography over the areas between borehole arrays and should only be used in conjunction with the radio-echo soundings that provide a greater number of data points that are more spatially distributed.

Similarities exist between subglacial topography in Figure 8.1 and Figure 8.2, indicating that the valley floor broadens and the point of lowest elevation becomes more greatly skewed towards the north side of the valley as the glacier descends in elevation. Both diagrams indicate that in the

areas between the three borehole arrays there are unlikely to be any significant ridges (riegels) or over-deepenings where the flow of subglacial water can become restricted or temporarily stored. This fits in with the conceptual models of subglacial water storage developed in chapter 6, which assume no major obstructions to water flow are presented by subglacial topography. Consequently, this further increases the validity of using constrictions and expansions in the CTD of subglacial channels as a means of understanding changes in subglacial water storage in chapters 8 and 9.

## 8.3 Spatial and temporal variations of water storage within the subglacial drainage network

Water pressure in subglacial channels is a reflection of the CTD (see chapter 6). Dimensions of the borehole are assumed to remain unaffected by englacial ice flow. It is also assumed no englacial channels intersect the borehole and the hydraulic connection between the base of a borehole and the nearest influencing subglacial channel remains constant throughout the monitoring period. Intersection of englacial channels was verified using borehole video, which only found one englacial channel intersection, in borehole 99.55 (see Figure 8.3), out of all the boreholes that were drilled in 1999. Lack of borehole inclinometry data or remote sensing of the subglacial environment, using imaging techniques such as GPR, meant verification of changing borehole dimensions and subglacial connections between the boreholes and the drainage network was not possible. Consequently, the assumption that borehole water levels (BWL) reflect water pressures in subglacial channels relies on changes in BWL occurring faster (by orders of magnitude) than changes in dimensions of the borehole, which are predominantly controlled by internal deformation of glacier ice. Little can be done to prevent misinterpretation of changes in BWL due to changes in connections between the base of a borehole and the drainage network rather than changes in the section of the subglacial drainage system itself. However, misinterpretation in this manner may be limited by considering interpretation of the absolute magnitudes of variations in BWL only within each borehole water level time series. Comparison of variations in BWL with TSR, discharge or BWL in another borehole must therefore be limited to comparison of relative changes within each time series. Not all of the twenty-one boreholes drilled in 1999 connected with the subglacial hydrological system and of those that connected, temporarily or permanently, five were subject to continuous measurements of BWL (see Figure 8.4 and Table 8.1). Another eight boreholes that connected were subject to regular spot height measurements (Table 8.2) allowing a temporal and spatial indication of variation in BWL across

the glacier between JD 201 and JD 260. It can be seen from Table 8.2 and Figure 8.4 that over a third of the boreholes were drilled into hydraulically isolated areas of the glacier bed and a similar proportion only slightly or intermittently connected.

| | Boreholes 1999 | | | | |
|---|---|---|---|---|---|
| | 99.10 | 99.30 | 99.33 | 99.52 | 99.54 |
| Measurement period | 15 August – 16 September | 20 July – 1 September | 29 July – 2 September | 29 July - 10 August | 29 July – 23 August |
| Missing data (%) | 40.7 | 73.2 | 64.8 | 0.3 | 35.4 |
| Reconstructed data (%) | 18.2 | 0.0 | 12.5 | 0.0 | 8.9 |
| Maximum water level - measured or *estimated* (metres a.s.l.) | 2721.8 (2742.6 – 18.6 above ice surface) | 2728.5 | 2728.6 (2746.6 – 3.6 above ice surface) | 2788.0 (surface) | 2787.4 (surface) |
| Minimum water level - measured or *estimated* (metres a.s.l.) | 2668.7 (2636.5) | 2645.3 | 2679.0 (2660.7) | 2776.3 | 2646.1 |
| Elevation of ice surface when drilled (metres a.s.l.) | 2724 | 2743 | 2743 | 2788 | 2788 |
| Elevation of borehole base (metres) | 2591 | 2593.5 | 2619 | 2643 | 2643.5 |

***Table 8.1 - Data describing boreholes subject to continuous measurement.***

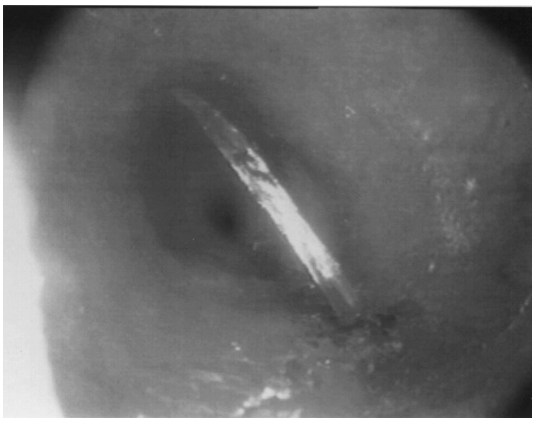


***Figure 8.3 - Englacial channel intersecting borehole 99.55.***

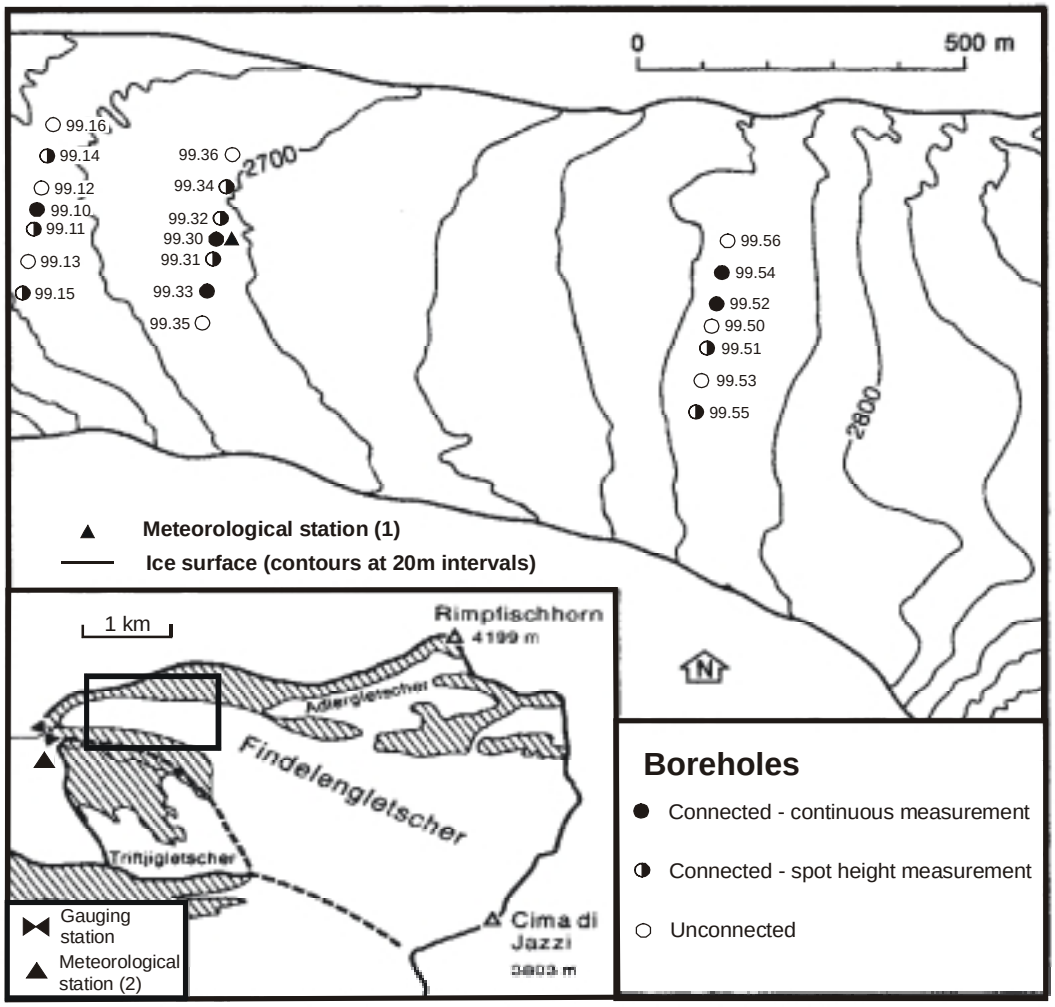



***Figure 8.4 – Map of borehole locations, their degree of connectivity with the subglacial hydrological system and measurement resolution at Findelengletscher, 1999.***

| Julian Day | Date | 99.11 | 99.14 | 99.15 | 99.31 | 99.32 | 99.34 | 99.51 | 99.55 |
|---|---|---|---|---|---|---|---|---|---|
| 180 | 29 Jun | | | | | | | D, S | |
| 181 | 30 Jun | | | | | | | U | D, S |
| 183 | 2 Jul | | | | | | | 67.5m | 11.0m |
| 188 | 7 Jul | | | | | D, S | D, S, | | |
| 189 | 8 Jul | | | | | U | U | U | U |
| 190 | 9 Jul | | | | D, S | | | | |
| 193 | 12 Jul | D, S | | | 7.0m | 6.0m | 32.0m | 64.0m | 10.5m |
| 194 | 13 Jul | | | D, S | | | | | |
| 195 | 14 Jul | S | | 15.5m | 38.5m | 6.0m | 7.0m | 64.0m | 11.0m |
| 197 | 16 Jul | S | D, S | 21.0m | 99.0m | 17.5m | 8.0m | 58.5m | 11.0m |
| 198 | 17 Jul | S | S | | | | | 15.5m | U |
| 204 | 23 Jul | | | | 86.0m | U | 48.0m | | |
| 205 | 24 Jul | S | S | 13.5m | | | | | |
| 208 | 27 Jul | | | | | | | 1.5m | U |
| 209 | 28 Jul | | | | 89.0m | | | | |
| 210 | 29 Jul | S | S | 8.0m | 86.0m | U | 26.0m | S | U |
| 212 | 31 Jul | | | | U | U | 17.5m | S | U |
| 217 | 5 Aug | 1.0m | 7.5m | 7.0m | U | U | 3.5m | S | U |
| 220 | 8 Aug | | | | | | | S | U |
| 222 | 10 Aug | 5.0m | 15.0m | S | U | S | 6.5m | | |
| 229 | 17 Aug | 13.0m | S | S | U | S | 2.0m | | |
| 230 | 18 Aug | 11.5m | 0.5m | 0.5m | U | S | 4.0m | | |
| 231 | 19 Aug | | | | | | | S | U |
| 237 | 25 Aug | | | | | | | S | U |
| 239 | 27 Aug | 6.0m | | | 32.0m | S | 2.5m | | |
| 243 | 31 Aug | S | S | S | U | S | 2.0m | S | U |
| 259 | 16 Sept | U | S | S | U | C | U | S | U |

***Table 8.2 – Spot height measurements of depth below the ice surface of water levels in boreholes that connected, temporarily or permanently, with the glacial hydrological system. Measurements in all boreholes were taken within a period of one hour between 12:00 and 19:00 each day. (D = borehole drilled, S = water level at surface, U = water level unknown, C = borehole closed through ice deformation).***

### 8.3.1 Detailed observations of borehole water levels

TSR estimates only begin on JD 212 due to prior periods of incomplete meteorological data. Discharge measurements are available from JD 145 to JD 297, except for a period of missing data between JD 202 and 207. Figure 8.6 shows records of borehole water levels begin on JD 201 in borehole 99.30 and although it cannot be compared to data representing both inputs, outputs and water balance until JD 212, an eleven-day period from 16:30 on JD 201 indicates that BWL fluctuate over a diurnal cycle within a range of 20m, which peak between 13:30 and 16:30 each day. Continuous data representing inputs and outputs to and from the glacial hydrological system begin at 12:30 on JD 212 allowing comparison of phase relationships with variations in BWL, in five boreholes that have semi-continuous data. The CTD of subglacial channels is unlikely to be spatially homogenous throughout the drainage network. Therefore spatial and temporal changes in storage and release of water within the system can be identified by comparing variations in BWL of separate boreholes that are varying in or out of phase with TSR and discharge.

Figure 8.5 to Figure 8.8 show that in the first water balance period (WB1) BWL were monitored in boreholes 99.30, 99.33 and 99.52. Inclusion of Figure 8.5 as well as Figure 8.6 describing BWL in borehole 99.30 is necessary as some recorded data, indicated by a pecked line in Figure 8.5, appears faulty. The data appears faulty because increases in BWL described by the pecked line are completely unrelated to the diurnal variations in TSR, discharge or other BWL in other boreholes and consequently, no firm conclusions will be made from this data. The smooth nature of the curvature of increases in BWL described by the pecked line, may be caused by a function of relaxation of the pressure transducer diaphragm and resolution of output that are unable to keep pace with rapidly changing subglacial water pressures. However, small peaks on JD 237 and JD 239 within an otherwise regular increase in BWL are synchronous with daily maximums of other variables. The spot height measurements of BWL taken using borehole video apparatus

on JD 222 and JD 239 (see section 11.5) indicate BWL are within the expected range of missing data on JD 222 and less than 4m from potentially 'faulty' data on JD 239 (an inaccuracy which can be justified due to manual error in absolute measurement of BWL elevation). This justifies the inclusion of 'faulty' data in section 8.3.1, with appropriate safeguards for interpretation, and indicates that gaps in BWL data shown in Figure 8.6 are primarily due to absence of a diurnal signal rather than an absence of data.

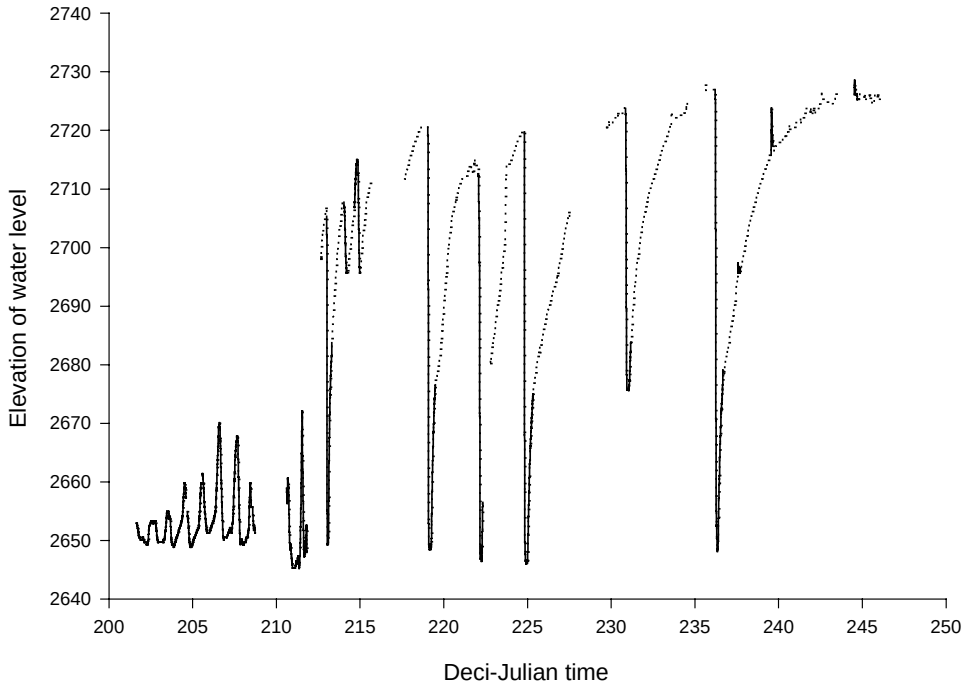



***Figure 8.5 - 10-minutely variation in elevation of water levels in borehole 99.30 (solid and pecked - see text for explanation) and elevation of glacier surface at time of drilling (dashed), 20 July - 3 September 1999.***

Increases in the water balance between JD 212 and 216, caused by TSR increasing at a faster rate than discharge, are reflected by increases in diurnal maximums of BWL in boreholes 99.30 and 99.33. A slight increase in diurnal minimums in borehole 99.52 between JD 212 and JD 216 also

indicates that increasing volumes of inputs during daytime, increases the overall water balance, causing higher water pressures in the glacial hydrological system at night. A steady increase in the total glacier water balance is reflected across all boreholes in-phase with TSR and discharge. Thus, hydraulic communication exists between subglacial areas around the base of all three boreholes located in separate parts of subglacial drainage.

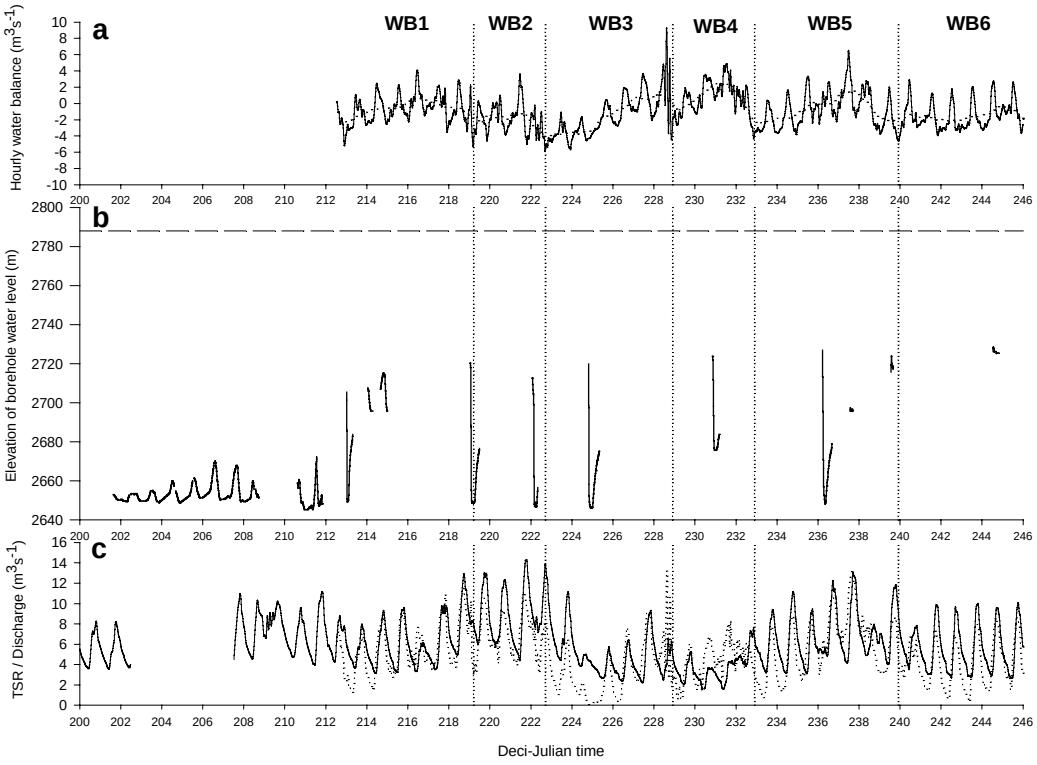



***Figure 8.6 - (a) Hourly water balance (solid) and 24-hour running average (pecked) demarcated into periods of rising and falling water balance at Findelengletscher, (b) 10-minutely variation in elevation of water levels in borehole 99.30 (solid), elevation of glacier surface at time of drilling (dashed), (c) hourly modelled total surface runoff (pecked) and pro-glacial river discharge (solid) in the Findelenbach, 20 July – 1 September 1999.***

The decrease in water balance during WB1, which begins on JD 217, is not immediately reflected by BWL in boreholes 99.52 and 99.33. The diurnal range of BWL in borehole 99.30 increases substantially so that it is juxtaposed over 60m higher up the borehole, whilst BWL in borehole 99.52 remain constantly high at or near the surface of the borehole up to and including JD 218. However, BWL in borehole 99.33 show an increase in daily maximum values between JD 217 and JD 219 that are in-phase with discharge and TSR as well as increasing daily minimum values that are in-phase with discharge but out of phase with TSR and water balance. A large rapid decrease in the water balance at 19:30 on JD 217 is not indicated by BWL in any of the three communicating boreholes. However, at 01:30 on JD 219 a similar rapid decrease in the water balance is reflected immediately by BWL in boreholes 99.30 and 99.33, but not in borehole 99.52. Data from borehole 99.30 during WB1 was only sporadic. It did indicate a rapid drop in BWL of approximately 71m taking approximately three and a half hours (a similar rapid drop in BWL of borehole 99.30 first occurred on just before WB1 on JD 212 and was repeated a further 5 times in subsequent water balance periods). Considering the decreasing BWL in borehole 99.30 in further detail between JD 218 and JD 219 TSR begins to rise during the otherwise descending diurnal limb at 21:30 on JD 218. TSR rises slowly from this point until 00:30 on JD 219 whereupon it increases rapidly until peaking at 01:30, which is synchronous with a precipitation event. The peak in TSR and the sharp drop in BWL in borehole 99.30 occur simultaneously at 01:30, causing an almost immediate rise in discharge that is out of phase with a decrease in the water balance. As TSR drops rapidly, discharge continues to increase and plateaus at 02:30 until 04:30 when it decreases at a similar rate to the descending discharge limb prior to the increase at 21:30 the previous day. In borehole 99.33 BWL follow the general, regular diurnal pattern although there is a slight increase at 23:40 on JD 218 that is proportionally maintained throughout the more erratic descending limb.

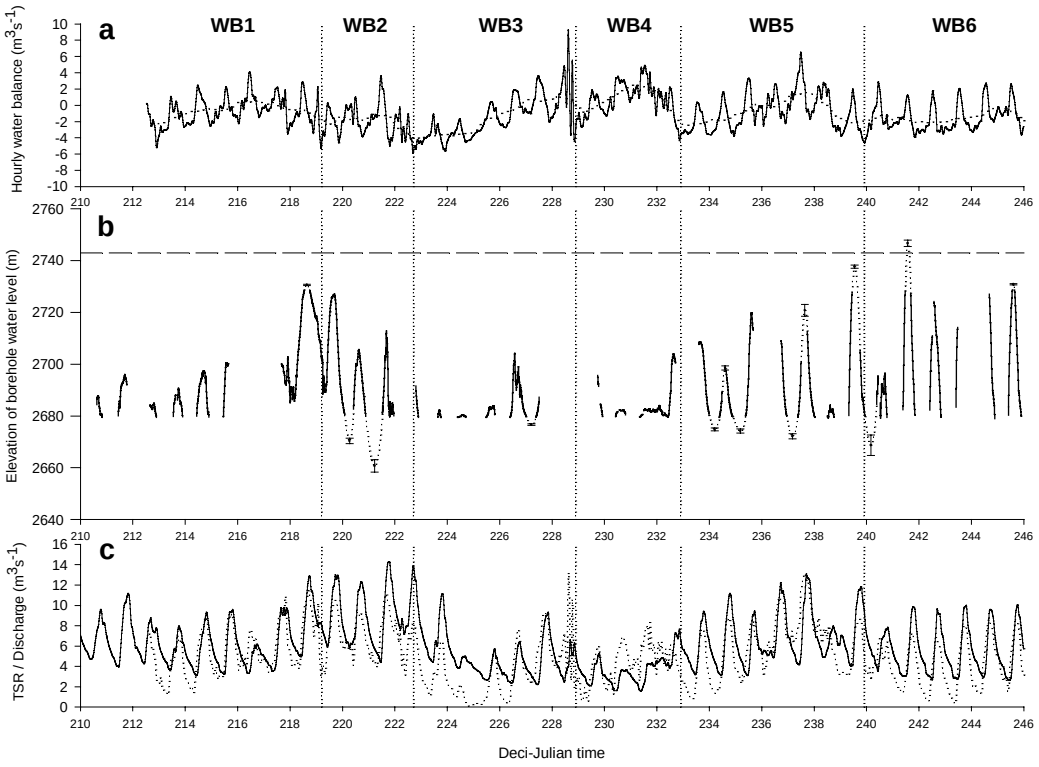



***Figure 8.7 - (a) Hourly water balance (solid) and 24-hour running average (pecked) demarcated into periods of rising and falling water balance at Findelengletscher, (b) 10-minutely variation in elevation of water levels in borehole 99.33 (solid), elevation of glacier surface at time of drilling (dashed), estimates of water levels during periods with missing data (pecked) and estimates of diurnal maximum and minimum borehole water level (including error bars at 95% confidence limits), (c) hourly modelled total surface runoff (pecked) and pro-glacial river discharge (solid) in the Findelenbach, 29 July – 2 September 1999.***

The increasing trend in water balance between daily minimums on JD 219 to JD 221 is only very slight during a period of consistently negative water balance. Throughout this period both daily maximum and minimum BWL in borehole 99.33 decreases, which is in-phase with decreasing TSR from the daily maximum on JD 219 to the daily minimum on JD 221. The slight increasing trend in water balance during this period only exists as discharge decreases at a slightly faster rate than TSR. BWL in borehole 99.52 are maintained at the borehole surface throughout until a decrease of just less than one metre, which is a significantly large variation relative to previous

observations in BWL, at a time during the diurnal cycle that is similar to previous diurnal minimums. BWL data from borehole 99.30 are absent from this period although the pecked line in Figure 8.5 may suggest that BWL have been increasing at a variable rate since the previous large rapid drop on JD 219.

After the maximum daily water balance during WB2 on JD 221, which is synchronous with the diurnally ascending limb of discharge substantially lagging that of TSR, the water balance declines rapidly. Daily maximum discharge on JD 221 and daily minimum discharge on JD 222, which are in and out of phase with TSR respectively, are the largest maximum and minimum discharge throughout the entire ablation season. BWL in borehole 99.33 drops abruptly and plateaus as the diurnally increasing pattern approaches the daily maximum on JD 221. At the same time BWL in borehole 99.52 starts to decrease at a uniform rate for 5.3m (over five times greater than any previous decrease) until 10:00 on JD 222 when BWL briefly increases synchronously with both TSR and discharge until the end of the borehole 99.52 data series. BWL in borehole 99.30 decreases rapidly early on JD 222 as the water balance is declining in a similar magnitude and pattern to decreases on JD 219 and JD 213. This rapid decrease lags the first of three small increases in the diurnally descending limb of TSR and precedes a short temporary increase in discharge just before the daily minimum on JD 222.

A declining water balance begins to level off late on JD 222 at the beginning of WB3 as in-phase decreases in daily maximum and minimum TSR and discharge maintain an approximately constant difference throughout their decline until late on JD 224. Although BWL data from borehole 99.33 is very incomplete throughout this period it suggests there is a decline in maximum daily BWL that reflects a reduction in subglacial water pressure. Daily maximum TSR and discharge on JD 224 and daily minimums on JD 225 are very low as they coincide with precipitation falling as snow. This temporarily decreases the elevation of the snow line to that of

the glacier snout. Decreasing BWL in borehole 99.54 (Figure 8.9) are synchronous with very low TSR on JD 224 and only show a very small diurnal increase that is superimposed on constantly declining BWL. As TSR becomes negligible on JD 224, at 19:30 another rapid decrease occurs in BWL in borehole 99.30 of a similar magnitude and pattern to rapid decreases on JD 219 and JD 222.

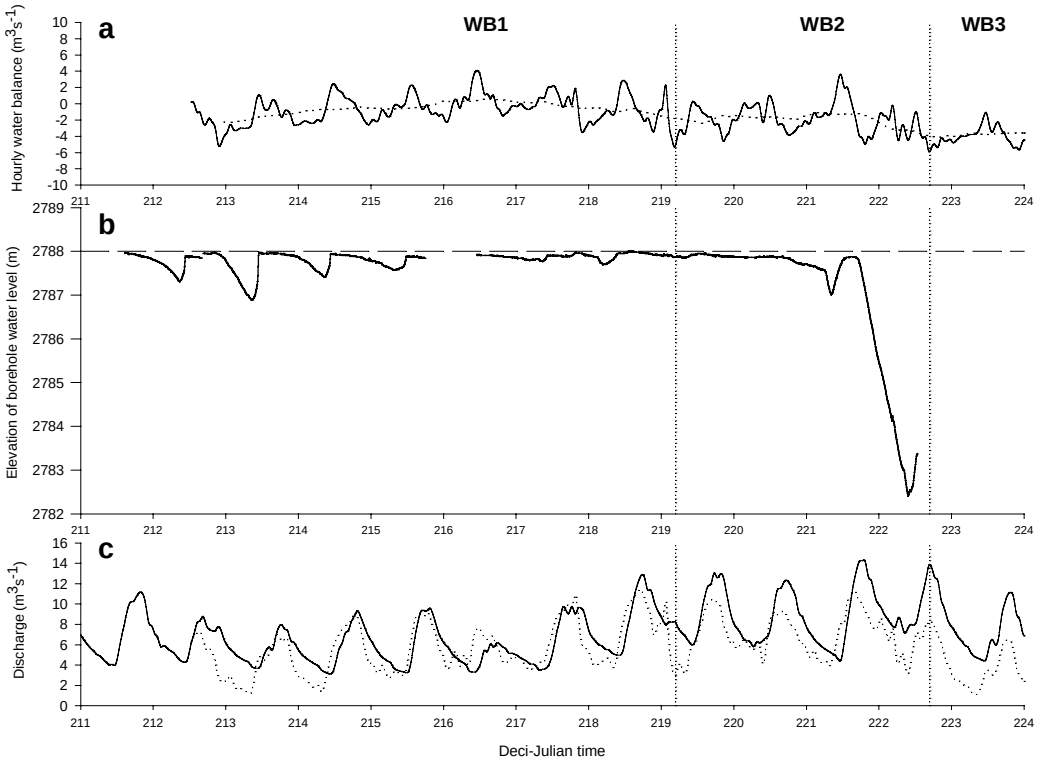



***Figure 8.8 - (a) Hourly water balance (solid) and 24-hour running average (pecked) demarcated into periods of rising and falling water balance at Findelengletscher, (b) 10-minutely variation in elevation of water levels in borehole 99.52 (solid), elevation of glacier surface at time of drilling (dashed), (c) hourly modelled total surface runoff (pecked) and pro-glacial river discharge (solid) in the Findelenbach, 30 July – 10 August 1999.***

Water balance within and under the glacier increases from JD 225 onwards as TSR increases at a faster rate than discharge. Although daily maximum TSR increases for three consecutive days in-

phase with daily maximum discharge, increased water balance is caused when daily minimum discharges throughout this period remain approximately equal to that on JD 225 whereas minimum daily TSR steadily increase. An increase in the daily maximum and the estimated minimum BWL in borehole 99.33, on JD 226 and JD 227 respectively, rapidly reflect an increase in subglacial water pressure in line with the increasing trend in water balance. Although maximum and minimum daily BWL in borehole 99.54 on JD 226 are slightly out of phase with TSR and discharge they also reflect the increase in water balance over a period of three consecutive days up to daily maximums on JD 228. The water balance on JD 228 continues the rising trend during the morning of JD 228 until shortly before midday TSR becomes dominated by a precipitation event consisting of two high magnitude, short duration rainfall events in quick succession. Although discharge reflects TSR by exhibiting two peaks in the diurnal pattern, which each lag their respective peaks in TSR by two hours, maximum daily discharge on JD 228 decreases out of phase with the precipitation dominated TSR, but in-phase with maximum daily BWL in borehole 99.54 and the trend in water balance throughout the second half of JD 228.

The trend of increasing water balance, prior to a short decrease during JD 228, re-continues throughout JD 229 until midday on JD 231. Throughout JD 229 and JD 230 daily maximum and minimum TSR increases out of phase with decreasing daily maximum and minimum discharge. Although estimates of daily maximum BWL in boreholes 99.10 (Figure 8.10), 99.33 and 99.54 all decrease in-phase with discharge and out of phase with TSR, daily minimum BWL in borehole 99.54 (the only borehole where minimum daily BWL data are available) increases in-phase with TSR and out of phase with discharge. A rapid decrease in BWL in borehole 99.30 occurs at 21:00, which is not preceded by precipitation and is similar in pattern to previous decreases, although the magnitude of the drop is smaller. Previously, four rapid decreases of BWL in borehole 99.30 have all terminated at elevations between 2647 - 2650m a.s.l. whereas the decrease on JD 230 terminates approximately 30m short of this elevation range. As well as

maximum daily discharge being unseasonably low, the shape of the highly attenuated diurnal discharge hydrographs exhibit a pronounced shoulder in the diurnally descending limb.

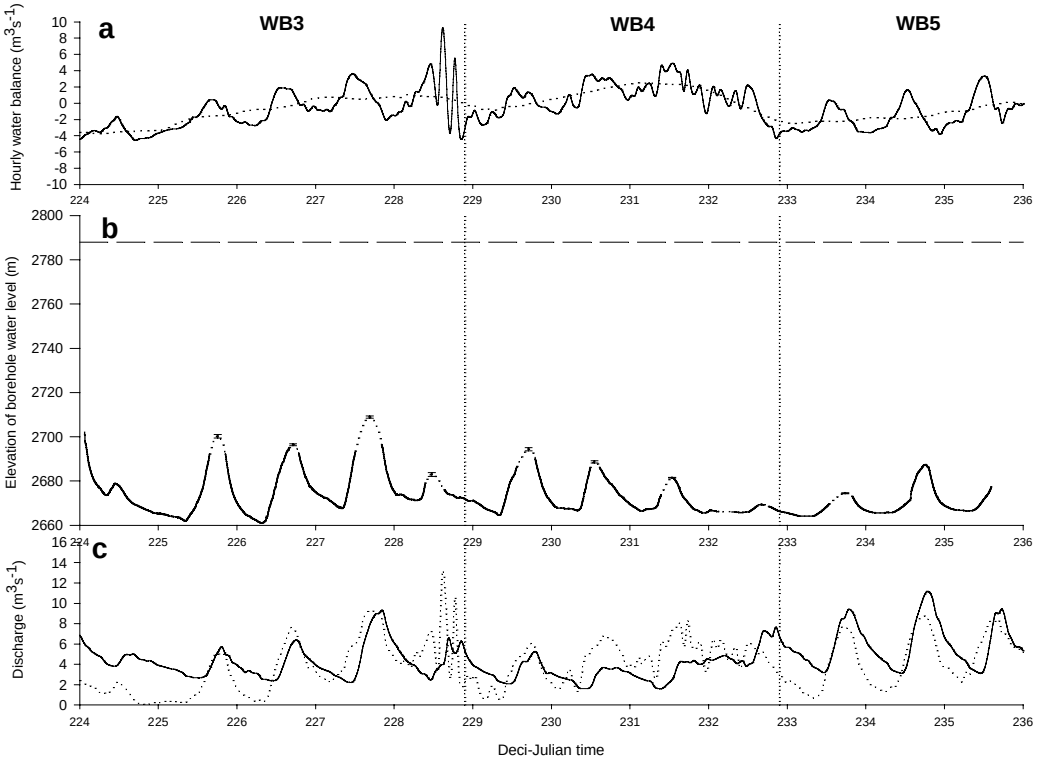



***Figure 8.9 - (a) Hourly water balance (solid) and 24-hour running average (pecked) demarcated into periods of rising and falling water balance at Findelengletscher, (b) 10-minutely variation in elevation of water levels in borehole 99.54 (solid), elevation of glacier surface at time of drilling (dashed), estimates of water levels during periods with missing data (pecked) and estimates of diurnal maximum and minimum borehole water level (including error bars at 95% confidence limits), (c) hourly modelled total surface runoff (pecked) and pro-glacial river discharge (solid) in the Findelenbach, 12 – 24 August 1999.***

On JD 231 minimum daily discharge and BWL in both boreholes 99.10 and 99.54 remain approximately equal to values the previous day as daily minimum and maximum TSR continue to increase. Daily maximum BWL in borehole 99.54 decrease whilst BWL maximums in boreholes 99.33 and 99.54 remain approximately equal to previous daily values. Discharge and BWL in

boreholes 99.33 and 99.54 then depart from the regular diurnal pattern by sustaining the daily maximum BWL until approximately 02:30 on JD 232, whereupon BWL only slightly decrease before the regular diurnal cycle is re-established shortly before midday. The duration of sustained high BWL relative to the previous diurnal cycle is synchronous with a high duration, low magnitude precipitation event that also sustains TSR albeit more erratically. Sustained high TSR and BWL in boreholes 99.10 and 99.33 vary out of phase with BWL in borehole 99.54, which maintains a regular diurnal pattern throughout JD 231 but only shows a slight increase in BWL during the diurnal cycle on JD 232. This continues the trend in decreasing daily maximums. The increasing trend in water balance during WB4 stops at the point when maximum daily discharge on JD 231 becomes maintained. As TSR then starts to decrease, gradually but erratically, a decreasing trend in water balance begins, which gets faster from 12:30 until 20:30 on JD 232 when a clear diurnal cycle in water balance recommences.

As diurnal cycles in water balance recommence late on JD 232 diurnal cycles in BWL in boreholes 99.10, 99.33 and 99.54 also resume. Water balance shows a slight increasing trend over JD 233 and JD 234 as although maximum daily TSR and discharge are in-phase with each other minimum daily discharges are approximately equal and out of phase with increasing daily minimum TSR. BWL in each of the three boreholes respond differently to the increasing trend in water balance. Maximum and minimum BWL in borehole 99.54 increase in-phase with the increasing trend. Maximum BWL in borehole 99.33 decrease out of phase with water balance and daily maximum and minimum BWL in borehole 99.10 remain approximately constant. During this relatively short time period, comparison of the three boreholes shows that maximum BWL in borehole 99.33 consistently peaks first, followed by BWL in borehole 99.54 and then borehole 99.10, whereas minimum BWL in boreholes 99.33 and 99.54 appear to be synchronous whilst BWL in borehole 99.10 lags both.

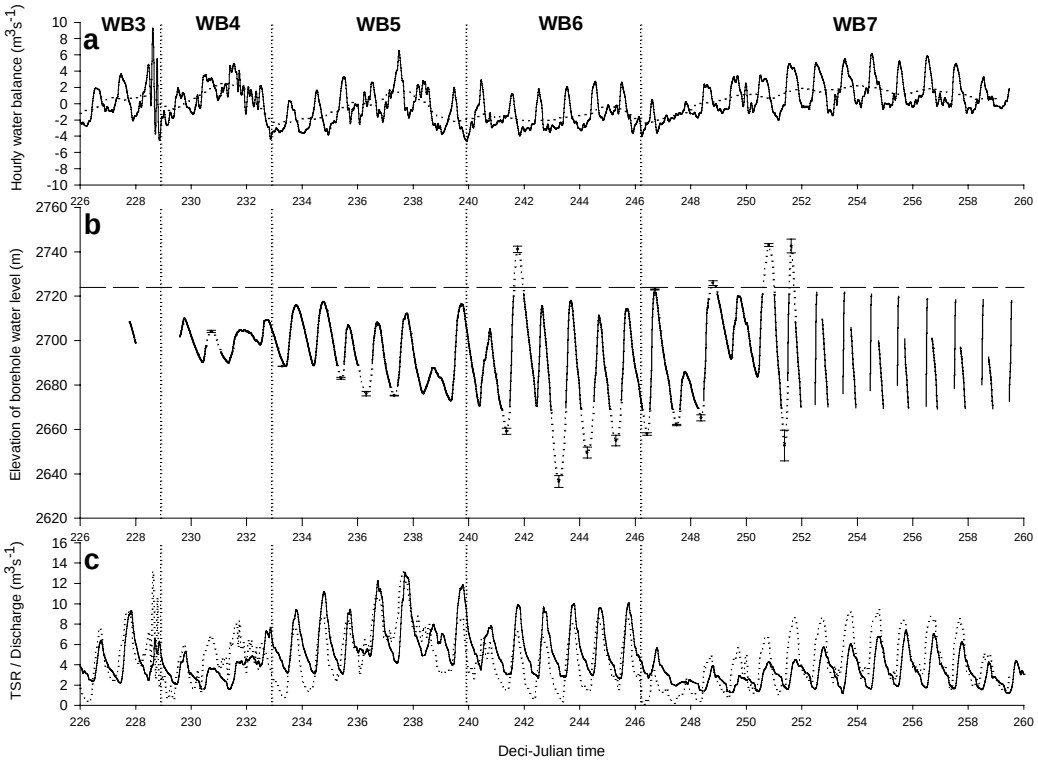



***Figure 8.10 – (a) Hourly water balance (solid) and 24-hour running average (pecked) demarcated into periods of rising and falling water balance at Findelengletscher, (b) 10-minutely variation in elevation of water levels in borehole 99.10 (solid), elevation of glacier surface at time of drilling (dashed), estimates of water levels during periods with missing data (pecked) and estimates of diurnal maximum and minimum borehole water level (including error bars at 95% confidence limits), (c) hourly modelled total surface runoff (pecked) and pro-glacial river discharge (solid) in the Findelenbach, 15 August – 16 September 1999.***

The trend in water balance again increases from JD 235 up to and including JD 237 and is caused by daily maximum and minimum TSR increasing in-phase with discharge, but at a faster rate. A relatively low magnitude precipitation event interrupts the diurnal pattern of water balance. This slightly lowers maximum daily TSR on JD 235 and slightly increases minimum daily discharge on JD 236, which causes brief out of phase variations within an overall trend of increasing water balance. A rapid decrease in BWL in borehole 99.30 coincides with the precipitation event and is synchronous with daily minimum BWL in borehole 99.10 on JD 236. Maximum BWL in

borehole 99.33 rises sharply on JD 235 and, despite discontinuous data, appears to maintain both the increase in maximum BWL as well as equality of previous minimum BWL as water balance increases. The diurnal range and absolute elevation of BWL in borehole 99.10 decreases slightly on JD 235 as the rate of rising water balance increases. However, the diurnal range then increases due to the combination of increasing maximum and decreasing minimum BWL in borehole 99.10 between JD 235 and JD 237.

A decreasing trend in water balance lasting from 12:00 on JD 237 to 00:00 on JD 240 is initiated by a fast decrease in TSR on JD 238 that fails to follow a recognisable diurnal pattern. Maximum and minimum discharge vary in-phase with TSR throughout the decline in water balance and on JD 238-239 discharge shows a diurnal cycle, albeit heavily attenuated, with a clear double peak despite TSR not following a regular diurnal pattern. BWL in both borehole 99.10 and 99.33 continue to follow the trends exhibited during the increasing period of water balance as both daily maximums increase in boreholes 99.33 and 99.10, whilst daily minimums in borehole 99.10 decrease. The decrease in TSR on JD 238 is represented by low maximum BWL in both boreholes without affecting the overall trends.

Maximum and minimum daily TSR, discharge and BWL data (where available) in boreholes 99.10 and 99.33 all vary in-phase with each other from when an increasing trend in water balance commences on JD 240 up to and including the daily maximums on JD 241. An extended length of decrease between 13:30 and 20:30 on JD 241 follows a decrease in the maximum daily water balance. This causes a slight negative blip in an otherwise continual increasing trend in water balance until midday on JD 245. Though BWL data in borehole 99.33 are sporadic from this point onwards (until the data series concludes on JD 246) available data suggests daily maximum BWL remain steady, reflecting similar variations in subglacial water pressures to those on JD 239 and JD 241. After daily minimum BWL in borehole 99.10 on JD 242 increase out of phase with

decreasing TSR and discharge, all three variables vary in-phase with each other at daily maximums and minimums. This continues until maximum daily TSR increases out of phase with both BWL in borehole 99.10 and discharge on JD 244, and minimum daily discharge decreases out of phase with BWL and TSR on JD 245. Between JD 241 and the end of JD 245 daily maximum and minimum discharges vary only within a range of less than 0.5m, therefore, the increasing trend in water balance is controlled by TSR, which continually increases between JD 242 and the end of JD 245.

The trend of increasing maximum and minimum BWL in borehole 99.10 over consecutive days since JD 244 continues until a decrease in the daily maximum on JD 247. Maximum discharge and both maximum and minimum TSR decrease on JD 246 out of phase with variations in BWL as the water balance remains negative throughout almost the entire day. The trend in water balance begins to increase on JD 247 as minimum daily BWL in borehole 99.10 increase out of phase with decreasing discharge and TSR. A diurnal cycle in discharge is unrecognisable on JD 247 producing the lowest maximum daily discharge since the monitoring period started on JD 212, which is in-phase with BWL and TSR. Very low discharge is synchronous with a decrease in the elevation of the transient snow line (TSL) as precipitation that began to fall as rain on JD 247 rapidly turned into snow, covering the glacier surface down to the elevation of the snout at just over 2500m a.s.l. A slight increase in daily minimum TSR on JD 248 is in-phase with BWL in borehole 99.10 but out of phase with discharge that continues to decrease.

Maximum and minimum daily TSR increase on JD 248 and continue to increase over successive days until JD 254, other than on JD 251 when the daily minimum only slightly decreases and on JD 252 when maximum TSR is equal to that of the previous day. Maximum and minimum daily discharge also increase on consecutive days over the same time period, other than a decease in daily maximum on JD 249 and a slight decrease in daily minimum on JD 253. The trend in the

water balance increases in-phase with both TSR and discharge over this time period as the rate of increase in TSR is greater than the rate of increase in discharge. Daily maximum and minimum BWL in borehole 99.10 do not show a similar smooth pattern over an identical time period. Although BWL increase in-phase with TSR and discharge on JD 248 maximum and minimum BWL decrease until the increase in daily maximum on JD 250. Maximum daily BWL on JD 249 decrease in-phase with discharge, but out of phase with TSR and the decrease in minimum daily BWL on JD 250 decrease out of phase with both the other two variables.

A large decrease in minimum daily BWL on JD 251 significantly increases the diurnal range of BWL variations as the daily maximum on JD 251 is maintained at a level approximately equal to that on the previous day. BWL data in borehole 99.10 become discontinuous from JD 251 onwards as the gaps of missing observations at peaks and troughs within the diurnal cycle are too large to interpolate with confidence. However, as the range over which BWL can be accurately observed (~2670 - 2720m) still remains unchanged after JD 251 discontinuous data thereon indicates that the diurnal range of subglacial water pressure remains high. The water balance remains high from JD 251 until JD 260, but shows a slight decrease in the trend from JD 255 onwards, which is caused by small decreases in TSR that are reflected in the discharge hydrograph.

### 8.3.2 Interpretation of water balance using borehole water levels

Timescales vary over which water balance increases and decreases in each of seven water balance periods as a consequence of variations in meteorological inputs interacting with changes in capacity of the subglacial drainage network to discharge inputs. Physical mechanisms controlling variations in duration of increasing and decreasing water balance trends, with consequent affects on daily water balance patterns, have contingent affects requiring a chronologically ordered discussion in order to interpret influences of major controlling physical mechanisms. Previous work at Findelengletscher (Iken and Bindschadler, 1986) suggested both distributed and concentrated forms of subglacial drainage coexist (see Figure 7.12), which provides a basis for discussion of temporal variation in subglacial configurations.

#### 8.3.2.1 Water balance period one (WB1)

In borehole 99.30, prior to JD 212, BWL show a regular diurnal cycle of water pressures within a 20m range fluctuating near the base of the borehole. Figure 8.11 shows that due to the sparseness of data describing BWL in borehole 99.30 after JD 212, phase relationships between daily maximum and minimum BWL, TSR and discharge cannot be compared over the period of decreasing water balance. However, as the negative water balance begins to decrease on JD 212, BWL increase to over 35m greater than previous daily maximums until a sudden decrease early on JD 213 returns the BWL to a daily minimum that is approximately similar to minimums prior to JD 212. The rapid decrease in BWL of over 50m is a departure from the previous trend of smoother diurnal cycles. Despite sporadic data, it appears that diurnal cycles in BWL in borehole 99.30 may be back within an approximate 20m daily range on JD 213 and JD 214 that is juxtaposed approximately 45m higher up the borehole. The high magnitude increase in water pressure between JD 211 and JD 213, relative to previous diurnal cycles, is a reflection of the

general increasing trend in the rate of subglacial water storage at the start of WB1 as TSR increases at a faster rate than the overall CTD.

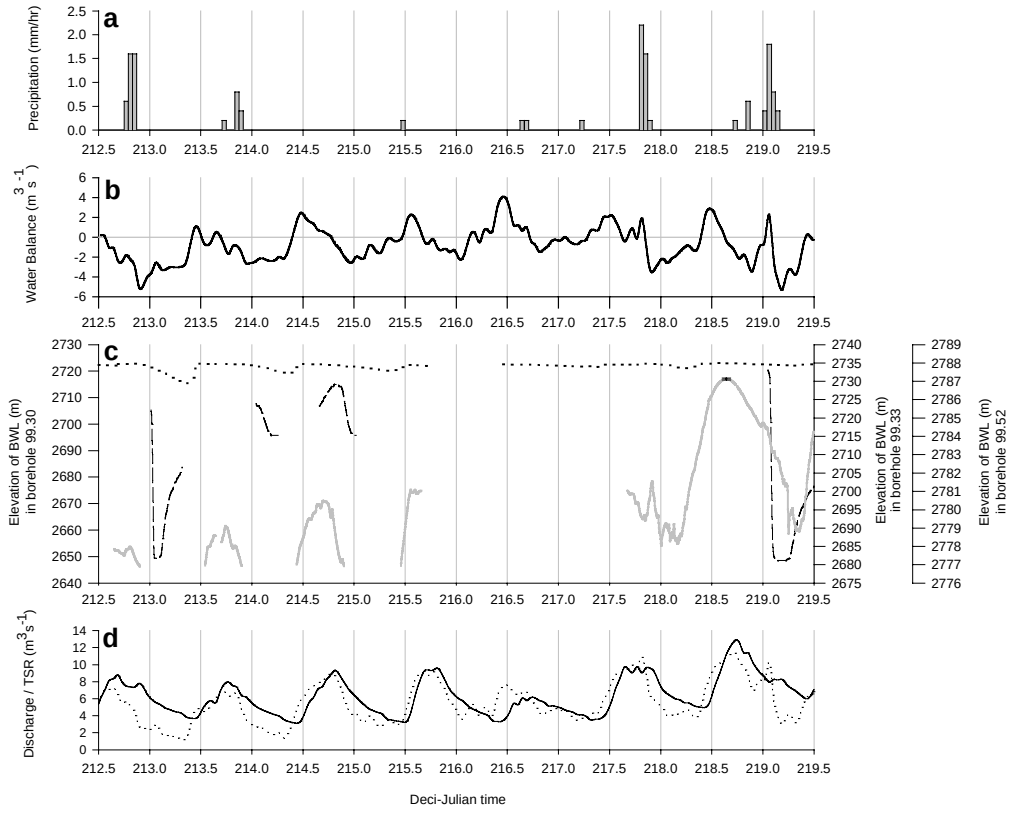



***Figure 8.11 - (a) hourly precipitation; (b) hourly water balance at Findelengletscher; (c) 10-minutely variation in elevation of water levels in borehole 99.30 (dashed), borehole 99.33 (grey), borehole 99.52 (pecked), estimates of water levels in borehole during periods with missing data (short dash) and estimates of diurnal maximum borehole water level (including error bars at 95% confidence limits); (d) hourly total surface runoff (pecked) and pro-glacial river discharge (solid) in the Findelenbach, 31 July - 7 August 1999.***

A large rapid decrease in BWL in borehole 99.30, which punctuates the increase in BWL, occurs early on JD 213 and is a result of precipitation contributing to TSR rather than TSR consisting solely of meltwater. The sequence of events that cause the rapid decrease in BWL in borehole 99.30 on JD 213 are as follows. A large proportion of TSR from a precipitation event on JD 212, which occurs as the transient snow line is still increasing in elevation, is rapidly discharged through the tunnel-conduit section of the subglacial drainage network. This is described by a synchronous rise in the otherwise diurnally decreasing limb of BWL in borehole 99.33 (the base of which is over a distance of 84m away - incorporating a 25.5m difference in elevation - see Figure 8.1), causing the second of two peaks in the diurnal discharge cycle. However, a smaller but significant proportion of TSR is englacially routed to distributed subglacial drainage structures, possibly of a linked-cavity nature, which are adjacent to the tunnel-conduit section of the network. As TSR declines, water pressures in the tunnel-conduit system, indicated by BWL in borehole 99.33, also decline. In comparison to water pressures in adjacent distributed networks, where water pressures are much higher by comparison as precipitation induced TSR has longer transit times, the water pressures in the tunnel-conduit system are low. Differences in water pressure are great enough to allow the hydraulic gradient, acting from the distributed section of drainage towards the tunnel-conduit network to force a new localised connection (or significantly increase the size of a pre-existing connection) between the two sections within the whole drainage network. BWL in borehole 99.52 show no obvious deviation from the partial diurnal signal, although the diurnal minimum early on JD 213 is lower than minimums on either the previous or following days. This may also reflect a drop in water pressures in subglacial areas adjacent to the tunnel-conduit network although it is also influenced by a similar trend in daily minimum TSR.

An increasing trend in water balance from JD 212 up to JD 216, which is superimposed over reasonably regular diurnal cycles, is caused by rates of TSR increasing faster than rates of

discharge and, therefore, also faster than the CTD. In-phase increases of maximum BWL in boreholes 99.30 and 99.33 indicate TSR is increasing subglacial water pressures and becoming temporarily stored throughout the subglacial network. Maintenance of similar minimum daily discharges as the water balance increases suggests increasing volumes of TSR are not becoming backed-up through the day and discharged during the night in the main tunnel-conduit section of the drainage network. Instead, longer-term subglacial storage is likely to occur in areas of distributed drainage adjacent to the tunnel-conduit section of the network where the CTD is much lower and transit times of water flow are longer.

The rate of temporary storage of TSR increases, causing a net increase in the positive water balance on JD 216 despite a decrease in maximum TSR that is in-phase with discharge. Consequently, when maximum daily TSR decreases on JD 216, subglacially stored water from the increasing water balance over the previous four days is not released to supplement low TSR. Although no BWL data exists in borehole 99.33 until the afternoon of JD 217 it is likely that water pressures in the tunnel-conduit section of the drainage network on JD 216 have declined due to low total daily TSR. Lower water pressures will reduce velocities of water flow, causing longer transit times in the tunnel-conduit network that temporarily increases the water balance. This is indicated by a longer delay between ascending limbs of TSR and discharge than on previous days, which suggests the tunnel-conduit and adjacent sections of the subglacial drainage network are operating almost as two separate systems. Physical mechanisms controlling temporary connections between the two sections are consequently of interest. Estimated low water pressures in the tunnel-conduit section on JD 216 have not been low enough, relative to water pressures in adjacent drainage sections, to increase the hydraulic gradient sufficiently to cause a connection from distributed to concentrated subglacial areas of drainage. Increased daily maximum TSR on JD 217 relative to JD 216 causes an increased velocity of water throughput in the glacial hydrological system as a greater proportion of total daily TSR is routed through the

tunnel-conduit system. A quicker response in the diurnally ascending limb of discharge, relative to increasing TSR, results in a lower temporary net increase in the water balance. This is achieved as low water pressure in the tunnel-conduit system during JD 216, in comparison to ice overburden pressure, has resulted in constriction of the CTD.

Precipitation events on 217 and 219 exert a large influence on the decreasing water balance in WB1 as they are synchronous with brief increases in water balance, which are followed by greater more rapid decreases. Such precipitation events have a greater affect on the increase in the CTD of the whole subglacial drainage network and the decrease in water balance than a twenty-four hour period of low TSR on JD 216. This is indicated by the diurnal increase in TSR on JD 217 that is out of phase with a decreasing maximum daily positive water balance signifying the subglacial hydrological system is discharging stored water despite the tunnel-conduit section of the drainage network not apparently storing much TSR over a timescale greater than 24 hours.

Prolonged peak TSR on JD 217 resulting from precipitation, temporarily maintains the diurnally positive component of the water balance though there is an extremely rapid decrease in the water balance after precipitation ends. An increase in BWL of borehole 99.33 is synchronous with the end of the precipitation event on JD 217, which suggests there has been direct supraglacial runoff of precipitation into the tunnel-conduit section of the subglacial drainage network. However, the water balance late on JD 217 rapidly decreased from a positive net balance to a much larger negative water balance than was experienced at any point over the previous three days. This was due to the low duration high magnitude nature of the precipitation-induced TSR input, which started an increase in the CTD of hydraulic connections between the tunnel-conduit and adjacent distributed sections within the subglacial drainage network. This is evident from the rate of release throughout the night of water stored subglacially since JD 212, causing an increase in daily minimum discharge on JD 218 that is out of phase with decreasing TSR and water balance.

Subglacial flow of water into the tunnel-conduit section from adjacent areas is reflected by an increase in the daily minimum BWL in borehole 99.33 on JD 218, which increases in-phase with discharge and out of phase with minimum TSR and water balance. As increased water pressure in the area of the subglacial drainage network in which the base of the borehole 99.33 terminates is in-phase with discharge it can be inferred that borehole 99.33 is highly influenced by concentrated water drainage in subglacial channels or conduits that are likely to transport a significant proportion of overall discharge.

The rapid increase in minimum daily discharge on JD 218 demonstrates that the tunnel-conduit system is well developed and is likely to have been previously discharging at less than the maximum potential CTD. Accordingly there has been little opportunity for back-up within the tunnel-conduit system, which is illustrated by the trend of declining discharge over the previous ten days during hydrological period VII (see Figure 7.4). Limitations to the increase in minimum discharge are imposed by the rate of development of the orifice size of channels connecting the tunnel-conduit sections of the network with adjacent areas that are more distributed in drainage character, and the maximum volume of water temporarily stored within adjacent areas that can be released.

Increased maximum TSR on JD 218 causes further increase in water balance within the network, hence the relatively large maximum water balance that is of similar magnitude in comparison to JD 217. Water balance decreases as part of the usual diurnal pattern, briefly increases late on JD 218 in response to precipitation and is then rapidly released at the same time as the precipitation event finishes. Precipitation on JD 219 causes another increase in the orifice size of the channels connecting the tunnel-conduit and adjacent sections of the whole drainage network on top of the increase initiated on JD 217. As the orifice size of connecting channels increases, so does the CTD of the entire subglacial drainage network, suggesting these channels provide a rate-limiting

factor to discharge within the glacierised area of the catchment. The increase in CTD is illustrated by the largest negative water balance of WB1 at 04:30 on JD 219 as the whole glacial hydrological system is able to discharge more of the temporarily stored water at a greater peak rate.

The descending diurnal limb of BWL in borehole 99.33 early on JD 219 reacts differently to the synchronous precipitation-induced increase in TSR in comparison to precipitation events on JD 212 and JD 217. Previously BWL have peaked in response to precipitation in a rapid but transitory manner, returning quickly to the usual diurnal pattern. However, on JD 219 the diurnal pattern of BWL, which is juxtaposed approximately one metre up the borehole at the onset of precipitation, continues to decrease in the usual, albeit more erratic daily pattern. Consequently, inputs of precipitation-induced TSR are not routed rapidly to the tunnel-conduit system. Instead it is likely that TSR is initially routed into adjacent areas of subglacial drainage, causing longer transit times through less efficient subglacial pathways until flowing water reaches enlarged connecting channels into the tunnel-conduit system. Water routed through the distributed drainage network is likely to be more widely spatially distributed and will have a larger range of transit times between supraglacial entry into moulins and crevasses and subglacial entry into the tunnel-conduit system through one of many small connecting channels. The sudden decrease in BWL in borehole 99.30 reflects a sudden decrease in water pressure as water is rapidly released from a section of the distributed drainage system into the tunnel-conduit system. The absolute volume of water that is released is likely to be small relative to overall discharge, through an equally small connecting channel, which accounts for the very large and sudden decrease in subglacial water pressure (see Figure 6.17). Water will be released in this manner when the hydraulic gradient towards the tunnel-conduit system increases to such an extent that the pressure exceeds thresholds of ice-sediment shear strength or thresholds of stability in subglacial hydraulic configuration, for example causing localised ice floatation. Although the volume of water

released into the tunnel-conduit section, which was reflected by BWL in borehole 99.30, is likely to be small the mechanism of subglacial water movement will be copied at many other spatially distinct subglacial areas, which in combination causes a pronounced shoulder in the descending limb of the discharge hydrograph and a synchronous decrease in water balance.

Release of temporarily stored water from the initially distributed drainage network to the tunnel-conduit system in this manner will enlarge the orifice size of channels connecting with the tunnel-conduit system through dissipation of heat from moving water. As a result the TSR peak on JD 219 has a more attenuated affect on the second peak in the diurnal discharge hydrograph than the TSR peak on JD 212 as a larger proportion of TSR on JD 219 is being routed through areas of subglacial drainage adjacent to the tunnel-conduit system. As more TSR during JD 219 has increased transit times through areas adjacent to the tunnel-conduit system than during JD 212, the increase in water balance is much more prominent and the peak in the discharge hydrograph is more attenuated. However, gradual improvement of hydraulic efficiency within distributed drainage means there are fewer physical barriers within subglacial hydraulic configurations, which increase the ease at which hydraulic gradients force water into the tunnel-conduit system through connecting pathways that are spatially limited in size and frequency. Such increases in the connectivity, efficiency and CTD of the entire glacier throughout JD 219 keep daily minimum discharge high and out of phase with both daily minimum TSR and a decreasing trend in water balance.

BWL in borehole 99.52 reflect just the troughs of diurnal cycles, which are synchronous with variations in TSR and discharge, and are otherwise maintained at the glacier surface throughout WB1. Although all attempts were made to prevent seepage of supraglacial water into the borehole some water may have entered the borehole supraglacially during times of peak daily ice melt. However, BWL in borehole 99.52 are still hydraulically communicating with the subglacial

drainage system but high water pressures are consistently maintained at greater levels than ice overburden pressure. A likely cause of consistently high water pressures is that the base of the borehole terminates in a saturated sediment of low hydraulic conductivity as when drilling ended lots of bubbles and a very gradual drop in water level were observed at the surface of the borehole (see section 11.6). Sedimentary substrates with a low hydraulic conductivity may maintain high subglacial water pressures that restrict spatial transfer of water pressure. Daily minimum BWL in borehole 99.52 do vary in-phase with the water balance as it increases between JD 213 and JD 216 and decreases on JD 217 and JD 218. The low amplitude of diurnal variations in BWL and the in-phase relationship with water balance further suggest the base of the borehole terminates in a saturated sedimentary substrate that is representative of variations in subglacial water pressures from the tunnel-conduit section of the subglacial drainage network.

#### 8.3.2.2 Water balance period two (WB2)

Sustained increased BWL in borehole 99.33 at the end of WB1, representing high water pressures in the tunnel-conduit section of the drainage network, have increased the entire CTD not only of the tunnel-conduit section but also the connections to, and hydraulic efficiency within, areas of the drainage network that are adjacent to the tunnel-conduit section. It is increases in CTD and hydraulic efficiency that allow temporarily stored water within adjacent subglacial areas to flow into the tunnel-conduit section of the system causing an increase in water pressures and consequently increasing both BWL in borehole 99.33 and discharge. As maximum and minimum BWL in borehole 99.33, TSR and discharge decrease in-phase with each other between the daily maximum on JD 219 and the daily minimum on JD 221 (Figure 8.12) the rate of release of water that is temporarily stored in subglacial areas adjacent to the tunnel-conduit section must also slowly decrease. Consequently, a slightly increasing trend in the water balance occurs (throughout a period of consistently negative water balance) as the rate of release of temporarily

stored water into the tunnel-conduit section of the drainage network, which supplements daily inputs of TSR, decreases faster than the decreasing rate of TSR. As discharge is the sum of TSR and volumes of water released from temporary subglacial storage, discharge will also decrease at a slightly faster rate than TSR, thereby causing an increasing trend in water balance. The decrease in water pressures in the drainage system as a whole at the time of minimum TSR on JD 221 are also reflected by a drop in BWL in borehole 99.52 and as this is the first decrease in this borehole throughout WB2 it indicates further exhaustion of the release of temporarily stored water over a wider spatial area.

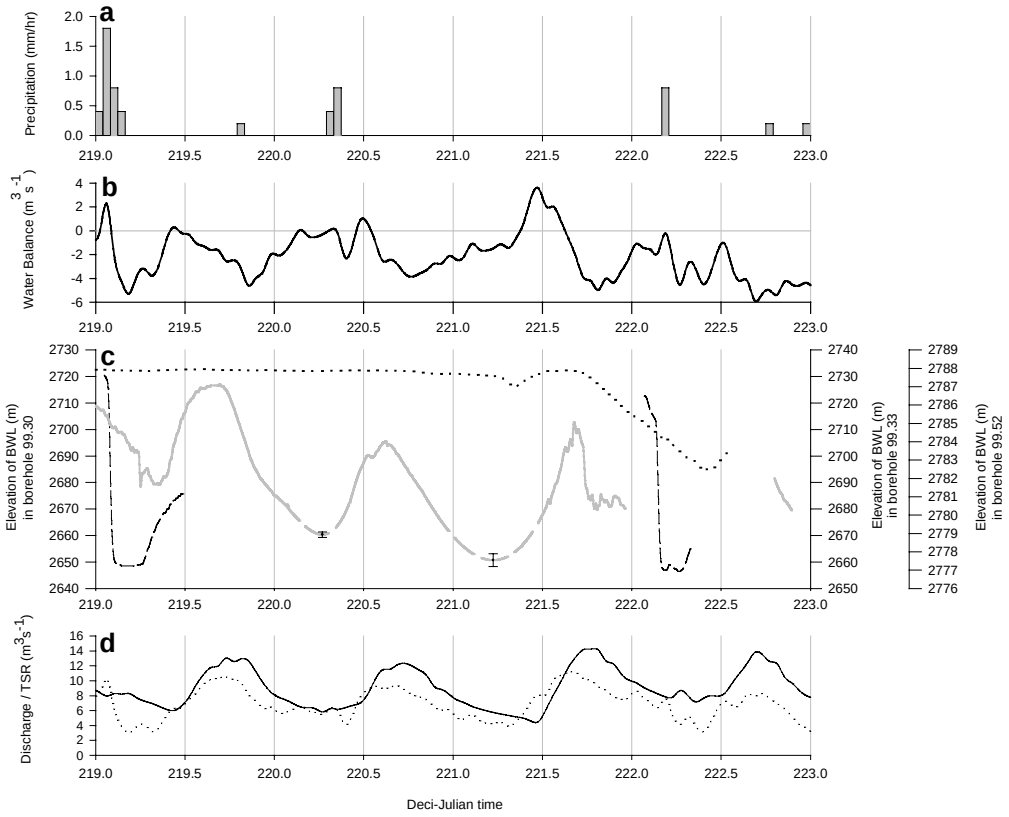



***Figure 8.12 - (a) hourly precipitation; (b) hourly water balance at Findelengletscher; (c) 10-minutely variation in elevation of water levels in borehole 99.30 (dashed), borehole 99.33 (grey), borehole 99.52 (pecked), estimates of water levels in borehole during periods with missing data (short dash) and estimates of diurnal maximum borehole water level (including error bars at 95% confidence limits); (d) hourly total surface runoff (pecked) and pro-glacial river discharge (solid) in the Findelenbach, 7 - 11 August 1999.***

A short-term increase in the water balance on JD 221 is caused when minimum daily discharge lags minimum daily TSR, which are both approximately equal in magnitude. The increase in water balance is more pronounced in comparison to previous days during WB2. This is a consequence of a decline in the release of subglacially stored water from temporary storage and an increase in the transit times of initial daily increases in TSR through the glacier. Variations in TSR become more influential over variations in discharge as TSR constitutes a larger proportion of total discharge and the transit times through the glacier become longer (as lower water pressures cause lower water velocities of decreasing volumes of water flow through subglacial channels that have recently enlarged in CTD).

After the peak in water balance on JD 221 a further decreasing trend in water balance is initiated. Daily maximum TSR increases on JD 221 in-phase with daily maximum discharge, which is a seasonal maximum. However, an otherwise increasing BWL in borehole 99.33 departs from the expected diurnal pattern at a time which is synchronous with maximum discharge by rapidly decreasing approximately 32m. At this point it levels out, albeit erratically, until there is a break in the time series. At the same time as BWL in borehole 99.33 decrease, BWL in borehole 99.52 also start to decrease, although at a slower rapid uniform rate. This suggests seasonal maximum discharge is caused by a rapid change in subglacial hydraulic connections causing the release of previously unexploited subglacially stored water through a different area of subglacial drainage to the section of the tunnel-conduit system that influences BWL in borehole 99.33. The decrease in BWL in borehole 99.52 are synchronous with BWL in borehole 99.33 provides further evidence that borehole 99.52 is also influenced by variations of water pressure in the tunnel-conduit system. Whatever subglacial hydraulic characteristics borehole 99.52 reflects, the rate of decrease is restricted by the hydraulic conductivity of the sediment resulting in a uniform rate in reduction of BWL.

An increase in minimum daily discharge on JD 222 (the largest in the entire ablation season) is out of phase with TSR, and hence release of subglacially stored water continues. BWL decreases rapidly in borehole 99.30 although as concurrent BWL data in borehole 99.33 is not available it is uncertain whether decreasing water pressures reflect release of subglacial water into the tunnel-conduit network or through possibly newly created subglacial hydraulic pathways adjacent to the tunnel-conduit section of the network. A rapid decrease of BWL in borehole 99.30 precede a short duration precipitation event at 04:40 on JD 222, which is reflected as a small peak in an otherwise minimum daily discharge at 06:30. Transit times of 110 minutes for precipitation-induced TSR through the glacial hydrological system are comparable with times for dye traces conducted previously at peak daily discharges. This indicates that surface inputs have unobstructed, swift passage through the tunnel-conduit system despite possibly major glaciological changes having occurred in the subglacial hydraulic environment to facilitate the high rate of discharge of subglacially stored water.

#### 8.3.2.3 Water balance period three (WB3)

Figure 8.13 shows that release of subglacially stored water, in combination with high TSR, which causes seasonally high maximum and minimum daily discharges on JD 221 and JD 222, continues to drain from the subglacial hydrological system maintaining high discharges until JD 224. Very low TSR on JD 224 is synchronous with an equally low discharge indicating that what little water was left in temporary subglacial storage has been allowed to drain. Decreases in subglacial water pressure appear, despite only sporadic availability of BWL data in borehole 99.33, to reflect this decrease across the subglacial network. Uncertainty exists regarding how quickly and for how long BWL in borehole 99.54 have decreased. However, daily peaks of BWL in borehole 99.33 (located approximately 450m down-glacier of borehole 99.54) appear to decrease rapidly on JD 222 and level off on JD 223 and JD 224, whereas rapid decline of BWL in

borehole 99.54 seem to occur a day later on JD 223. A lag in the decrease of BWL between boreholes suggests they reflect hydraulically dissimilar sections of subglacial drainage. This prevents a rapid wave-like movement of decreasing water pressures to propagate up-glacier as TSR decreases sharply in combination with drainage of water from temporary subglacial storage.

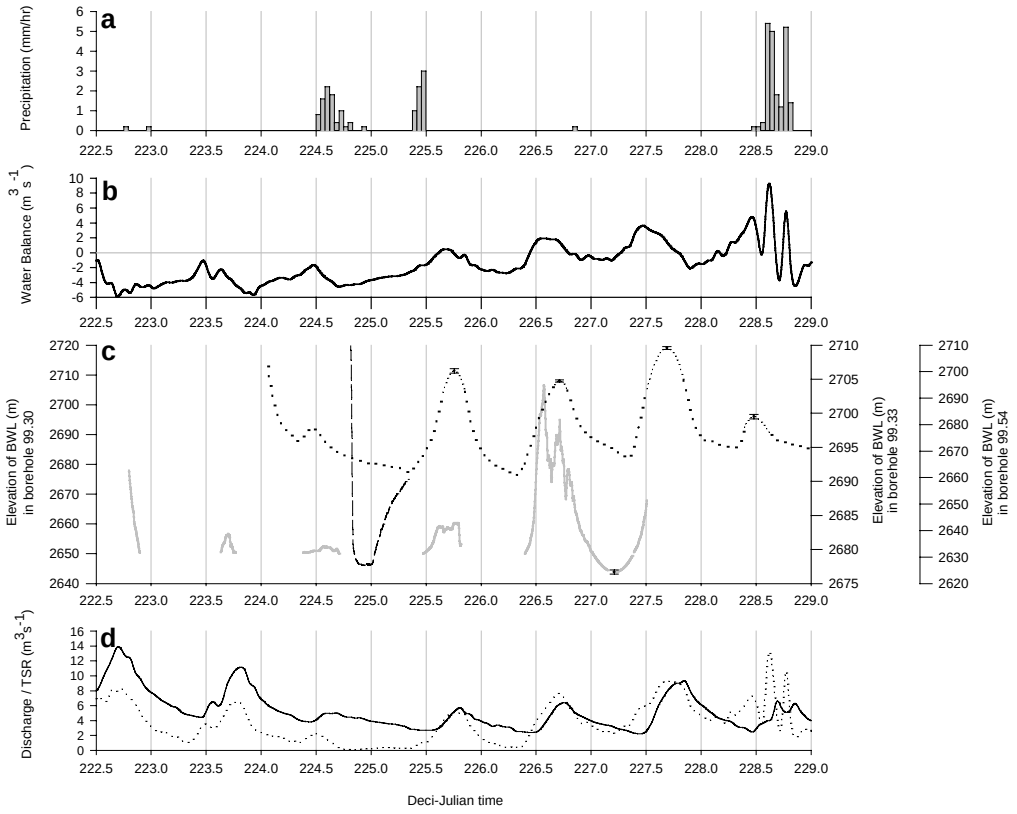



***Figure 8.13 - (a) hourly precipitation; (b) hourly water balance at Findelengletscher; (c) 10-minutely variation in elevation of water levels in borehole 99.30 (dashed), borehole 99.33 (grey), borehole 99.54 (pecked), estimates of water levels in borehole during periods with missing data in boreholes 99.54 (light pecked) 99.33 (short dash) and estimates of diurnal maximum borehole water level (including error bars at 95% confidence limits); (d) hourly total surface runoff (pecked) and pro-glacial river discharge (solid) in the Findelenbach, 10 - 17 August 1999.***

Figure 8.14 shows precipitation on JD 224 and 225 does not have the same direct impact on discharge and water balance as previous precipitation events. Relatively low air temperatures late on JD 224, especially air temperatures measured within the boundary layer of the glacier surface caused much of the overnight precipitation to fall as snow. Precipitation commences at 12:00 on JD 224 and although it is initially dominated by rain (until 16:00) an increasingly larger proportion of precipitation consists of snow as the day progresses. Precipitation recorded between 09:00 and 12:00 on JD 225 is likely to be caused by the snow, which has accumulated in the rain gauge overnight, melting due to diurnal increases in incoming solar radiation and air temperature (especially that of on-glacier air temperature increasing above 0°C). Rainfall early on during the precipitation event is not reflected in TSR, or the water balance, due to the temporal resolution of estimation of elevation of the transient snow line (TSL). TSL was estimated at a daily resolution, therefore, as snow was lying at 2500m a.s.l. during the late afternoon and early morning on JD 224 and JD 225 respectively. The entirety of both days were designated as having a TSL at 2500m a.s.l. As precipitation falling at higher elevations than 2500m a.s.l. was considered to fall as snow and was excluded from calculations of TSR. This physical inaccuracy in calculations of TSR may cause underestimation. Consequently, the lag time of a rapid decrease in BWL in borehole 99.30 after peak precipitation on JD 224 is approximately four hours, which is similar in duration to a previous decrease caused by precipitation-induced TSR on JD 212 but longer than the decrease on JD 219. Similarities in lag times on JD 224 with those on JD 219 correspond to periods of low subglacial water pressures influencing BWL in borehole 99.33, whereas much shorter lag times occur when subglacial water pressures are high.

As the water balance increases for three consecutive days from JD 225 onwards, due to TSR increasing at a faster rate than discharge, trends of BWL in borehole 99.33 and 99.54 also increase reflecting rising subglacial water pressures. Comparison of daily maximum TSR and discharge on JD 227 (the third consecutive day of increasing water balance) with JD 222 (prior to

the large decrease in TSR) shows that a higher maximum daily TSR on JD 227 than JD 222 produces a lower maximum discharge. It is unlikely that a reduction in maximum daily discharge on JD 227 is a result of very low water pressures during JD 224 allowing ice overburden pressure to reduce the CTD of subglacial channels. Although this would restrict subglacial water flow, increase subglacial water pressures and limit the increase in daily maximum discharge, subglacially routed water during the daytime would back-up in subglacial channels, increasing minimum daily discharges at night. Daily minimum discharges do not increase throughout the period of increasing water balance indicating TSR is not being temporarily stored within major subglacial drainage pathways such as the tunnel-conduit section of the drainage network. Alternatively, comparison of maximum daily TSR on JD 227 with an equivalent maximum TSR on JD 217 (before the release of stored water that caused seasonally high TSR and discharge) shows that maximum daily discharges are also approximately equal between the two dates. This comparison indicates the larger maximum discharge on JD 222, relative to JD 227, is still being supplemented by the release of subglacially stored water, which is coming to an end.

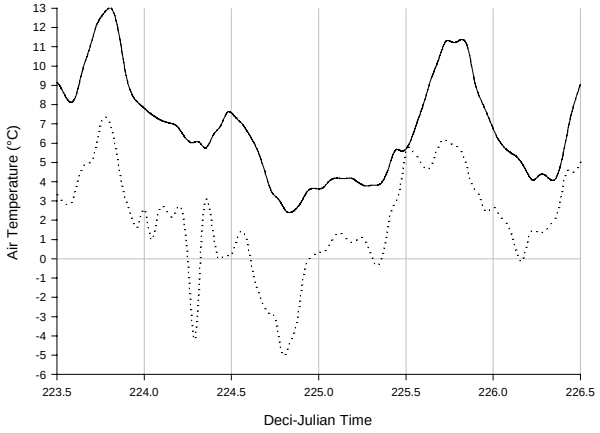



***Figure 8.14 - Hourly boundary layer air temperature measured off-glacier (solid) and on-glacier (pecked), 11 - 14 August 1999.***

After JD 224, when the release of stored water has definitely ended, two processes will combine to increase the water balance. Relatively small volumes of TSR flowing through subglacial channels enlarged by seasonally high discharges will increase the water balance by increasing transit times of TSR through the glacier as water pressures are lower and frictional resistance from the channel sides increase. Although this increases the magnitude of the water balance within a diurnal cycle, the increasing trend over three days is mainly caused by storage of TSR in areas of the subglacial drainage system other than the main tunnel-conduit network. Subglacial water pressures on JD 224 in channels connecting areas of subglacial drainage that act as storage reservoirs to the tunnel-conduit network, which released temporarily stored water between JD 221 and JD 223, have been low enough for long enough (relative to ice overburden pressures) to deform shut. Water flow through the glacier is not restricted by a decrease in the CTD of the tunnel-conduit section of the system, which is too large and structurally stable to be significantly affected during the window of opportunity for closure when ice overburden pressures exceed low channel water pressures. Instead, the efficiency has been significantly reduced within adjacent areas of the drainage network that are characterised by tortuous small channels, linked cavities or low broad channels, either in isolation or in combination, which may possibly be incised into a sedimentary substrate. Out of phase variations between an increasing maximum daily BWL in borehole 99.33 and a decreasing BWL in borehole 99.54 on JD 226 illustrate that within an overall trend of increasing water balance, spatial variations occur in preferential subglacial routing of TSR from one diurnal cycle to the next, as a relatively larger proportion of daily maximum TSR is routed towards borehole 99.33 rather than borehole 99.54 on JD 226 than on JD 225.

The decreasing water balance in WB3 lasts only nine hours from 11:30 to 20:30 on JD 228. Despite a large magnitude rainfall event, also lasting for nine hours and incorporating two short periods of the highest intensity rainfall experienced throughout the measured meteorological time

series, total TSR is low due to high cloud and lower air temperatures combining to reduce melt rates. The two peaks in precipitation are shown clearly by a double peak in discharge, which reflects that transit times through the glacier take two hours and that the majority of precipitation-induced TSR is routed as quick flow through the tunnel-conduit section of the subglacial system. Measured BWL data in borehole 99.54 are missing between 09:20 and 16:40 on JD 228, and precipitation-induced peaks in TSR occur at 14:30 and 18:30. Therefore, as BWL in borehole 99.54 do not reflect any variation in subglacial water pressure associated with the second TSR or discharge peak of the day it is likely that BWL in borehole 99.54 do not reflect water pressure variations in the tunnel-conduit system.

#### 8.3.2.4 Water balance period four (WB4)

As the period of decreasing water balance on JD 228 constitutes a temporary reduction in inputs rather than an increase in the rate of release of subglacially stored water, continuation of an increasing trend in the water balance up to JD 231 due to TSR increasing at a greater rate than discharge, would be expected to cause a similar increase in rising subglacial water pressures. Instead, the trend of decreasing maximum daily discharge is in-phase with decreasing maximum daily BWL in boreholes 99.10, 99.33 and 99.54 (Figure 8.15). A rapid decrease in BWL in borehole 99.30 is also synchronous with the trend of decreasing maximum daily subglacial water pressures. Daily minimum discharge and BWL in boreholes 99.10 and 99.54 are maintained at approximately the same level throughout the increasing trend in water balance (minimum BWL in borehole 99.33 are unknown). This suggests that the subglacial drainage network has changed during JD 228 causing inputs to the network around the times of daily maximum TSR on JD 229 and JD 230 to be routed to areas of the network that do not influence BWL. Decreasing BWL in borehole 99.33 (revealed despite only sporadic availability of data) indicates that preferential routing of TSR away from the tunnel-conduit section of subglacial drainage has occurred during

JD 229. Consequently, less water becomes backed-up within the tunnel-conduit network during times of peak discharge and minimum daily discharge decreases. This requires an assumption that the rate of release of temporarily stored water from adjacent areas of the subglacial drainage network towards the tunnel-conduit network has not increased, which is likely as the total glacial water balance is increasing.

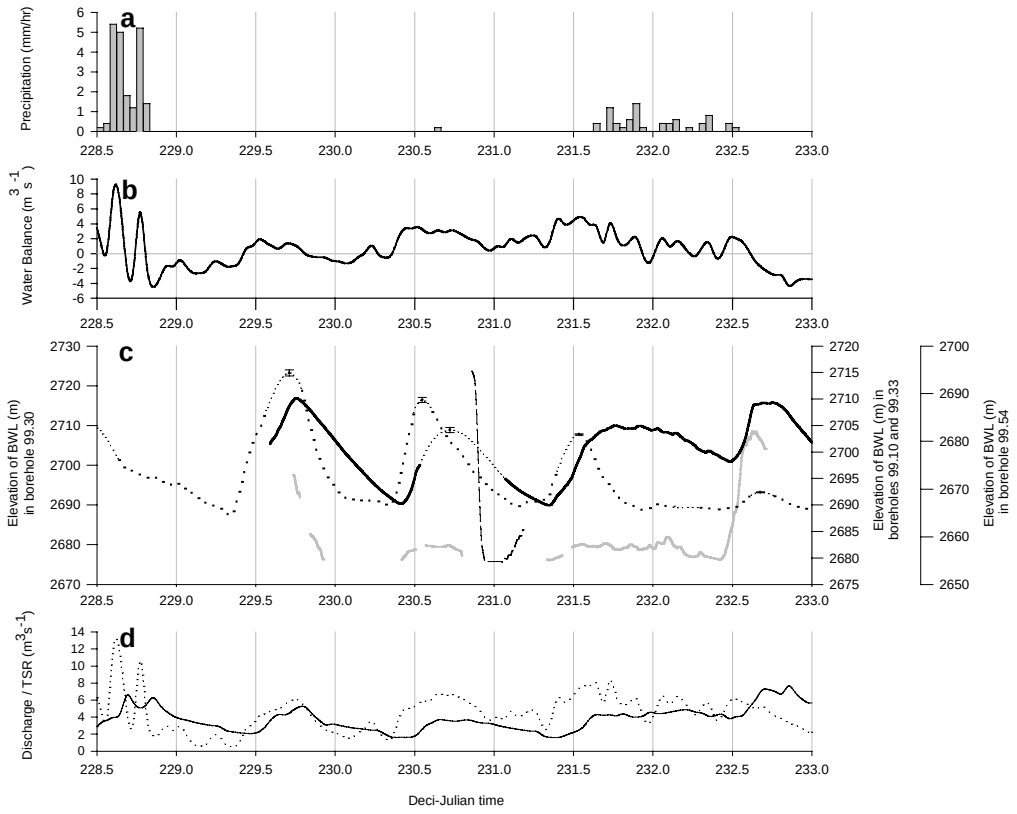



***Figure 8.15 - (a) hourly precipitation; (b) hourly water balance at Findelengletscher; (c) 10-minutely variation in elevation of water levels in borehole 99.10 (solid), borehole 99.30 (dashed), borehole 99.33 (grey), borehole 99.54 (pecked), estimates of water levels in borehole during periods with missing data in boreholes 99.10 and 99.54 (light pecked) and estimates of diurnal maximum borehole water level (including error bars at 95% confidence limits); (d) hourly total surface runoff (pecked) and pro-glacial river discharge (solid) in the Findelenbach, 16 - 21 August 1999.***

Preferential routing of inputs into temporary storage at the time of maximum daily TSR may also account for the pronounced shoulder in the shape of the diurnal hydrograph on JD 229 and JD 230. The shoulder is exaggerated as TSR that would normally contribute to peak daily discharge is withheld within the subglacial drainage network, resulting in a decrease of an otherwise increasing discharge on JD 229 and a totally non-existent peak discharge on JD 230. The shoulder is caused as lower subglacial water pressures, occurring after peak TSR later in the diurnal cycle, cause subglacial routing of TSR back through the tunnel-conduit network, which reduces the rate of decrease in discharge and appears as a shoulder in the diurnal hydrograph.

Low water pressures during the night in subglacial areas such as the tunnel-conduit network can cause the hydraulic gradient to force water in temporary storage from the adjacent subglacial area that influences borehole 99.30. The increase in hydraulic gradient that allows the strength threshold of basal ice and substrate to be exceeded is not, unlike many previous rapid decreases in BWL in borehole 99.30, linked to precipitation-induced TSR. However, BWL on JD 230 only drop approximately two thirds of the height of previous decreases. This may be due to spatial heterogeneity in the shear strength of local basal ice conditions. It could also be due to the extent to which the strength threshold of basal ice has been exceeded without precipitation-induced TSR.

The trend of increasing water balance begins to reverse late on JD 231 and is synchronous with the high duration precipitation event. Water that has been temporarily stored since JD 228 is released into subglacial areas influencing boreholes 99.10 and 99.33 causing BWL to initially be maintained at maximum daily values throughout the rest of the day and then causes further increases in BWLs when diurnal TSR cycles recommence on JD 232. The release of temporarily stored subglacial water indirectly influences water pressure in the subglacial area influencing borehole 99.54. Decreasing maximum BWL in borehole 99.54 from JD 229 to JD 231 indicate

that preferential subglacial routing and temporary storage of daily maximum TSR (prior to late afternoon on JD 231) has not been directly towards borehole 99.54. However, when stored water is released water pressures initially maintain a regular diurnal BWL cycle on JD 231 but only a very small, highly attenuated cycle on JD 232. It is likely that water has become temporarily stored in areas of the subglacial drainage network adjacent to the tunnel-conduit system, down-glacier of borehole 99.54 but up-glacier of boreholes 99.10 and 99.33. As water storage increases there is no hydraulic connection between areas of temporary storage and borehole 99.54, as water from maximum daily TSR is preferentially routed away from borehole 99.54 during this period. However, as water is released, decreasing pressures in areas of temporary storage increase the hydraulic gradient between the spatially separate areas, causing a hydraulic connection to form. Subglacial water influencing borehole 99.54 then drains away through new hydrological connections and ultimately into the tunnel-conduit section of the network. As BWL initially dropped very slowly after drilling and spot height measurements of BWL prior to JD 224 observe large rapid variations in BWL it is likely that the base of borehole 99.54 terminates in subglacial sediment in a similar manner to borehole 99.52 situated 50m away. Hydraulic connection from the borehole to the subglacial drainage system through sediment allows immediate transfer of water pressure when sediment is saturated, occasional evacuation of water within the borehole due to failure within the sediment matrix and, at very low water pressures, it will also act as a rate-limiting factor to actual water movement through the substrate due to low hydraulic conductivities. As a result on JD 232 water does not drain completely from the borehole, in which BWL are already diurnally fluctuating in the lowest 15%. The very small, highly attenuated diurnal cycle later that day is caused by a combination of an indistinguishable diurnal TSR cycle and spatial variation in the saturation and hydraulic conductivity of subglacial sediment.

#### 8.3.2.5 Water balance period five (WB5)

Figure 8.16 shows that as the trend in water balance starts to increase slightly on JD 233 and JD 234, BWL in borehole 99.54 increase out of phase with BWL in borehole 99.33. This relationship is a reversal of the phase relations that occurred when water balance decreased during WB4 (when BWL in borehole 99.33 increased out of phase with 99.54). This indicates that TSR is again becoming temporarily stored in areas of subglacial drainage adjacent to the tunnel-conduit network between boreholes 99.33 and 99.54.

During the decrease in water balance in WB4 (JD 231 and JD 232) BWL in 99.10 exhibited a very similar pattern to BWL in borehole 99.33 suggesting the subglacial areas influencing both boreholes were closely hydraulically connected. However, from JD 233 to JD 234 daily maximum and minimum BWL in borehole 99.10 increase only very slightly as BWL in borehole 99.33 decrease. Also, comparison of the lag times between maximum and minimum BWL in each of the three boreholes between JD 233 and JD 235 shows that during regular diurnal cycles maximum and minimum BWL in borehole 99.10 and 99.33 are asynchronous. In fact maximum and minimum BWL in borehole 99.10 are more synchronous with BWL in borehole 99.54 as BWL in borehole 99.33 always lead similar stationary points in borehole 99.54 that in turn lead borehole 99.10 (see section 11.8). Time lags between daily maximum BWL in boreholes 99.10 and 99.33 are about 210 minutes over a distance of about 350m, compared to transit times of half that time for dye traces of over one kilometre between the glacier surface close to both boreholes and the proglacial river. Consequently, the extent to which BWL in boreholes 99.10 and 99.33 are asynchronous suggests that although the two boreholes are hydraulically connected via the tunnel-conduit network. Inputs of water into the subglacial area that influences BWL in borehole 99.10 are derived from a combination of sources and not exclusively from the section of the tunnel-conduit network that also influences borehole 99.33. Glaciological changes in the size and

efficiency of the tunnel-conduit network that contributed to a decreasing water balance in WB4 may have exaggerated the extent to which the BWL are asynchronous.

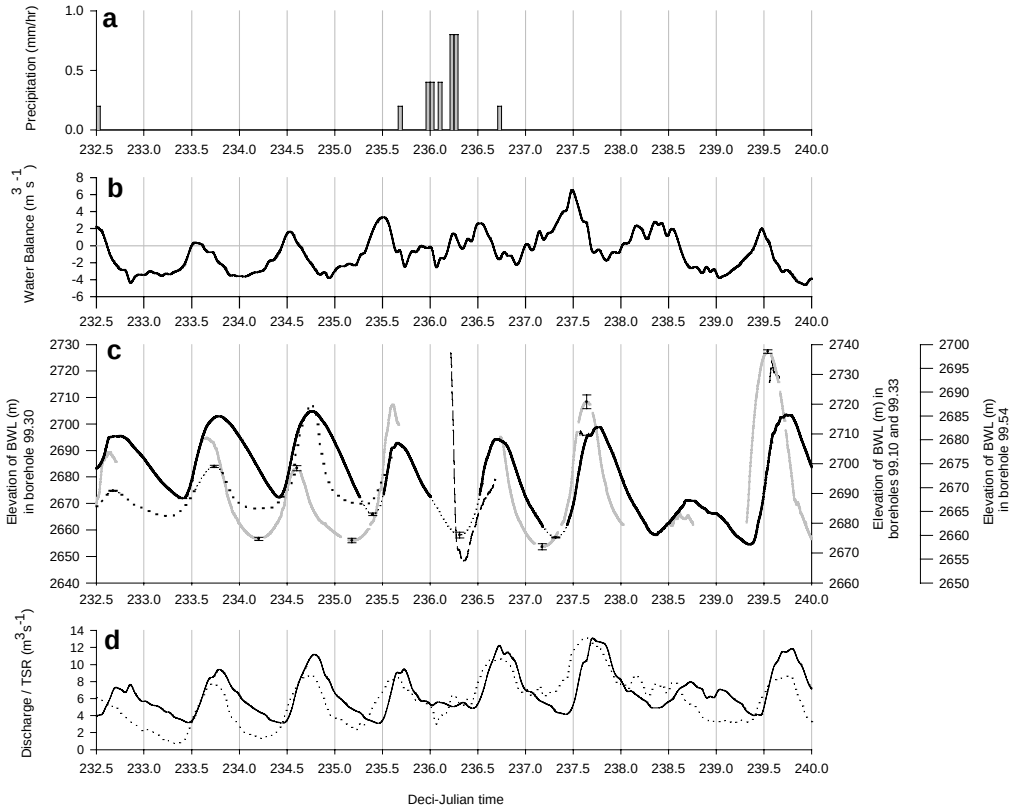



***Figure 8.16 - (a) hourly precipitation; (b) hourly water balance at Findelengletscher; (c) 10-minutely variation in elevation of water levels in borehole 99.10 (solid), borehole 99.30 (dashed), borehole 99.33 (grey), borehole 99.54 (pecked), estimates of water levels in borehole during periods with missing data in boreholes 99.33 (short dash) 99.10 and 99.54 (light pecked) and estimates of diurnal maximum borehole water level (including error bars at 95% confidence limits); (d) hourly total surface runoff (pecked) and pro-glacial river discharge (solid) in the Findelenbach, 20 - 28 August 1999.***

The water balance starts to increases at a greater rate on JD 235 as minimum daily BWL in boreholes 99.10 and 99.33 decrease, which reflect decreasing water pressures in the tunnel-conduit section of the network. BWL in borehole 99.54 continue to increase, reflecting increasing water pressure in sections of the drainage network adjacent to the tunnel-conduit system where TSR is becoming temporarily stored.

On JD 235 maximum daily BWL in borehole 99.10 decrease out of phase with the increasing maximum daily BWL in borehole 99.33, whilst still maintaining a diurnal pattern. BWL in borehole 99.33 increase out of phase with TSR, discharge and borehole 99.10 as some of the temporarily stored subglacial water, which contributes to the rate of increase in the water balance on JD 235, is released into the channel that influences borehole 99.33. It is likely such temporarily stored water, in subglacial areas of less efficient drainage, are released into the tunnel-conduit system through intermittent hydraulic connections. These have improved in efficiency as a result of a similar release of subglacially stored water that caused an increase in BWL in borehole 99.33 on JD 231. It is possible that a large constriction or a significant re-routing of water in the hydraulic connection between boreholes 99.33 and 99.10 could prevent in-phase movement in BWL between the two boreholes. However, it is more likely that borehole 99.33 reflects a tributary within the tunnel-conduit system that contributes relatively small volumes of water compared to the total volumes influencing borehole 99.10. If this is the case, the out of phase movement on JD 235 may be due to localised release of water into the channel section that influences borehole 99.33, in comparison to the release on JD 231 that occurred over a much wider subglacial area. Consequently, the small release of temporarily stored water does not have a large impact on BWL in borehole 99.10 that reflects continued water storage throughout the subglacial drainage network. This indicates new hydraulic connections from subglacial areas adjacent to the tunnel-conduit network are becoming increasingly dominant in controlling preferential flow pathways of daily TSR.

Minimum daily BWL in borehole 99.10 on JD 236 decrease out of phase with TSR and discharge as TSR that results from a low magnitude precipitation event of reasonably high duration early on JD 236 is not predominantly routed through the tunnel-conduit section of the subglacial network. Instead, rainfall runoff that is not incorporated into temporary storage has a slightly longer, more dispersed transit time through the glacier, which results in a more attenuated response in the hydrograph by levelling the usual diurnal trough, rather than producing a 'flashy' response. Precipitation induced TSR also contributes to increasing water pressures in areas of subglacial drainage influencing borehole 99.30. This increases the pressure difference in comparison to low pressures in nearby sections of the tunnel-conduit network, causing the hydraulic gradient to exceed thresholds of basal ice stability and force temporarily stored water into the tunnel-conduit network. As a result BWL in borehole 99.30 decrease rapidly on JD 236 just prior to minimum daily water pressures in the tunnel-conduit system, as indicated by BWL in borehole 99.10.

Water balance continues to increase due to increasing TSR that culminates in the largest daily maximum and minimum TSR throughout the entire ablation season on JD 237. The highest TSR of the ablation season does not cause the highest discharge, but it does cause the largest diurnal water balance (excluding the brief precipitation-induced increases in water balance on JD 228). Increasing water balance is caused by subglacial retention of TSR between 22:30 on JD 236 and 11:30 on JD 237. Subglacial retention is not caused by TSR backing-up in the tunnel-conduit system as although maximum daily BWL in boreholes 99.10 and 99.33 do increase, minimum BWL the following day do not also increase.

Water balance decreases over JD 238 as a direct result of TSR failing to follow a recognisable diurnal pattern. Large volumes of water in temporary subglacial storage are not released over JD 238 causing maximum daily discharge and water pressures in the tunnel-conduit section of the

drainage network, represented by BWL in boreholes 99.10 and 99.33, to reflect the decrease in TSR. However, the discharge hydrograph on JD 238 shows a double peak that is completely unrelated to a slow decline in TSR. The second peak in discharge is caused by release of water from temporary storage into the tunnel-conduit system from adjacent subglacial areas both up- and down-glacier of borehole 99.10. BWL in borehole 99.10 show a shoulder in the diurnally decreasing limb implying some connections between hydraulically separate sections of the subglacial drainage network up-glacier of the borehole have temporarily connected, releasing water into the relatively low pressure tunnel-conduit network thereby increasing water pressures in the channel. It is likely that this mechanism is repeated down-glacier of borehole 99.10, causing more water to be released from temporary storage into the tunnel-conduit network, as the distinction between peaks in the discharge hydrograph are clearer than in the diurnal pattern of BWL. Release of temporarily stored water into the tunnel-conduit system increases dramatically during JD 239, increasing maximum daily BWL in both boreholes 99.10 and 99.33 and supplementing TSR to maintain a high maximum daily discharge as the overall water balance decreases.

#### 8.3.2.6 Water balance period six (WB6)

An increasing trend in water balance is initiated during low maximum daily TSR on JD 240 when discharge and BWL in boreholes 99.10 and 99.33 all decrease in-phase with each other (Figure 8.17). In a similar manner to the low maximum TSR on JD 238 water in temporary subglacial storage is not noticeably released into the tunnel-conduit network to supplement TSR and maintain discharge. Although all variables remain in-phase with each other during the daily maximum on JD 241 the magnitude of diurnal increase in BWL in both boreholes 99.10 and 99.33 are much greater than previously observed. The large increases in maximum BWL are synchronous with an extended decrease in the water balance (between 13:30 and 20:30) that

temporarily interrupts an increasing trend in water balance. Simultaneous increase of BWL in both boreholes indicates release of stored water from temporary subglacial storage into the tunnel-conduit system is likely to occur over a wide subglacial area. As the release of stored water through the tunnel-conduit system continues throughout the night into JD 242, raising minimum BWL in borehole 99.10, volumes of released water combine with a decrease in minimum TSR to create an equivalent minimum daily discharge to that on JD 241. The rate at which stored water is released into the tunnel-conduit system decreases throughout JD 242 causing a reduction in maximum and minimum daily BWL in borehole 99.10. Despite BWL data from borehole 99.33 being discontinuous it also appears to show a reduction in the daily maximum on JD 242. Release of temporary storage must still be continuing into JD 243 further down-glacier of borehole 99.10 as despite minimum daily TSR decreasing in-phase with BWL in borehole 99.10 the minimum discharge is still equivalent to that on JD 241 and JD 242.

From JD 242 onwards, diurnal variations in the water balance have a very similar pattern for three consecutive days, which is superimposed on a rising trend. Increases in the water balance over a 24-hour period are short-lived and are a function of the transit times through the glacier of the initial daily increase in TSR. Duration of lag times between the beginning of ascending limbs of TSR and discharge and the degree to which one variable is out of phase with the other dictates the magnitude of the increase. Decreases in water balance over the same time-scale start when the rate of increase in discharge exceeds that of TSR and the rate of decline depends on individual fluctuations in either variable from then on. Consequently, the regular form of ascending and descending diurnal limbs of TSR and discharge throughout the three consecutive days from JD 242 mean that the increasing water balance occurs as a constant background rate rather than by rapid fluctuations within increasing or decreasing limbs as a result of variation in hydrometeorological or glaciological conditions. The vast majority of TSR appears to be routed through the tunnel-conduit system. Constant rates of storage from JD 242 until the daily

maximum on JD 245 are not likely to be a result of a reduction in the CTD of this section of subglacial drainage as both subtle variations in daily maximum discharge and the consecutive increase in minimum TSR are all reflected in maximum and minimum variations of BWL in borehole 99.10. Consequently, a small proportion of TSR is likely to become temporarily stored at a constant rate within subglacial areas that are adjacent to the tunnel-conduit section of the drainage network.

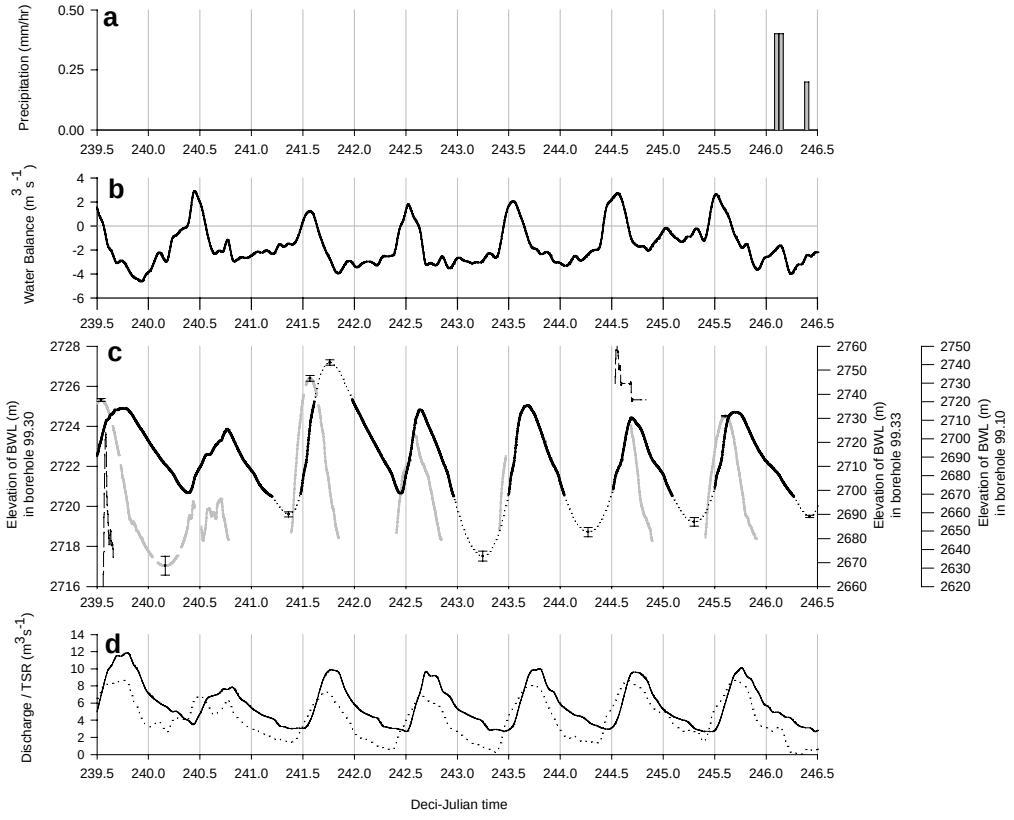



***Figure 8.17 - (a) hourly precipitation; (b) hourly water balance at Findelengletscher; (c) 10-minutely variation in elevation of water levels in borehole 99.10 (solid), borehole 99.30 (dashed), borehole 99.33 (grey), estimates of water levels in borehole during periods with missing data in borehole 99.10 (light pecked) 99.33 (short dash) and estimates of diurnal maximum borehole water level (including error bars at 95% confidence limits); (d) hourly total surface runoff (pecked) and pro-glacial river discharge (solid) in the Findelenbach, 27 August - 3 September 1999.***

#### 8.3.2.7 Water balance period seven (WB7)

Although TSR decreases sharply on JD 246, release of stored water associated with the decreasing water balance on JD 246 maintains the daily minimum discharge and increases the minimum BWL in borehole 99.10, which is associated with increasing water pressures in the tunnel-conduit section of the drainage network. However, it is likely that the CTD of the tunnel-conduit system decreases rapidly throughout JD 246 as lower maximum discharge and TSR (the latter of which is still being supplemented by release of water from temporary subglacial storage - as indicated by the water balance) are out of phase with increasing daily maximum BWL in borehole 99.10. Figure 8.18 shows an increasing trend in water balance begins on JD 247 and the CTD of the tunnel-conduit network continues to decrease, which is indicated by minimum BWL in borehole 99.10 on JD 247 continuing to increase out of phase with TSR and discharge. Whilst BWL in borehole 99.10 decreases in-phase with TSR (as snowfall reduced the elevation of the transient snowline) and discharge later that day. Minimum BWL on JD 248 increases in-phase with TSR but out of phase with decreasing discharge, indicating further constriction to water flow has occurred in the tunnel-conduit section of the drainage network.

Maximum BWL in borehole 99.10 increase on JD 248 in-phase with TSR and discharge, but comparison with JD 246 shows maximum TSR is higher and discharge is lower on JD 248 than JD 246 providing comparative evidence for a reduction in the CTD of subglacial drainage. Increasing temporary storage within the tunnel-conduit section continues to contribute to the overall trend in water balance as a proportion of minimum TSR, which increases out of phase with discharge on JD 249, becomes temporarily stored and increases BWL in borehole 99.10. However, later on JD 249 temporary subglacial storage occurs in areas of the drainage network other than the tunnel-conduit section as maximum daily TSR increases out of phase with BWL as well as discharge. Further decreases in minimum BWL on JD 250 that are out of phase with both

discharge and TSR, which has been supplemented by precipitation-induced runoff, suggest the increase in subglacially stored water during the daytime has increased the CTD of the tunnel-conduit system influencing borehole 99.10. Increased CTD enables an increase in maximum daily discharge on JD 250 that is in-phase with TSR and BWL. Although the increase in CTD on JD 250 has been exceeded by the increase in TSR, continued increase in CTD throughout JD 250 causes a brief decrease in the water balance as water in temporary subglacial storage is released on JD 251 when minimum discharge increases out of phase with TSR and BWL in borehole 99.10. The CTD continues to increase during JD 251 as increasing maximum discharge, in response to increasing maximum TSR, causes approximate equality of maximum BWL in borehole 99.10 in comparison to JD 250. Despite discontinuous BWL data from JD 252 onwards it appears, from the stability of minimum daily discharges and the magnitude of maximum daily discharges relative to maximum daily TSR, that the CTD of the tunnel-conduit network is both sensitive to and responds quickly to variations in TSR. This maintains the subglacial hydrological system at levels very close to optimal hydraulic efficiency.

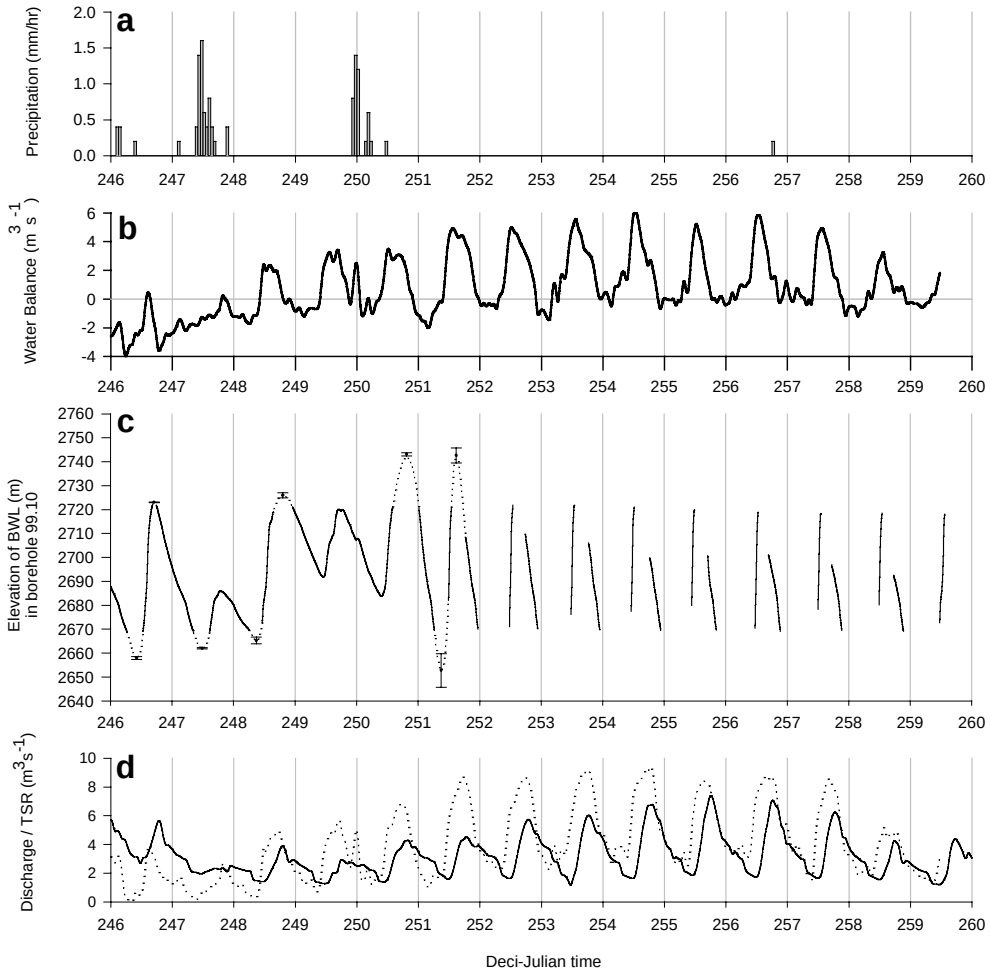



***Figure 8.18 - (a) hourly precipitation; (b) hourly water balance at Findelengletscher; (c) 10-minutely variation in elevation of water levels in borehole 99.10 (solid), estimates of water levels in borehole during periods with missing data (light pecked) and estimates of diurnal maximum borehole water level (including error bars at 95% confidence limits); (d) hourly total surface runoff (pecked) and pro-glacial river discharge (solid) in the Findelenbach, 3 - 17 September 1999.***

## 8.4 Water balance and ice motion

Measurements of ice surface movement were made in both vertical (displacement) and horizontal (fall line) directions using stakes drilled into the ice surface at seven positions along the fall or centre line of the glacier. Vertical displacement due to ablation was accounted for and removed from final measurements. Figure 8.19 shows five of the stakes covered the area between the three arrays of boreholes that run across the width of the ice surface. Ice surface movement was measured at a daily resolution incorporating total cumulative movement between daily measurements (over approximately a 24 hour period). In comparison, TSR, proglacial discharge and water balance values are the hourly average of measurements every ten minutes and precipitation is the cumulative hourly total measurements taken every ten minutes. Vertical displacement and fall line velocity were measured relative to a point of fixed elevation in front of the glacier terminus. Measurements of vertical displacement are presented as the difference in height from the fixed point at each of the five stakes located around the borehole arrays. Measurements of fall line velocities are calculated from the daily average horizontal displacement at all stakes and are presented as a rate in mm $hr^{-1}$. Different temporal resolutions of measurement between daily variations in both fall line velocity and vertical displacement, in comparison to hourly measurements of subglacial water balance and resultant water pressures. These necessitate interpretation of phase and synchroneity relationships as trends over consecutive days rather than within diurnal cycles.

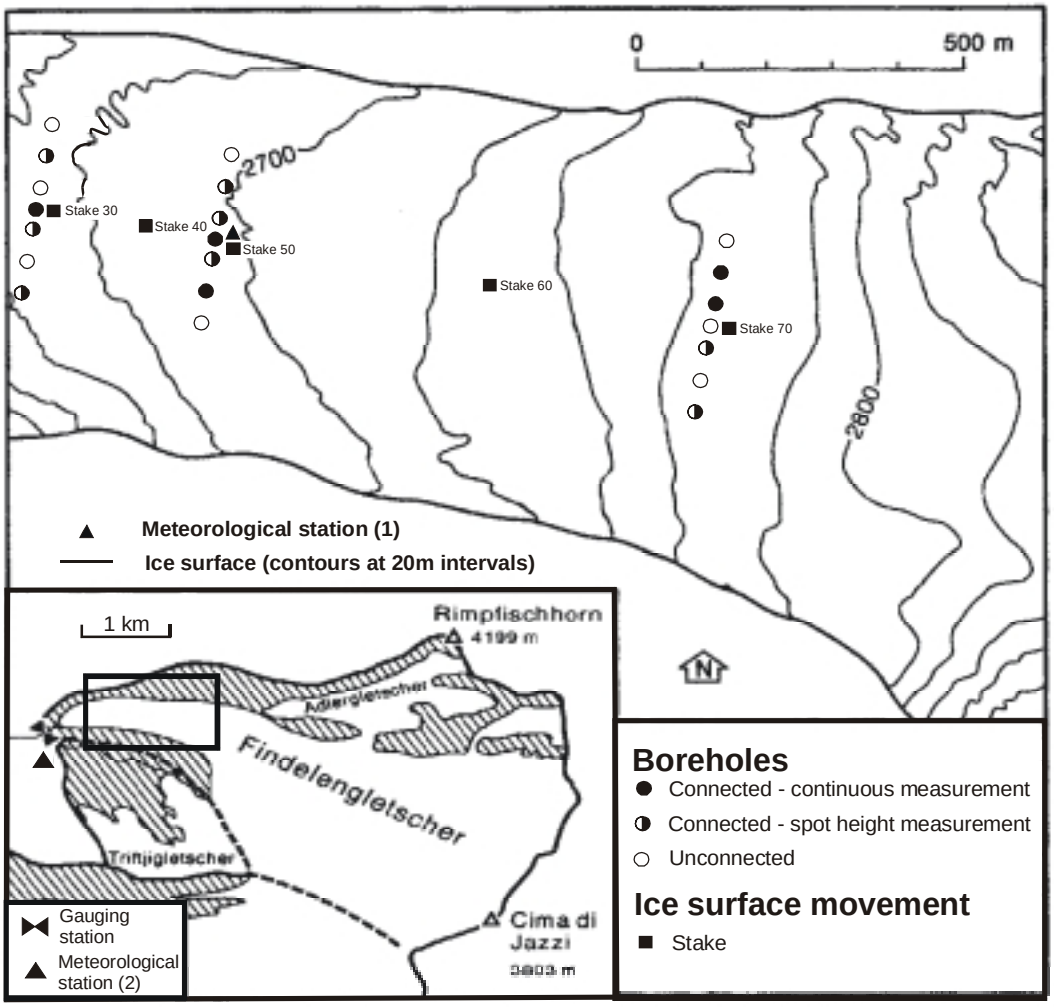



***Figure 8.19 - Positions of stakes used to determine ice surface movement relative to the positions of boreholes.***

### 8.4.1 Detailed observations of ice motion

It can be seen from Figure 8.20 that although day-to-day variations in mean fall line velocity can be erratic, between JD 201 and JD 211 velocities exhibit a trend of gradual increase followed by a rapid decease. This cycle is repeated between JD 212 and JD 220. Figure 8.21 shows a sudden increase in vertical displacement occuring at all five stakes between JD 208 and JD 210. The height of all stakes, except stake 60, decrease shortly after JD 210 and exhibit trends of relatively constant heights similar to those prior to the increase, but at positions of increased elevation.

Trends of decreasing height prior to the abrupt displacement continue at stake 60 after the displacement. Vertical displacement is synchronous with intermittent precipitation between 17:00 on JD 208 and 20:00 on JD 210, which reaches the highest measured intensity of the entire ablation season. A high daily minimum discharge on JD 209, the highest of the ablation season to date, is followed by an erratic diurnally ascending limb and is also synchronous with abrupt vertical displacement.

Between JD 212 and JD 220 a similar slow gradual increase is followed by a rapid decrease in mean fall line velocity. The peak in mean fall line velocity on JD 218 and JD 219 is synchronous with decreasing water balance in WB1 and a precipitation event, although it is lower in magnitude and duration than the precipitation event that accompanied the previous velocity peak. An increase in vertical displacement at all stakes lag by two to three days behind the peak mean fall line velocity on JD 218, but are synchronous with decreasing water balance. Continuation of similar trends prior to the increase in height occur after the increase, therefore, maintaining the increased height at all stakes except at stake 60 where the decreasing trend again occurs.

Mean fall line velocities maintain a gradual declining trend, albeit erratically from day-to day, between JD 220 and JD 228 until a rapid increase occurs on JD 229, which is again synchronous with a high magnitude precipitation event and a decrease in water balance. No vertical displacement is associated with a pattern of gradual decrease followed by a rapid increase in mean fall line velocity, which is the opposite of the previous two cycles of gradual increase followed by rapid decrease.

Mean fall line velocities are maintained at a near constant rate from JD 230 JD 243, other than a transitory decrease on JD 238 that is synchronous with decreasing water balance during WB5 and variations in vertical displacement. Heights of stakes 30, 40 and 50 decrease in-phase with mean

fall line velocity whereas stakes 60 and 70 increase out of phase. On JD 239 all stakes other than stake 40 either maintain the increase in height or rise to heights greater than before the displacement on JD 238.

### 8.4.2 Affect of ice motion on water balance

#### 8.4.2.1 Mean fall line velocities and water balance

Figure 8.20 shows trends and peaks in mean fall line velocity. These have an inconsistent relationship with variations in subglacial water pressures and water balance due to changes in the configuration and efficiency of the subglacial drainage network throughout the ablation season. High subglacial water pressures, which cause low net effective pressures, are linked with increased surface velocity in valley glaciers (Jansson, 1995). Increased water pressures are generated and maintained when increased volumes of TSR are routed into subglacial areas and exceed the localised CTD. The wider the spatial distribution of low net effective pressures beneath basal ice, the smaller the proportion of basal ice is left remaining in contact with the substrate. Although 'sticky spots' may exist where basal friction exceeds the local driving stress causing resistance to movement (Fischer *et al.*, 1999), if shear stresses from overlying ice are concentrated over a smaller subglacial area they are more likely to increase rates of regulation, plastic deformation and shear strengths of material at the ice-bedrock interface. At an ice-sediment interface within the subglacial environment increasing shear stresses can cause an increase in rates of deformation or shearing within the sediment matrix (Boulton and Hindmarsh, 1987) although evidence for large areas of subglacial sediment beneath Findelengletscher is limited. Consequently, increased surface velocity correlates with high subglacial water pressures causing low net effective pressures to be distributed over a wide subglacial area.

Distributed drainage systems, in particular linked cavity systems (Kamb, 1987), would allow rapid spatial distribution of increased water pressures resulting from subglacial routing of increased TSR from precipitation or ice-melt. Theoretically an increase in water pressure within a linked cavity system would be immediately distributed over an increased area of the glacier subsole as orifices that link cavities increase instantaneously and maintain constant levels of water pressure. However, in reality the response of the CTD of the orifices linking cavities to increased water pressure is not instantaneous, ubiquitous or unbounded. Consequently, subglacial water pressures are increased and maintained until the efficiency and connectivity of distributed drainage increases to compensate. In contrast, increasing water pressures as a result of subglacially routed TSR exceeding the CTD of the tunnel-conduit system (concentrated drainage) are only reflected over small subglacial areas within the boundaries of R-channels. Consequently, low net effective pressures in the tunnel-conduit system do not affect subglacial areas sufficient enough to increase surface velocities.

The peak in mean fall line velocity between JD 208 and JD 210 appears to be a result of bed separation caused by low effective pressures resulting from increased precipitation induced TSR. Although BWL data from borehole 99.30 are missing between 18:00 on JD 208 and 15:00 on JD 210 comparison of diurnal BWL patterns over five days before and five days after the increase in mean fall line velocity indicates that there has been a change in diurnal patterns of water pressure affecting borehole 99.30. Before JD 208, BWL in borehole 99.30 exhibit a regular diurnal pattern and after JD 210, despite discontinuous data, diurnal cycles of BWL become more erratic and then are juxtaposed ~60m higher up the borehole. Although water balance data are unavailable it is fair to assume that precipitation between JD 208 and JD 210, which caused high daily minimum discharge on JD 209 and an erratic diurnally ascending limb, has increased water pressures over a wide area of distributed drainage. This causes low effective pressures necessary to increase the mean fall line velocity. Increased water pressures, caused when TSR exceeds the

CTD of distributed drainage, have resulted in basal sliding which in turn has altered the configuration of distributed drainage. The base of borehole 99.30 no longer terminates in an area reflecting a regular diurnal cycle of water pressure and instead begins to reflect a more erratic diurnal pattern incorporating greater increases in water pressures and sudden drops.

The affect of increased mean fall line velocity on the configuration of distributed subglacial drainage is uncertain. Linked cavity systems require high sliding velocities to prevent ice creep into cavities in the lee of bedrock protrusions. Increased rates of subglacial water flow will cause increased efficiency and connectivity of pipes or small channels formed through dissipation of friction energy from enhanced water flow rates. However, high sliding velocities may destroy such enhanced channels, especially if they run transverse to the direction of ice flow. Consequently, distributed drainage after the peak in mean fall line velocity is likely to be left in a transitional period where some areas have an increased hydraulic efficiency, some have maintained a linked cavity system and others have become temporarily hydraulically isolated.

The second major peak in mean fall line velocity between JD 218 and JD 219 is again synchronous with a precipitation event, albeit of lower magnitude and duration than during the first velocity peak, and with a decreasing trend in water balance. Precipitation routed towards the distributed drainage system exceeds the CTD of subglacial hydrological pathways that have developed since the last major velocity peak. Increased water pressures cause rapid expansion in the extent of the distributed drainage network. The expansion forces connections with the tunnel-conduit system, causing increasing daily maximum water pressures affecting BWL in borehole 99.33 and increasing daily minimum water pressures affecting BWL in borehole 99.52. Increases in BWL in both boreholes reflect subglacial movement of water towards tunnel-conduit systems from adjacent areas of less efficient distributed style drainage and a reduction in the overall water balance.

The timing of increased mean fall line velocity occurs after increased water pressures, resulting from a period of increased water balance, combines with low hydraulic transmissivity to reach a pressure threshold for glacier sliding. Consequently, only further short increases in water pressures, caused by precipitation, are necessary to exceed pressure thresholds that cause rapid cavity growth or till shearing events required to increase rates of sliding. Increased mean fall line velocities are likely to result from multiple events of this kind happening simultaneously throughout the distributed drainage system when water pressures are maintained close to the threshold for glacier sliding.

A third increase in mean fall line velocity occurs on JD 229 and again is synchronous with a precipitation event and a decrease in water balance. However, after this increase the mean fall line velocity remains steady suggesting that water flow in distributed drainage has evolved to become spatially more constricted and less affected by changes in TSR and water balance. It is possible distributed drainage now reflects a multibranched arborescent drainage system (Hock and Hooke, 1993) consisting of numerous small channels that are more hydraulically efficient and have more permanent connections with the tunnel-conduit network. Drainage systems like this develop an increased stability and CTD within distributed drainage, which diminishes both the spatial coherency and propagation of down-glacier velocity waves through low net effective pressures.

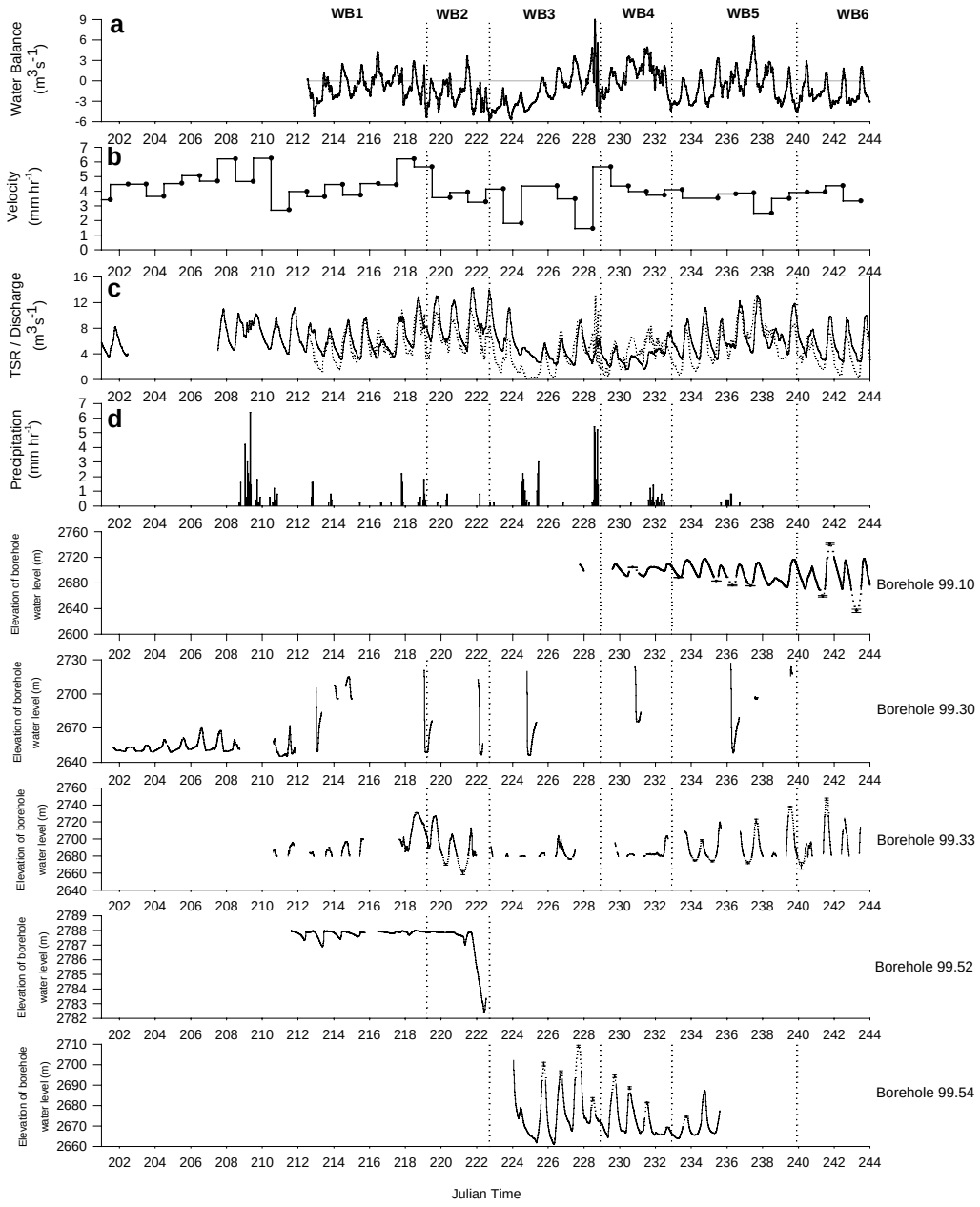



***Figure 8.20 - (a) Hourly water balance demarcated into periods of rising and falling water balance at Findelengletscher, (b) mean daily horizontal glacier surface velocity along fall line, (c) hourly total surface runoff (pecked) and pro-glacial discharge (solid), (d) hourly precipitation. All other graphs indicate 10-minutely variation in elevation of water levels in boreholes (solid), estimates of water levels during periods with missing data (pecked) and estimates of diurnal maximum and minimum borehole water level (including error bars at 95% confidence limits), 20 July - 1 September 1999.***

#### 8.4.2.2 Vertical displacement and water balance

Figure 8.21 demonstrates how vertical displacement of the glacier surface exhibits an inconsistent relationship with periods of decreasing water balance and precipitation. Clear relationships between displacement and subglacial water pressures are also undeterminable. Consequently, vertical displacement is likely to be caused by combinations of subglacial hydraulic jacking and longitudinal strain in response to compressive and extensive glacier ice flow.

Hydraulic jacking causes increased vertical displacement of the glacier surface when increasing TSR is routed into subglacial cavities, increasing subglacial water pressures and decreasing the net effective pressure (Iken *et al.*, 1983). Iken and Bindschadler (1986), referring to bed separation in this manner as the mechanism of formation of water-filled cavities, suggests that periods of hydraulic jacking are likely to be synchronous with increased mean fall line velocities. The first ice surface uplift event on JD 209 and JD 210 is synchronous with increased mean fall line velocity. This suggests that cavity formation within the subglacial drainage network is large enough in spatial extent to be the dominant influence over total ice movement.

The magnitude of increase in vertical displacement, the duration of the increase and the extent to which the following decrease returns to the pre-displacement height are all variable between stakes. This indicates that spatial variation exists in rates of movement in both vertical and horizontal axes within the glacier, which is not moving as a single body.

Rates of ice flow vary within a valley glacier, increasing where flow is extensive and decreasing where flow is compressive. The gradient of basal topography, amongst other factors, is highly influential over the location of fast and slow flowing ice within valley glaciers. Compressive flow exists where the bedrock gradient in a longitudinal down-glacier direction decreases and

where the gradient increases extensive flow occurs. Resulting longitudinal compressive and tensile stresses within glacier ice cause deformation and fracture when stresses exceed critical strain rates within glacier ice (when ice can no longer respond to stress by elastic deformation). Variations in surface displacement, as well as fall line velocities, can occur when fractures in compressive ice flow form along a shear plane where faster moving blocks of ice thrust above slower moving blocks in a manner analogous to tectonic movement. The direction of fracture planes within ice depends on the down slope inclination of the angle of orientation of the principal stress deviator. If fractures occur in upper layers of ice, vertical displacement is not great as the orientation of the principal stress deviator is parallel to the surface. However, with increasing ice depth the down-slope inclination of the angle of orientation of the principal stress deviator also increases, causing ice to thrust upwards along shear planes at higher angles. This produces greater vertical displacement and fall line velocities.

Variations in rates of ice flow are evident from the location and orientation of crevasses. Large crevasse fields exist down-glacier of stake 30 and much smaller crevasse fields exist on the south side of the glacier centre line between stake 60 and stake 70. Both crevasse fields are a result of compressive flow, when the down-slope gradient of bedrock topography decreases, followed by extensive flow, when the down-slope gradient increases. Compressive flow causes ice to expand laterally (Nye, 1952), resulting in slightly splayed crevasses when flow then becomes extensive as the down-slope bedrock gradient increases. Evidence for a small change in bedrock gradient between stake 60 and stake 70 can be seen from measurements of the glacier subsole in Figure 8.2 and the larger gradient change below stake 30 is evident from surface topography. Consequently, variations in the magnitude of longitudinal strain throughout the length of the glacier will also affect the localised response of surface ice displacement at individual stakes in addition to hydraulic jacking, both during vertical increases and subsequent declines in surface height.

The second ice uplift event between JD 221 and JD 222 lags two to three days behind the second peak in mean fall line velocity, suggesting that hydraulic jacking is no longer the dominant influence over mean fall line velocities and that difference in longitudinal strain rates within glacier ice has an increased influence. Time taken for glacier ice to respond, through deformation and fracture, to increases in compressive stress may account for the lag in vertical displacement behind peak mean fall line velocities. Increased efficiency within the distributed section of subglacial drainage, which contributes to the decrease in water balance, will also account for the reduction in spatial extent of water filled cavities throughout the glacier subsole that are required for hydraulic jacking to dominate ice movement. Also, after the second uplift event the increase in vertical displacement is permanent implying the increase is a result of internal thrusting along shear planes within glacier ice rather than temporary affects of changing subglacial water pressure.

The third vertical displacement event on JD 238, which is synchronous with a temporary decrease in mean fall line velocity, shows much spatial variation in both direction and permanency of vertical displacement between the stakes. A decrease in surface height of stakes 30, 40 and 50 may be a result of localised negative or reverse motion of glaciers when subglacial water pressures drop and ice drops back into unpressurised cavities (Willis, 1991). Although this decrease is synchronous with decreasing TSR and water balance, it is likely distributed drainage has evolved so that cavities no longer have as great a spatial influence within subglacial drainage as they did during the first uplift event. Differences in longitudinal strain rates that cause vertical straining, ice deformation and thrusting along internal slip planes are equally, if not more important. Consequently, extensive flow, as a result of tensile stresses that also influence mean fall line velocity, causes relaxation in vertical straining of glacier ice and descent of ice blocks along internal shear planes around stakes 30, 40 and 50. Meanwhile, compressive flow causes

vertical straining within ice and ascent of ice blocks along internal shear planes affecting the glacier surface around stakes 60 and 70.

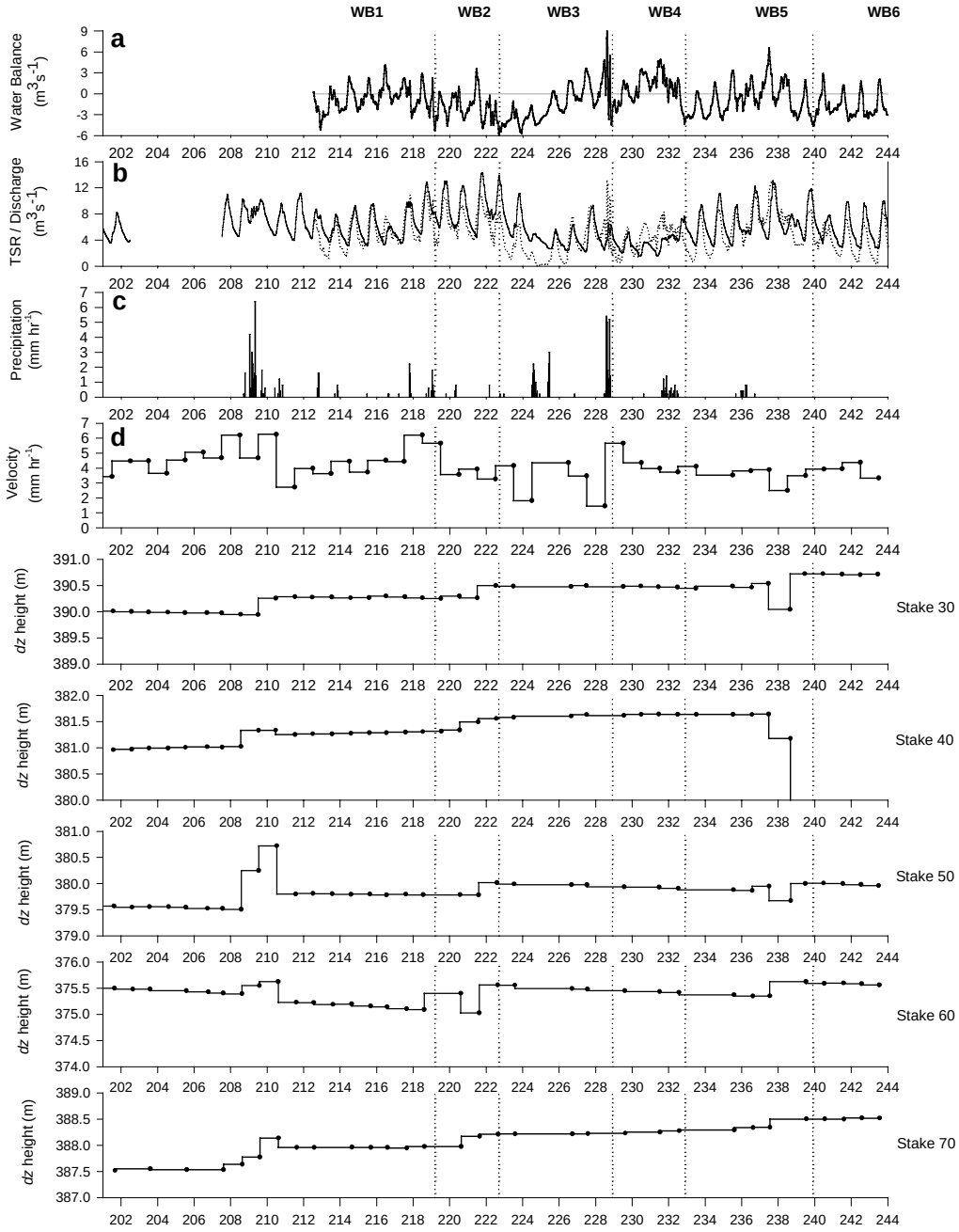



***Figure 8.21 - (a) Hourly water balance demarcated into periods of rising and falling water balance at Findelengletscher, (b) hourly total surface runoff (pecked) and pro-glacial discharge (solid), (c) hourly precipitation, (d) mean daily horizontal glacier surface velocity along fall line. All other graphs show vertical displacement of the glacier surface at positions along the fall line, 20 July - 1 September 1999.***

# 9 WATER BALANCE AND SUBGLACIAL DRAINAGE STRUCTURE

## 9.1 Introduction

Chapter 9 provides a synthesis of the causes of water storage at Findelengletscher. In section 9.2 the utility of boreholes as a method of investigating changes in subglacial drainage are discussed using the conceptual background developed in chapter 6. This focuses on temporal changes in the efficiency and type of subglacial drainage (tunnel-conduit or distributed) reflected by particular boreholes. The nature of hydraulic connections between boreholes and the subglacial drainage system are also considered. As a result, the configuration of the subglacial drainage during the ablation season is hypothesised in section 9.3.

Section 9.4 discusses individual hydrometeorological and glaciological causes of water storage and release within the subglacial drainage system. The implications of storage and release of water on the drainage system itself are then discussed for high magnitude runoff events in the late ablation season.

## 9.2 Hydraulic connection of boreholes

High spatial variation is evident in the hydraulic characteristics of the glacial hydrological system as over a third of the twenty-one boreholes drilled in 1999 are hydraulically isolated and a similar proportion only slightly or intermittently connected. Gordon *et al.* (2001) highlighted the affect on BWL of supraglacial and englacial sources of inputs to and outputs from boreholes that are not hydraulically isolated. Such affects are superimposed on the primary hydraulic connections with the subglacial drainage network.

Although it is almost practically impossible to completely prevent all surface runoff from entering the borehole, either directly via surface streams or through inter-granular seepage in surface layers of ice, visual estimates and analysis of BWL around peak daily TSR suggest volumes of water entering the borehole supraglacially are not significant in comparison to basal inputs and outputs. During drilling at Findelengletscher englacial drainage was encountered as pockets of pressurised water were occasionally intersected and the temporary connection of a small englacial channel with borehole 99.55 was identified using borehole video. Video profiling was conducted in all boreholes where borehole video equipment could fit down the diameter of the borehole, which included all boreholes where water levels were continuously monitored, suggesting that englacial connections were restricted to borehole 99.55. In the absence of hydrostratigraphic profiling (Smart and Ketterling, 1997) or the use of 'hydrology units' incorporating EC cells and turbidity sensors (Stone and Clarke, 1996), video profiling helped indicate the provenance of water fluxes that cause diurnal variations in BWL by highlighting the presence of sediment in suspension (Figure 9.1) and its turbid nature within boreholes. Although the connection with the subglacial environment does not provide an exclusive source for sediment in suspension within boreholes it is by far the most likely and the turbid nature of the particles in suspension implies that sediment is maintained in suspension by fluxes of water into the base of

the borehole. Consequently, of the boreholes that were not hydraulically isolated, diurnal variations in BWL were assumed to result from inputs to and outputs from the base of borehole.

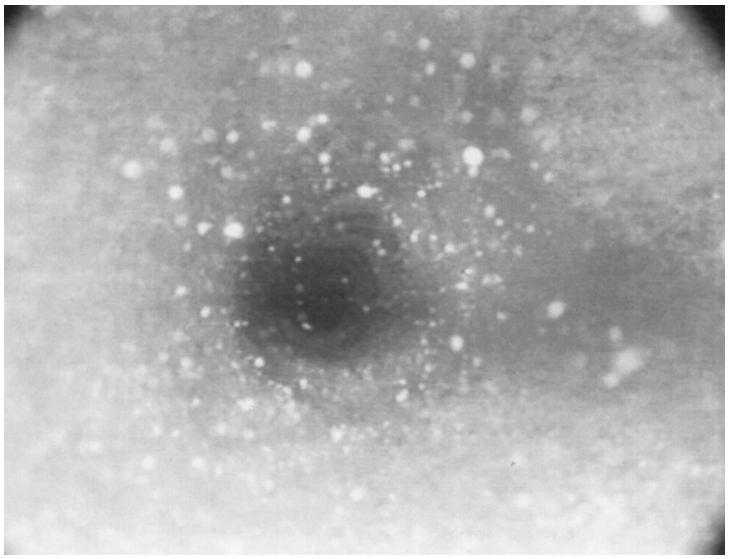


***Figure 9.1 - Sediment in suspension within borehole 99.54***

Boreholes 99.33 and 99.10 are interpreted as connecting with the tunnel-conduit section of the drainage network. As water evacuated out of borehole 99.33 immediately after connection with the glacier bed it is likely to have terminated either in the subglacial channel itself or close enough to the channel to cause a direct connection through ice and sediment at the bedrock interface. Although the connection of the base of borehole 99.10 with the subglacial channel was less immediate, a hydraulic connection rapidly developed. A pilot study in 1998 indicated that a borehole drilled in the same area as 99.10 connected directly with a large subglacial channel. Therefore, although borehole 99.10 did not connect directly, due to the likely proximity between the borehole base and the channel in the tunnel-conduit network it is unlikely that any significant time delay occurs in subglacial transfer of water pressure across the small distance linking the two.

Borehole 99.30 is interpreted as having a variable connection with the subglacial drainage network that exhibits different BWL patterns before and after JD 209. A combination of high mean fall line velocities and a large temporary increase in vertical displacement coincides with this change in the pattern of BWL from a regular diurnal cycle to an erratic cycle of periodic large drops, which possibly result from slowly increasing subglacial water pressures. Even after re-drilling the basal section of borehole 99.30 to ensure it had reached the glacier bed, hydraulic connection to the subglacial drainage system was not immediate. Instead, over the following six diurnal cycles of water pressure a connection developed, possibly with the tunnel-conduit system, at either ice-sediment or ice-bedrock interfaces. Stability of this connection was greatly affected by the ice movement event and subsequently reflected erratic diurnal cycles at increasing elevations and diurnal ranges within the borehole until BWL observed cycles of slowly increasing water levels followed by a rapid drop back to water levels that were equivalent to diurnal minimums prior to the ice movement event.

The regularity of the elevation in water levels that triggered the drop, which is the approximate height of an isolated englacial cavity that was intersected whilst drilling (between 2720m and 2727m a.s.l.), suggested that a pressure threshold had been exceeded. This caused dilation and failure as the yield strength of the sediment was exceeded or a reduction in the net effective pressure required for localised ice floatation. Rapid decreases in BWL were synchronous with either (or a combination of) decreasing water balance or increased hydraulic potential between the tunnel-conduit system and surrounding areas most probably of distributed drainage. Similar patterns of sub-hourly decreases in BWL of such magnitudes are rare in previous published borehole work. The closest comparisons of BWL patterns can be seen in breakthrough curves as boreholes created by hot water drilling intersect unfrozen water-saturated basal till, for example at South Cascade Glacier, USA (Fountain, 1994) or at Ice Stream B, West Antarctica (Engelhardt and Kamb, 1997). A theoretical treatment of BWL in water-filled boreholes that break-through

into subglacial sedimentary aquifers is given in (Stone and Clarke, 1993). However, despite the similarity in comparison of BWL patterns the exact nature of the subglacial drainage system with which borehole 99.30 connects remains uncertain.

Boreholes 99.52 and 99.54 are interpreted as reflecting variations in subglacial water pressure in the tunnel-conduit and adjacent distributed systems respectively. Spot height measurements of BWL in both boreholes 99.52 and 99.54 before JD 209 indicates they are hydraulically connected. However, increased ice surface displacement and mean fall line velocity, resulting from a high magnitude precipitation event, disrupts the stability of the subglacial connection causing BWL in borehole 99.52 to increase out of phase with decreasing BWL in borehole 99.54.

The resulting change in subglacial hydraulic connection causes increasing BWL in borehole 99.52 to reach the surface and subsequently follow a diurnal cycle of low amplitude. Due to continuously high subglacial water pressures only the troughs in diurnal cycles may sometimes be observed. It is highly likely the borehole terminates subglacially at an ice-sediment interface and consequently, diurnal variations of water pressure in the tunnel-conduit system are reflected through a saturated sediment layer instead of the previously more direct hydraulic connection. Such theoretical configurations have previously been suggested to explain patterns of BWL and their connection to subglacial drainage system at Findelengletscher (Barrett and Collins, 1997) and other glaciers such as South Cascade Glacier, USA (Fountain, 1994).

Low hydraulic conductivity of subglacial sediment restricts the rate of water flow in to and out of the base of the borehole, which maintains high BWL at times of low water pressure in subglacial channels. The low amplitude of diurnal variations in BWL is caused by distance decay of the pressure wave further away from the channel (see section 6.5). Daily minimum BWL data in other boreholes, which allows reliable comparison of possible delay in the timing of daily

minimum BWL in borehole 99.52, is limited. However, daily minimum BWL in borehole 99.33, which is directly hydraulically connected to the tunnel-conduit system, lead daily minimum BWL in borehole 99.52 on JD 218 and JD 221. As topographic shadowing causes the daily cycle of ice and snow melt to commence first at the highest elevations up-glacier, the daily minimum BWL in borehole 99.52 would be expected to lead those in borehole 99.33. Consequently, variable hydraulic conductivity within the sediment layer is likely to delay the transfer of water pressure from the tunnel-conduit system to the base of borehole 99.52. Low conductivity of subglacial sediment equally provides resistance to water flow from the borehole to the tunnel-conduit system when the hydraulic gradient is reversed on JD 221. A sudden decrease in water pressure within the tunnel-conduit system is reflected immediately by BWL in borehole 99.33 through a direct hydraulic connection, but BWL in borehole 99.52 reflect a slower uniform rate of decrease controlled by the hydraulic conductivity of the sediment.

Spot height measurements of BWL in borehole 99.54 are erratic until JD 224, reflecting both the changing configurations within distributed drainage systems and the nature of the hydraulic connection between the system and the borehole. Rapid changes in BWL, sometimes involving variations in water level of the order of the entire borehole depth, suggest subglacial drainage consists of many small channels or cavities, each with a low CTD, which may have transient connections with each other. A section of such a variable, distributed drainage system is likely to be hydraulically connected to borehole 99.54 through a sediment layer. Rapid changes in BWL of a distributed drainage system are not likely to be caused by ice floatation as water pressures can be distributed over a wide subglacial area. Consequently, it is more likely that large hydraulic gradients exceed the yield strength of sediment causing abrupt failure within the sediment matrix. Borehole video profiling shows a large amount of sediment in suspension towards the base of the borehole (Figure 9.1) and when the water balance decreases in WB4 and water flows from areas of distributed drainage towards the tunnel-conduit network the low

hydraulic conductivity of subglacial sediment prevents water from draining out of the borehole completely on JD 232.

In comparison to the borehole drainage classification system developed by Gordon *et al.* (2001) at Haut Glacier d'Arolla, boreholes drilled through Findelengletscher do not show the same degree of connection with active englacial drainage. Although there is some evidence of 'complex' boreholes, where boreholes intersect hydraulically isolated cavities, most appear to be 'simple' and basally connected. If turbidity and EC data in boreholes had been available such conclusions may be different, however, only using drilling records, borehole video profiling and analysis of BWL these conclusion are justified. Whether boreholes that were classified as unconnected were 'blind' or 'apparently unconnected' is uncertain and extremely difficult, if not impossible, to discern. Although it is possible for boreholes at Findelengletscher to have terminated in basal ice, short of the ice-bedrock interface and classified as 'blind', drilling records suggest boreholes terminated in areas impermeable to over one hour of pressurised hot water drilling and are herein considered to be 'apparently unconnected' after reaching the glacier base.

## 9.3 Configuration of subglacial drainage

Subglacial drainage results from the coexistence of two broadly separate hydrological systems that vary in hydraulic character throughout seasonal evolution. A discrete tunnel-conduit drainage system consisting of large efficient subglacial conduits fed englacially by supraglacial runoff into moulins is the dominant influence over diurnal discharge cycles. Such channels, of a form related to R-channels (Röthlisberger, 1972) or possibly N-channels (Nye, 1973) where bedrock topography allows, are intra-annually persistent. Although the CTD of the channel will decrease over winter months due to closure from ice overburden pressures, as Findelengletscher has been retreating since the early 1980's, down-glacier ice velocities are not likely to be great

enough to enable surging to occur that would irrevocably damage the configuration. Evidence for the existence and inter-annual persistence of a tunnel-conduit section of subglacial drainage at Findelengletscher comes from comparison of BWL and dye tracing in a pilot study during 1998, and work (unpublished) by members of the Alpine Glacier Project and other authors, notably Iken and Truffer (1997). Development of the tunnel-conduit system at the start of the ablation season occurs in response to increasing hydrometeorologically driven surface runoff into the glacier. The CTD of the tunnel-conduit system to discharge inputs in 1999 appears to peak about the time of the highest maximum and minimum daily discharge on JD 221 and JD 222 respectively. From this point onwards, increased efficiency within subglacial drainage is likely to be a consequence of increased CTD and connectivity within other sections of the subglacial drainage system and their connection with the tunnel-conduit system.

Figure 9.2 shows a schematic representation of subglacial drainage beneath Findelengletscher in the mid to late ablation season resulting from a combination of drilling records, BWL in continuously monitored boreholes, spot height measurements in other borehole and borehole video profiling. This is by no means a definitive picture of the spatial configuration of subglacial drainage. However, it is a useful visual tool to aid understanding of interrelationships between the tunnel-conduit system and adjacent areas of distributed drainage.

Distributed drainage consists of numerous small inefficient channels and hydraulically isolated cavities that are fed englacially from crevasses and discontinuities in the glacier surface that capture minor, possibly intermittent, supraglacial streams. Pressure melting of the glacier subsole provides water for distributed systems that is stored as thin films (Weertman, 1972), inside cavities in bedrock and within sedimentary substrates. Connectivity and subsequent flow of water between such areas constitutes distributed drainage. As connectivity and hydraulic efficiency of small channels and linked cavities (Kamb, 1987) within the distributed drainage

system are susceptible to sub-seasonal changes caused by both hydrometeorologically derived inputs and basal sliding drainage, drainage configurations are unlikely to have inter-annual persistence and instead are highly changeable throughout the ablation season. Direct evidence for the existence of distributed drainage over significant subglacial areas that contributes to total proglacial discharge is provided by diurnal variations in EC that are out of phase with discharge. Out of phase movement between variables results from slow flow rates with a high solute content from distributed drainage becoming diurnally diluted by high flow rates with a low solute content from the tunnel-conduit system. Indirect evidence is provided by analysis of out of phase trends between water storage and water pressures in the tunnel-conduit system, without any noticeable accompanying change in the CTD of the tunnel-conduit system.

As subglacial drainage evolves throughout the ablation season, hydrological interaction occurs between both the tunnel-conduit and distributed drainage systems. Development throughout the ablation season of increasingly efficient drainage within the distributed system and development of hydraulic pathways connecting both systems become dominant factors in controlling the CTD of the entire subglacial drainage network.

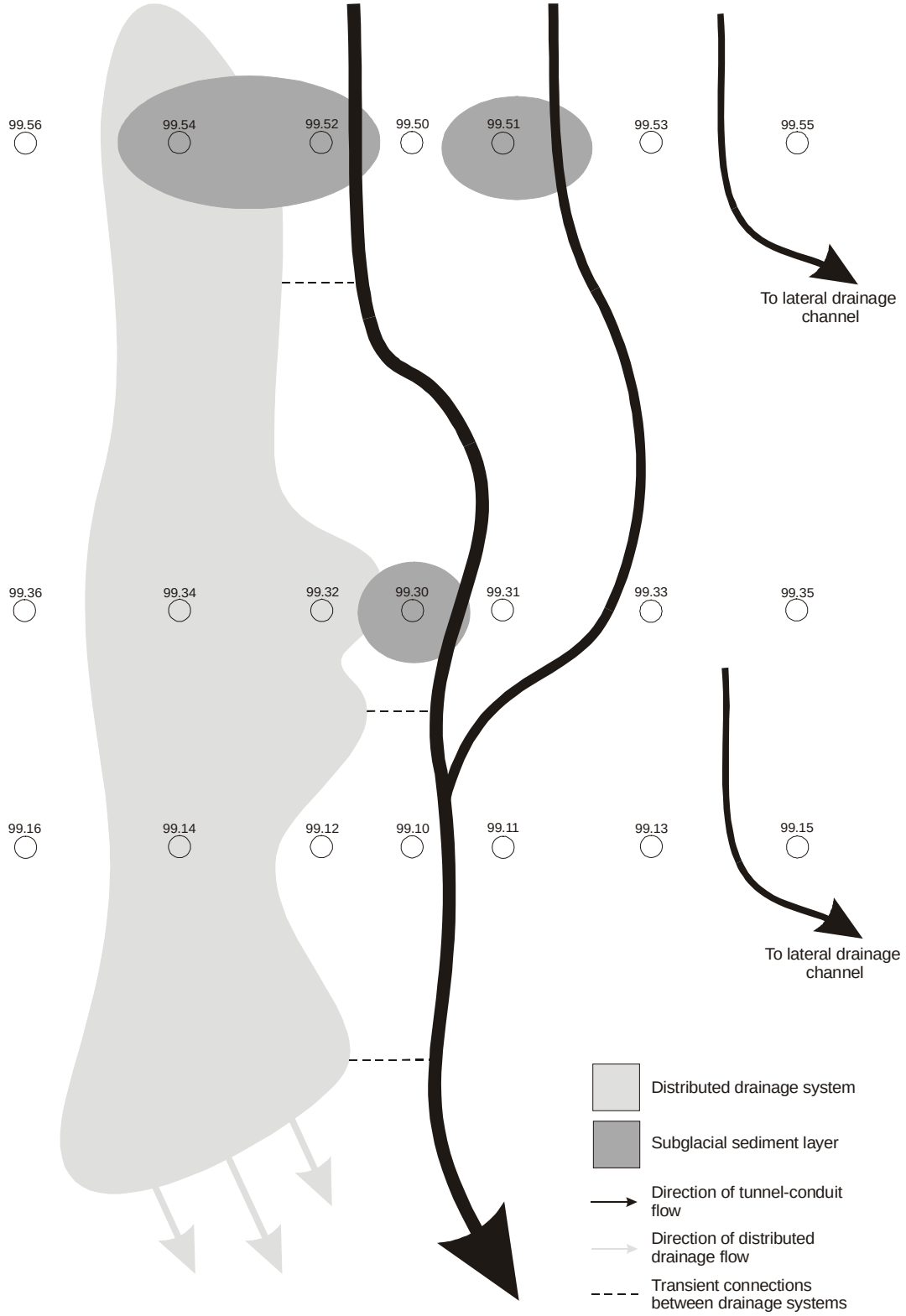



***Figure 9.2 - Schematic diagram of subglacial drainage configuration beneath Findelengletscher in the mid to late ablation season (not to scale).***

## 9.4 Causes of storage and release of subglacially routed water

Conceptually separating the subglacial drainage network into two coexisting systems of efficient and inefficient flow, which may occasionally interact, is commonplace in glacial hydrological studies. Whether drainage systems are termed 'well connected or 'poorly connected' at Trapridge Glacier (Murray and Clarke, 1995; Stone and Clarke, 1996), or whether subglacial flow is transmissive along a variable pressure axis or resistive through a distributed network at Haut Glacier d'Arolla (Gordon *et al.*, 1998; Hubbard *et al.*, 1995) theoretical separation of the drainage network by lumped hydrological characteristics for interpretation of seasonal evolution is widespread.

Broad conceptual divisions are appealing for interpretation of data presented in section 7.3. Strong diurnal cycles of water pressure in a relatively stable, discrete and efficient tunnel-conduit system are large and clear enough to be evident in BWL, whether or not boreholes directly connect with channels or communicate though a hydraulically connective sediment layer. However, it is less easy to distinguish areas of distributed drainage using BWL. Distributed drainage, through relatively inefficient tortuous networks of small channels and linked cavities, may be able to disperse diurnal variations in subglacial water pressure throughout a system of variable connectivity, which maintains areas of stable water pressures. Erratic changes in flow pathways cause sporadic disconnection and reconnection of areas within the distributed system and possible suppression of diurnal cycles of water pressure, which can make BWL in hydraulically connected boreholes confusing to interpret.

Consequently, as BWL data reflecting subglacial areas of distributed drainage are limited, water balance data are used in an analogous manner to BWL in distributed drainage in comparison with BWL data that reflects the tunnel-conduit network. This works on the assumption that if phase

relationships between water balance and BWL in boreholes reflecting the tunnel-conduit network are out of phase with each other the discrepancy is caused by the 'other' distributed section of the subglacial drainage network.

Connection of the distributed and tunnel-conduit sections of subglacial drainage, which are highly influential over storage and release of subglacially routed water, are greatly effected by the seasonal evolution of the entire drainage network. Remnants of R-channels have been identified at Findelengletscher from dye traces in late winter (Moeri and Leibundgut, 1986). Initial spring surface runoff is likely to take advantage of intra-annual permanence of the tunnel-conduit system by exploiting sub- and englacial channels that developed during the previous ablation season (Röthlisberger, 1996). By the end of winter it is likely only the main conduits within the tunnel-conduit system remain open while more peripheral conduits have become disconnected through ice overburden pressures and basal sliding. Consequently, depending on the extent of the disconnections, peripheral areas of the tunnel-conduit system may become hydraulically isolated or incorporated into the distributed drainage system.

The extent to which the distributed drainage system deteriorates over the winter is less certain. Although smaller channels that characterise distributed drainage are more susceptible to closure by ice overburden pressures, the ability for flow to switch between multiple pathways may help to maintain hydraulic connectivity, albeit at a greatly reduced level, within configurations of distributed drainage. Re-establishment of hydraulic connections within distributed drainage resulting from initial spring surface runoff is likely to be faster than re-establishment of the tunnel conduit network. Many configurations of distributed drainage, for example linked cavity systems, require only small volumes of water from surface runoff to connect hydraulically isolated water filled cavities that resulted from deterioration of the system during the winter. Positive feedback mechanisms between increased rates of basal sliding and higher subglacial

water pressures, which are distributed over a wide area of the glacier subsole, will allow maintenance and continuing evolution of distributed drainage, rather than causing disruption of hydraulic pathways in the tunnel-conduit system.

Flow through distributed drainage dominates proglacial discharge early in the ablation season, as indicated by EC records, until evolution of the more efficient tunnel-conduit system causes rates of flow to exceed that of distributed drainage. As discharge from the glacier terminus is concentrated in one major channel, water flow from distributed drainage is likely to subglacially connect with the tunnel-conduit system at some point near to the glacier terminus. The location and permanency of connections between the two systems is uncertain. However, the glacier has been in retreat since the early 1980's (Iken and Truffer, 1997), without any major periods of surging having been observed in the intervening time that would have completely restructured the drainage configuration. Season by season the number of R-channels in the tunnel-conduit system at Findelengletscher will decrease and those remaining will become more arterial (Iken and Truffer, 1997). Consequently, some permanent connections between the two systems may exist towards the terminus.

As the configuration of subglacial drainage evolves throughout the ablation season, temporary connections between both distributed and tunnel-conduit systems develop in addition to more permanent connections. Stone and Clarke (1996) suggested evolution of subglacial drainage passageways resulted from complex physical mechanisms, principally combining water pressures and hydraulic jacking, in which boundaries of well-connected and poorly-connected drainage spread and then returned to their previous state. This would account for temporary connections between each system. Murray and Clarke (1995) has shown that temporary connections between tunnel-conduit and distributed systems at Trapridge Glacier can switch back and forth throughout the ablation season. No defined threshold of subglacial water pressure was identified at which

switch-opening (or switch-closing) occurs, suggesting links between each system are stochastic rather than deterministic in nature. Consequently, as thresholds of water pressure that cause connections between both systems vary, the connecting mechanisms are referred to as a 'sticky switch'.

Physical mechanisms that cause temporary connections within a predominantly sedimentary substrate beneath Trapridge Glacier, were suggested to be the consequence of either substrate compression (causing rapid connections) or porewater diffusion (causing slower connections) (Murray and Clarke, 1995). Iken and Truffer (1997) suggest Findelengletscher slides over a predominantly bedrock substrate, but although there is little evidence for a ubiquitous subglacial layer of sediment, large pockets of saturated basal sediments are likely to be present (Barrett and Collins, 1997). Complex combinations of physical processes including ice-melt, bed separation, and diffusion, compression, erosion or failure of sediment will cause cycling between enlargement and shrinkage of subglacial drainage passageways at Findelengletscher. Temporary connections between tunnel-conduit and distributed systems that result from primarily transverse enlargements of subglacial channels are a consequence of large hydraulic gradients (Gordon *et al.*, 1998).

Sequences of hydrometeorological and glaciological factors, which create the difference in hydraulic potential between the drainage systems needed to open and shut the hydraulic connections, have been discussed in chapter 7 . The requisite difference in hydraulic potential to connect the systems, which influences water balance, is caused by either precipitation, low daily TSR or glaciological changes unrelated to hydrometeorological conditions, all of which may affect both glacier sliding velocity and vertical displacement. Their impact on subglacial storage and release of water as the ablation season progresses is highlighted below.

### 9.4.1 Precipitation

Two precipitation events in WB1 cause a decreasing trend in water balance. Precipitation increases water pressures in distributed drainage at a faster rate than the tunnel-conduit network, causing an increase in hydraulic gradient between the two sections of subglacial drainage. As the forcing pressure exceeds the strength of ice and sediment between the two sections of subglacial drainage, hydraulic connections develop causing water to flow from areas of distributed drainage into the tunnel-conduit network. Water pressures in the tunnel-conduit section increase as a result. Initial increases of water pressure in distributed drainage, and the likely expansion of interconnected channels and cavities across the glacier subsole, has increased bed separation so that shear strength is exceeded at remaining points of contact at ice-sediment or ice-bedrock interfaces causing mean fall line velocity to increase. After water is discharged from the distributed drainage network through the tunnel-conduit system effective pressure increases and closes recently established hydraulic connections as water pressures required to maintain enlarged channel orifices are no longer available.

Although water balance data are not available on JD 209 and JD 210 a much larger precipitation event causes a similar increase in mean fall line velocity and in addition an increase in surface displacement. The same hydraulic mechanism that acts during WB1 is proposed to cause this event. However, the increase in magnitude of precipitation is responsible for uplift as well as a larger response in discharge. Precipitation has such a large influence on subglacial water pressures and ice motion due to the sudden nature of the input in combination with potentially greater access to the subglacial environment, as precipitation may runoff into crevasses and englacial connections not normally utilised by diurnally ephemeral supraglacial streams. This combination of factors causes a sudden, synchronous increase in subglacial water pressure as the CTD of small channel orifices across a wide area of distributed drainage are exceeded at the same

time. Resulting reduction in effective pressure causes increased bed separation, fall line velocity and hydraulic jacking if subglacial pressures are high enough.

Precipitation events on JD 224 and JD 225 during WB3 are larger than during WB1, but they do not sufficiently increase the hydraulic gradient to create connections between tunnel-conduit and distributed systems. Precipitation occurs after three days of declining water balance and is synchronous with very low rates of ice-melt (as elevation of the transient snowline decreases). Low rates of melt in combination with precipitation reduces the total volume of TSR routed subglacially and it is likely previous periods of high water pressure and connections between the two systems have increased the efficiency and CTD within distributed drainage. Consequently, water pressures and the hydraulic gradient are likely to be smaller and not great enough to cause connections between distributed and tunnel-conduit systems.

Decreasing water balance at the end of WB3 is more a consequence of low ice-melt, as heavy rain clouds block out incoming solar radiation, rather than high intensity bursts of precipitation causing connections between tunnel-conduit and distributed drainage. However, precipitation does appear to have affected the hydraulic connectivity within distributed drainage, possibly connecting new englacial pathways to surface runoff. Increased subglacial water pressures have contributed to an increase in mean fall line velocity on JD 229 and increased the difference in hydraulic potential within the distributed drainage system. This causes preferential storage of water away from the section of distributed drainage that influences borehole 99.54, as well as the tunnel-conduit system, as water balance increases during WB4.

Precipitation at the end of WB4 dominates TSR and causes the decrease in water balance. The hydraulic gradient created by increased water pressures from prolonged, rather than intense, precipitation in the section of distributed drainage away from borehole 99.54 (most likely down-

glacier) increases the CTD of connections between the distributed and tunnel-conduit drainage systems. The hydraulic gradient increases rates of water flow into the tunnel-conduit system and away from the section of distributed drainage influencing borehole 99.54. Effective pressures appear to close or reduce the CTD of connections shortly after the water balance stops decreasing as diurnal cycles in TSR recommence.

Precipitation on JD 247 has little affect on hydraulic gradients and connectivity within subglacial drainage as a rapid reduction in meltwater, caused by a decrease in the transient snow line, means total volumes of TSR are actually very low. An increase in water balance during precipitation suggests precipitation is becoming stored within distributed drainage. However, a combination of increased efficiency and low absolute volumes of water in storage do not increase water pressures enough to force the hydraulic gradient to make connections with the tunnel-conduit system. Later during WB7 on JD 249 and JD 250 a precipitation event of similar magnitude is again not great enough to cause a major increase in connectivity within subglacial drainage and instead augments the increasing trend in water balance.

### 9.4.2 Low daily surface runoff

Despite rainfall before and after low elevation snowfall on JD 224, low daily TSR resulting from the fall in elevation of the snow line is the dominant influence over water balance. Very low daily TSR allows water to drain from temporary subglacial storage through existing hydraulic pathways. This causes a decrease in the overall rate of release (starting an increasing trend in water balance) and as water pressures fall in both distributed and tunnel-conduit systems total volumes of water in storage decline. Low TSR is unlikely to have an immediate impact on the configuration of subglacial drainage, although a lagged glaciological impact may occur as a result of increased effective pressure.

A drop in air temperature on JD 238 decreases TSR and causes an in-phase decrease in water pressure in the tunnel-conduit system. Lower water pressures in the tunnel-conduit system increase the hydraulic potential between distributed and tunnel-conduit systems causing hydraulic connections to develop between the systems and water to flow into the tunnel-conduit system from adjacent areas. As the hydraulic gradient increases sufficiently to increase connectivity, water is rapidly discharged from the distributed drainage system causing the second peak in the diurnal discharge cycle early on JD 238. The temporary decrease in subglacial water pressures result in both a decrease in mean fall line velocity and vertical displacement of the glacier surface. The magnitude and direction of vertical displacement is spatially variable as a consequence of longitudinal strain fields within the ice.

Low daily TSR on JD 247, resulting from a decrease in the elevation of the snowline, causes a rapid decrease in the CTD of the tunnel-conduit drainage system and probably closure of hydraulic connections linking to distributed drainage. An increasing trend in water balance commences as a result.

### 9.4.3 Glaciological changes

During WB2 the hydraulic gradient increases suddenly on JD 221 forcing water away from the tunnel-conduit influencing boreholes 99.33 and 99.52. Diurnal patterns of TSR remain relatively unchanged throughout this period when there is no precipitation. However, this change is synchronous with an increase in surface displacement, which is most likely due to deformation and fracture within the ice rather than a direct result of hydraulic jacking (although the effect may possibly be lagged from high water pressures on JD 218). The sudden nature of the fall in water pressure suggests a rapid increase in hydraulic efficiency is caused by bed separation resulting

from an abrupt ice movement. Bed separation is most likely to increase the efficiency of distributed drainage, causing water to coalesce to form larger channels that are less sinuous and have a larger CTD. Bed separation is less likely to have a similar affect on the tunnel-conduit system; therefore, the rapid increase in hydraulic gradient will cause increased connections between drainage systems. Increased connectivity and efficiency throughout the subglacial drainage network causes the decreasing trend in water balance during WB2 to commence.

As water balance is increasing during WB3 slight glaciological changes appear to control subglacial routing within a trend of increasing TSR. During a period of increasing subglacial water pressures throughout the entire subglacial system, out of phase variation of maximum daily BWL in boreholes 99.54 and 99.33 on JD 226 indicates that connections, between the distributed and tunnel-conduit systems respectively, allow hydraulic gradients to briefly direct water flow away from the distributed drainage system. Although this is only a temporary fluctuation in preferential flow pathways it is not synchronous with any hydrometeorological input. Consequently, the change in hydraulic gradient is caused by local subglacial conditions that may possibly be responding to a lagged effect of low daily TSR on JD 224.

Glaciological changes within the tunnel-conduit system, result from the decrease in water balance at the end of WB4. These changes cause volumes of water flowing through the section of the tunnel-conduit system that influences borehole 99.33 to become a smaller proportion of the water subglacially routed through a down-glacier section of the same system that influences borehole 99.10. Comparison of absolute BWL elevations in both boreholes as part of a long-section of the tunnel-conduit system (see section 6.2) indicates that during WB4 maximum daily BWL in borehole 99.10 are at higher elevations than BWL in borehole 99.33. However, during WB5 elevations of maximum daily BWL in borehole 99.33 begin to exceed those in borehole 99.10 implying a constriction in the channel orifice has developed in the connecting channel between

the two boreholes, which increase water pressures up-glacier of the constriction. The reduction in CTD is a consequence of ice overburden pressures exceeding lower water pressures. Lower water pressures result from changes in the configuration of the subglacial drainage network as the water balance decreases during WB4, which causes preferential routing of TSR away from the channel that influences borehole 99.33.

### 9.4.4 Implications for high magnitude runoff in the late ablation season

Heavy rainfall events have produced flood events in the Swiss Alps, which occasionally resulted in debris flows (Rebetez *et al.*, 1997; Zimmermann, 1990), throughout increasingly warm summers during the 1980's and 1990's (Collins, 1998b). Rates of runoff from rainfall in highly glacierised catchments increase throughout the summer as the proportion of the glacier surface that is snow-free (allowing rapid runoff) increases with greater elevation of the transient snowline (TSL). The basin hypsometry of Findelengletscher is such that the snow-free proportion of the glacier surface is highly sensitive to increases in the TSL between 3000m and 3500m a.sl. An increase in elevation of the TSL between 3000m and 3500m a.s.l. increases the snow-free area within the Findelengletscher basin from ~20% to ~80% (~20km$^2$) (Collins, 1998a). Consequently, in late summer when the TSL is at its highest annual elevation, high magnitude rainfall-induced TSR will rapidly increase the volume of inputs to the subglacial drainage system. How the subglacial drainage system, through which almost all surface runoff in the catchment is channelled, reacts to the sudden input provides a major controlling factor over the form of the proglacial river hydrograph and the potential for flooding.

In tunnel-conduit style subglacial drainage systems the CTD is high and will allow rapid throughput of initial volumes of rainfall-induced TSR. Conduits in a tunnel-conduit system are very stable due to their shape and hydraulically efficient configuration. Consequently, as

conduits can withstand large hydrostatic pressures, as the rate of inputs exceeds the rate at which the tunnel-conduit system can discharge, TSR becomes backed up and temporarily stored within the system. Increase water pressures resulting from temporarily stored water will increase the velocity of water flow and causes enlargement by melt widening of the channel sides, adding meltwater to volumes of TSR, and mechanical erosion. Enlargement will happen progressively causing a slow increase in proglacial discharge.

However, if subglacial drainage is dominated by distributed systems of inefficient, poorly connected channels and cavities water pressures resulting from a sudden input of rainfall-induced TSR may cause destabilisation of the drainage configuration (Walder and Driedger, 1995). Destabilisation can cause switching of drainage configuration from a distributed, inefficient network to a more hydraulically efficient system of conduits. Switching will incorporate areas of previously hydraulically isolated, subglacially stored water that enhances TSR and increases proglacial discharge. Rapid reorganisation of drainage configurations can cause temporary formation of multiple outlets at the glacier terminus, which may be caused by combinations of subglacial erosion, fracturing, ice melt and hydraulic jacking, witnessed at Bas Glacier d'Arolla during floods in July 1987 (Warburton and Fenn, 1994).

Walder and Costa (1996), using drainage of glacier-dammed lakes as the trigger for outburst flooding, suggested that routing of water through tunnel-conduit style drainage configurations caused slow rising, attenuated hydrographs, limiting the potential outburst flooding effect of high rainfall events. However, the sudden release of water due to reorganisation of more inefficient, distributed drainage systems causes a rapidly ascending limb of 'flashy' discharge hydrographs, resulting in a higher peak discharge. Consequently, increasing temporary water storage and subglacial water pressures within internal glacier drainage systems in response to large, high

elevation rainfall events are fundamental to the timing and magnitude of any resulting outburst flooding (Collins, 1998a).

Barrett and Collins (1997) observed a high rainfall event at Findelengletscher between 22-24 September 1993. Water levels of a borehole connecting to subglacial drainage via a layer of sediment fell at an increasing rate, which was considered to be indicative of progressive channel growth in existing conduits and small pipes. Much instability of the drainage system was caused by the increase in inputs as meltwater had access to areas of the subsole not normally integrated into the drainage network, which entrained large amounts of sediment that choked-up adduction galleries that had remained clear during comparative discharges earlier in the ablation season. A similar pattern was observed at Matanuska Glacier, Alaska where an intense rain event late in the ablation season caused an eight-fold increase in discharge and a forty-seven-fold increase in sediment transport (Denner *et al.*, 1999). Interpretations again focussed on water being forced under pressure into distributed drainage systems.

Interpretation of data from Findelengletscher throughout the ablation season in 1999 shows that whilst distributed and tunnel-conduit systems coexist, temporary storage of TSR occurs predominantly within the distributed drainage network. Release of stored water is most likely, although not exclusively, a consequence of increased pressures in distributed drainage, increasing local hydraulic gradients and forcing connections with the tunnel-conduit system. Although hydraulic efficiency within distributed drainage does increase during the ablation season, connections linking it to the tunnel-conduit network are only temporary and provide the rate-limiting factor to potential water flow within the entire subglacial network from a sudden rainfall-induced input event. After prolonged periods of declining or negative water balance in the late ablation season, for example during WB6, periods of low daily TSR, such as at the beginning of WB7, and resulting low water pressures in the tunnel-conduit system primarily cause

deterioration of connecting channels between distributed and tunnel-conduit drainage systems. Hydraulic connections close, as there is little water to be released from temporary storage in distributed drainage to maintain the connections.

The resulting subglacial drainage network in the late ablation season consists of systems that are increasingly hydraulically isolated from each other and that have reduced CTD. An increasing diurnal range of BWL in borehole 99.10 during WB7 reflects a reduction in the size of channels in the tunnel-conduit system towards the end of the ablation season (see section 6.4). Reduction in CTD of the channel section, caused by low daily TSR on JD 247, subsequently increases the diurnal range in water pressures without increasing the daily range or magnitude of TSR. Although the size of the relatively small channels in distributed drainage are unlikely to decrease to a similar extent, the connectivity of small pipes and linked cavities will decrease causing increasing storage and isolation of areas of the distributed drainage system.

However, if a large magnitude rainfall event were to take place initial rates of temporary storage are likely to be high as precipitation can exploit more englacial connections that connect with distributed drainage. Also, reduced CTD of the channels in the tunnel-conduit network will cause temporary storage and increased water pressures forcing water into storage in distributed drainage. Although decreased connectivity within distributed drainage will allow greater volumes of TSR to become temporarily stored, when water pressures within distributed drainage exceed thresholds of subglacial stability, discharge will increase exponentially as recently disconnected hydraulic pathways will reconnect at a rate greater than if they had been completely destroyed over winter long periods of low TSR. Precipitation in the late ablation season can, therefore, trigger the release of increasing volumes of temporarily stored water, through rapid expansion into previously isolated areas of distributed drainage and re-integration of hydraulic

connections formed earlier in the ablation season, in combination with the release of TSR backed up in tunnel-conduit systems of reduced CTD.

## 9.5 Conclusions

No significantly large overdeepenings or riegels exist in bedrock topography beneath the subglacial area between borehole arrays at Findelengletscher. Consequently, general changes in bedrock gradient influence, but do not dominate, the course of subglacial water flow and instead have a greater impact on longitudinal strain rates that affect ice-flow.

The subglacial hydrological network is broadly divided into two systems that differ in hydraulic character and vary throughout the ablation season. There is evidence for inter-annual persistence of the hydraulically efficient tunnel-conduit system but the configuration of the distributed drainage system, which has a lower hydraulic connectivity and efficiency, is much less persistent and is affected to a greater extent by seasonal evolution in response to hydrometeorological inputs. Hydraulic connections that exist between both systems, which are mostly intermittent, have a large influence on storage and release of subglacially routed water. Opening and closure of these connections are caused by hydraulic gradients exceeding undefined thresholds of subglacial stability that are locally variable depending on the strength of the ice-sediment or ice-bedrock interface.

Rainfall events can increase water pressures in the distributed drainage system, forcing hydraulic connections into the tunnel-conduit system that initiates release of water from subglacial storage. Rainfall provides relatively short but intense inputs of water that can exploit a wider network of englacial connections to subglacial drainage than meltwater runoff alone. If water storage is already causing pressures that are approaching stability thresholds, inputs from rainfall can

rapidly force widespread temporary hydraulic connections within distributed drainage and between both drainage systems. Increasing subglacial water pressures resulting from increasing daily maximum TSR (as part of a regular diurnal pattern), have a greater affect on the CTD of the tunnel-conduit system than on connections between drainage systems. Consequently, they have less affect on the release of subglacially stored water. Hydraulic connections can also form when low daily maximum TSR reduces water pressures in the tunnel-conduit system, which can sufficiently increase the difference in hydraulic potential relative to water pressures in adjacent areas of distributed drainage to cause connections and initiate release of water from subglacial storage. Occasionally release of water from temporary subglacial storage is not synchronous with either hydrometeorological causal factor. Instead, glaciological changes occur that alter preferential subglacial flow pathways, such as ice movement on JD 221, although such changes may be lagged effects (over a number of days) of high water pressures from rainfall or low water pressures from low daily TSR.

Boreholes that do not terminate in hydraulically isolated areas are rarely 'complex' and variations in BWL are reliant on relatively 'simple' basal connections with the subglacial drainage network. Subglacial hydraulic connections exist through pressure waves in saturated sediment or by direct interception of subglacial channels. Variation of water pressures in the tunnel-conduit system were easier to detect using BWL than the influence of the distributed drainage system due to the characteristically large magnitude of diurnal ranges and greater regularity of diurnal pattern. When direct measurements of BWL in areas of distributed drainage are unavailable water balance calculations can be used in an analogous manner allowing continuing comparison with variations of BWL in the tunnel-conduit system.

Relationships between subglacial water pressure and ice movement (both fall line velocity and vertical displacement) are inconsistent due to changes in configuration of subglacial drainage. A

relationship is evident between increased subglacial water pressure, fall line velocity and surface uplift during rainfall events between JD 208 and JD 210, which cause hydraulic jacking and bed separation. As hydraulic efficiency and connectivity increases within areas of distributed drainage, bed separation and hydraulic jacking have less of an influence over ice velocity and uplift. Instead the magnitude and direction of fall line velocity and vertical displacement become influenced to a greater extent by spatial difference in longitudinal strain within glacier ice in areas of compressive and extensive flow.

In the event of a large rainfall event in the late ablation season connectivity of channels within distributed drainage and the CTD of the tunnel-conduit system will have decreased sufficiently to cause temporary retention of a large proportion of TSR, predominantly within distributed drainage. However, once water pressures exceed thresholds of subglacial stability, discharge will increase exponentially as recently disconnected hydraulic pathways will reconnect at a greater rate than if they had been completely destroyed over long winter periods of low TSR. The potential for rapid runoff of rainfall over the annual maximum snow-free area within the catchment, in combination with temporary storage followed by re-integration of hydraulic connections formed earlier in the ablation season, increases the potential for proportionally large discharge events (relative to the volumes of inputs) in the late ablation season.

# SECTION IV - CONCLUSIONS

# 10 CONCLUSIONS

This thesis contains the results of investigations into subglacial water storage within a temperate Alpine glacier. An essential part of these investigations are *in situ* measurements of hydrometeorological and glaciological variables, which allow direct examination of the subglacial environment. It is shown that the subglacial drainage system is very capable of modifying the discharge hydrograph through temporary subglacial storage of water and its subsequent release. Consequently, the response of the subglacial drainage system to rainfall events at high elevation or snowfall events at low elevation during the late ablation season is highly influential over the form of the discharge hydrograph. This has significance for water resource decision-making and safety of resident populations in high mountain environments, and emphasises the importance of the dynamic nature of subglacial drainage in response to large rainfall events in the late ablation season that have only recently been highlighted by Barrett and Collins (1997) and Denner *et al.* (1999).

A thorough synthesis of our current understanding of physical mechanisms that control surface runoff and drainage through glacierised catchments has been presented. This allowed development of a model to calculate surface runoff, determination of changes in subglacial water storage and development of a theoretical framework through which to interpret the capacity of the subglacial drainage network to store and release surface runoff.

Accurate predictions of total surface runoff (TSR), which combines meltwater and precipitation, are made using a spatially distributed energy balance model. The model is data driven, using measurements of air temperature, incoming solar radiation, precipitation and snowline elevation, which maintain a conceptually correct interpretation of the factors controlling inputs to the glacial hydrological system. The model is based on that of Hock (1999) but it includes only one non-

physically based parameter instead of three. As model output is optimised without using a discharge routing component, no prior assumptions are made about the nature of the subglacial drainage network. Consequently, TSR is derived from a 'new' spatially distributed energy balance model that has as few non-physically based parameters as possible.

Spatial variation in subglacial water storage is observed through measurements of subglacial water pressures, using water levels in boreholes that connect with the subglacial hydrological system either directly or through a layer of saturated sediment. Development of a theoretical framework through which to interpret variations in subglacial water pressures from borehole water levels is an important part of this work. Whereas Gordon *et al.* (2001) concentrated on the influence of englacial channels intersecting boreholes, this work focuses more on the influence of subglacial hydraulic connections between the base of a borehole and the subglacial drainage system, which have not been developed in previous studies. Influences on borehole water levels over diurnal and seasonal timescales include variations in subglacial conduit size, if the borehole directly intersects subglacial conduits, or saturation and hydraulic conductivity of sediment, if the borehole indirectly connects with subglacial drainage. The theoretical framework demonstrates great caution must be used when interpreting changes in borehole water levels when either direct or indirect connections have been made with the subglacial drainage system. This justifies the use of semi-quantitative analysis as a method of interpreting subglacial drainage at Findelengletscher.

Calculations of water storage in combination with measurements of borehole water levels suggest that the subglacial drainage network is broadly divided into two systems (tunnel-conduit and distributed) that differ in hydraulic character and vary throughout the ablation season. There is evidence for inter-annual persistence of the hydraulically efficient tunnel-conduit system but the configuration of the distributed drainage system, which has a lower hydraulic connectivity and

efficiency, is much less persistent and is affected to a greater extent by seasonal evolution in response to hydrometeorological inputs. Glaciological responses that cause release of stored water focus on hydraulic connections that exist between tunnel-conduit and distributed systems. Intermittent opening and closure of these connections are caused by hydraulic gradients exceeding undefined thresholds of subglacial stability that are locally variable depending on the strength of the ice-sediment or ice-bedrock interface. Identification of rapid changes in hydraulic pathways and high pressure gradients are crucial to understanding the dynamic nature of subglacial drainage at Findelengletscher and are similar to rapid changes at Trapridge Glacier, Canada, where areas of the glacier bed also rapidly switched back and forth from being part of connected and unconnected drainage systems (Murray and Clarke, 1995).

Rainfall events at high elevation are shown to be a highly influential controlling factor over release of water from subglacial storage. Rainfall events can increase water pressures in the distributed drainage system, forcing hydraulic connections into the tunnel-conduit system that initiates release of water from subglacial storage. Rainfall events provide relatively short but intense inputs of water, which can exploit a wider network of englacial connections to subglacial drainage than meltwater runoff alone. If subglacial water storage is already causing pressures that are approaching stability thresholds, inputs from rainfall can rapidly force widespread temporary hydraulic connections within distributed drainage and between both drainage systems.

Hydraulic connections can also form when low daily maximum TSR reduces water pressures in the tunnel-conduit system. This can sufficiently increase the difference between water pressures in the tunnel-conduit system and adjacent areas of distributed drainage, so that the increased hydraulic potential causes increased connectivity between both systems and initiates release of water from subglacial storage.

Occasionally, release of water from temporary subglacial storage is not synchronous with either hydrometeorological causal factor. Instead glaciological changes such as glacier sliding or vertical displacement, as identified previously in Willis (1995), alter preferential subglacial flow pathways. However, such changes may be the result of lagged effects (over a number of days) of high water pressures from rainfall or low water pressures from low daily TSR due to the time taken to transfer longitudinal strain within glacier ice.

High elevation rainfall, low daily TSR and glacier movement (both sliding and uplift) are low duration events within the context of the ablation season. However, they have been shown to have a disproportionately large impact on the hydraulic connectivity and efficiency of the subglacial drainage system, greatly influencing periods of water storage and release throughout the ablation season.

In the event of a large rainfall event in the late ablation season connectivity of channels within distributed drainage and the capacity of the tunnel-conduit system to discharge will have decreased sufficiently to cause temporary retention of a large proportion of TSR, predominantly within distributed drainage. However, once water pressures exceed thresholds of subglacial stability, discharge will increase exponentially as recently disconnected hydraulic pathways will reconnect at a greater rate than if they had been completely destroyed over long winter periods of low TSR. The potential for rapid runoff of rainfall over the annual maximum snow-free area within the catchment, in combination with temporary storage followed by re-integration of hydraulic connections formed earlier in the ablation season, increases the potential for proportionally large discharge events (relative to the volumes of inputs) in the late ablation season. Flooding in glacierised basins becomes more likely as a result.

Future work should aim to prolong the monitoring period throughout the late ablation season until well after the elevation of the transient snow line descends beneath the elevation of the glacier. Continuous monitoring of water levels within a spatially distributed array of boreholes during this period would allow the 'window of opportunity' for late season flooding to be more adequately covered should there be a rainfall event. If this monitoring period were repeated over successive annual cycles it would also yield valuable information on the rate of closure of hydraulic pathways within the subglacial drainage system towards the end of the ablation season. Information describing the release of water during this period or the spatial extent of water storage within the subglacial drainage network throughout the winter is of use for investigation of glacier movement and proglacial discharge before and during the start of the following ablation season.

Other work that attempts to understand the physical basis for water flow through glacierised catchments will require monitoring of further variables that are involved in water flow, within an integrated approach such as Richards *et al.* (1996) from Haut Glacier d'Arolla, Switzerland. Frequent measurement of transit times of surface runoff from different areas on the glacier surface to the proglacial river, as well as hourly measurements of dissolved and suspended load, would be particularly useful in combination with borehole water level data. In combination, such data may be able to increase the spatial understanding of how temporary connections within the subglacial drainage network occur. The impact of periods of subglacial water storage and release throughout the ablation season could then be considered on flooding, hydrograph attenuation, $CO_2$ sequestration and rates of glacier erosion amongst other areas of glaciological study.

## 11 REFERENCES

Aizen, V., Aizen, E., and Melack, J. (1995). "Characteristics of runoff formation at the Kirgizskiy Alatoo, Tien Shan." *IAHS*, 228, 413-430.

Alley, R. B. (1989). "Water-pressure coupling of sliding and bed deformation: I. Water system." *Journal of Glaciology*, 35(119), 108-118.

Alley, R. B., Blankenship, D. D., Bently, C. R., and Rooney, S. T. (1986). "Deformation of till beneath ice stream B, West Antarctica." *Nature*, 322, 57-59.

Ambach, W. (1986). "Nomographs for the determination of meltwater from snow- and ice surfaces." *Berichte des naturwissenschaftlich-medizinischen Vereins in Innsbruck*, 73, 7-15.

Ångström, A., and Tryselius, O. (1934). "Total radiation from sun and sky at Abisko (68°21'·2 N, 18°49'·3 E)." *Geografiska Annaler*, 16(1), 53.

Arnold, N. S., Willis, I. C., Sharp, M. J., Richards, K. S., and Lawson, W. J. (1996). "A distributed surface energy-balance model for a small valley glacier. I. Development and testing for Haut Glacier d'Arolla, Valais, Switzerland." *Journal of Glaciology*, 42(140), 77-89.

Baker, D., Escher-Vetter, H., Moser, H., Oerter, H., and Reinwarth, O. (1982). "A glacier discharge model based on results from field studies of energy balance, water storage and flow." *IAHS*, 138, 103-112.

Barrett, A. P., and Collins, D. N. (1997). "Interaction between water pressure in the basal drainage system and discharge from an Alpine glacier before and during a rainfall-induced subglacial hydrological event." *Annals of Glaciology*, 24, 288-292.

Barry, R. G. (1992). *Mountain Weather and Climate*, Routledge, London and New York.

Bearth, P. (1953). "*Geologischer Atlas der Schweiz.*", Swiss Geological Commission, Bern.

Behrens, H., Bergmann, H., Moser, H., Rauert, W., Stichler, W., Ambach, W., Eisner, H., and Pessel, K. (1975). "Study of the discharge of Alpine glaciers by means of environmental isotopes and dye tracers." *IAHS*, 104, 219-224.

Benn, D. I., and Evans, D. J. A. (1998). *Glaciers and Glaciation*, Arnold, London.

Berner, P. (1963). "Der Einfluss der Bewölkung auf die Himmelsstrahlung." *Archiv für Meteorologie, Geophysik und Bioklimatologie*, Ser. B(12 (3-4)), 442.

Bezinge, A. (1987). "Glacial meltwater streams, hydrology and sediment transport: the case of the Grande Dixence hydroelectricity scheme." *In Glacio-fluvial sediment tranfer: an Alpine perspective*, A. M. Gurnell and M. J. Clark, eds., John Wiley and Sons Ltd, Chichester, 473-498.

Blake, E. W., and Clarke, G. K. C. (1992). "Interpretation of borehole-inclinometer data - a general-theory applied to a new instrument." *Journal of Glaciology*, 38(128), 113-124.

Blake, E. W., Fischer, U. H., and Clarke, G. K. C. (1994). "Direct measurement of sliding at the glacier bed." *Journal of Glaciology*, 40(136), 595-599.

Blalock, H. M. (1979). *Social statistics*, McGraw-Hill, New York.

Boulton, G. S., and Hindmarsh, R. C. A. (1987). "Sediment deformation beneath glaciers: rheology and geological consequences." *Journal of Geophysical Research*, 92(B9), 9059-9082.

Braithwaite, R. J. (1995). "Aerodynamic stability and turbulent sensible-heat flux over a melting ice surface, the Greenland ice sheet." *Journal of Glaciology*, 41(139), 562-571.

Braithwaite, R. J., Konzelmann, T., Marty, C., and Olsen, O. B. (1998). "Reconnaissance study of glacier energy balance in North Greenland, 1993-94." *Journal of Glaciology*, 44(147), 239-247.

Braithwaite, R. J., and Olesen, O. B. (1989). "Calculation of glacier ablation from air temperature, West Greenland." *In Glacier Fluctuations and Climatic Change*, J. Oerlemans, ed., Kluwer, Dodrecht-Boston-London, 219-233.

Braithwaite, R. J., and Olesen, O. B. (1990). "A simple energy-balance model to calculate ice ablation at the margin of the Greenland ice sheet." *Journal of Glaciology*, 36(123), 222-228.

Brown, G. H., Sharp, M. J., Tranter, M., Gurnell, A. M., and Nienow, P. W. (1994). "Impact of post-mixing chemical reactions on the major ion chemistry of bulk meltwaters draining the Haut Glacier d'Arolla, Valais, Switzerland." *Hydrological Processes*, 8, 465-480.

Burkimsher, M. (1983). "Investigations of glacier hydrological systems using dye tracer techniques: observations at Pasterzengletscher, Austria." *Journal of Glaciology*, 29(103), 403-416.

Clague, J. J., and Mathews, W. H. (1973). "The magnitude of jökulhlaups." *Journal of Glaciology*, 12(66), 501-504.

Clarke, G. K. C. (1996). "Lumped-element analysis of subglacial hydraulic circuits." *Journal of Geophysical Research*, 101(B8), 17547-17559.

Cline, D. (1995). "Snow surface energy exchanges and snowmelt at a continental alpine site." *IAHS*, 228, 157-166.

Cohen, D., Hooke, R. L., Iverson, N. R., and Kohler, J. (2000). "Sliding of ice past an obstacle at Engabreen, Norway." *Journal of Glaciology*, 46(155), 599-610.

Collins, D. N. (1977). "Hydrology of an Alpine glacier as indicated by the chemical composition of meltwater." *Zeitschrift für Gletscherkunde und Glazialgeologie*, 13, 219-238.

Collins, D. N. (1979a). "Hydrochemistry of meltwaters draining from an alpine glacier." *Arctic and Alpine Research*, 11(3), 307-324.

Collins, D. N. (1979b). "Quantitative determination of the subglacial hydrology of two Alpine glaciers." *Journal of Glaciology*, 23(89), 347-362.

Collins, D. N. (1979c). "Sediment concentration in melt waters as an indicator of erosion processes beneath an Alpine glacier." *Journal of Glaciology*, 23(89), 247-257.

Collins, D. N. 1982a; "Temporal variations of meltwater runoff from an Alpine glacier." *Proc. Symp. Hydrolog. Research Basins Sonderh. Landeshydrologie*, Bern , 781-789.

Collins, D. N. (1982b). "Water storage in an Alpine glacier." *IAHS*, 138, 113-122.

Collins, D. N. (1988). "Suspended sediment and solute delivery to meltwaters beneath an alpine glacier." *Mitteilungen der Versuchsanstalt für Wasserbau, Hydrologie und Glaziologie*, 94, 147-161.

Collins, D. N. (1989a). "Hydrometeorological conditions, mass balance and runoff from Alpine glaciers." *In Glacier Fluctuations and Climatic Change*, J. Oerlemans, ed., Kluwer, Dodrecht-Boston-London, 235-260.

Collins, D. N. (1989b). "Seasonal development of subglacial drainage and suspended sediment delivery to melt waters beneath an Alpine glacier." *Annals of Glaciology*, 13, 45-50.

Collins, D. N. (1995). "Diurnal variations of flow-through velocity and transit time of meltwaters traversing moulin-conduit systems in an alpine glacier." *IAHS*, 228, 363-369.

Collins, D. N. (1996). "A conceptually based model of the interaction between flowing meltwater and subglacial sediment." *Annals of Glaciology*, 22, 224-232.

Collins, D. N. (1998a). "Outburst and rainfall-induced peak runoff events in highly glacierized Alpine basins." *Hydrological Processes*, 12, 2369-2381.

Collins, D. N. (1998b). "*Rainfall-induced flood events in a glacierised Alpine basin during warm summers.*", Alpine Glacier Project Working Papers, Manchester, 13.

Collins, D. N. (1999). "Solute flux in meltwaters draining from a glacierized basin in the Karakoram mountains." *Hydrological Processes*, 13(18), 3001-3015.

Collins, D. N., and Lowe, A. T. (1997). "*Remote sensing of the seasonal ascent of the transient snow-line for analysis of variability of runoff from large glacierised basins in the Karakoram mountains.*", Alpine Glacier Project Working Papers, Manchester, 21.

Copland, L., Harbor, J., Minner, M., and Sharp, M. (1997a). "The use of borehole inclinometry in determining basal sliding and internal deformation at Haut Glacier d'Arolla, Switzerland." *Annals of Glaciology*, 24, 331-337.

Copland, L., Harbor, J., and Sharp, M. (1997b). "Borehole video observation of englacial and basal ice conditions in a temperate valley glacier." *Annals of Glaciology*, 24, 277-282.

Cuffey, K. M., Thorsteinsson, T., and Waddington, E. D. (2000). "A renewed argument for drystal size control of ice sheet strain rates." *Journal of Geophysical Research - Solid Earth*, 105(B12), 27889-27894.

Cutler, P. M. (1998). "Modelling the evolution of subglacial tunnels due to varying water input." *Journal of Glaciology*, 44(148), 485-497.

Dansgaard, W., Johnsen, S. J., Clausen, H. B., Dahl-Jensen, D., Gundestrup, N. S., Hammer, C. U., Hvidberg, C. S., Steffensen, J. P., Sveinbjörnsdottir, A. E., Jouzel, J., and Bond, G. (1993). "Evidence for general instability of past climate from a 250-kyr ice-core record." *Nature*, 364, 218-220.

Davis, J. C. (1986). *Statistics and data analysis in geology*, John Wiley and Sons, New York.

Denner, J., Lawson, D. E., Larson, G. J., Evenson, E. B., Alley, R. B., Strasser, J. C., and Kopczynski, S. (1999). "Seasonal variability in hydrologic-system response to intense rain events, Matanuska Glacier, Alaska, U.S.A." *Annals of Glaciology*, 28, 267-271.

Drewry, D. J. (1983). "*Antarctica, Glaciological and Geophysical Folio.*", Scott Polar Research Institute Report, University of Cambridge, Cambridge, 16 sheets.

Drosdov, O. A., and Mosolova, G. I. (1975). "Method for estimating the melting of snow on glaciers." *IAHS*, 104, 70-73.

Engelhardt, H. (1978). "Water in glaciers: observations and theory of the behaviour of water levels in boreholes." *Zeitschrift für Gletscherkunde und Glazialgeologie*, 14, 35-60.

Engelhardt, H., and Kamb, B. (1997). "Basal hydraulic system of a West Antarctic ice stream: constraints from borehole observations." *Journal of Glaciology*, 43(144), 207-230.

Engelhardt, H. F., Humphrey, N., Kamb, B., and Fahnestock, M. (1990). "Physical conditions at the base of a fast-moving Antarctic ice stream." *Science*, 248(4951), 57-59.

Ersi, K., Ohmura, A., and Lang, H. (1995). "Simulation of runoff processes of a continental mountain glacier in the Tian Shan, China." *IAHS*, 228, 455-465.

Eschelmeyer, K., and Harrison, W. D. (1990). "Jakobshavns Isbrae, West Greenland: seasonal variations in velocity - or lack thereof." *Journal of Glaciology*, 36(122), 82-88.

Escher-Vetter, H. (1985). "Energy balance calculations for the ablation period 1982 at Vernagtferner, Oetztal Alps." *Annals of Glaciology*, 6, 158-160.

Fairchild, I. J., Bradby, L., Sharp, M. J., and Tison, J.-L. (1994). "Hydrochemistry of carbonate terrains in alpine glacial settings." *Earth Surface Processes and Landforms*, 19, 33-54.

Fenn, C. R. (1987). "Sediment transfer processes in alpine glacier basins." *In Glacio-fluvial sediment transfer: an alpine perspective*, A. M. Gurnell and M. J. Clark, eds., John Wiley and Sons Ltd, Chichester, 59-86.

Fenn, C. R. (1989). "Quantifying the errors involved in transferring suspended sediment rating equations across ablation seasons." *Annals of Glaciology*, 13, 64-68.

Fischer, U. H., and Clarke, G. K. C. (1994). "Ploughing of subglacial sediment." *Journal of Glaciology*, 40(134), 97-106.

Fischer, U. H., Clarke, G. K. C., and Blatter, H. (1999). "Evidence for temporally-varying "sticky spots" at the base of Trapridge Glacier, Yukon Territory, Canada." *Journal of Glaciology*, 45(150), 352-360.

Fischer, U. H., Iverson, N. R., Hanson, B., Hooke, R. L., and Jansson, P. (1998). "Estimation of hydraulic properties of subglacial till from ploughmeter measurements." *Journal of Glaciology*, 44(148), 517-522.

Fountain, A. G. (1993). "Geometry and flow conditions of subglacial water at South Cascade Glacier, Washington State, U.S.A.; an analysis of tracer injections." *Journal of Glaciology*, 39(131), 143-156.

Fountain, A. G. (1994). "Borehole water-level variations and implications for the subglacial hydraulics of South Cascade Glacier, Washington State, U.S.A." *Journal of Glaciology*, 40(135), 293-304.

Fowler, A., and Walder, J. (1993). "Creep closure of channels in deforming subglacial till." *Proceedings of the The Royal Society, London, A*, 441, 7-31.

Fowler, A. C. (1987). "Sliding with cavity formation." *Journal of Glaciology*, 33(115), 255-267.

Freeze, R. A., and Cherry, J. A. (1979). *Groundwater*, Prentice-Hall, Englewood Cliffs, New Jersey.

Fröhlich, C. (1993). "Changes of total solar irradiance." *In Interactions between global climate subsystems: the Legacy of Hann*, G. A. McBean and M. Hantel, eds., American Geophysical Union, Washington DC, 123-129.

Gordon, S., Sharp, M., Hubbard, B., Smart, C., Ketterling, B., and Willis, I. (1998). "Seasonal reorganization of subglacial drainage inferred from measurements in boreholes." *Hydrological Processes*, 12, 105-133.

Gordon, S., Sharp, M., Hubbard, B., Willis, I., Smart, C., Copland, L., Harbor, J., and Ketterling, B. (2001). "Borehole drainage and its implications for the investigation of glacier hydrology: experiences from Haut Glacier d'Arolla, Switzerland." *Hydrological Processes*, 15(5), 797-813.

Grainger, M. E., and Lister, H. (1966). "Wind speed, stability and eddy viscosity over melting ice surfaces." *Journal of Glaciology*, 6(43), 101-127.

Gudmundsson, G. H., Bauder, A., Luthi, M., Fischer, U. H., and Funk, M. (1999). "Estimating rates of basal motion and internal ice deformation from continuous tilt measurements." *Annals of Glaciology*, 28, 247-252.

Gurnell, A. M. (1993). "How many reservoirs ? An analysis of flow recessions from a glacier basin." *Journal of Glaciology*, 39(132), 409-414.

Gurnell, A. M., Hodson, A., Clark, M. J., Bogen, J., Hagen, J. O., and Tranter, M. 1994; "Water and sediment discharge from glacier basins: an arctic and alpine comparison." *Variability in Stream Erosion and Sediment Transport*, Canberra Symposium , IAHS; 224; 325-334.

Haeberli, W., and Funk, M. (1991). "Borehole temperatures at the Colle Gnifetti core-drilling site (Monta-Rosa, Swiss-Alps)." *Journal of Glaciology*, 37(125), 37-46.

Haefeli, R. (1970). "Changes in the behaviour of the Unteraargletscher in the last 125 years." *Journal of Glaciology*, 9, 195-212.

Hallet, B. (1979). "Subglacial regelation water film." *Journal of Glaciology*, 23(89), 321-334.

Hallet, B., and Anderson, R. S. (1980). "Detailed glacial geomorphology of a proglacial bedrock area at Castlegurad Glacier, Alberta, Canada." *Zeitschrift für Gletscherkunde und Glazialgeologie*, 16, 171-184.

Hanson, B., Hooke, R. L., and Grace, E. M., Jr. (1998). "Short-term velocity and water-pressure variations down-glacier from a riegel, Storglaciären, Sweden." *Journal of Glaciology*, 44(147), 359-367.

Hantz, D., and Lliboutry, L. (1983). "Waterways, ice permeability at depth, and water pressures at glacier d'Argentière, French Alps." *Journal of Glaciology*, 29(102), 227-239.

Harbor, J., Sharp, M., Copland, L., Hubbard, B., Nienow, P., and Mair, D. (1997). "Influence of subglacial drainage conditions on the velocity distribution within a glacier cross section." *Geology*, 25(8), 739-742.

Harper, J. T., and Humphrey, N. F. (1995). "Borehole video analysis of a temperate glacier's englacial and subglacial structure: Implications for glacier flow models." *Geology*, 23(10), 901-904.

Harper, J. T., Humphrey, N. F., Pfeffer, W. T., Huzurbazar, S. V., Bahr, D. B., and Welch, B. C. (2001). "Spatial variability in the flow of a valley glacier: Deformation of a large array of boreholes." *Journal of Geophysical Research - Solid Earth*, 106(B5), 8547-8562.

Harrison, W. D., Echelmeyer, K. A., and Englehardt, H. (1993). "Short-period observations of speed, strain and seismicity on Ice Stream B, Antarctica." *Journal of Glaciology*, 39(133), 463-470.

Harrison, W. D., Raymond, C. F., and Mackeith, P. (1986). "Short period motion events on Variegated Glacier as observed by automatic photography and seismic methods." *Annals of Glaciology*, 8, 82-89.

Hay, J. E., and Fitzharris, B. B. (1988). "A comparison of the energy-balance and bulk-aerodynamic approaches for estimating glacier melt." *Journal of Glaciology*, 34(117), 145-153.

Hieltala, M. (1989). "*En utvärdering av areella nederbördsmetoder och mätarplaceringar i Tarfaladalen.*", Examensarbete, Stockholm Universitet. Naturgeografiska Institutionen, Stockholm.

Hock, R. (1998). "*Modelling of glacier melt and discharge.*" Ph.D thesis, ETH Zürich, Zürich.

Hock, R. (1999). "A distributed temperature-index ice- and snowmelt model including potential direct solar radiation." *Journal of Glaciology*, 45(149), 101-111.

Hock, R., and Holmgren, B. (1996). "Some aspects of energy balance and ablation of Storglaciären, Northern Sweden." *Geografiska Annaler*, 78 A(2-3), 121-131.

Hock, R., and Hooke, R. L. (1993). "Evolution of the internal drainage system in the lower part of the ablation area of Storglaciären, Sweden." *Geological Society of America Bulletin*, 105, 537-546.

Hock, R., Iken, A., and Wangler, A. (1999). "Tracer experiments and borehole observations in the over-deepening of Aletschgletscher, Switzerland." *Annals of Glaciology*, 28, 253-260.

Hock, R., and Noetzli, C. (1997). "Areal melt and discharge modelling of Storglaciären, Sweden." *Annals of Glaciology*, 24, 211-216.

Hodge, S. M. (1976). "Direct measurement of basal water pressures: a pilot study." *Journal of Glaciology*, 16(74), 205-218.

Hodge, S. M. (1979). "Direct measurement of basal water pressures: progress and problems." *Journal of Glaciology*, 23(89), 309-319.

Hodgkins, R. (1996). "Seasonal trend in suspended-sediment transport from an Arctic glacier, and implications for drainage-system structure." *Annals of Glaciology*, 22, 147-151.

Hodgkins, R., Hagen, J. O., and Hamran, S. E. (1999). "20th century mass balance and thermal regime change at Scott Turnerbreen, Svalbard." *Annals of Glaciology*, 28, 216-220.

Hodgkins, R., Tranter, M., and Dowdeswell, J. A. (1998). "The hydrochemistry of runoff from a 'cold based' glacier in the High Arctic (Scott Turnerbreen, Svalbard)." *Hydrological Processes*, 12(1), 87-103.

Hodson, A., Tranter, M., and Vatne, G. (2000). "Contemporary rates of chemical denudation and atmospheric $CO_2$ sequestration in glacier basins: An Arctic perspective." *Earth Surface Processes and Landforms*, 25(13), 1447-1471.

Hodson, A. J., and Ferguson, R. I. (1999). "Fluvial suspended sediment transport from cold and warm-based glaciers in Svalbard." *Earth Surface Processes and Landforms*, 24(11), 957-974.

Holmlund, P. (1988). "Internal geometry and evolution of moulins, Storglaciären, Sweden." *Journal of Glaciology*, 34(117), 242-248.

Hooke, R. L. (1984). "On the role of mechanical energy in maintaining subglacial water conduits at atmospheric pressure." *Journal of Glaciology*, 30(105), 180-187.

Hooke, R. L. (1989). "Englacial and subglacial hydrology: a qualitative review." *Arctic and Alpine Research*, 21(3), 221-233.

Hooke, R. L. (1998). *Principles of Glacier Mechanics*, Prentice Hall, New Jersey.

Hooke, R. L., Brzozowski, J., and Bronge, C. (1983). "Seasonal variations in surface velocity, Storglaciären, Sweden." *Geografiska Annaler*, 65 A, 263-277.

Hooke, R. L., Hanson, B., Iverson, N. R., Jansson, P., and Fischer, U. H. (1997). "Rheology of till beneath Storglaciären, Sweden." *Journal of Glaciology*, 43(143), 172-179.

Hooke, R. L., and Iverson, N. R. (1995). "Grain-size distribution in deforming subglacial tills: Role of grain fracture." *Geology*, 23(1), 57-60.

Hooke, R. L., Laumann, T., and Kohler, J. (1990). "Subglacial water pressures and the shape of subglacial conduits." *Journal of Glaciology*, 36(122), 67-71.

Hooke, R. L., Pohjola, V. A., Jansson, P., and Kohler, J. (1992). "Intraseasonal changes in deformation profiles revealed by borehole studies, Storglaciären, Sweden." *Journal of Glaciology*, 38(130), 348-358.

Huang, M. H., and Wang, Z. X. (1987). "Research on the tunnel excavated in Urumqi Glacier No. 1, Tianshan Glaciological Station, China." *Journal of Glaciology*, 33(113), 99-104.

Hubbard, B., Binley, A., Slater, L., Middleton, R., and Kulessa, B. (1998). "Inter-borehole electrical resistivity imaging of englacial drainage." *Journal of Glaciology*, 44(147), 429-434.

Hubbard, B., and Nienow, P. (1997). "Alpine subglacial hydrology." *Quaternary Science Reviews*, 16, 939-955.

Hubbard, B. P., Sharp, M. J., Willis, I. C., Nielsen, M. K., and Smart, C. C. (1995). "Borehole water-level variations and the structure of the subglacial hydrological system of Haut Glacier d'Arolla, Valais, Switzerland." *Journal of Glaciology*, 41(139), 572-583.

Humphrey, N., Raymond, C., and Harrison, W. (1986). "Discharges of turbid water during mini-surges of Variegated Glacier, Alaska, U.S.A." *Journal of Glaciology*, 32(111), 195-207.

Humphrey, N. F., and Raymond, C. F. (1994). "Hydrology, erosion and sediment production in a surging glacier: Variegated Glacier, Alaska, 1982-83." *Journal of Glaciology*, 40(136), 539-552.

Iken, A., and Bindschadler, R. A. (1986). "Combined measurements of subglacial water pressure and surface velocity of Findelengletscher, Switzerland: conclusions about drainage system and sliding mechanism." *Journal of Glaciology*, 32(110), 101-119.

Iken, A., Fabri, K., and Funk, M. (1996). "Water storage and subglacial drainage conditions inferred from borehole measurements on Gornergletscher, Valais, Switzerland." *Journal of Glaciology*, 42(141), 233-248.

Iken, A., Röthlisberger, H., Flotron, A., and Haeberli, W. (1983). "The uplift of Unteraagletscher at the beginning of the melt season - a consequence of water storage at the bed ?" *Journal of Glaciology*, 29(101), 28-47.

Iken, A., and Truffer, M. (1997). "The relationship between subglacial water pressure and velocity of Findelengletscher, Switzerland, during its advance and retreat." *Journal of Glaciology*, 43(144), 328-338.

Iverson, N. R., Baker, R. W., Hooke, R. L., Hanson, B., and Jansson, P. (1999). "Coupling between a glacier and a soft bed: I. A relation between effective pressure and local shear stress determined from till elasticity." *Journal of Glaciology*, 45(149), 31-40.

Iverson, N. R., Hanson, B., Hooke, R. L., and Jansson, P. (1995). "Flow mechanism of glaciers on soft beds." *Science*, 267(5194), 80-81.

Iverson, N. R., Jansson, P., and Hooke, R. L. (1994). "In-situ measurement of the strength of deforming subglacial till." *Journal of Glaciology*, 40(136), 497-503.

Jackson, M. (2000). "*Svartisen Subglacial Laboratory*." *Document 14*, Norwegian Water Resources and Energy Directorate.

Jania, J., Mochnacki, D., and Gadek, B. (1996). "The thermal structure of Hansbreen, a tidewater glacier in southern Spitsbergen, Svalbrd." *Polar Research*, 15(1), 53-66.

Jansson, P. (1995). "Water pressure and basal sliding on Storglaciären, northern Sweden." *Journal of Glaciology*, 41(138), 232-240.

Jones, D. P., Ricker, K. E., Desloges, J. R., and Maxwell, M. (1985). "*Glacier outburst flood on the Noeick River - the draining of Ape Lake, British Columbia, October 20, 1984*." *Open-File Report 1139*, Geological Survey of Canada.

Kamb, B. (1987). "Glacier Surge Mechanism Based on Linked Cavity Configuration of the Basal Water Conduit System." *Journal of Geophysical Research*, 92(B9), 9083-9100.

Kamb, B., Englehardt, H. F., and Harrison, W. D. (1979). "The ice-rock interface and basal sliding process as revealed by direct observation in bore holes and tunnels." *Journal of Glaciology*, 23(89), 416-419.

Kamb, B., Raymond, C. F., Harrison, W. D., Englehardt, H., Echelmeyer, K. A., Humphrey, N., Brugman, M. M., and Pfeffer, T. (1985). "Glacier Surge Mechanism: 1982-1983 Surge of Variegated Glacier, Alaska." *Science*, 227(4686), 469-479.

Kasser, P. (1973). "Influences of changes in the glacierized area on summer runoff in the Porte du Scex drainage basin of the Rhône." *IAHS*, 95, 219-225.

Kavanaugh, J. L., and Clarke, G. K. C. (2000). "Evidence for extreme pressure pulses in the subglacial water system." *Journal of Glaciology*, 46(153), 206-212.

Koerner, R. M., Fisher, D. A., and Parnandi, M. (1981). "Bore-hole video and photographic cameras." *Annals of Glaciology*, 2, 34-38.

Konzelmann, T., and Braithwaite, R. J. (1995). "Variations of ablation, albedo and energy balance at the margin of the Greenland ice sheet, Kronpins Christian Land, eastern north Greenland." *Journal of Glaciology*, 41(137), 174-182.

Krimmel, R. M., Tangborn, W. V., and Meier, M. F. 1973; "Water flow through a temperate glacier." *The Proceedings of the Role of Snow and Ice in Hydrology Symposium*, Banff , UNESCO-WMO-IAHS Publication 107; Vol 1; 401-416.

Kuhn, M. (1987). "Micro-meteorological conditions for snow melt." *Journal of Glaciology*, 33(113), 24-26.

Lamb, H. R., Tranter, M., Brown, G. H., Hubbard, B. P., Sharp, M. J., Gordon, S., Smart, C. C., Willis, I. C., and Nielsen, M. K. (1995). "The composition of subglacial meltwaters sampled from boreholes at the Haut Glacier d'Arolla, Switzerland." *IAHS*, 228, 395-403.

Lang, H. (1973). "Variations in the relation between glacier discharge and meteorological elements." *IAHS*, 95, 85-94.

Lang, H. (1985). "Höhenabhängigkeit der Niederschläge." *In Die Niederschlag in der Schweiz (Berträge zur Geologie der Schweiz - Hydrologie, no. 31)*, B. Sevruk, ed., Kummerly and Frey, Berne, 149-57.

Lawson, D. E. (1993). "*Glaciohydrologic and glaciohydraulic effects on runoff and sediment yield in glacierized basins.*" *93-2*, US Army Corps of Engineers, Cold regions Research and Engineering Laboratory, Hanover, New Hampshire.

Lecce, S. A. (1993). "Flow separation and diurnal variability in the hydrology of Conness Glacier, Sierra Nevada, California, U.S.A." *Journal of Glaciology*, 39(132), 216-222.

Lewkowicz, A. G. (1985). "Use of an ablatometer to measure short-term ablation of exposed ground ice." *Canadian Journal of Earth Sciences*, 22, 1767-1773.

Liestøl, O. (1967). "Storbreen Glacier in Jotunheimen, Norway." *Norsk Polarinstitutt, Skrifter*, 141, 1-63.

Linacre, E. (1992). *Climate data and resources: a reference and guide*, Routledge, London.

Linacre, E., and Geerts, B. (1997). *Climates and weather explained*, Routledge, London and New York.

Lliboutry, L. (1968). "General theory of subglacial cavitation and sliding of temperate glaciers." *Journal of Glaciology*, 7(49), 21-58.

Lliboutry, L. (1971). "Permeability, brine content and temperature of temperate ice." *Journal of Glaciology*, 10(58), 15-29.

Lliboutry, L. (1983). "Modifications to the theory of intraglacial waterways for the case of subglacial ones." *Journal of Glaciology*, 29(102), 216-226.

Lliboutry, L. (1987). "Realistic, Yet Simple Bottom Boundry Conditions for Glaciers and Ice Sheets." *Journal of Geophysical Research*, 92(B9), 9101-9109.

Lundquist, D. (1982). "Modelling runoff from a glacierized basin." *IAHS*, 138, 131-136.

Mader, M., and Kaser, G. (1994). "Application of a linear reservoir model to the discharge of a glacierized basin in the Silvretta mountains." *Zeitschrift für Gletscherkunde und Glazialgeologie*, 30, 125-140.

Meier, M., Lundstrom, S., Stone, D., Kamb, B., Engelhardt, H., Humphrey, N., Dunlap, W. W., Fahnestock, M., Krimmel, R. M., and Walters, R. (1994). "Mechanical and hydrologic basis for the rapid motion of a large tidewater glacier. 1. Observations." *Journal of Geophysical Research - Solid Earth*, 99(B8), 15219-15229.

Meier, M. F. (1965). "Glaciers and climate." *In The Quaternary of the United States*, H. E. Wright and D. G. Frey, eds., Princeton University Press, Princeton, NJ, 795-805.

Menzies, J. (1995). *Modern glacial environments. Processes, dynamics and sediments*, Butterworth Heinemann, Oxford.

Moeri, T., and Leibundgut, C. (1986). "Winter dye tracer experiments on the Findelengletscher (Canton Wallis, Switzerland)." *Zeitschrift für Gletscherkunde und Glazialgeologie*, 22, 33-41.

Moore, J. C., Palli, A., Ludwig, F., Blatter, H., Jania, J., Gadek, B., Glowacki, P., Mochnacki, D., and Isaksson, E. (1999). "High-resolution hydrothermal structure of Hansbree, Spitsbergen, mapped by ground-penetrating radar." *Journal of Glaciology*, 45(151), 524-532.

Morin, R. H., Descamps, G. E., and Cecil, L. D. (2000). "Acoustic televiewer logging in glacier boreholes." *Journal of Glaciology*, 46(155), 695-699.

Müller, F., and Iken, A. (1973). "Velocity fluctuations and water regime of Arctic valley glaciers." *IAHS*, 95(165-182).

Müller, H. (1985). "On the radiation budget in the Alps." *Journal of Climatology*, 5, 445-462.

Munro, D. S. (1989). "Surface roughness and bulk heat transfer on a glacier: comparison with eddy correlation." *Journal of Glaciology*, 35(121), 343-348.

Munro, D. S. (1990). "Comparison of melt energy computations and ablatometer measurements on melting ice and snow." *Arctic and Alpine Research*, 22(2), 153-162.

Murray, T. (1997). "Assessing the paradigm shift: deformable glacier beds." *Quaternary Science Reviews*, 16, 995-1016.

Murray, T., and Clarke, G. C. (1995). "Black-box modeling of the subglacial water system." *Journal of Geophysical Research*, 100(B7), 10231-10245.

Nash, J. E., and Sutcliffe, J. V. (1970). "River flow forecasting through conceptual models. Part 1. A discussion of principles." *Journal of Hydrology*, 10(3), 282-290.

Ng, F. S. L. (2000). "Coupled ice-till deformation near subglacial channels and cavities." *Journal of Glaciology*, 46(155), 580-598.

Nienow, P. 2001; "Supraglacial drainage processes on High Arctic Glaciers: implications for subglacial hydrology and glacier dynamics." *International Glaciological Society (British Branch)*, Cambridge , .

Nienow, P., Sharp, M., and Willis, I. (1996a). "Temporal switching between englacial and subglacial drainage pathways: dye tracer evidence from the Haut Glacier d'Arolla, Switzerland." *Geografiska Annaler*, 78A(1), 51-60.

Nienow, P. W., Sharp, M., and Willis, I. C. (1996b). "Velocity-discharge relationships derived from dye tracer experiments in glacial meltwaters: implications for subglacial flow conditions." *Hydrological Processes*, 10, 1411-1426.

Nye, J. F. (1952). "A method of calculating the thickness of ice sheets." *Nature*, 169, 529-530.

Nye, J. F. (1965). "The frequency response of glaciers." *Journal of Glaciology*, 5, 567-587.

Nye, J. F. (1973). "Water at the bed of a glacier." *IAHS*, 95, 189-194.

Nye, J. F., and Frank, F. C. (1973). "Hydrology of the intergranular veins in a temperate glacier." *IAHS*, 95, 157-161.

Odegard, R. S., Hamran, S. E., Bo, P. H., Etzelmuller, B., Vatne, G., and Sollid, J. L. (1992). "Thermal regime of a valley glacier, Erikbreen, northern Spitzbergen." *Polar Research*, 11(2), 69-79.

Oerlemans, J. (1989). "On the response of valley glaciers to climatic change." *In Glacier Fluctuations and Climatic Change*, J. Oerlemans, ed., Kluwer Academic Publishers, Dodrecht-Boston-London, 353-371.

Oerlemans, J., and Knap, W. H. (1998). "A 1 year record of global radiation and albedo in the ablation zone of Morteratschgletscher, Switzerland." *Journal of Glaciology*, 44(147), 231-238.

Oke, T. R. (1995). *Boundary layer climates*, Routledge, London.

Östling, M., and Hooke, R. L. (1986). "Water storage in Storglaciären, Kebnekaise, Sweden." *Geografiska Annaler*, 68A(4), 279-290.

Østrem, G. (1975). "Sediment transport in glacial meltwater streams." *In Glaciofluvial and Glaciolacustrine Sedimentation*, A. V. Jopling and B. C. McDonald, eds., Society of Economic Paleontologists and Mineralogists, Tulsa, Oklahoma, U.S.A., 101-122.

Østrem, G., and Brugman, M. (1991). "*Glacier mass balance measurements: a manual for fieldwork and office work.*" *4*, NHRI Science Report.

Pangallo, E. (1995). "Alluvione del 5-6 novembre 1994 in Italia NW: analisi meteorologica." *Nimbus*, 6-7, 13-21.

Parker, G. (1979). "Hydraulic geometry of active gravel rivers." *Journal of the Hydraulics Division, American Society of Civil Engineers*, 105(HY9), 1185-1201.

Paterson, W. S. B. (1994). *The physics of glaciers*, Pergamon, Oxford.

Pfeffer, W. T., Humphrey, N. F., Amadei, B., Harper, J., and Wegmann, J. (2000). "In situ stress tensor measured in an Alaskan glacier." *Annals of Glaciology*, 31, 229-235.

Pohjola, V. A. (1994). "TV-video observations of englacial voids in Storglaciären, Sweden." *Journal of Glaciology*, 40(135), 231-240.

Pohjola, V. J. (1993). "TV-video observations of bed and basal sliding on Storglaciären, Sweden." *Journal of Glaciology*, 39(131), 111-118.

Raiswell, R. (1984). "Chemical models of solute aquisition in glacial meltwaters." *Journal of Glaciology*, 30, 49-57.

Raymo, M. E., and Ruddiman, W. F. (1992). "Tectonic forcing of late Cenozoic climate." *Nature*, 359, 117-122.

Raymond, C. F. (1971). "Flow in a transverse section of Athabasca Glacier, Alberta, Canada." *Journal of Glaciology*, 10(58), 55-84.

Raymond, C. F., and Harrison, W. D. (1975). "Some observations on the behavior of the liquid and gas phases in temperate glacier ice." *Journal of Glaciology*, 14(71), 213-231.

Rebetez, M., Lugon, R., and Baeriswyl, P.-A. (1997). "Climatic change and debris flows in high mountain regions: the case study of the Ritigraben torrent (Swiss Alps)." *Climatic Change*, 36, 371-389.

Richards, K., Sharp, M., Arnold, N., Gurnell, A., Clark, M., Tranter, M., Nienow, P., Brown, G., Willis, I., and Lawson, W. (1996). "An integrated approach to modelling hydrology and water quality in glacierised catchments." *Hydrological Processes*, 10, 479-508.

Robinson, G. D. (1958). "Some observations from aircraft of surface albedo and the albedo and absorption of cloud." *Archiv für Meteorologie, Geophysik und Bioklimatologie*, Ser. B, 9(1), 28.

Rohrer, M. (1989). "Determination of the transition air temperature from snow to rain and intensity of precipitation." *In Precipitation Measurement*, B. Sevruk, ed., Swiss Federal Institute of Technology, Zurich, 475-483.

Röthlisberger, H. (1972). "Water pressure in intra- and subglacial channels." *Journal of Glaciology*, 11(62), 177-203.

Röthlisberger, H. 1996; "The Physics of Englacial and Subglacial Meltwater Drainage - Theory and Observations." *4th International Symposium on Glacier Caves and Crypkarst in Polar and High Mountain Regions*, Rudolfshütte, Saltzburg, Austria , 13-23.

Röthlisberger, H., Iken, A., and Spring, U. (1979). "Piezometric observations of water pressure at the bed of Swiss glaciers." *Journal of Glaciology*, 23(89), 429-430.

Röthlisberger, H., and Lang, H. (1987). "Glacial Hydrology." *In Glacio-fluvial Sediment Transfer*, A. M. Gurnell and M. J. Clark, eds., John Wiley and Sons Ltd., 207-284.

Rott, H. (1979). "Vergleichende Untersuchungen der Energiebilanz in Hochgebirge." *Arch. Met. Geophys. Biokl.*, A(28), 211-32.

Sauberer, F., and Dirmhirn, I. (1952). "Der Strahlungshaushalt horizontaler Gletscherflächen auf dem Hohen Sonnblick." *Geografiska Annaler*, 34((3-4)), 261.

Schweizer, J., and Iken, A. (1992). "The role of bed separation and friction in sliding over an undeformable bed." *Journal of Glaciology*, 38(128), 77-92.

Seaberg, S. Z., Seaberg, J. Z., Hooke, R. L., and Wiberg, D. (1988). "Character of the englacial and subglacial drainage system in the lower part of the ablation area of Storglaciären, Sweden, as revealed by dye-trace studies." *Journal of Glaciology*, 34(117), 217-227.

Seidov, D., Barron, E., and Haupt, B. J. (2001). "Meltwater and the global ocean conveyor: northern versus southern conenctions." *Global and Plantary Change*, 30, 257-270.

Sharp, M. 1996; "Weathering pathways in glacial environments: hydrological and lithological controls." *Proceedings of the Fourth International Symposium on the Geochemistry of the Earth's surface*, Ilkley , 652-655.

Sharp, M., Tranter, M., Brown, G. H., and Skidmore, M. (1995a). "Rates of chemical denudation and $CO_2$ drawdown in a glacier-covered alpine catchment." *Geology*, 23, 61-64.

Sharp, M., Brown, G. H., Tranter, M., Willis, I. C., and Hubbard, B. (1995b). "Comments on the use of chemically based mixing models in glacier hydrology." *Journal of Glaciology*, 41, 241-246.

Shoemaker, E. M. (1986). "Subglacial hydrology for an ice sheet resting on a deformable aquifer." *Journal of Glaciology*, 32(110), 20-30.

Shreve, R. L. (1972). "Movement of water in glaciers." *Journal of Glaciology*, 11(62), 205-214.

Singh, A. K. (1999). "An investigation of the thermal conductivity of snow." *Journal of Glaciology*, 45(150), 346-351.

Sivia, D. S. (1996). *Data analysis: a Bayesian tutorial*, Clarendon Press, Oxford.

Skidmore, M. L., and Sharp, M. J. (1999). "Drainage system behaviour of a High-arctic polythermal glacier." *Annals of Glaciology*, 28, 209-215.

Smart, C. C. (1996). "Statistical evaluation of glacier boreholes as indicators of basal drainage systems." *Hydrological Processes*, 10, 599-613.

Smart, C. C., and Ketterling, D. B. (1997). "A low-cost electrical conductivity profiler for glacier boreholes." *Journal of Glaciology*, 43(144), 365-369.

Stenborg, T. (1969). "Studies of the internal drainage of glaciers." *Geografiska Annaler*, 51A(1-2), 13-41.

Stone, D. B., and Clarke, G. K. C. (1993). "Estimation of subglacial hydraulic properties from induced changes in basal water pressure: a theoretical framework for borehole-response tests." *Journal of Glaciology*, 39(132), 327-340.

Stone, D. B., and Clarke, G. K. C. (1996). "*In situ* measurements of basal water quality and pressure as an indicator of the character of subglacial drainage systems." *Hydrological Processes*, 10, 615-628.

Stone, D. B., Clarke, G. K. C., and Blake, E. W. (1993). "Subglacial measurement of turbidity and electrical conductivity." *Journal of Glaciology*, 39(132), 415-420.

Stone, D. B., Clarke, G. K. C., and Ellis, R. G. (1997). "Inversion of borehole-response test data for estimation of subglacial hydraulic properties." *Journal of Glaciology*, 43(143), 103-113.

Sugden, D. E., and John, B. S. (1976). *Glaciers and Landscape*, Edward Arnold, London.

Süsstrunk, A. E. (1959). "*Rapport sur les sondages sismiques du Glacier de Findelen effectués en octobre 1959.*" , Grande Dixence S.A., Lausanne.

Tabony, R. C. (1985). "The variation of surface temperature with altitude." *The Meteorological Magazine*, 114, 37-48.

Tarboton, D. G., Chowdhury, T. G., and Jackson, T. H. (1995). "A spatially distributed energy balance snowmelt model." *IAHS*, 228, 141-155.

Tranter, M., Brown, G., Raiswell, R., Sharp, M., and Gurnell, A. (1993). "A conceptual model of solute aquisition by Alpine glacial meltwaters." *Journal of Glaciology*, 39, 573-581.

Tranter, M., Brown, G. H., Hodson, A. J., and Gurnell, A. M. (1996). "Hydrochemistry as an indicator of subglacial drainage system structure: a comparison of Alpine and sub-Polar environments." *Hydrological Processes*, 10, 541-556.

Tranter, M., and Raiswell, R. (1991). "The composition of the englacial and subglacial component in bulk meltwaters draining the Gornergletscher, Switzerland." *Journal of Glaciology*, 37(125), 59-66.

Tranter, M., Sharp, M. J., Brown, G. H., Willis, I. C., Hubbard, B. P., Nielsen, M. K., Smart, C. C., Gordon, S., Tulley, M., and Lamb, H. R. (1997). "Variability in the chemical composition of in situ subglacial meltwaters." *Hydrological Processes*, 11(1), 59-77.

Truffer, M., Harrison, W. D., and Echelmeyer, K. A. (2000). "Glacier motion dominated by processes deep in underlying till." *Journal of Glaciology*, 46(153), 213-221.

Truffer, M., Motyka, R. J., Harrison, W. D., Echelmeyer, K. A., Fisk, B., and Tulaczyk, S. (1999). "Subglacial drilling at Black Rapids Glacier, Alaska, USA: drilling method and sample descriptions." *Journal of Glaciology*, 45(151), 495-505.

Turpin, O. C. (1998). "*Development and testing of a glacier runoff model.*" Ph.D thesis, University of Sheffield.

Tweed, F. S., and Russell, A. J. (1999). "Controls on the formation and sudden drainage of glacier-impounded lakes: implications for jokulhlaup characterisitcs." *Progress in Physical Geography*, 23(1), 79-110.

Viessman, W., Jr, and Lewis, G. L. (1996). *Introduction to Hydrology*, Harper Collins (College Publishers).

Vivian, R. (1975). *Les Glaciers des Alpes Occidentales*, Allier, Grenoble.

Wächter, H.-P. (Unpublished). "*Radio-Echolotungen auf dem Findelengletscher. Versuchsanstalt für Wasserbau, Hydrologie und Glaziologie an der Eidgenössischen Technischen Hochschule (Zürich).*" .

Waddington, B. S., and Clarke, G. K. C. (1995). "Hydraulic properties of subglacial sediment determined from the mechanical response of water-filled boreholes." *Journal of Glaciology*, 41(137), 112-124.

Wadham, J. L., Hodson, A. J., Tranter, M., and Dowdeswell, J. A. (1998). "The hydrochemistry of meltwaters draining a polythermal-based, high Arctic glacier, south Svalbard: I. The ablation season." *Hydrological Processes*, 12(12), 1825-1849.

Walder, J., and Hallet, B. (1979). "Geometry of former subglacial water channels and cavities." *Journal of Glaciology*, 23(89), 335-346.

Walder, J. S. (1982). "Stability of sheet flow beneath temperate glaciers and implications for glacier surging." *Journal of Glaciology*, 28(99), 273-293.

Walder, J. S. (1986). "Hydraulics of subglacial cavities." *Journal of Glaciology*, 32(112), 439-445.

Walder, J. S., and Costa, J. E. (1996). "Outburst floods from glacier-dammed lakes: the effect of mode of drainage on flood magnitude." *Earth Surface Processes and Landforms*, 21, 701-723.

Walder, J. S., and Driedger, C. L. (1995). "Frequent outburst floods from South Tahoma Glacier, Mount Rainier, USA: relation to debris flows, meteorological origin and implications for subglacial hydrology." *Journal of Glaciology*, 41(137), 1-10.

Walder, J. S., and Fowler, A. (1994). "Channelized subglacial drainage over a deformable bed." *Journal of Glaciology*, 40(134), 3-15.

Wallen, C. C. (1948). "Glacial-meteorological investigations on the Harsa Glacier in Swedish Lappland 1942-48." *Geografiska Annaler*, 30, 451-672.

Warburton, J., and Fenn, C. R. (1994). "Unusual flood events from an Alpine glacier: observations and deductions on generating mechanisms." *Journal of Glaciology*, 40(134), 176-186.

Weertman, J. (1964). "The theory of glacier sliding." *Journal of Glaciology*, 5(39), 287-303.

Weertman, J. (1972). "General Theory of Water Flow at the Base of a Glacier or Ice Sheet." *Reviews of Geophysics and Space Physics*, 10(1), 287-333.

Willis, I. C. (1991). "*The hydrological context and geomorphological significance of glacier motion: Midtdalsbreen, Norway.*" Ph.D, University of Cambridge, Cambridge.

Willis, I. C. (1995). "Intra-annual variations in glacier motion: a review." *Progress in Physical Geography*, 19(1), 61-106.

Willis, I. C., Richards, K. S., and Sharp, M. J. (1996). "Links between proglacial stream suspended sediment dynamics, glacier hydrology and glacier motion at Midtdalsbreen, Norway." *Hydrological Processes*, 10(4), 629-648.

Willis, I. C., Sharp, M. J., and Richards, K. S. (1991/1992a). "Studies of the water balance of Midtdalsbreen, Hardangerjökulen, Norway. I. The calculation of surface water inputs from basic meteorological data." *Zeitschrift für Gletscherkunde und Glazialgeologie*, 27/28, 97-115.

Willis, I. C., Sharp, M. J., and Richards, K. S. (1991/1992b). "Studies of the water balance of Midtdalsbreen, Hardangerjökulen, Norway. II. Water storage and runoff prediction." *Zeitschrift für Gletscherkunde und Glazialgeologie*, 27/28, 117-138.

Zeller, J., and Röthlisberger, G. (1988). "Umwetterschaden in der Schweiz im Jahre 1987." *wasser Energie*, Luft(80), 29-42.

Zimmermann, M. (1990). "Debris flows 1987 in Switzerland: geomorphological and meteorological aspects." *IAHS*, 194, 387-393.

Zongtai, W. (1989). "Recent variations of glaciers and the influence of climate and glacier fluctuations on runoff in China." *IAHS*, 183, 45-52.

# 12 APPENDICES

## 12.1 Data processing

Audit trail for boreholes 99.10, 99.52 and 99.54 are as follows :

Data in logger from borehole 99.10 downloaded on 22/08/99



Term.com (from Campbell PC208W 2.3 Software)



Bo102208.dat

(Generic names for such files are Bo10####.dat indicating a borehole on array 10. Day and month of download fills the following four hashed digits)



Split.com (from Campbell PC208W 2.3 Software)



Bo100899.prn



Exported directly in to an Excel workbook using the text import wizard



Bore_join 10.xls

Once exported into the *.xls file the B, C and D columns (JD, hr:mm and water height above the transducer respectively) from the *.prn file are separated and joined alongside a deci-julian time series thus joining files from consecutive downloads. Total borehole depth, transducer depth from surface and height of water above the transducer enabled calculation of height of water in a hole.

A similar sequence was observed for boreholes 99.52 and 99.54. Data from both boreholes was downloaded on the same *.dat file which bore the generic name bo50####.dat indicating a borehole on array 50. Day and month of download fills the following four hashed digits. Once exported into the *.xls file columns containing JD, hr:mm and water height for each individual hole (column B for 99.52 and column C for 99.54) were isolated from *.prn files and joined alongside a deci-julian time series thus joining files from consecutive downloads.

Audit trail for boreholes 99.30 and 99.33 are as follows:

Data in logger from boreholes 99.30 and 99.33 downloaded on 20/08/99



Xtalk.exe
(Tinylog option)





Bo200899.dat

(Generic names for such files are Bo######.dat indicating a borehole on array 30. Day, month and year of download fills the following six hashed digits)



Manual addition of 9999 after the last data point recorded in each data channel in *.dat to act a marker in subsequent programs



Bo200899.999



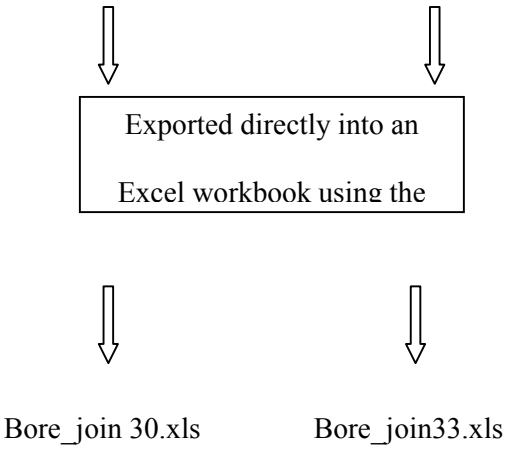
TLBORE99.bas (on *.999 before and including Bo290799.999) or TLBOR99B.bas (on *.999 after Bo290799.999)





Bo302008.pro Bo332008.pro

(Two separate files are created each showing deci-julian time, mA output and water height above transducer in columns A, B and C respectively)




Once exported into the *.xls file data is separated and joined alongside a deci-julian time series thus joining files from consecutive downloads. Total borehole depth, transducer depth from surface and height of water above the transducer enabled calculation of height of water in a hole.

## 12.2 Calibration of pressure transducers

Calibration of pressure transducers was carried out mathematically and then checked through testing in the field. Transducers used in boreholes 99.10, 99.33, 99.52 and 99.54 were manufactured by Gems Instruments to measure hydraulic head between the magnitude of 0-40m. In borehole 99.30 a vented Druck transducer measuring hydraulic head between 0-160m was used. Both types of transducer outputted current over a 4-20 mA range.

For boreholes 99.10, 99.52 and 99.54 calibration coefficients of Gems transducers were included within programs downloaded directly to Campbell CR10X and CR10 loggers. A 100 Ω resistor was included in each measuring circuit to create the following mathematical relationship allowing the output in current to be converted to a voltage output that can be detected by Campbell loggers.

Hydraulic head measurement range : 0 – 40 m
Transducer Output : 4 – 20 mA
Campbell logger measurement range : 0 – 2500 mV
Resistance in circuit : 100 Ω

At 0m of hydraulic head:

V = I * R
V = 0.004 * 100
V = 0.4 V or 400 mV

At 40m of hydraulic head:

V = I * R
V = 0.02 * 100
V = 2.0 V or 2000 mV

As there is a linear relationship between increase in hydraulic pressure and transducer output:

hydraulic head = M * mV output

$$M = \frac{\text{Range of hydraulic head}}{\text{Range of mV output}}$$

$$M = \frac{(40 - 0)}{(2000 - 400)}$$

M = 0.025

To calculate offset (c) substitute M into equation where hydraulic head is 40m and mV output is 2000 mV:

40 = 0.025 * 2000 + c
-10 = c

The linear relationship:

Hydraulic head (m) = 0.025 * mV output – 10

is incorporated in a Campbell downloading program in instruction lines five and six:

```
Volt (Diff) (P2)
; 1: 1       Reps
; 2: 5       2500 mV Slow Range
; 3: 1       DIFF Channel
; 4: 1       Loc [ _________ ]
; 5: 0.025    Mult
; 6: -10      Offset
```

In borehole 99.30 a Druck transducer measuring a hydraulic range of 0-160m was logged using a 4-20 mA Tinylog logger. Calibration was made during processing using code in Quickbasic programs Tlbor99b.bas and Tlbore99.bas that use a direct linear relationship of 1 mA = 10m.

In borehole 99.33 a Gems transducer measuring a hydraulic range of 0-40m was logged using a 4-20 mA Tinylog logger. Calibration was made during processing in similar Quickbasic programs that use a direct linear relationship of 1 mA = 2.5m.

It is essential that such mathematical relationships are corroborated by measurements in the field. Ideally all transducers should be calibrated in boreholes using logging equipment that will be permanently attached throughout the monitoring period. However, limitations exist in the form of number of available working loggers, computer battery power, proximity of boreholes that are filled with water to the surface, availability of borehole video to find water levels in boreholes that are not at the surface, available manpower, vulnerability of transducers to freezing into sides of boreholes and poor weather conditions. Consequently, one Gems (0-40m) transducer and one Druck (0-160m) transducer were calibrated using a Campbell CR10X and a Tinylog logger respectively. Although this does not give all permutations of transducer and logger types it does include an example of the use of each type, although not the combined set-up, of all measurement instruments.

Physical calibration was carried out by lowering a transducer down a series of known depths in a borehole that is filled to the surface with water. Use of a full borehole gave greater assurance of where the transducer was in relation to the water surface, something that was hard to achieve in other boreholes where water levels had to be found using borehole video. As distance below the surface water level increases so does the opportunity for false depth readings created by transducers snagging against the borehole sides, wire getting caught or tangled and wire stretching under strain of movement. Tinylog loggers were user friendly as they had a visual display giving an immediate actual output (not an average output) that related the position of hydraulic head, however, Campbell loggers needed to be connected to a laptop to produce a visual output at a designated monitoring interval (usually ten minutes). Calibration using a

transducer connected to a Campbell logger was, therefore, restricted by availability and battery power of the in situ laptop.

The range over which calibrations took place differed between loggers. As Tinylog loggers gave a visual output in mA (to one decimal place) it was convenient to lower the transducer so that a particular depth could be obtained for a known mA output. Campbell loggers produced an output in metres (due to mathematical conversion routines in its downloaded measurement programme) so a transducer could be lowered a known distance and compared directly to an output in similar measuring units. Distances that transducers were lowered were in the lower region of the measuring range to enable accurate measurements to be taken without danger of overburden pressures affecting the sensor, which may occur near the maximum end of the range.

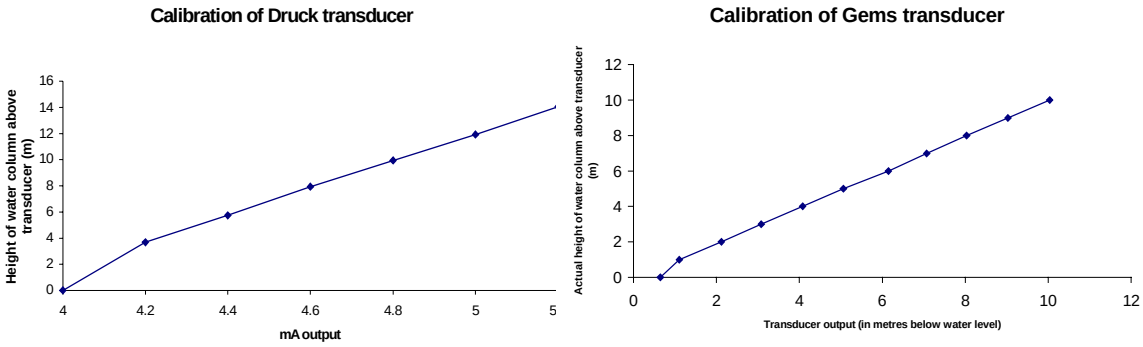



***Figure 12.1 - Field calibration of Druck and Gems TransInstument pressure transducers.***

Figure 12.1 shows calibration curves for both Gems and Druck transducers. Both show an excellent linear fit between sensor depth and logger output until depth measurements that approached zero, whereupon there was a slight deviation. The linear fit for the Gems and Druck transducers, excluding depth values approaching zero, are excellent giving $R^2$ values of 0.9999 and 0.9998 respectively. A regression line approximating Gems transducer data predicts a logger output of 0.126m when the transducer is at the water surface (0m below water level), which gives

an error of 1.26% over the calibration range and 0.31% if extrapolated to the whole 0-40m range. A regression line approximating Druck transducer predicts a transducer depth of 1.629m below water level at 4mA (i.e. when the logger should be out of the water), which gives an error of 11.23% over the 14.5m calibration range and 1.02% if extrapolated to the whole 0-160m range. Causes of error may occur in the elastic memory of the sensor and its deformation under very small pressures, resolution relative to the entire range (i.e. a change of 1m of the Druck transducer is only 0.625% of the total range), manual error in maintaining the transducer a set level in the calibration process and logger output error (minimal in a Campbell output at 5 significant figures but higher in a Tinylog where judgment of a change in boundary position between mA output to 1 decimal place on the visual display is done manually). Such absolute errors are relatively small when considered over the entire measurement range and are insignificant when data points are considered relative to one another.

In summary, as water levels in boreholes drop below that of transducers, output from Campbell loggers is not exactly zero and output from Tinylog loggers is not exactly 4.0 mA. Such differences are usually explainable, small and regular and have been treated as a relative zero point for each respective transducer. Slight changes in 'out of water' readings over a season can be produced by high over burden pressures causing changes in elastic memory of the sensor membrane. However, these are insignificant in terms of relative changes in borehole water level records over the monitoring period. During data management of borehole water level records, periods where transducers are deemed out of water have been removed manually. This was considered the most accurate method of quality control as each ‘out of water’ period could be individually assessed and the start and end points of descending and ascending limbs either side of 'out of water' periods could be identified as accurately as possible. Periods where water levels are far above measurement ranges the sensor is unable to measure change and produces a constant output. In a similar manner to ‘out of water’ periods these intervals were manually

removed from the record and note was taken that subsequent data may be influenced by damage caused to the sensor. Other than during extremes in the measurement ranges relationships between hydraulic head and logger output remained accurate and linear, allowing confidence in using mathematical conversions within Campbell download programmes and Tinylog processing programmes to convert raw data into the distance at which the water level is above the transducer.

### 12.3 Pressure sensor construction, operation and overburden

Change in borehole water levels above a submerged transducer are recorded by a piezoresistive sensor housed in a transducer (Figure 12.2). Piezoresistive sensors can take many physical forms, traditionally constructed from wire or foil ribbon adhesively bonded to a metal diaphragm, or more recently, a chemically milled boron and silicon wafer. However, the measurement principal is similar in that it reflects a change in resistance caused by an applied strain of the diaphragm. The diaphragm in a silicon wafer sensor is a homogenous single crystalline medium, implanted with piezoresistors that act in a similar manner to wire strain gauges, with important advantages. Within the designated measurement range silicon wafer sensors can measure higher sensitivities, of up to 100 times greater than wire strain gauges, at levels of accuracy equivalent to between ±1.5% and ±0.8% of the total error band, which combines parameters attributable to repeatable and non-repeatable errors, including static and thermal errors, linearity, hysteresis and repeatability under a range of operating conditions. This is achieved using silicon wafers as the actual sensing diaphragm, which does not suffer to the same degree from inherent instabilities and hysteresis (see Figure 12.3) caused by thermoelastic strain and the complex fabrication processes of traditionally constructed sensors bonded to dissimilar materials. Consequently, as silicon is a perfect crystal, it has extremely good elasticity within its operating range and returns to its original shape. As the pressure causes the thin silicon diaphragm to flex it induces a strain in the buried piezoresistors converting a change in mechanical input to a change in electrical output. The arrangement of piezoresistors are theoretically approximated by Figure 12.4 (where $R \pm \Delta R$ represent the actual resistor values at the applied pressure force). The signal voltage generated by the full Wheatstone bridge arrangement is, therefore, proportional to the amount of supply voltage and the amount of pressure applied, which generates the resistance change $\Delta R$.

When a sensor has been taken marginally outside its intended operating range and has exceeded the overburden pressure, the elastic memory of the silicon diaphragm may be affected, exhibiting permanent change over daily hysteresis cycles in borehole water levels. However, increasingly large measurement errors caused by successive periods of overburden pressure are more pronounced on older designs of transducers, whereas silicon diaphragms normally fail only by rupturing. Unlike a single wire or foil-ribbon sensor, progressive failure of the silicon-based sensor is less likely and may be tolerant to two or three times the designed overburden pressure before rupturing completely. Consequently, although the electrical output from the sensor at water levels above the intended measurement range will not be reliable, the sensor will not rupture and will produce reliable output when pressures return to within the intended operating range. Tolerance of the sensor to overburden pressures will depend on its contingency to the magnitude and frequency of high pressure events and the individual characteristics of the sensor.

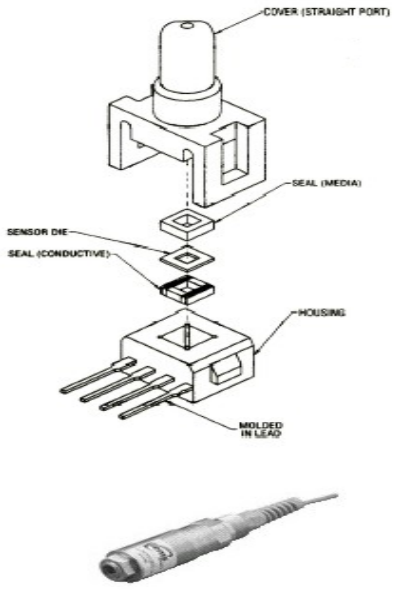



***Figure 12.2 – Exploded diagram of a pressure sensor (Honeywell) and a typical housing (Gems sensors).***

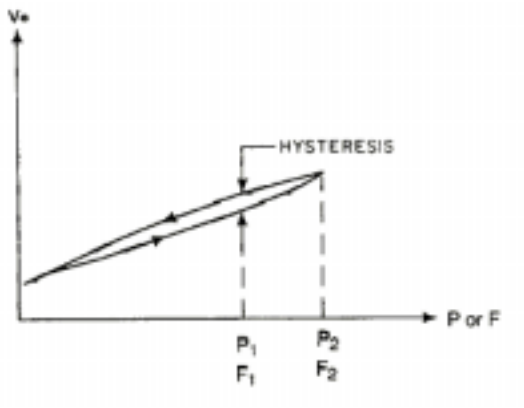



***Figure 12.3 – Hysteresis error (combined temperature and mechanical hysteresis).***

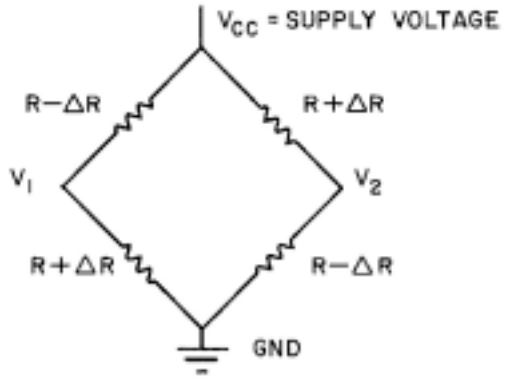



***Figure 12.4 – Full Wheatstone bridge arrangement of resistor connections***

### 12.4 Worked example of curve fitting

Reconstruction of missing data used a maximum of twenty observed data points either side of the period of missing data. They were linearly scaled to absolute values of between ±2.0 to limit computational error (Table 12.1). Confidence limits of the fit were obtained by comparing the mean of the distribution of noise between the observed data and the fitted curve with the students 't' distribution. The t-statistic at nineteen degrees of freedom at the 99% significance level is 2.539. Hence, there is a 99% probability that any data points lying within an area of 2.539 standard deviations above or below the curve are represented by the line. To calculate the maximum potential peak or trough values from the fitted regression curve, the first and last five observed data points of the twenty used to construct the curve, were lowered by the product of 2.539 and the standard deviation. The middle ten values were raised by the same amount (Figure 12.5). A regression curve was then fitted to this new data set to produce a curve of maximum possible values within a 99% confidence range (Figure 12.6). Minimum potential y values were calculated by raising the first and last five values by the same product and lowering the middle ten values. Differentiating the equations of the cubic curves and solving the resulting quadratic equation to find the relevant stationary point, enabled the identification of maximum and minimum points. On completion, the scaled x and y values, used to limit computational error in calculation of the equations of the curves, were re-scaled back to represent deci-julian time and borehole water levels respectively. The position of peak and trough values within the periods of missing data were located on the regression curve by differentiating the cubic regression equation, to become a quadratic equation and then solving this equation to find the stationary points. Missing data between the peak and trough values and observed data were approximated by re-scaled regression curves (Figure 12.7). To avoid discontinuities between observed and reconstructed data, interpolation using cubic spline curves through observed data and either the reconstructed peak or trough value (and its error) allowed a smooth transition. As a result, a

continuous visual interpretation of all points during periods of missing data including the magnitude and the timing of maximum and minimum points was created.

| X real | Y real | X scaled | Y scaled | Y fitted | Y scaled - Y fitted | (Y scaled - Y fitted)$^2$ |
|---|---|---|---|---|---|---|
| 251.486 | 81.465 | 0.486 | -0.213 | -0.170 | 0.044 | 0.0019 |
| 251.493 | 91.159 | 0.493 | 0.029 | 0.029 | 0.000 | 0.0000 |
| 251.500 | 95.904 | 0.500 | 0.148 | 0.211 | 0.063 | 0.0040 |
| 251.507 | 104.832 | 0.507 | 0.371 | 0.379 | 0.008 | 0.0001 |
| 251.514 | 114.508 | 0.514 | 0.613 | 0.536 | 0.077 | 0.0059 |
| 251.521 | 121.206 | 0.521 | 0.780 | 0.677 | 0.103 | 0.0106 |
| 251.528 | 124.309 | 0.528 | 0.858 | 0.808 | 0.050 | 0.0025 |
| 251.535 | 127.128 | 0.535 | 0.928 | 0.925 | 0.003 | 0.0000 |
| 251.542 | 129.939 | 0.542 | 0.998 | 1.032 | 0.033 | 0.0011 |
| 251.549 | 130.780 | 0.549 | 1.020 | 1.126 | 0.106 | 0.0113 |
| 251.764 | 118.211 | 0.764 | 0.705 | 0.744 | 0.038 | 0.0015 |
| 251.771 | 117.481 | 0.771 | 0.687 | 0.699 | 0.012 | 0.0002 |
| 251.778 | 116.472 | 0.778 | 0.662 | 0.657 | 0.005 | 0.0000 |
| 251.785 | 115.398 | 0.785 | 0.635 | 0.619 | 0.016 | 0.0003 |
| 251.792 | 114.331 | 0.792 | 0.608 | 0.583 | 0.025 | 0.0006 |
| 251.799 | 112.995 | 0.799 | 0.575 | 0.552 | 0.023 | 0.0005 |
| 251.806 | 111.632 | 0.806 | 0.541 | 0.525 | 0.016 | 0.0003 |
| 251.813 | 110.264 | 0.813 | 0.507 | 0.503 | 0.004 | 0.0000 |
| 251.819 | 108.895 | 0.819 | 0.472 | 0.486 | 0.014 | 0.0002 |
| 251.826 | 107.474 | 0.826 | 0.437 | 0.474 | 0.038 | 0.0014 |

***Table 12.1 - Values used in reconstruction of missing data.***

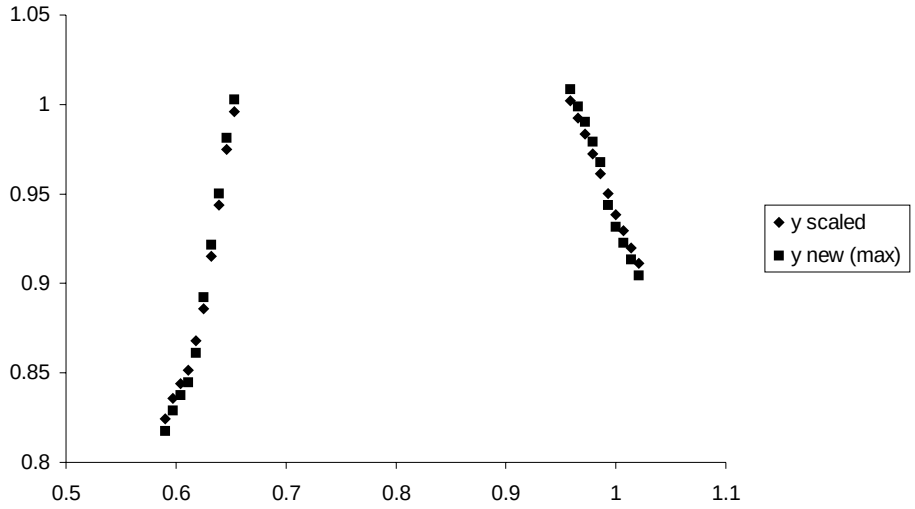



***Figure 12.5 - Original scaled data points and new data points raised and lowered to find maximum values from the curve within the 99% confidence limits.***

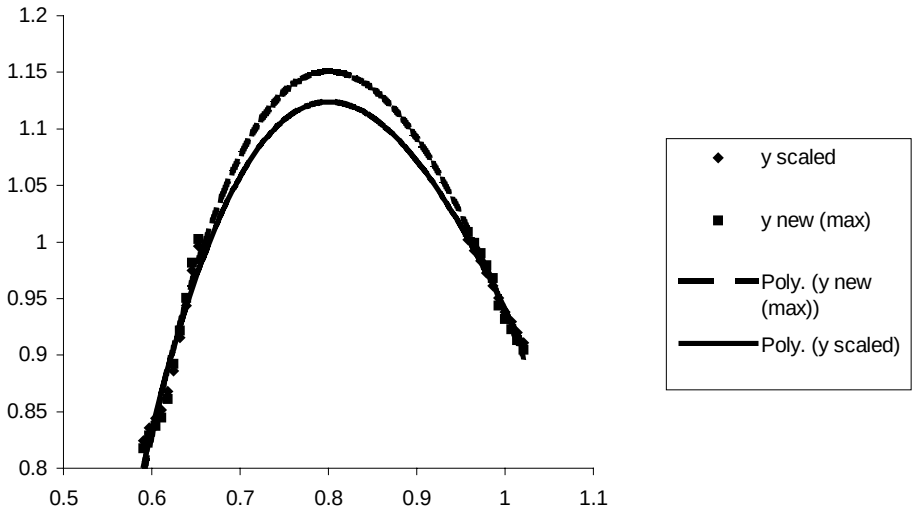



***Figure 12.6 - Regression curves through original scaled data points and data points lowered and raised to produce a curve of maximum possible values within a 99% confidence range.***

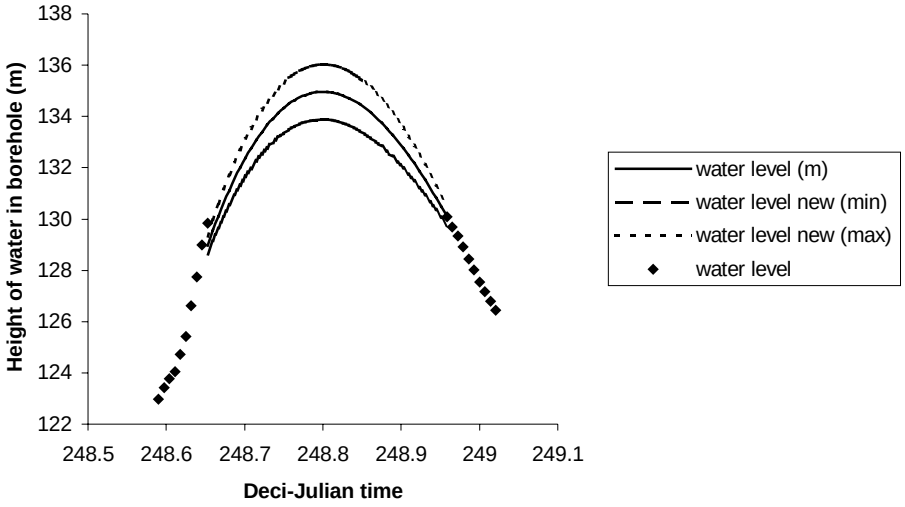



***Figure 12.7 - Observed data and re-scaled regression curves during periods of missing data.***

## 12.5 Borehole Summary - spot height measurements

U = W/L unknown
S = W/L at surface
E = W/L electronically monitored
Values indicate spot measurements

#1 = Possible very slow draining rate
#2 = Camera diameter too big to fit in hole
#3 = Surface water running into hole

| JD | Date | 99.10 | 99.11 | 99.12 | 99.13 | 99.14 | 99.15 | 99.16 |
|---|---|---|---|---|---|---|---|---|
| 168 | 17-Jun-99 | | | | | | | |
| 169 | 18-Jun-99 | | | | | | | |
| 170 | 19-Jun-99 | | | | | | | |
| 171 | 20-Jun-99 | | | | | | | |
| 172 | 21-Jun-99 | | | | | | | |
| 173 | 22-Jun-99 | | | | | | | |
| 174 | 23-Jun-99 | | | | | | | |
| 175 | 24-Jun-99 | | | | | | | |
| 176 | 25-Jun-99 | | | | | | | |
| 177 | 26-Jun-99 | | | | | | | |
| 178 | 27-Jun-99 | | | | | | | |
| 179 | 28-Jun-99 | | | | | | | |
| 180 | 29-Jun-99 | | | | | | | |
| 181 | 30-Jun-99 | | | | | | | |
| 182 | 01-Jul-99 | | | | | | | |
| 183 | 02-Jul-99 | | | | | | | |
| 184 | 03-Jul-99 | | | | | | | |
| 185 | 04-Jul-99 | | | | | | | |
| 186 | 05-Jul-99 | | | | | | | |
| 187 | 06-Jul-99 | | | | | | | |
| 188 | 07-Jul-99 | | | | | | | |
| 189 | 08-Jul-99 | | | | | | | |
| 190 | 09-Jul-99 | | | | | | | |
| 191 | 10-Jul-99 | | | | | | | |
| 192 | 11-Jul-99 | | | | | | | |
| 193 | 12-Jul-99 | | Drilled S | | | | | |
| 194 | 13-Jul-99 | | | | Drilled S | | Drilled S | |
| 195 | 14-Jul-99 | Drilled S | S | | S | | 15.5m | |
| 196 | 15-Jul-99 | | | | | | | |
| 197 | 16-Jul-99 | S | S | Drilled S | S | Drilled S | 21.0m | |
| 198 | 17-Jul-99 | | | | | | | |
| 199 | 18-Jul-99 | | | | | | | |
| 200 | 19-Jul-99 | | | | | | | |
| 201 | 20-Jul-99 | | | | | | | |
| 202 | 21-Jul-99 | | | | | | | Drilled #1 |
| 203 | 22-Jul-99 | | | | | | | |
| 204 | 23-Jul-99 | | | | | | | |
| 205 | 24-Jul-99 | 14.0m | S | S | S | S | 13.5m | 9.5m |
| 206 | 25-Jul-99 | | | | | | | |
| 207 | 26-Jul-99 | | | | | | | |
| 208 | 27-Jul-99 | | | | | | | |
| 209 | 28-Jul-99 | | | | | | | |

| JD | Date | 99.10 | 99.11 | 99.12 | 99.13 | 99.14 | 99.15 | 99.16 |
|---|---|---|---|---|---|---|---|---|
| 210 | 29-Jul-99 | 8.5m | S | S | S | S | 8.0m | 14.0m |
| 211 | 30-Jul-99 | | | | | | | |
| 212 | 31-Jul-99 | | | | | | | |
| 213 | 01-Aug-99 | | | | | | | |
| 214 | 02-Aug-99 | | | | | | | |
| 215 | 03-Aug-99 | | | | | | | |
| 216 | 04-Aug-99 | | | | | | | |
| 217 | 05-Aug-99 | 10.0m | 1.0m | S | S #3 | 7.5m | 7.0m | 11.5m |
| 218 | 06-Aug-99 | | | | | | | |
| 219 | 07-Aug-99 | | | | | | | |
| 220 | 08-Aug-99 | | | | | | | |
| 221 | 09-Aug-99 | | | | | | | |
| 222 | 10-Aug-99 | 16.0m | 5.0m | S | S | 15.0m | S | 11.0m |
| 223 | 11-Aug-99 | | | | | | | |
| 224 | 12-Aug-99 | | | | | | | |
| 225 | 13-Aug-99 | | | | | | | |
| 226 | 14-Aug-99 | | | | | | | |
| 227 | 15-Aug-99 | | | | | | | |
| 228 | 16-Aug-99 | | | | | | | |
| 229 | 17-Aug-99 | 27.5m E | 13.0m | S | S | S | S | 7.0m |
| 230 | 18-Aug-99 | 27.5m E | 11.5m | S | S | 0.5m | S | 5.5m |
| 231 | 19-Aug-99 | | | | | | | |
| 232 | 20-Aug-99 | | | | | | | |
| 233 | 21-Aug-99 | | | | | | | |
| 234 | 22-Aug-99 | | | | | | | |
| 235 | 23-Aug-99 | | | | | | | |
| 236 | 24-Aug-99 | | | | | | | |
| 237 | 25-Aug-99 | | | | | | | |
| 238 | 26-Aug-99 | | | | | | | |
| 239 | 27-Aug-99 | 9.5m E | 6.0m | | S | | S | 4.0m |
| 240 | 28-Aug-99 | | | | | | | |
| 241 | 29-Aug-99 | | | | | | | |
| 242 | 30-Aug-99 | | | | | | | |
| 243 | 31-Aug-99 | 6.0m E | S | | S | S | 3.0m | 10.0m |
| 244 | 01-Sep-99 | | | | | | | |
| 245 | 02-Sep-99 | | | | | | | |
| 246 | 03-Sep-99 | | | | | | | |
| 247 | 04-Sep-99 | | | | | | | |
| 248 | 05-Sep-99 | | | | | | | |
| 249 | 06-Sep-99 | | | | | | | |
| 250 | 07-Sep-99 | | | | | | | |
| 251 | 08-Sep-99 | | | | | | | |
| 252 | 09-Sep-99 | | | | | | | |
| 253 | 10-Sep-99 | | | | | | | |
| 254 | 11-Sep-99 | | | | | | | |
| 255 | 12-Sep-99 | | | | | | | |
| 256 | 13-Sep-99 | | | | | | | |
| 257 | 14-Sep-99 | | | | | | | |
| 258 | 15-Sep-99 | | | | | | | |
| 259 | 16-Sep-99 | E | U | S | U | S | U | U |
| 260 | 17-Sep-99 | | | | | | | |
| 261 | 18-Sep-99 | | | | | | | |
| 262 | 19-Sep-99 | | | | | | | |
| 263 | 20-Sep-99 | | | | | | | |

U = W/L unknown
S = W/L at surface
E = W/L electronically monitored
Values indicate spot measurements

#1 = Possible very slow draining rate
#2 = Camera diameter too big to fit in hole
#3 = Surface water running into hole

| JD | Date | 99.30 | 99.31 | 99.32 | 99.33 | 99.34 | 99.35 | 99.36 |
|---|---|---|---|---|---|---|---|---|
| 168 | 17-Jun-99 | | | | | | | |
| 169 | 18-Jun-99 | | | | | | | |
| 170 | 19-Jun-99 | | | | | | | |
| 171 | 20-Jun-99 | | | | | | | |
| 172 | 21-Jun-99 | | | | | | | |
| 173 | 22-Jun-99 | | | | | | | |
| 174 | 23-Jun-99 | | | | | | | |
| 175 | 24-Jun-99 | | | | | | | |
| 176 | 25-Jun-99 | | | | | | | |
| 177 | 26-Jun-99 | | | | | | | |
| 178 | 27-Jun-99 | | | | | | | |
| 179 | 28-Jun-99 | | | | | | | |
| 180 | 29-Jun-99 | | | | | | | |
| 181 | 30-Jun-99 | | | | | | | |
| 182 | 01-Jul-99 | | | | | | | |
| 183 | 02-Jul-99 | | | | | | | |
| 184 | 03-Jul-99 | | | | | | | |
| 185 | 04-Jul-99 | | | | | | | |
| 186 | 05-Jul-99 | Drilled S | | | | | | |
| 187 | 06-Jul-99 | | | | | | | |
| 188 | 07-Jul-99 | | | Drilled S | | Drilled S #1 | | |
| 189 | 08-Jul-99 | 1.5m #2 | | U | | U | | Drilled #1 |
| 190 | 09-Jul-99 | | | | | | | |
| 191 | 10-Jul-99 | | | | | | | |
| 192 | 11-Jul-99 | | | | Drilled U | | Drilled U | |
| 193 | 12-Jul-99 | 8.0m | 7.0m | 6.0m | 46.5m | 32.0m | 6.0m | 46.5m |
| 194 | 13-Jul-99 | | | | | | | |
| 195 | 14-Jul-99 | 38.5m | 38.5m | 6.0m | 51.5m | 7.0m | 4.0m | S |
| 196 | 15-Jul-99 | | | | | | | |
| 197 | 16-Jul-99 | 94.0m | 99.0m | 17.5m | 58.0m | 8.0m | 4.0m | S |
| 198 | 17-Jul-99 | E | | | | | | |
| 199 | 18-Jul-99 | | | | | | | |
| 200 | 19-Jul-99 | | | | | | | |
| 201 | 20-Jul-99 | | | | | | | |
| 202 | 21-Jul-99 | | | | | | | Drilled #1 |
| 203 | 22-Jul-99 | | | | | | | |
| 204 | 23-Jul-99 | E | 86.0m | U #2 | 60.0m | 48.0m | 3.5m | U #2 |
| 205 | 24-Jul-99 | | | | | | | |
| 206 | 25-Jul-99 | | | | | | | |
| 207 | 26-Jul-99 | | | | | | | |
| 208 | 27-Jul-99 | | | | | | | |
| 209 | 28-Jul-99 | | 89.0m | | 54.0m E | | | |

| JD | Date | 99.30 | 99.31 | 99.32 | 99.33 | 99.34 | 99.35 | 99.36 |
|---|---|---|---|---|---|---|---|---|
| 210 | 29-Jul-99 | 83.0m E | 86.0m | U #2 | E #2 | 26.0m | 5.0m | U #2 |
| 211 | 30-Jul-99 | | | | | | | |
| 212 | 31-Jul-99 | 94.0m E | U | U #2 | E #2 | 17.5m | 11.0m | U #2 |
| 213 | 01-Aug-99 | | | | | | | |
| 214 | 02-Aug-99 | | | | | | | |
| 215 | 03-Aug-99 | | | | | | | |
| 216 | 04-Aug-99 | | | | | | | |
| 217 | 05-Aug-99 | 93.5m E | U | U #2 | E #2 | 3.5m | 4.0m | U #2 |
| 218 | 06-Aug-99 | | | | | | | |
| 219 | 07-Aug-99 | | | | | | | |
| 220 | 08-Aug-99 | | | | | | | |
| 221 | 09-Aug-99 | | | | | | | |
| 222 | 10-Aug-99 | 76.0m E | U #2 | S #3 | E U #2 | 6.5m | 4.5m | U #2 |
| 223 | 11-Aug-99 | | | | | | | |
| 224 | 12-Aug-99 | | | | | | | |
| 225 | 13-Aug-99 | | | | | | | |
| 226 | 14-Aug-99 | | | | | | | |
| 227 | 15-Aug-99 | | | | | | | |
| 228 | 16-Aug-99 | | | | | | | |
| 229 | 17-Aug-99 | E U #2 | U #2 | S | E U #2 | 2.0m | 4.5m | U #2 |
| 230 | 18-Aug-99 | E U #2 | U #2 | S | E U #2 | 4.0m | 4.5m | U #2 |
| 231 | 19-Aug-99 | | | | | | | |
| 232 | 20-Aug-99 | | | | | | | |
| 233 | 21-Aug-99 | | | | | | | |
| 234 | 22-Aug-99 | | | | | | | |
| 235 | 23-Aug-99 | | | | | | | |
| 236 | 24-Aug-99 | | | | | | | |
| 237 | 25-Aug-99 | | | | | | | |
| 238 | 26-Aug-99 | | | | | | | |
| 239 | 27-Aug-99 | 32.0m E | 32.0m | S | E U #2 | 2.5m | 18.5m | U #3 |
| 240 | 28-Aug-99 | | | | | | | |
| 241 | 29-Aug-99 | | | | | | | |
| 242 | 30-Aug-99 | | | | | | | |
| 243 | 31-Aug-99 | E U #2 | U #2 | S | E U #2 | 2.0m | 4.0m | U #2 #3 |
| 244 | 01-Sep-99 | | | | | | | |
| 245 | 02-Sep-99 | | | | | | | |
| 246 | 03-Sep-99 | | | | | | | |
| 247 | 04-Sep-99 | | | | | | | |
| 248 | 05-Sep-99 | | | | | | | |
| 249 | 06-Sep-99 | | | | | | | |
| 250 | 07-Sep-99 | | | | | | | |
| 251 | 08-Sep-99 | | | | | | | |
| 252 | 09-Sep-99 | | | | | | | |
| 253 | 10-Sep-99 | | | | | | | |
| 254 | 11-Sep-99 | | | | | | | |
| 255 | 12-Sep-99 | | | | | | | |
| 256 | 13-Sep-99 | | | | | | | |
| 257 | 14-Sep-99 | | | | | | | |
| 258 | 15-Sep-99 | | | | | | | |
| 259 | 16-Sep-99 | U #3 | U | Closed | U | U | U | U |
| 260 | 17-Sep-99 | | | | | | | |
| 261 | 18-Sep-99 | | | | | | | |
| 262 | 19-Sep-99 | | | | | | | |
| 263 | 20-Sep-99 | | | | | | | |

U = W/L unknown
S = W/L at surface
E = W/L electronically monitored
Values indicate spot measurements

#1 = Possible very slow draining rate
#2 = Camera diameter too big to fit in hole
#3 = Surface water running into hole

| JD | Date | 99.50 | 99.51 | 99.52 | 99.53 | 99.54 | 99.55 | 99.56 |
|---|---|---|---|---|---|---|---|---|
| 168 | 17-Jun-99 | | | | | | | |
| 169 | 18-Jun-99 | | | | | | | |
| 170 | 19-Jun-99 | | | | | | | |
| 171 | 20-Jun-99 | | | | | | | |
| 172 | 21-Jun-99 | | | | | | | |
| 173 | 22-Jun-99 | | | | | | | |
| 174 | 23-Jun-99 | | | | | | | |
| 175 | 24-Jun-99 | | | | | | | |
| 176 | 25-Jun-99 | | | | | | | |
| 177 | 26-Jun-99 | | | | | | | |
| 178 | 27-Jun-99 | | | | | | | |
| 179 | 28-Jun-99 | | | | | | | |
| 180 | 29-Jun-99 | Drilled S | Drilled U | | | | | |
| 181 | 30-Jun-99 | S | U | | Drilled S | | Drilled U | |
| 182 | 01-Jul-99 | | | | | | | |
| 183 | 02-Jul-99 | S | 67.5m | | S | | 11.0m | |
| 184 | 03-Jul-99 | | | Drilled #1 | | | | |
| 185 | 04-Jul-99 | | | U | | Drilled #1 | | Drilled #1 |
| 186 | 05-Jul-99 | | | | | | | |
| 187 | 06-Jul-99 | | | | | | | |
| 188 | 07-Jul-99 | | | | | | | |
| 189 | 08-Jul-99 | S | U | U | S | U | U | U |
| 190 | 09-Jul-99 | | | | | | | |
| 191 | 10-Jul-99 | | | | | | | |
| 192 | 11-Jul-99 | | | | | | | |
| 193 | 12-Jul-99 | S | 64.0m | 37.0m | S | S | 10.5m | 22.0m |
| 194 | 13-Jul-99 | | | | | | | |
| 195 | 14-Jul-99 | S | 64.0m | 37.0m | S | S | 11.0m | U #2 |
| 196 | 15-Jul-99 | | | | | | | |
| 197 | 16-Jul-99 | S | 58.5m | 36.5m | S | S | 11.0m | S |
| 198 | 17-Jul-99 | | | | | | | |
| 199 | 18-Jul-99 | | | | | | | |
| 200 | 19-Jul-99 | | | | | | | |
| 201 | 20-Jul-99 | | | | | | | |
| 202 | 21-Jul-99 | | | | | | | |
| 203 | 22-Jul-99 | | | | | | | |
| 204 | 23-Jul-99 | | | | | | | |
| 205 | 24-Jul-99 | S | 15.5m | 32.0m | 2.0m | 31.0m | U #2 | S |
| 206 | 25-Jul-99 | | | | | | | |
| 207 | 26-Jul-99 | | | | | | | |
| 208 | 27-Jul-99 | S | 1.5m | 24.0m E | U | 90.0m E | U #2 | |
| 209 | 28-Jul-99 | | | | | | | |

| JD | Date | 99.50 | 99.51 | 99.52 | 99.53 | 99.54 | 99.55 | 99.56 |
|---|---|---|---|---|---|---|---|---|
| 210 | 29-Jul-99 | S | S | E #2 | 6.5m | 40m E | U #2 | S |
| 211 | 30-Jul-99 | | | E S #3 | | E S | | |
| 212 | 31-Jul-99 | S | S | E #3 | S | E S #3 | U #2 | S |
| 213 | 01-Aug-99 | | | | | 140.0m E | | |
| 214 | 02-Aug-99 | | | | | | | |
| 215 | 03-Aug-99 | | | | | | | |
| 216 | 04-Aug-99 | | | | | | | |
| 217 | 05-Aug-99 | 1.0m | S | S | S | S #3 | U #2 | Closed |
| 218 | 06-Aug-99 | | | | | | | |
| 219 | 07-Aug-99 | | | | | | | |
| 220 | 08-Aug-99 | U | S | E S | S | E U #2 | U #2 | Closed |
| 221 | 09-Aug-99 | | | | | | | |
| 222 | 10-Aug-99 | U | S | E S | S | E U #2 | U #2 | Closed |
| 223 | 11-Aug-99 | | | | | | | |
| 224 | 12-Aug-99 | | | | | | | |
| 225 | 13-Aug-99 | | | | | | | |
| 226 | 14-Aug-99 | | | | | | | |
| 227 | 15-Aug-99 | | | | | | | |
| 228 | 16-Aug-99 | | | | | | | |
| 229 | 17-Aug-99 | S | S | E S | S | E U #2 | | Closed |
| 230 | 18-Aug-99 | | | | | | | |
| 231 | 19-Aug-99 | S | S | E S #3 | S | E U #2 | U #2 | Closed |
| 232 | 20-Aug-99 | | | | | | | |
| 233 | 21-Aug-99 | | | | | | | |
| 234 | 22-Aug-99 | | | | | | | |
| 235 | 23-Aug-99 | | | | | | | |
| 236 | 24-Aug-99 | | | E S #3 | | E S | | |
| 237 | 25-Aug-99 | S | S | S | S | S | U #2 | Closed |
| 238 | 26-Aug-99 | | | | | | | |
| 239 | 27-Aug-99 | | | | | | | |
| 240 | 28-Aug-99 | | | | | | | |
| 241 | 29-Aug-99 | | | | | | | |
| 242 | 30-Aug-99 | | | | | | | |
| 243 | 31-Aug-99 | S | S | S | S | S | U #2 | Closed |
| 244 | 01-Sep-99 | | | | | | | |
| 245 | 02-Sep-99 | | | | | | | |
| 246 | 03-Sep-99 | | | | | | | |
| 247 | 04-Sep-99 | | | | | | | |
| 248 | 05-Sep-99 | | | | | | | |
| 249 | 06-Sep-99 | | | | | | | |
| 250 | 07-Sep-99 | | | | | | | |
| 251 | 08-Sep-99 | | | | | | | |
| 252 | 09-Sep-99 | | | | | | | |
| 253 | 10-Sep-99 | | | | | | | |
| 254 | 11-Sep-99 | | | | | | | |
| 255 | 12-Sep-99 | | | | | | | |
| 256 | 13-Sep-99 | | | | | | | |
| 257 | 14-Sep-99 | | | | | | | |
| 258 | 15-Sep-99 | | | | | | | |
| 259 | 16-Sep-99 | U | S | Closed | S | Closed | U #2 | Closed |
| 260 | 17-Sep-99 | | | | | | | |
| 261 | 18-Sep-99 | | | | | | | |
| 262 | 19-Sep-99 | | | | | | | |
| 263 | 20-Sep-99 | | | | | | | |

## 12.6 Drilling Record

| JD | Date | Hole No. | Information |
|---|---|---|---|
| 179 | 28-Jun-99 | 99.50 | Start drilling @ 13:27. Drill stopped descending 20:10 - left for 1hr. 20:30 drilled dropped 1.5m suddenly under own weight. Stopped 20:35. |
| 180 | 29-Jun-99 | 99.50 | Start drilling @ 13:00. Drill reached previous night's position - feels light and only gets heavy when pulled up to mark where it was thought to stop initially. Unconnected. Depth 183.0m |
| 180 | 29-Jun-99 | 99.51 | Start drilling 15:55. @ 60m lots of bubbles. Stopped 18:25. Connected. Depth 132.0m |
| 180 | 29-Jun-99 | 99.53 | Started drilliing 19:05, stopped 19:50 - 67m down. |
| 181 | 30-Jun-99 | 99.53 | Moved drill sled nearer the hole. Start drilling 13:15. 14:05 drill stopped descending. Stopped drilling 15:00. Unconnected. Depth 113.0m |
| 181 | 30-Jun-99 | 99.55 | Drilling started @ 15:20. Connection after ~5m - area heavily crevassed / faulted in SW direction. ~20m down ice mass moved (Increased water pressure reduced friction allowing englacial movement ?) 16:31 drill appears to stop dropping @ ~97m. 17:00 drilling stopped. Connected - likely to be englacial - Depth 98.0m. |
| 184 | 03-Jul-99 | 99.52 | Start Drilling @ 14:40. Drill stopped descending @ 17:20. Stopped @18:30. Possibility it's draining at a slower rate than input from hose. Once drilling ended lots of bubbles and v. gradual drop in water level. Depth 145.0m |
| 185 | 04-Jul-99 | 99.54 | Start @ 11:29. Stopped descending @13:40. Stopped drilling @ 14:20. Uncertainty over whether or not connected as drain rate is v.v. slow, if at all. Depth 144.5m |
| 185 | 04-Jul-99 | 99.56 | Start drilling @ 15:10. Drill stopped descending 17:15 - left running till 18:00 no change and unconnected (cause of water drop was the drill displacing water). Depth 11.5m |
| 186 | 05-Jul-99 | 99.30 | Start 15:06. @ ~73m water drained away from hole but refilled within 3 mins. 17:15 drill stopped descending. Left to run until 18:15 - it had descended but was very difficult to judge where slack had been taken up (joined with remnants of 98.30 ?) Depth 132.5m *see later* |
| 187 | 06-Jul-99 | 99.32 | Start 17:14. Stopped 18:39 ~105m |
| 188 | 07-Jul-99 | 99.32 | Start 14:00 , drill stopped descending 14:45, finally stopped @15:45, unconnected. Depth 161.0m |
| 188 | 07-Jul-99 | 99.34 | Start 16:20. Stopped descending 18:30, stopped drilling @ 19:15. Once stopped water level started to drop at a very slow rate. Depth 150.5m |
| 189 | 08-Jul-99 | 99.36 | Start 13:25. Drained and quickly refilled @ ~37.5m. Drill stopped descending ~ 15:20, stopped @ 16:10. Uncertainty whether or not it's draining. Depth 136.0m |
| 189 | 36349 | 99.30 (RE-DRILL) | Started around 140 -145m water coming to surface was dirty. Still no obvious connection. Depth 149.m |

| JD | Date | Hole No. | Information |
|---|---|---|---|
| 190 | 09-Jul-99 | 99.31 | Start 13:00. Stopped descending @ 15:00, stopped drilling @ 15:47. Water exiting hole is highly turbid and milky (like water from 99.30). Depth 139.0m |
| 192 | 11-Jul-99 | 99.33 | Start 13:34. ~ 122.5m water drained quickly. Water pumped down for 10mins and stopped @ 15:10. Connected. Depth 124.0m |
| 192 | 11-Jul-99 | 99.35 | Start 16:10. @ ~8m connected englacially near fracture lines in the ice. 17:50 drill seems to stop descending. Borehole keeps accepting hose - maybe it has connected with a fissure and is running along it? Hose down > 150m but taught at ~107.5m. Depth 106.0m |
| 193 | 12-Jul-99 | 99.11 | Start 15:45, drill stopped descending @ 18:00 - left running till 18:50. Unconnected. Depth 133.5m |
| 194 | 13-Jul-99 | 99.13 | Start 13:55. @ ~1.5m water filled an englacial hole. @ ~5m pressure forced a local ice movement. ~16:00 drill not descending, drilling stopped ~17:00. Depth 121.0m |
| 194 | 13-Jul-99 | 99.15 | Start 17:13. 18:15 drill not descending. 18:50 stopped drilling. Unconnected. Depth 98.0m |
| 195 | 14-Jul-99 | 99.10 | Start 14:20. Stopped descending 16:45, stopped drilling 17:14. Unconnected. Depth 133.0m |
| 195 | 14-Jul-99 | 99.12 | Start 18:28, stopped 19:55 restart tomorrow. |
| 196 | 15-Jul-99 | 99.12 | Re-start 15:30. Stopped ~14:45. Unconnected. Depth 134.0m |
| 196 | 15-Jul-99 | 99.14 | Started 15:10. Unknown when stopped. Unconnected. Depth 150.m |
| 202 | 21-Jul-99 | 99.16 | Start 14:56. Drill stopped descending 16:30. Stopped 17:30. May have v.v. slow drain rate - uncertainty whether connected. Depth 136.5m |

## 12.7 Surface runoff model computer code (FORTRAN 90)

```
! program to evaluate combined hourly volumes of melt and precipitation
runoff from a glacierised catchment - with data set to calculate ranges

! Nick Rutter 28/02/01


program melt


! declare the variables and parameters

implicit none

real, dimension(1104) :: djd1, SiteMeasuredISR, djd2, Temp,
SitePotentialISR, SolarElev, d, Zenith, H, Tls, Tt

real, dimension(1104) :: SimMelt, MeasuredQ, LnMeasuredQ,
SumLnMeasuredQ, Num1, Num2, Denom1, Denom2

real, dimension(1104) :: Met2CosAzimuths, Met2CosTheta,
Met2CosAzimuthAngle, Met2SinAzimuthAngle

real, dimension(1104) :: CountMeasuredQ, Counter, B, EofT, TSL, djd3,
djd4, ppt, Runoff

integer, dimension(1104) :: Year, JD, Nm, Equinox

real, dimension(16) :: Angle, Elev, Pres, AreaTot, AreaGlac,
PressureCell, heightKM

real, dimension(1104,16) :: CellTemp, TotMelt, MeltRate, PotentialISR,
CosAzimuthAngle, CosAzimuths, CosTheta, SinAzimuthAngle, Ppt1

real, dimension(1104,16) :: CellStatus, RadCoef, TotPpt, CellStatus2

real, Parameter :: PressureSea = 1013, SolarCon = 1368, Transmissivity =
0.75, n = 24, MeltFactor = 3.35

real, Parameter :: Lat = 46.006, Long = 7.821, Aspect = 270.0, TLR =
0.6, ElevMet1 = 2530.0, ElevMet2 = 2740.0

real, Parameter :: snow = 0.0000195, ice = 0.00007, pi = 3.141593,
AngMet2 = 5.0, dtr = (3.141593/180), zero =0

integer, Parameter :: StandLong = 0

integer :: temperature_unit=11, cell_parameter=13, radiation_unit=14,
TotalMelt_unit1=17, TotalMelt_unit2=15

integer :: sim_melt = 16, measured_Q = 12, tsl_unit=18, ppt_unit = 19,
ppt_unit2=20, tot_runoff=21
```

```
real Met2heightKM, Met2pressureCell, TotNum1, TotNum2, TotDenom1,
TotDenom2, AveQ, Rsquared, Rlnsquared

real AveMelt, Num3, Denom3, Rsquared2

integer I, J


! Routine to open the data files and work out surface runoff due to melt
over the whole glacierised catchment

open (UNIT = radiation_unit,
FILE='/nimbus/pg/nrutter/Fort/test_data/sensitivity_trials/range_rad99.t
xt', STATUS='OLD')

open (UNIT = temperature_unit,
FILE='/nimbus/pg/nrutter/Fort/test_data/sensitivity_trials/range_temp99.
txt', STATUS='OLD')

open (UNIT = cell_parameter, FILE='/nimbus/pg/nrutter/Fort/cell99.txt',
STATUS='OLD')

open (UNIT = tsl_unit,
FILE='/nimbus/pg/nrutter/Fort/test_data/sensitivity_trials/range_tsl99.t
xt', STATUS='OLD')

open (UNIT = ppt_unit,
FILE='/nimbus/pg/nrutter/Fort/test_data/sensitivity_trials/range_rain99.
txt', STATUS='OLD')

! Retrive cell parameters

Do J=1,16

    read (cell_parameter,*) Elev(J), Angle(J), AreaTot(J), AreaGlac(J)

EndDo


! Retrieve array variables

Do I=1,1104

      read (radiation_unit,*) Year(I), djd1(I), SiteMeasuredISR(I)

      read (temperature_unit,*) djd2(I), Temp(I)

      read (tsl_unit,*) djd3(I), TSL(I)

      read (ppt_unit,*) djd4(I), ppt(I)


EndDO


! Seta any values of ISR that are negative (i.e. due to resolution and
accuracy of the radiometer)to zero
```

```
Where (SiteMeasuredISR <= (0.0))
   SiteMeasuredISR = 0
EndWhere

! Establish the correct radiation coefficient (snow or ice) for the cell
depending on the location of the TSL
Do I=1,1104
Do J=1,16
CellStatus(I,J) = TSL(I) - Elev(J)
Enddo
Enddo

Where (CellStatus <= 0)
      RadCoef = snow
Elsewhere
      RadCoef = ice
Endwhere

! Calculation of atmospheric pressure above the cell
heightKM = (Elev/1000)
PressureCell = 1013 * 10**(-0.12 * heightKM)

! Work out the JD from the djd value
JD = Floor(djd1)

! Work out the value of Nm
Where (MOD(Year, 4) == 0)
   Equinox = 81
Elsewhere
   Equinox = 80
Endwhere
```

```
Where (JD >= Equinox)

   Nm = JD - Equinox

Elsewhere

   Nm = 285 + JD

Endwhere


! Work out the declination, solar elevation and zenith angles

d = 23.45 * Sin(0.986*Nm*dtr)

SolarElev = 90 - Lat + d

Zenith = 90 - SolarElev


! Calculate the equation of time (by approximation)

B = 360 * (JD - Equinox) / 365

EofT = 9.87*sin(2*B*dtr) - 7.53*cos(B*dtr) - 1.5*sin(B*dtr)


! Calculation of the Local clock time (in decimal hours) including
subtratction of one hour daylight saving time (N.B. as the timing of
start and end of daylight saving time are controlled by law this part of
the program must be changed by hand and not automatically)

Tls = (djd1 - JD - 1/24)*24


! As longitude is east the time-difference between the standard
longitude and actual longitude of the place is negative (i.e. multiply
by -1.0).  Standard Longitude is the longitude at the beginning of the
zone (i.e. 0 degrees for Findelengletscher, which is at 7 degrees East)

Tt = Tls - ((-1.0) *((Long - StandLong)/15)) + (EofT/60)

H = (Tt - 12) * 15


! Calculation of the Cos(theta) component i.e. the effect of the sun's
position in the sky

Do I=1,1104

Do J=1,16

CosAzimuthAngle(I,J) = (Sin(Angle(J)*dtr) - Sin(Lat*dtr) *
Sin(SolarElev(I)*dtr)) / Cos(Lat*dtr) * Cos(SolarElev(I)*dtr)

SinAzimuthAngle(I,J) = -cos(d(I)*dtr) * Sin(H(I)*dtr) /
Cos(SolarElev(I)*dtr)
```

```
CosAzimuths(I,J) = Cos(Aspect*dtr) * CosAzimuthAngle(I,J) -
Sin(Aspect*dtr) * SinAzimuthAngle(I,J)

CosTheta(I,J) = Cos(Angle(J)*dtr) * Sin(SolarElev(I)*dtr) +
Sin(Angle(J)*dtr) * Cos(SolarElev(I)*dtr) * CosAzimuths(I,J)

Enddo

Enddo


! working out potential ISR

do I=1,1104

do J=1,16

PotentialISR(I,J) = SolarCon *
Transmissivity**((PressureCell(J)/PressureSea)/cos(Zenith(I)*dtr)) *
CosTheta(I,J)

EndDo

Enddo


! Calculation of atmospheric pressure above the measurement site

Met2heightKM = (ElevMet2/1000)

Met2PressureCell = 1013 * 10**(-0.12 * Met2heightKM)


! Calculation of the Cos(theta) component above the measurement site

Do I=1,1104

Met2CosAzimuthAngle(I) = (Sin(AngMet2*dtr) - Sin(Lat*dtr) *
Sin(SolarElev(I)*dtr)) / Cos(Lat*dtr) * Cos(SolarElev(I)*dtr)

Met2SinAzimuthAngle(I) = -cos(d(I)*dtr) * Sin(H(I)*dtr) /
Cos(SolarElev(I)*dtr)

Met2CosAzimuths(I) = Cos(Aspect*dtr) * Met2CosAzimuthAngle(I) -
Sin(Aspect*dtr) * Met2SinAzimuthAngle(I)

Met2CosTheta(I) = Cos(AngMet2*dtr) * Sin(SolarElev(I)*dtr) +
Sin(AngMet2*dtr) * Cos(SolarElev(I)*dtr) * Met2CosAzimuths(I)

Enddo


! Calculation of site potential ISR
```

```
SitePotentialISR =  SolarCon *
Transmissivity**(Met2PressureCell/PressureSea)/cos(Zenith*dtr) *
Met2CosTheta


! Calculate temperature of the cell

do I=1,1104

do J=1,16

   CellTemp(I,J)=Temp(I) - TLR*((Elev(J) - ElevMet1)/100)

enddo

enddo


! Set any temperature values to zero if the cell elevation is greater
than the 0 degree isotherm  (i.e. avoiding negative melt)

where   (CellTemp <= 0)

        CellTemp = 0

Endwhere


! Hock's radiation calculation

do I=1,1104

do J=1,16

   MeltRate(I,J) = ((1/n) * MeltFactor + RadCoef(I,J) *
PotentialISR(I,J) * SiteMeasuredISR(I) / SitePotentialISR(I))
*CellTemp(I,J)

Enddo

EndDo


! Calculate total volumes of melt in cubic metres per hour, per gridcell

Do I = 1,1104

Do J = 1,16

TotMelt(I,J) = MeltRate(I,J) * 0.001 * AreaGlac(J)

EndDo

EndDo


! Calculate total volumes of surface runof from precipitation
```

```
! Calculate potential precipitation volumes per cell in mm per hour

do I=1,1104

   Ppt1(I,:)=Ppt(I) *(1.0001301**((Elev-ElevMet2)/100))

!print'(17F6.1)', djd1(I), Ppt1(I,:)

enddo

!stop
! Separate precipitation into liquid or solid using the 0 deg isotherm

where   (CellTemp <= 0)

         Ppt1 = zero

Endwhere


! Separate precipitation into liquid or solid using the TSL

Do I = 1, 1104

Do j = 1,16

CellStatus2(I,J) = TSL(I) - Elev(J)

Enddo

Enddo

where  (CellStatus2 <= 0)

       Ppt1 = zero

Endwhere

!do I=1,1104
!print'(17F6.1)', djd1(I), Ppt1(I,:)
!enddo
!stop


! Calculate the total runoff from precipitation over the whole catchment
in cubic metres per hour

TotPpt = Ppt1 * 0.001 * spread(AreaTot,1,1104)

!do I=1,1104
!print'(17F7.0)', djd1(I), TotPpt(I,:)
!enddo
!stop

! Calculate discharge (in cumecs) per hour from the whole glacier
```

```
Do I = 1,1104

Runoff(I) = Sum(TotPpt(I,:)/3600) + Sum(TotMelt(I,:)/3600)

print'(17F8.1)', djd1(I), Runoff(I)
enddo
!stop

! close the original data files

close (radiation_unit)

close (temperature_unit)

close (cell_parameter)

close (tsl_unit)

close (ppt_unit)


! Open new files to write the results

open (UNIT=TotalMelt_unit1,
File='/nimbus/pg/nrutter/Fort/test_data/sensitivity_trials/range_TotRuno
ff.txt', STATUS='REPLACE')

open (UNIT=TotalMelt_unit2,
File='/nimbus/pg/nrutter/Fort/SensitiveTest.txt', STATUS='REPLACE')

open (UNIT=ppt_unit2, File='/nimbus/pg/nrutter/Fort/SimRunoff.txt',
STATUS='REPLACE')


do I=1,1104

   write (TotalMelt_unit1,'(2F15.7)') djd1(I), Runoff(I)

   write (TotalMelt_unit2,'(17F15.7)') djd1(I), (TotMelt(I,J),J=1,16)

   write (ppt_unit2,'(17F15.7)') djd1(I), (TotPpt(I,J),J=1,16)

EndDo

Close (TotalMelt_unit1)

Close (TotalMelt_unit2)

Close (ppt_unit2)


end program melt
```

## 12.8 Time lags between stationary points in BWL time series

| | Time (hh:mm) | | | Time lag (hh:mm) | | |
|---|---|---|---|---|---|---|
| Julian Day | Maximum BWL 99.33 | Maximum BWL 99.54 | Maximum BWL 99.10 | 99.33 leads 99.54 by | 99.33 leads 99.10 by | 99.54 leads 99.10 by |
| 229 | | 17:10 | 18:10 | | | 1:00 |
| 230 | | 13:20 | 17:20 | | | 4:00 |
| 231 | | 12:50 | | | | |
| 232 | 15:10 | 16:20 | | 1:10 | | |
| 233 | 15:40 | 17:50 | 19:00 | 2:10 | 3:20 | 1:10 |
| 234 | 14:30 | 18:20 | 18:20 | 3:50 | 3:50 | 0:00 |
| 235 | 14:30 | | 15:50 | | 1:20 | |
| 236 | | | 17:00 | | | |
| 237 | 15:30 | | 18:00 | | 2:30 | |
| 238 | | | 17:00 | | | |
| 239 | 13:00 | | 17:40 | | 4:40 | |
| 240 | | | 18:20 | | | |
| 241 | 13:40 | | 18:20 | | 4:40 | |
| 242 | | | 15:20 | | | |
| 243 | | | 16:30 | | | |
| 244 | | | 16:40 | | | |
| 245 | 14:30 | | 17:00 | | 2:30 | |
| 246 | | | 17:10 | | | |
| 247 | | | 19:10 | | | |
| 248 | | | 19:10 | | | |
| 249 | | | 17:50 | | | |
| 250 | | | 19:40 | | | |
| 251 | | | 14:50 | | | |

| | Time (hh:mm) | | | Time lag (hh:mm) | | | |
|---|---|---|---|---|---|---|---|
| Julian Day | Minimum BWL 99.33 | Minimum BWL 99.54 | Minimum BWL 99.10 | 99.33 leads 99.54 by | 99.54 leads 99.33 by | 99.33 leads 99.10 by | 99.54 leads 99.10 by |
| 229 | | 8:10 | | | | | |
| 230 | | 8:00 | 10:00 | | | | 2:00 |
| 231 | | 3:50 | 8:20 | | | | 4:30 |
| 232 | 10:10 | 9:50 | | | 0:20 | | |
| 233 | | 6:50 | 10:00 | | | | 3:10 |
| 234 | 5:00 | 8:20 | 10:10 | 3:20 | | 5:10 | 1:50 |
| 235 | 4:20 | 7:30 | 9:40 | 3:10 | | 5:20 | 2:10 |
| 236 | | | 7:30 | | | | |
| 237 | 4:30 | | 7:40 | | | 3:10 | |
| 238 | | | 8:50 | | | | |
| 239 | | | 8:30 | | | | |
| 240 | 4:00 | | 9:20 | | | 5:20 | |
| 241 | | | 8:50 | | | | |
| 242 | | | 10:50 | | | | |
| 243 | | | 6:10 | | | | |
| 244 | | | 6:40 | | | | |
| 245 | | | 7:10 | | | | |
| 246 | | | 10:10 | | | | |
| 247 | | | 11:50 | | | | |
| 248 | | | 9:00 | | | | |
| 249 | | | 11:00 | | | | |
| 250 | | | 9:40 | | | | |
| 251 | | | 9:00 | | | | |